PREDICTION OF THE FATIGUE OF METAL MATRIX COMPOSITES USING THE THEORY OF CELLS

William Fleming B.Sc (Hons) MSc

A thesis submitted in partial fulfilment
of the requirements of
Northumbria University for the
degree of Doctor of Philosophy

February 2006

Abstract

Discontinuous and particulate metal matrix composites have emerged as a set of materials which has found increasing niche areas of use. They are now widely used in both diesel and petrol internal combustion engines, as well as in sports bicycles and other areas where their combination of unique properties can be exploited to advantage.

The inclusion of fibres into a base matrix produces a complex material both in its make up and mechanical properties and it would be an advantage to be able to predict a candidate metal matrix composite material's mechanical and thermal properties prior to that material's development. One such approach, the so called Theory of Cells, is a micromechanical approach which uses the analysis of repeating cells within the composite to make prediction of the composite's mechanical properties.

In the present study, this approach has been employed to predict the fatigue life of a series of different metal matrix composites at ambient temperature. These composites include some materials with SiC fibres and some with Al_2O_3 fibres. Using data obtained from the monolithic matrix material and the individual fibres theoretical S/N and Strain/N curves were produced. This was possible by assuming that the matrix material in the composite fails at the same fatigue stress level as does the monolithic matrix material or, if fibres fail, this will be at the failure level of the individual fibres. These curves were then compared to experimental data for all metal matrix composites and good agreement was obtained for all but the low cycle fatigue regime.

A finite element programme was employed to predict fatigue life in the low cycle fatigue regime and the results were compared to the predictions made by the Theory of Cells. It was found that the finite element was no better at predicting the fatigue life of the composite than the Theory of Cells. Both systems however predicted an area of high stress in front of the fibre in the direction of loading.

Fatigue tests were carried out on one particular material at both 200°C and 300°C and the fatigue life was compared to that predicted by the Theory of Cells. It was found that the predictions became increasingly inaccurate with increasing temperature.

Table of Contents

Table of Figures and Tables

Chapter 1

1.0 Introduction

1.1 Metal Matrix Composites

Strong materials are always of interest to both the designer and the engineer. Often strong materials are also of high density as is the case of steel compared to for example standard polymers. A material that combines the properties of both lightweight and strength would be particularly desirable. One such material is aluminium, which in its many alloy forms can show both high ultimate strength and high yield strength. In ambient conditions it is only the relatively high cost of aluminium that precludes its use in many more high strength situations. Although all materials will have much degraded mechanical properties at elevated temperatures this degradation starts at only 200°C for aluminium when both stiffness and strength start to deteriorate. At 300°C creep will start to play a significant part in the life history of the material.

Initially the inclusion of stiff, high strength fibres into aluminium was to produce a super high strength, high stiffness material. To achieve this, long continuous fibres were used in a lightweight matrix. A typical example being the boom/waveguide for the Hubble space telescope[1] made from an aluminium alloy and carbon fibres. With high stiffness and low density it was ideally suitable for the harsh environment in which it was installed. Due to the high cost of producing unidirectional continuous fibre metal matrix composites, they have only been used in these very specialist areas up till recently.[2]

To reduce cost, short fibres have been used when producing metal matrix composites. These short fibres are relatively easy to handle and allow the use of such standard production methods as squeeze casting[3] and extruding[4]. Short fibre composites will show much reduced mechanical properties when compared to an equivalent long fibre composite. However because the fibre direction is usually randomly orientated throughout the material, the properties will be the same in all directions unlike the situation found in a continuous composite.

Originally, fibres were added to metals to improve their strength and their stiffness. This was possible because of the superior stiffness and strength exhibited by certain ceramic fibres. However in short fibre composites the fibres are divided and the matrix material must now take some of the load. The resulting loss of strength experienced by the composite can often be such that it is weaker than the equivalent base material. However, even these short fibre composite materials find a use in high temperature environments. Metal matrix composites will tolerate much greater temperatures than an aluminium alloy before their strength or stiffness is affected. These composites have been used as pistons in internal combustion engines that may experience temperatures of 290°C. At such temperatures, the metal matrix composite maintains its strength and is not affect by creep.

An area of concern when using composites is fatigue. The introduction of fibres into a material has also introduced potential stress raisers into that material. The fibres themselves, as inclusions, could act as sites for crack initiation: the area around the fibre could be seen as a void, and the mismatch in the stiffness of fibre and matrix could lock in stresses during production or during loading. An attempt to look at ways of predicting metal matrix composite fatigue life will be a valuable and useful tool for future composite development.

The analysis of materials with a complex morphology such as a composite is important for the safe and confident use of such materials. While work has been done in the area of predicting static material properties such as Young's Modulus, Poisson's Ratio and also attempts have been made to predict the stress strain behaviour of metal matrix composites, little work has been done on the fatigue behaviour of such materials. One useful area of fatigue analysis is to predict the fatigue life for a given material. This information is often presented as a maximum stress against number of cycles to failure (S/n) curve or a maximum strain against number of cycles to failure curve. This information is necessary to perform fatigue damage calculations on any structure or artefact.

Although many factors may come into play to affect the fatigue life of a material, stress levels within that material are a major factor. Although the make-up of a metal matrix composite is complex a number of methods are available to analyse the stress strain behaviour on a microscopic level. The finite element method appears to be a good candidate to carry out this analysis, but the time required and the complexity of the analysis places severe limitations on its use. A micromechanical model of the material structure would appear to offer a solution to the many problems faced in mechanically modelling a composite.

In this work a micromechanical model, the Theory of Cells, is used to predict the stress within and around a fibre in a metal matrix composite. Using this information the assumption is made that the fatigue behaviour of the matrix will be the same as the fatigue behaviour of the bulk homogeneous material, while the fibres will fail statistically as they reach their overall failure stress. A prediction is then made of the fatigue life of a number of metal matrix composites using both the maximum stress and maximum strain approach. This prediction is then compared with experimental results and also a finite element prediction.

1.2 Commercial Use of Discontinues and Particulate Metal Matrix Composites

With the possibility of producing materials with many improved properties it is rather surprising that the introduction of short fibre composites into commercial production has been rather slow. The problem has not been producing suitable composites but producing a composite whose cost is comparable to that of the monolithic material.

The automotive industry has used metal matrix composites for a number of years. AE, Kolben Schmidt, Mahle and Toyota have used fibre reinforced aluminium pistons for diesel engines.[5] Although some pistons have been used which are made wholly from metal matrix composites, one company at least[6] has chosen to selectively reinforce the piston head with fibres. This has allowed them to exploit

the advantages of reinforced aluminium in the high temperature area of the diesel engine whilst saving costs by using conventional aluminium in the rest of the piston.

Honda has pioneered the use of aluminium metal matrix composites as an alternative material to cast iron for use in automotive engine blocks. Such blocks have been used in Accord, Ascot Innova and the S2000 models. The use of metal matrix composites has both reduced the engine length and allowed a weight saving of around 4.5 kg.

Chevrolet and General Motors have replaced steel with aluminium metal matrix composite in their automotive drive shafts on a range of pick up trucks.[7,8] As the drive shaft rotates at high speed, dynamic stability depends on the material modulus and density with an ideal material having high modules and low density. When steel is replaced with aluminium no dynamic stability benefit is obtained, as although aluminium is lighter than steel, its modulus is less than steel. The only way of significantly increasing the modulus of aluminium is by adding stiff ceramic fibres. Aluminium metal matrix composite drive shafts can run at significantly higher speed than the steel drive shafts they replace.

To allow ease of handling and yet be capable of high speed, a stiff but lightweight material is an advantage in high performance bicycle frames. Aluminium metal matrix composites have been incorporated into the design of a number of racing bicycles. Extensive tests have shown that not only do the bicycles have superior specific stiffness but have an improved fatigue resistance compared to the aluminium equivalent.

In the aerospace industry metal matrix composites have made some progress. Pratt and Whitney have used metal matrix composites in guide vanes on their 4000 series engines whilst Lockheed Martin's F16 fighter aircraft incorporates metal matrix ventral fins and also fuel access covers on the main airframe[7].

1.3 Aims and Objectives.

The aim of the study was to provide a theoretical and experimental framework for the prediction of fatigue life of commercial metal matrix composites using the Theory of Cells.

The following is a list of the objectives addressed in the study.

1. Reformulate the Theory of Cells to allow it to be incorporated into a computer program.
2. Write a computer program, using the Theory of Cells, to allow fatigue predictions to be made on candidate metal matrix composite materials.
3. Enable the programme to predict other relevant mechanical properties of the metal matrix composite. For example the various moduli , the Poisson's Ratio and the yield stress.
4. Carry out a series of fatigue tests varying both the fibre type and volume fraction of fibres in the selected metal matrix composites.
5. Carry out testing at elevated temperatures.
6. Compare experimentally derived mechanical properties with those predicted by the Theory of Cells for a number of metal matrix materials.
7. Compare experimentally determined fatigue life predictions with those forecast by the Theory of Cells for all materials tested.
8. Compare fatigue life predictions provided by the Theory of Cells with those fatigue life predicated by the finite element method.

Chapter 2

2.0 Overview

2.1 Definition of a Composite

A composite material is comprised of two or more dissimilar materials. However this leaves the range of materials that would fall under the heading of composite too broad. It is therefore necessary to define an engineering composite material.[9] Firstly the material must be manufactured, it must be a combination of at least two materials possibly separated by an interface and it should have properties that could not be achieved using any of the individual constituents. Unlike an alloy the constituents of the composite remain separated and do not form compounds or solutions. In commercial use the composite is usually a two-constituent material comprising the base matrix material and a second reinforcing fibre material.

2.2 Matrix and Fibres

Metal matrix composites are one of three basic composite material systems. The distinguishing feature of each is the matrix material can be a polymer, a metal or a ceramic. In a commercial metal matrix composite the base matrix material is usually an alloy of aluminium or titanium although copper, steel and other materials have been used. The fibre is normally an oxide, carbide or a nitride but prototype composites with metal fibres have been produced. The fibres used in metal matrix composites are usually SiC or Al_2O_3 but again a number of other fibres are reported in the literature.[10] As well as differing in their material of construction the fibres are also available, in different forms: as continuous fibres, whiskers, short fibres or particles. Long fibre composites give the metal matrix composites superior properties compared to short fibre and particulate composites but the latter type offers significant cost reduction.

2.3 Continuous Fibre Composites

The earliest metal matrix composites had continuous fibres, which produced a sophisticated class of materials whose properties were highly anisotropic but had compensating improvements of properties in at least one direction in the material. The advantages of these materials compared to the matrix material, from which they are produced, would include high strength, high elastic modulus, high toughness and impact properties and much-reduced tendency to creep over a wide temperature range. The composite will also tend to maintain its ambient yield stress, its maximum strength and also its stiffness at a wide range of elevated temperatures. In these composite systems the primary role of the fibres was to carry the load, while the function of the matrix was to hold the fibres together and to distribute the load amongst the fibres. In this case, the properties of the metal matrix composites were determined by the properties of the fibres, the matrix being chosen for its density or corrosion resistance or some other property. For economic reasons long fibre metal matrix composites have found only limited use in aerospace and military applications[11].

2.4 Short Fibre Composites

Because of their economic advantage discontinuous metal matrix composites have found many uses in conventional engineering situations[12]. As their name suggests, the fibres in this type of composite are short but only composites having a fibre length to a diameter ratio of less than 100 can truly be called short fibre composites. Not only are the discontinuous fibres in themselves cheaper and easier to handle but also these composite materials can be shaped and formed by standard engineering processes such as forging, rolling and extrusion. Also, as machining, drilling and grinding do not break critical fibres these processes do not alter the mechanical properties of the composite.

By using discontinuous fibres instead of continuous fibres the great improvements in the strength and stiffens of the composite, compared to the base material, is

reduced. However discontinuous metal matrix composites will retain their mechanical properties at higher temperatures than their comparable matrix material.[13]

In this type of metal matrix composite certain parts of the matrix can play a significant role in load bearing. The stress pattern over the area of the composite is somewhat complex but within the elastic range of the composite, high stress regions of matrix can be seen to take a significant share of the load compared to the fibres. Once yield in the matrix takes place, this situation rapidly changes however, with the stress in the fibre increasing significantly with load while the stress in the matrix rises at a much slower rate.

2.5 Types of Discontinuous Metal Matrix Composites

As well as the different materials that can be used for the matrix and the reinforcement, the length of fibres is perhaps the next most important variable in a metal matrix composite. Short fibre composites have fibre lengths less than 100 times their diameter while particulate composites have particles whose diameter and length are of the same order. This length to diameter ratio is called the aspect ratio (ASP) and in particulate composites the ASP would be expected to be 1 but because of varying manufacture methods it is assumed that it will be between 1 and 2. Both short fibres and particles can be of a polycrystalline nature while the short fibre may also be made from a single crystal with a high aspect ratio called a whisker. These whiskers in themselves are much stronger than the polycrystalline material but they are more expensive and may not realise their full strength in the metal matrix composite system.

2.6 History

Although the first metal matrix composites were developed in the 1920's[14] no serious research was carried out on these materials until the 1960's. A lot of the early work was involved in producing two-constituent materials, which have

similar properties to metal matrix composites. With these materials, a precipitate second phase is formed within the structure. This phase behaves in a similar way to a fibre or a particulate, its properties being radically different from the other phase in the structure. The 60's also saw the production of the first modern metal matrix composites. The matrix used for these composites was aluminium and copper while the reinforcements were long boron and tungsten fibres. Economic considerations saw the development of discontinuous reinforced fibres in the 1980's with aluminium-based composites using SiC and Al_2O_3 reinforcements being used in commercial products.[15]

2.7 Problems of Analysis

The introduction of fibres into a base metal may give greatly enhanced mechanical properties to the resultant metal matrix composite. These properties will be dependent on many factors that involve both the properties of the base matrix and the fibre used.

It would be advantageous to be able to predict some of these properties in the material design stage. It would then be possible to calculate the potential usefulness of a material or a range of materials before embarking on a costly production process. It would also narrow the range of materials that need to be considered. However the reason for needing to carry out this study, the vast range of possible variables when mixing the materials together, is what makes the analysis difficult. The base material may suggest itself by its end use, but producing the metal matrix composite may alter its microstructure. There is often a limited choice of fibre types, but also fibre diameter, cross sectional area and also length are amongst some of the variables. The volume ratio of fibre to matrix needs to be considered as well as the fibre orientation. The fibres may be aligned in one direction within the composite or may be randomly distributed through the matrix. A metal matrix composite also includes an interface between fibre and matrix whose function is to transmit stress between fibre and matrix but may also be an area of weakness.[16]

The range of properties that it would be useful to predict is the Young's Modulus, Shear Modulus, Poisson Ratio, Yield Stress and Ultimate Stress. Because the material may be anisotropic, it is important to predict these properties in different directions within the material. As fatigue life is of great importance to the safe operation of many highly stresses structures it would also be useful to predict the way any potential material might behave under cyclic stress.

2.8 Topics of Interest in the Review.

The following review will look at various micromechanical models that predict mechanical properties of a composite. Then using the method called the Theory of Cells, show how it has been adapted to include continuous and discontinuous fibres, and how it may be used to predict fatigue life. A review of current knowledge of the fatigue behaviour of metal matrix composites will also be given. An account will also be given of the current knowledge of both the nature of the fibre-matrix interface and its role in determining metal matrix composite properties. A brief review will also be given on possible ways of modelling the plastic behaviour of the matrix and metal matrix composite.

Chapter 3

3.0 Review of the Literature

3.1 Predicting Properties of Metal Matrix Composites

3.1.1 Introduction

In deciding the potential value of any metal matrix composite system it would be useful to forecast the major mechanical properties of such a system. The possible methods available are: using empirical relationships, using a finite element system or deriving a set of relationships using some micromechanical system derived from the properties of the constituent parts of the composite.

3.1.2 Rule of Mixtures

One popular empirical method is the so-called Rule of Mixtures.[17] This rule assumes that the composite mechanical property under consideration will have a value in ratio to the volume fraction of each of the constituents, i.e.

$$P_c = \sum_{i=0}^{N} V_i P_i$$

Where

$$\sum_{i=0}^{N} V_i = 1$$

P_c is the property of the metal matrix composite under consideration

P_i is the property of the constituent material under consideration

V_i is the volume fraction of the constituent material

N is the number of constituent materials

Although there is no analytical basis for this rule, it has proven useful when analysing aligned continuous fibre composites for properties in the direction of the fibres.

3.1.3 Finite Element Method

While in principle a numerical method such as finite element analysis can be used to determine mechanical properties the amount of time and expertise required for such an enterprise is prohibitive.

3.1.4 Analytical Methods

3.1.4.1 Introduction

In an early review article[18] four micromechanical models were highlighted which could predict a variety of mechanical properties of metal matrix composites by knowing the properties of the composite's constituent parts. Each of the four models was intended for use with continuous aligned fibres and each of the methods could predict both transverse and axial properties. The methods were The Discrete Fibre Matrix Model[19], the Vanishing Fibre Diameter Model[20], the Multi Cell Model[21] and the Theory of Cells[22].

3.1.4.2 The Discrete Fibre Matrix Model

This method as originally proposed uses the computational method of differences and assumed that both the matrix and the fibre were linear elastic.

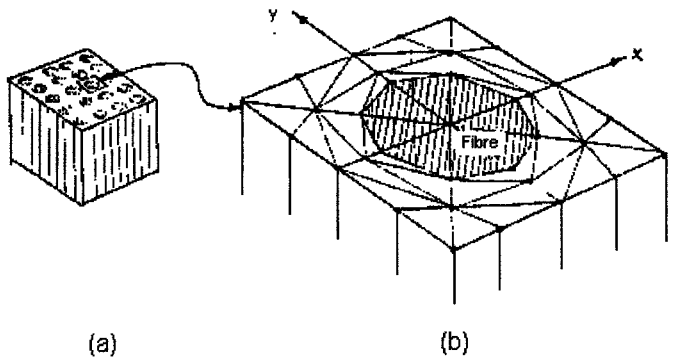

Figure 3.1(a) & (b): Idealised Cross Section of Composite

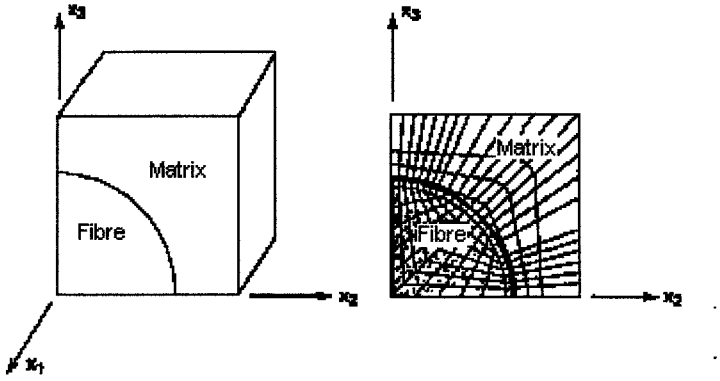

Figure 3.1 (c) Quarter Fibre with associated matrix and associated Finite Difference Mesh

Figure 3.1a shows an idealised cross section of a composite. It is not necessary to analyse the whole structure to obtain accurate results, a region comprising a ¼ of a fibre plus its surrounding area has proven sufficient. Figure 3.1 (b) shows a fibre and surrounding area while Figure 3.1 (c) shows the smallest volume that is required to completely characterise the material's behaviour. This region is then subdivided into triangular elements to allow a finite difference analysis to be carried out. The resultant computer program is written in a manner to predict the transverse Young's modulus and the transverse shear modulus for a chosen fibre/matrix system over a range of volume fractions. Some experimental evidence has been produced to show the validity of this method. The limitations of the method, at least as it was first proposed, are quite severe. It only forecasts a limited number of properties with severe restrictions on the types of composite systems to be used.

3.1.4.3 The Multi Cell Model

This approach uses a 'Mechanics of Material' approach to predict both mechanical and thermal properties of a proposed metal matrix composite.

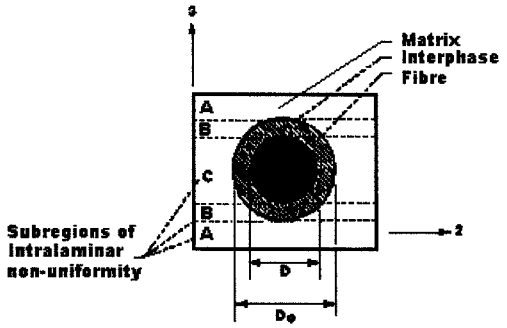

Figure 3.2 Multi-cell model showing sub-region

This approach uses an idealised cross section of a square array of fibres within a composite. In this approach only one sub region need be analysed as shown in Figure 3.2. This region comprises a fibre, its surrounding area of matrix and an interfacial area between the two. This allows for the properties of any material that may be produced due to fibre/matrix interaction to be used in the governing equations.

The backbone of the analysis is the assumption that the sum of the forces on each of the composite constituent parts will equal the overall force in the composite:

$$P_{overall} = P_{fiber} + P_{interface} + P_{matrix}$$

and that the overall strain in the composite will be the same as the strain in each of the constituent parts:

$\varepsilon_{overall} = \varepsilon_{fibre} = \varepsilon_{interface} = \varepsilon_{matrix.}$

Knowledge of each of the constituent's various moduli and other elastic properties, coupled with a basic mechanics of material approach, makes it is possible to predict a set of homogenous properties of the composite. The mechanical properties predicted are the various moduli, the Poisson's ratios and the uni-axial strength.

Carrying out a similar analysis using the thermal properties of the constituent parts it is also possible to predict the conductivity, coefficients of expansion and heat capacity of the overall composite. In the early stages of this theory the predictions were checked favourably with results obtained by finite element analysis.

3.1.4.4 Vanishing Fibre Diameter Model

This is one of the methods that use a rigorous mathematical approach to the prediction of composite properties. It follows from work on the mathematical modelling of the macroscopic behaviour of a heterogeneous media from constituent properties and interactions[23]. This work was extended[24] to incorporate an elastic inclusion embedded within the media. This solution as it stands is known to suffer from problems that the vanishing fibre model seeks to address.

In the classical solution of this problem, the retention of the actual physical boundaries of the constituent parts is assumed. However, in the case of a composite, problems occur when one of the materials is plastically deforming while the other remains elastic. Local stress concentrations in the matrix are ignored, thus causing errors in the calculation of stress and plastic strain both during and after yielding. This is overcome by assuming that although the fibres occupy a finite space within the composite, their diameter is so small that they do not interfere with the matrix deformation in the transverse and thickness direction. Some experimental evidence and finite element analysis has been offered to show the validity of this method.[25]

3.1.4.5 Theory of Cells.

In this method an analytical approach is taken to the modelling of an elasto-plastic metal matrix composite. A micromechanical analysis is carried out which allows both the fibre and matrix to be either elastic or inelastic. The material is assumed to have a regular array of doubly periodic square fibres arranged in a matrix material. This arrangement of a continuous fibre unidirectional composite is shown in Figure 3.3.

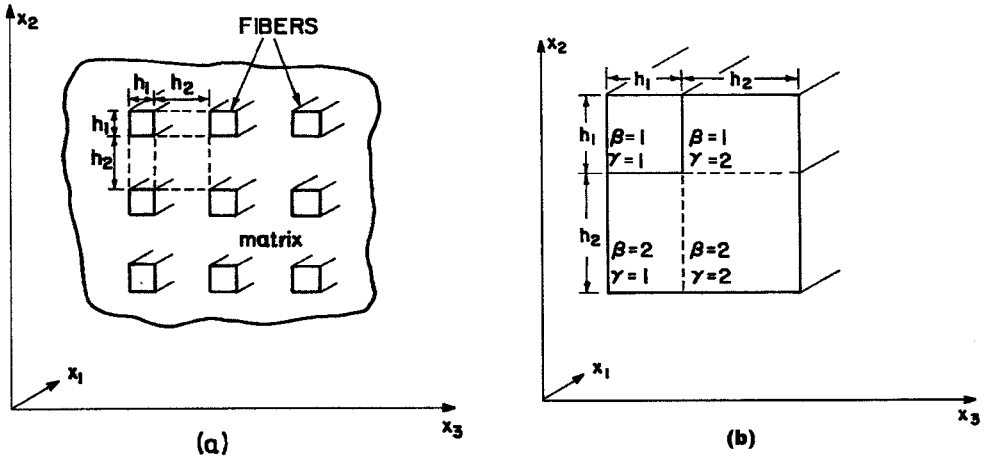

Figure 3.3 (a) An idealised array of unidirectional continuous fibres embedded in a composite matrix (b) One fibre and its associated matrix represented as four sub-cells

Because of the periodic arrangement, it is sufficient to analyse only a representative cell of the material as shown in Figure 3.3 (b). This cell is divided into 4 sub-cells as shown in the figure, one cell being fibre the other 3 made up of the surrounding matrix. The micro-mechanical analysis between these four sub-cells is carried out taking into account continuity of displacement and traction at the interfaces of the sub-cells. The equilibrium within the cell is also taken into consideration.

Determination of overall composite properties in all three dimensions is possible with this system of analysis. A considerable amount of experimental evidence is available to verify the validity of this method.

3.2 Developments in the Theory of Cells.

3.2.1 Introduction

The Theory of Cells is a robust model that has been extended into many areas of composite analysis. The continuous fibre version has been used to analyse materials with polymeric, metal or ceramic matrix materials. The continuous fibre theory is fully three-dimensional, allowing both fibre and matrix to be anisotropic and consequently predicting anisotropic properties for the resultant composite. Elasticity is not imposed on either the fibre or the matrix but using the ideas of Bodner,[26] plastic modelling is included within the theory. Extensions of the theory have included the modelling of non-linear behaviour of resin matrix composites, allowing for imperfect bonding of fibre and matrix, a method for predicting yield and ultimate strength of the composite and finally a re-casting of the theory to allow for analysis of short fibre and particulate composites. With the continuous and short fibre versions of the Theory of Cells a refinement has been added that allows analyses of randomly oriented fibres.

3.2.2 Short Fibre Composites.

In the modelling of short fibre composites the fibres are assumed to be aligned rectangular parallelepipeds imbedded in a matrix and to form a triply periodic array as shown in Figure 3.4.

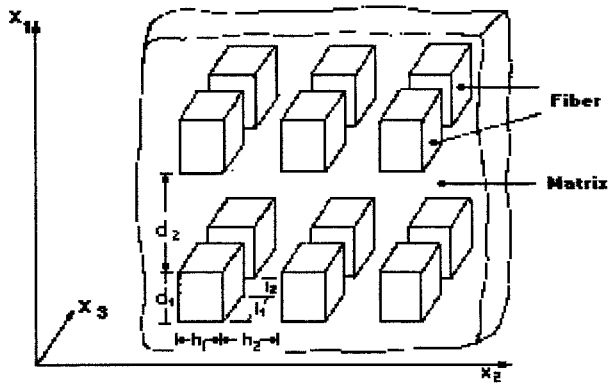

Figure 3.4 Schematic of an MMC with periodic array of fibres

As with the long fibre composite, only a representative volume of the composite need be analysed. This cell of material comprises one fibre and seven sub-cells of matrix material. This is shown in Figure 3.5.

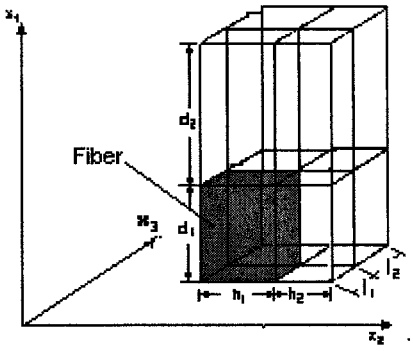

Figure 3.5 A representative cell of the composite showing the eight sub-cells

The system of algebraic equations that needed to solve this problem is far more complex than that which is required to solve the continuous fibre model. A summary of the method is given in Chapter 3. As with the continuous fibre version of the Theory of Cells, the analysis not only predicts the various moduli in all three directions but will give the overall stress in the composite during each stage of loading as well as the corresponding stress in each of the sub-cells.

This version of the Theory of Cells can be used to analyse metal matrix composites with fibres of any dimension and therefore long fibre and short fibre metal matrix composites are handled in the same manner. For the special case of particulate composites the computation is carried out with all dimensions of the fibre equal.

3.2.3 The Fibre Interface in the Theory of Cells.

A metal matrix composite is composed of at least two very dissimilar materials, which must however form a good bond at their interface to produce a useful material. Difficulties in obtaining data on the mechanical or physical properties at the interface meant that in all early versions of the Theory of Cells, perfect bonding was assumed between fibre and matrix. However, in a real material this requirement of perfect bond is quite demanding since it requires adhesion of materials that by their nature may not directly adhere. Even a material that on production has good bonding between fibre and matrix may suffer some level of de-bonding during service use.

The first attempt to modify the Theory of Cells to take into account a real interface assumed a metal matrix composite that had suffered total de-bonding of the fibres[27]. This is of course an extreme situation, as actual de-bonding would be assumed to be partial and non-uniform throughout the metal matrix composite.

The total de-bonding of the fibres is achieved in the theory by allowing free tangential slip at the fibre matrix interface, while still demanding the continuity of the normal displacement there. This ideal of tangential slip was first used in the study of periodical bi-laminated composites[28] but is here used in conjunction with a first order expansion, to determine average constitutive equations for a fibre matrix composite. It should be stated that as presented this theory could only be used with continuous reinforced composites.

Due to the limited applications of this method, Aboudi uses a totally different approach when looking at the more general case of imperfect bonding[29]. This approach was first suggested by Jones and Whittier[30] and consists of assuming that

the interface is a thin film. Imperfect bonding can then be represented in this model by two parameters, one dependent on the level of adhesion in the tangential direction the other on the level of adhesion in the normal direction at the interface. This method has been used to analyse a unidirectional continuous aluminium/ boron metal matrix composite and the results checked against results obtained using finite element analysis with good agreement.

3.2.4 Inelastic Behaviour of Metal Matrix Composites

A typical metal matrix composite comprises a fibre that behaves in an elastic manner up to the breaking stress and a matrix that will show the typical elasto-plastic behaviour of a ductile material. In order to model a composite an allowance must be made for the plastic deformation of the ductile matrix. In the development of the Theory of Cells a unified theory of plasticity, developed by Bodner and Partom, was used.[31] In this approach, plasticity is assumed to be always present throughout the loading process, and deformation is represented by the sum of the elastic strain and the plastic strain throughout the whole of the loading history of the material. The elastic strain is calculated in the standard manner, using linear elastic theory while plasticity is represented by a plastic flow rule which couple plasticity and creep functions together. In this unified theory, five experimentally determined parameters are used to represent inelastic behaviour. These parameters can represent both creep and plastic behaviour. They are strain rate sensitive and can also represent work hardening of the material.

It should be noted that there is no yield function in this theory as elastic, plastic and creep deformation is assumed to be taking place at all time during loading. However at low loads and ambient temperatures the inelastic strain term is insignificant for an aluminium metal matrix composite.

3.2.5 The Generalised Cells Model

In the original Theory of Cells a continuous fibre composite was modelled as one sub-cell of fibre and three sub-regions of matrix material. However a more generalised version of the Theory of Cells has been developed[32] in which the area selected for analysis is divided into any number of rectangular sub-cells as opposed to the four sub-cells in the original formulation shown in Figure 3.6.

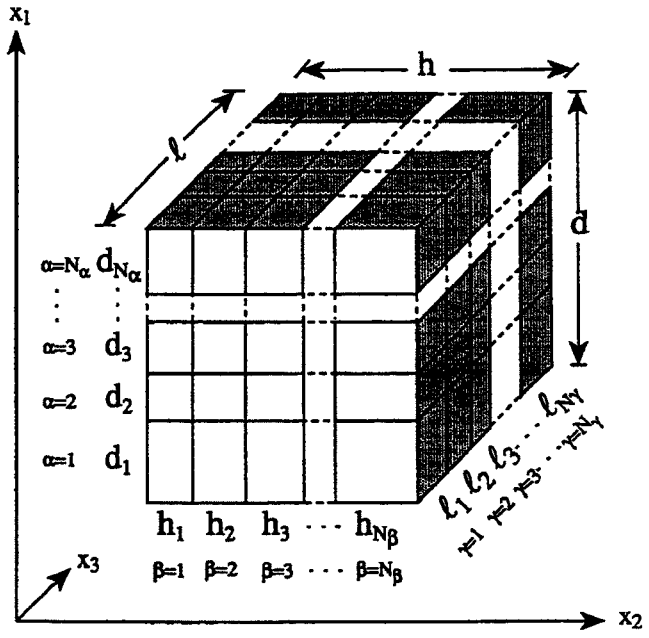

Figure 3.6. A repeating cell for the generalised version of the Theory of Cells

In this model the fibre may be represented by a single cell or a group of cells and the remaining cells may represent the matrix or the fibre/matrix interface. Increasing the number of sub-cells to be analysed will allow for a more detailed modelling of the plastic behaviour of the matrix and therefore a more accurate prediction of the stress strain curve of the proposed metal matrix composite might be expected. This model is more sensitive to yield and plastic flow in the matrix

when these values might be expected to vary significantly across the cell. With the increased number of sub-cells it is also possible to represent multiphase composite material and to model such areas as the interface.

The Generalised Theory of Cells model has been used to predict the axial and transverse stress strain curve for aluminium boron aligned continuous metal matrix composite. With a 16 sub-cell configuration good agreement is shown between the model and a finite element prediction in the transverse direction while only a 4 sub-cell configuration is necessary to show excellent agreement with a finite element prediction in the axial direction.

3.3 Composite Interfaces

An important component of any composite system is the fibre-matrix interface. The interface in a composite can be defined as a boundary surface between dissimilar materials. The interface is important because it controls the degree of bonding between matrix and fibre, and it is also the cohesive forces that exist within the interface which govern the load transfer within the composite structure.[33] This interface load transference often dictates the performance of the whole composite structure. The nature of the interface is dependent not only on the make up of the constituent parts of the composite but on the way the composite was manufactured. Knowledge of the interface will allow a margin of control of its properties both during the composite production process and any subsequent post process treatments.

When casting one material around, another the chemical reaction that results at their interface is obviously governed by the nature of the two materials. In a successful composite, this interface will act as a bond between the two constituent parts of the composite and the type of bond can be divided into three categories:

The bonds may be mechanical in nature, they may be chemical (either dissolution or wet-ability bonding) or reaction bonds.

Due to the roughness of the fibres[34] and contraction of the matrix during cooling, a strong mechanical bond can be set up within the composite material. If the fibre and matrix have a good wet-ability interaction[35] the bonding will be caused by electron interchange and so as this force is of short range it is essential that their surfaces come into intimate contact. This is achieved by ensuring that the fibres are treated to remove any impurities that may exist on their surface before they are incorporated into the composite. In reaction bonding, there is an interchange of atoms between materials which is caused by the high temperatures during composite production. This reaction bonding will tend to create an interfacial material with different properties from both the fibre and matrix.

The modelling of any interfacial region within a mechanical theory of composites is very difficult. Direct testing of the interfacial region to determine mechanical properties is extremely difficult due to the size of the region. Some information can be obtained about the bond strength of the interface by using a fibre pullout test. This is carried out on a specially prepared test specimen which has a single fibre half-embedded in a matrix under an axial load and displacement is then measured due to the increasing load.[36]

Unfortunately, because of preparation and handling difficulties, this and other similar tests are not practical for metal matrix composites. For this reason it is normally assumed that the interface forms a perfect bond[37] between fibre and matrix and that the forces and displacements will be transmitted across the region.

However, as perfect bonding would seem to be a rather difficult to achieve or maintain in a system, it may be achieved in only a few composites. Certainly under a highly stressed situation, failure or partial failure of the interface may be expected. Failure will usually be by one of two failure mechanisms[38]: cavitation or de-bonding.

The dominant mode of interface failure in short fibre and particulate metal matrix composites is by cavitation. It is assumed that in these systems strong interfacial bonds exist between fibre and matrix, then ductile failure is precipitated by

nucleation, followed by growth and then coalescence of voids within the vicinity of the fibre reinforcements.

In composites containing weakly bonded fibre and matrix it would be expected that interfacial de-bonding would occur. This happens in a brittle manner once local conditions reach a critical value. This could be that the local stress has exceeded the interfacial bond strength or the strain energy release rate exceeds the interfacial fracture toughness.

The manufacture of a composite material has an influence on the interface, encouraging solution segregation, local dislocation density precipitation reaction and fibre clustering. These will tend to cause imperfections and flaws near the interface and cause cracks to form and cavitation nucleation to occur. The nucleation of voids however requires an amount of plastic strain and so would occur under a high stress regime[39]. In strongly bonded interfaces voids will grow from the matrix and conversely for weak interfaces voids form at the ends of fibres.

Damage will tend to occur at weak interfaces because this will be the area at which stress are concentrated due to abrupt change of materials and the geometric distribution of fibres. The weak interface itself may be caused by weak or brittle phases within itself or porosity generated during manufacture. These items will add to the tendency for the fibre within the composite to de-bond from the matrix.

Several attempts appear in the literature that incorporates the resistance and effect of imperfect bonding in composites. They mainly consist of the introduction of a third phase (inter-phase) between the fibre and matrix constituents. The effect of the degree of adhesion is represented by a proper choice of the material constants, density and thickness of inter-phases[40]. The difficulty is of course devising a test procedure to obtain these parameters. After all, the fibres themselves are measured on the micron scale and the area of interest, the interface, is embedded within the metal matrix composite itself.

3.4 Fatigue of Materials under Cyclic Stress

Although some static fatigue failure has been reported for certain glasses[41] failure by fatigue usually takes place under cyclic loading and involves the initiation and progressive growth of a crack across the specimen. Failure usually occurs when the remaining area of material can no longer resist the applied load and because of the presence of the area of high stress in front of the fatigue crack tip failure is usually sudden and catastrophic.

Unless the material initially contains a crack or other such default it is believed that crack initiation may not occur until quite late in the fatigue life of the material.[42] Initiation is therefore quite an important factor in the general fatigue life of any material. The factors affecting initiation are many and their interaction quite complex. The maximum and minimum cyclic stresses are obviously important but so is the sign of both these stresses. The rate of stress cycling may play a part, as may the form of the stress pattern (i.e. sinusoidal, step or triangulated). The specimen size and shape, the specimen surface finish and microstructure are other factors to be considered.

3.5 Fatigue Behaviour of Fibre Composite

3.5.1 Introduction

All fibre composites possess a unique combination of characteristics that must be recognised from the outset if their fatigue behaviour is to be understood. Major factors are heterogeneity, anisotropy, strengthening by load transfer, and interfaces between fibre and matrix. Although many of these factors may be found in conventional engineering materials it is their combination and extent that presents problems in composite materials. Combined, these characteristics result in

unprecedented complexities in composite fatigue behaviour, but they also provide unparalleled opportunity to design more fatigue-resistant materials.

A composite material is of course at least a two-component material and the fatigue behaviour of both the fibre and the matrix need to be considered. Ceramic fibres do not often suffer from fatigue damage and typically their endurance limit will be their static strength[43]. The metal matrix within the composite will of course be subject to fatigue failure in much the same way as it would if it were a monolithic material.

The inclusion of fibres into the matrix material multiplies the possibility of defects occurring and defects are candidate areas for fatigue crack initiation and growth. These defects may often occur at the interface or they may occur at fibre ends. If they have not occurred during material manufacture they will often be induced upon the first loading of the composite. During cyclic loading some fibres may break at weak points but more importantly the fibre and matrix will try to strain at different rates perhaps causing damage at the interface. If the mix of fibre and matrix is such that the fibres take most of the load it will be difficult to damage the matrix even if there are readily available defects.

In a homogeneous material fatigue damage is usually associated with one crack only, which may cause catastrophic failure. For composites the situation is far more complex. Even if a fatigue crack is initiated and starts to grow it may encounter a fibre that could deflect the crack into a less damaged direction. Because of this behaviour the first fatigue crack that starts to propagate may be deflected and thus arrested by a fibre that may allow another and then many cracks to grow. This is most likely to occur in long fibre composites that may then sustain damage throughout the stressed region. A decrease in the Young's modulus of the material will result as fatigue damage is sustained, and as a consequence material failure may occur by a loss of material stiffness rather than actual tensile failure[44].

Reinforcement occurs by the transfer of loads via shear stresses across fibre-matrix interfaces and the fibres, which are stiffer than the matrix, will carry most of the applied axial loads. Interfaces play another important role in fracture resistance

by controlling the modes of crack growth; they can deflect growing cracks and impede crack growth[45].

3.5.3 Fatigue of Polymer Composites

In polymeric composites, fatigue testing can generate a considerable amount of heat depending on the frequency. This makes the test both temperature and frequency dependent. Due to the temperature effect on fatigue strength, obtaining valid experimental data in the form of S/n curves and endurance limits has proven difficult. However it has been shown that fatigue strength dependence on temperature is a function of tensile strength dependence on temperature, and temperature against tensile strength data is easily obtained.[46] Therefore any fatigue tests carried out at above ambient temperature, which is normal if a moderately high frequency of stress reverses is used, can be recalculated for ambient temperature. This allows an S/n curve to be generated for a composite and a fatigue life prediction to be made at ambient temperatures.

The fatigue failure modes in long fibre reinforced polymer matrix composites are controlled by the fibre, the matrix and by the fibre/matrix interface. That is, if the matrix requires much less cyclic strain to fatigue than the fibre, then the matrix damage will occur first. If on the other hand, the fibre requires less cyclic strain to fail than does the matrix, the fibre damage will occur first

3.5.4 Fatigue of Metal Matrix Composites

The unique combination of stiffness, strength and density offered by metal matrix composites has made them leading material candidates for advanced engineering application. A key factor in the safe design and use of any material in a highly stressed situation is the rate at which fatigue cracks initiate and the rate at, once initiated, they will propagate. For optimum fatigue life in a composite system,

the right balance of interfacial strength and, where applicable, fibre bridging must be obtained[47].

When considering metal matrix composites we must distinguish between long fibre composites and short or particulate composites. Even when these two types of composites have identical matrix and fibre, the material properties of each composite can be radically different and this is also true of their fatigue properties.

Often long fibre metal matrix composite materials can appear to be very fatigue resistant. However, if they undergo damage during cyclic loading at high stress this can lead to a significant reduction in stiffness that may cause "failure" in components where the stiffness is critical. Fatigue damage in a long fibre laminated metal matrix composite can reduce the laminate stiffness by as much as 50% without causing laminate failure.[48] Stiffness loss in long fibre metal matrix composites has been a useful paramount for detecting fatigue damage initiation.

Compared to a polymeric composite the matrix material of a metal matrix composite is of relatively high strength and stiffness compared to the fibre and consequently contributes more to the composite properties than does a polymer material. The metal matrix may have a modulus of the same order of magnitude as the fibre and while under static loading the fibres reach their ultimate strain first and fail before the matrix, under fatigue loading the matrix yields at strain level far below fibre ultimate strain. As a consequence of this, fatigue and therefore fatigue damage will be matrix dominated.

A model of fatigue behaviour of unidirectional MMC has been developed which takes into account both crack initiation at fibres and crack stopping by fibres. If we imagine a crack growing in the composite matrix, this may grow according to the Paris Power Law :-

$$\frac{da}{dn} = C(\Delta K)^n$$

The crack will grow until it reaches a fibre then it must either break the fibre at this point or change direction and move parallel to the fibre. It can only cross the fibre at a weak point. As long as it grows parallel to the fibre it will not contribute to final failure of the composite. Fibres with no weak points are called perfect fibres and if the material has mostly perfect fibres the S/N curve will be flat with the fatigue endurance stress being almost the same as the fibre tensile stress and this appears not to follow the Paris hypothesis. Fibres which contain a high number of weak points will behave in much the same way as the matrix material where crack growth is a function of ΔK, and follow the Paris Power Law.

In practice, we usually get a mixed type of crack growth, with the crack taking some time to find the weakness in the fibre, but nevertheless finding it. This results in long fibre metal matrix composites possessing high fatigue strengths in the longitudinal direction..

As with polymers, the first sign of fatigue damage may be loss of material stiffness and will be due to extensive matrix cracking. However in some materials when the failure is mostly due to fibre breakage the ultimate fatigue failure is caused by a relatively strong crack at 90° to loading.

It has been suggested that the overall crack growth is controlled by the fibre/matrix interface and the fibre spacing. It has also been shown that bundles of fibres can inhibit crack growth in a titanium metal matrix composite. The bundles halted the crack growth across the fibres and forced the crack to grow parallel to the fibres until weaker fibre sections allowed the crack growth to continue across the fibres again[49].

Fatigue behaviour of a unidirectional metal matrix composite is usually superior to that of the un-reinforced material but short-fibre composites tend to have lower fatigue strength than that of the un-reinforced material. The difference in behaviour is explained by the stress distribution within these two types of composite. In long fibre materials, the matrix function is to hold the fibres apart and the matrix will experience trivial stress levels compared to the fibres. In short fibre materials whilst the fibres can still withstand high stress, the load must be transferred from

one fibre to another via the matrix material. Some sections of the matrix will be experiencing high stress, stress high enough to initiate fatigue damage. These stresses can be higher, for a given loading, than that experienced by the non-reinforced material. In short fibre materials it is only when the matrix has undergone yielding that the stresses in the fibres become significantly larger than that experienced by the matrix.[50]

The present understanding of fatigue crack initiation in metal matrix composites can be summarised as follows: Metal matrix composite fatigue crack initiation differs from fatigue crack initiation in metals in only one principal way, namely that, in addition to free surfaces acting as sites of initiation, fractured fibres serve as a new source of fatigue cracks in the composite. This problem is naturally more pronounced for brittle fibres, brittle coatings on fibres, or brittle interface reaction products. More importantly, these are interior sites, not readily accessible to observation and non-destructive inspection techniques. Whether or not fatigue cracks actually initiate at broken fibres depends on the association stress intensity factor, which is proportionate to the fibre diameter and the stress amplitude. Subsequent crack growth is controlled by the elastic property, yield strength and work hardening characteristics of the constituents and the fibre matrix interfacial bond strength and microstructure.

In metal matrix composites fatigue failure can affect both the fibre and the matrix. Should a fibre fail, either by reaching its failure stress or by conventional fatigue damage, the load carried by this fibre will be transferred to the matrix and/or onto the other fibres. The fibre break point is also an area of potential crack growth. Fatigue failure of the matrix itself will normally cause instantaneous failure of the composite.

The ideal fatigue-resistant fibre-reinforced metal appears to be one having a low yield strength ductile matrix, a high yield strength brittle fibre and a weak interfacial bond. Then failure will occur at the interface instead of within the matrix.

3.6 Effect of Temperature on Metal Matrix Composites

Many metal matrix composites are specifically designed to be used in thermal environments where most conventional materials fail to sustain their properties. Because of their multi-constituent nature, metal matrix composites can be sensitive to temperature change. The metal matrix base of the composite will have a high coefficient of thermal expansion compared to the ceramic reinforcing fibres. When the composite is exposed to elevated temperatures the constituent parts will expand and contract at different rates, causing thermal stress fields around the fibres. Even though yielding or creep of the matrix may relax some of this thermal stress, premature yielding in the composite may still occur.[51]

The creep nature of the metal matrix composite may be significantly different from that of the matrix material. Not only will the ceramic fibres, which in themselves are creep free materials, slow the creep of the matrix but they will also impair the movement of dislocations within the material. It has been suggested[52] that the speed of dislocation movement can control creep rate. With a two material system in which the heat capacity of both materials are significantly different, there will be thermal gradients throughout the material thus causing 'micro hot spots' which will enhance plastic strain at these areas.

3.7 The Prediction of Fatigue Behaviour

Early published works on fatigue of metal matrix composites were mostly concerned with reporting experimental results of specific material behaviour. Some of these studies were on continuous fibre composites and lead to a realisation that fatigue could be dominated by the static strength of the fibres contained in the composites.[53]

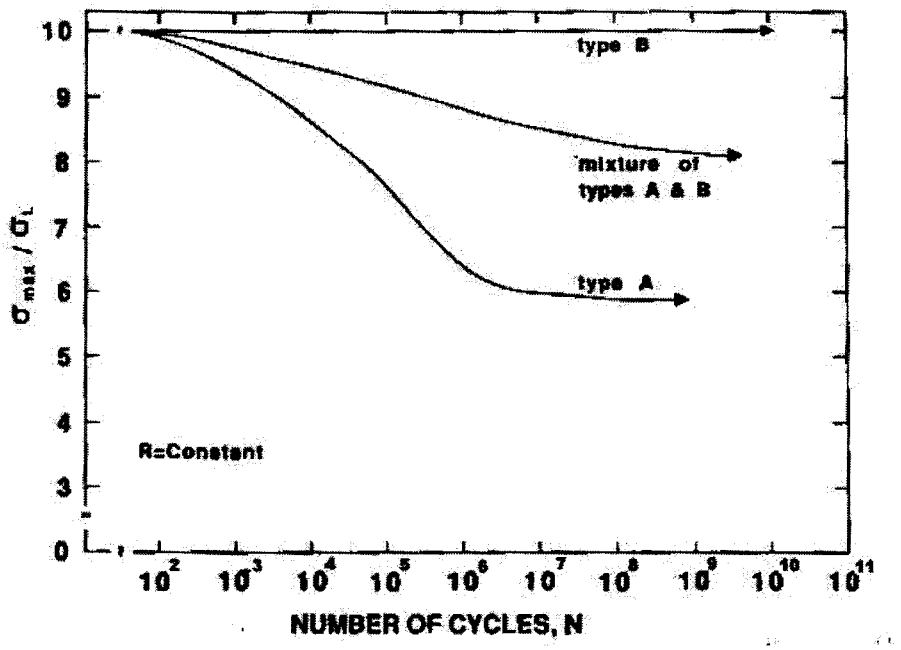

Figure 3.7 Three Types of S/n Curves of Metal Matrix Composites A) Sigmoidal B) Flat Mixture of Type A and Type B.

Figure 3.7 shows three types of S/n curve,

- Type A is fatigue dominated by matrix fatigue,
- Type B is fatigue dominated by fibre brakeage
- Type C is a mixture of both modes of failure.

In type B failure, which was seen to be the case with most continuous fibre composites, failure is occurring because fibres are reaching their failure stress and not because they are being cyclically damaged. If the fibres within the composite all had approximately the same static strength the composite would not suffer from cyclic fatigue failure and failure would only occur if the working stress reached the static failure stress. However, seemingly identical fibres will exhibit a wide range of failure stresses. On the first loading of a composite, a small number of the weaker fibres break, on the second loading there are fewer fibres to withstand the stress so failure of other fibres occurs and this continues throughout the cyclic process until failure occurs.

Experimental work on the fatigue of discontinuous fibre metal matrix composites did not start in earnest till the 1990's[54] and in addition to work reporting the fatigue performance of various composites, attempts were being made to understand and predict some aspects of the fatigue behaviour. The predictions revolved around two major areas:-

- crack growth
- fatigue life prediction.

For crack growth, the Paris relationship has been show to be applicable for a range of short fibre composites. For example, in tests carried out on two particulate metal matrix composites, both with a matrix material Al2014 but with different volume fractions of SiC, the Paris law was shown to apply and the parameters calculated.[55] The results are shown in Figure 3.8 and, as can be seen, the rate is different for both composites. It can be seen that by adding fibres to the composite the crack growth rate is much increased over all load levels.

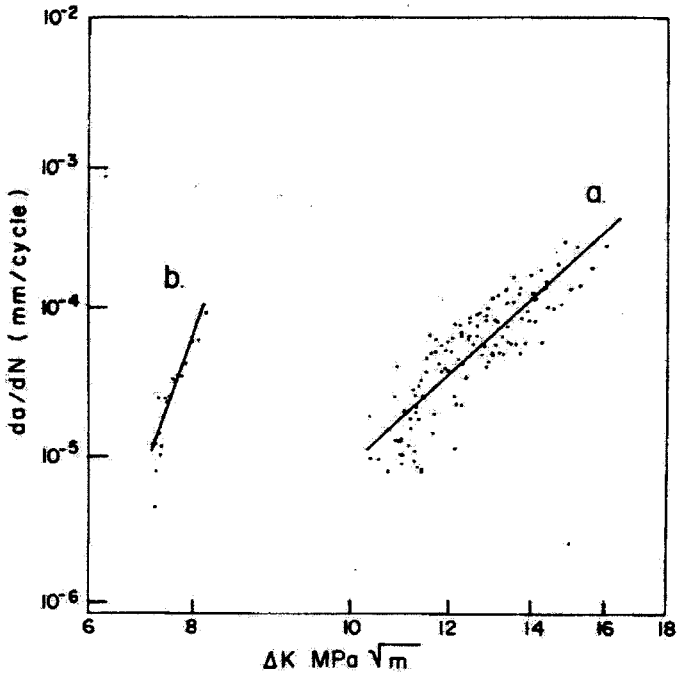

Figure 3.8. The fatigue crack propagation rate for two metal matrix composites a) Al7091 30% volume SiC_p and b) Al2014 40% SiC_p

For these materials, crack propagation occurred in the matrix layer with preference in areas with fibre clumping. Crack branching was also noted, which indicates that the SiC particles could effectively hamper crack growth. The reason for accelerated crack growth in the metal matrix composite with the higher fibre volumes is that this composite was more prone to large clusters of fibres, these causing rapid crack growth along what was believed to be weakened interfaces between fibre and matrix.

This work was concerned with predicting what would happen to existing material but the Paris Law does not help with predicting on what happens to an as yet untried matrix fibre combination. The work did however point out the problems with excessive volume fraction of fibres in a composite.

The Paris Law does not model all types of cracks. It was first reported by Pearson[56] that very short cracks propagated at rates different from long cracks. It has now been recognised that microscopically small cracks are fundamentally different from both mechanically small cracks and long cracks.[57] This concept of microscopically small cracks has lead to the defect tolerance approach to the prediction of both crack growth and fatigue life forecast.[58] Using the effective range of the J-integral to characterise the elasto-plastic fatigue crack growth rate of the microscopically small crack. Both R-curves and crack closure need to be determined experimentally and then it is claimed that this method can model all modes of crack growth. With these results, a theoretical S/n curve can be generated for a specific metal matrix composite type[59].

The results using this method are shown in Figure 3.9. Experimental and predicted results are shown on the same diagram. Although it has been claimed that these results are in close agreement with each other, serious doubts must be raised as it is impossible to draw a line through either set of results. It is obvious that more experimental evidence is required to validate this approach to fatigue life.

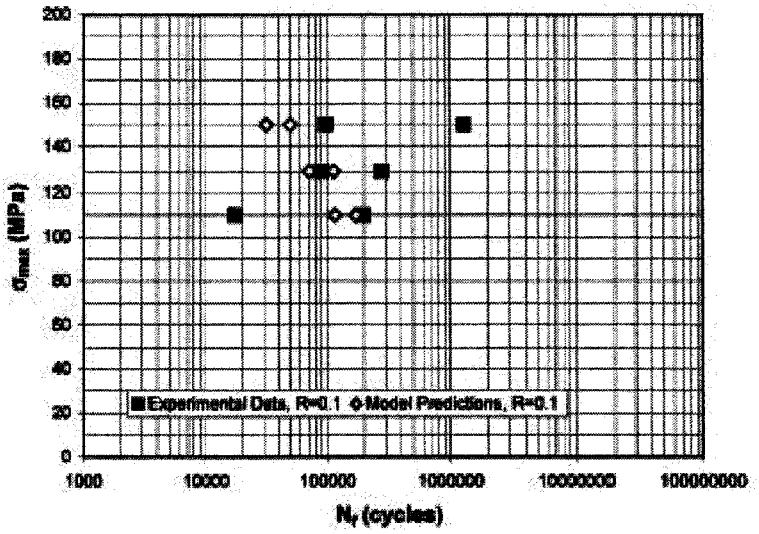

Figure 3.9. Predicted Fatigue Lives of the Al 359 Metal Matrix Composite Using Pre-Determined Initial Defect Sizes.

This approach is not applicable to predicting the fatigue properties of proposed metal matrix composite systems, as a defect size to cause failure for a given stress is required for any material being analysed. As it is not possible to know the defect size within a particular material, it must either be calculated from experimental results or a typical defect size must be used. Experimentation has shown that for a particular metal matrix composite defect sizes range from 0.04 mm to 0.1 mm. This variable quantity must be looked on as a major weakness of this method.

Another fracture mechanics approach has been used by Ding et al[60] to predict the low cycle fatigue crack growth behaviour and fatigue life of a short fibre metal matrix composite. If the crack growth in this type of composite is treated as a succession of crack initiations by accumulated cyclic plastic deformation, this deformation must occur at the crack tip. Within this cyclic plastic zone there is also a fatigue damage zone where the degradation process must take place. The stress levels within this zone must be in the region of the ultimate stress of the matrix material, as this is what causes the crack to grow. The cyclic J integral for this fatigue damage zone can be calculated, and therefore a range of crack tip opening displacements correlated. The crack growth per cycle can then be determined and by using the concept of a critical crack length the fatigue life calculated.

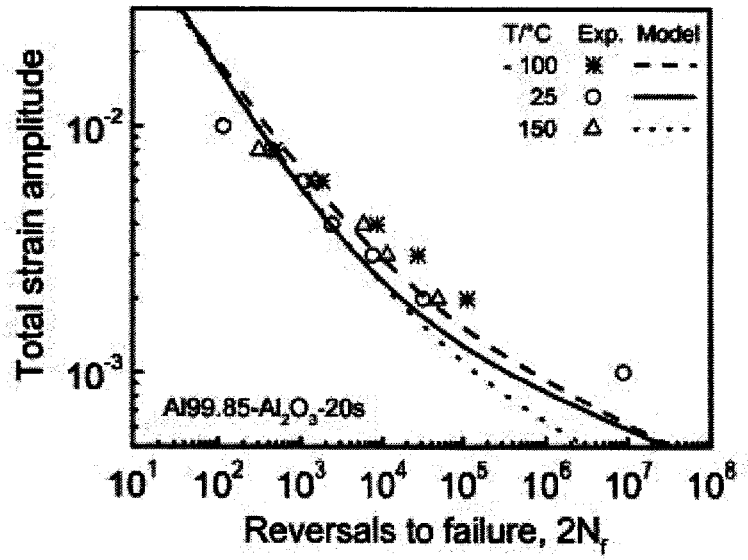

Figure 3.10 Total Strain Amplitude against Reversals to Failure for experimental and model predictions for Al99.85 with 20% volume of Al_2O_3 at three temperatures.

The results from this work are shown in Figure 3.10 where total strain amplitude is plotted against reversals to failure. The material used is pure aluminium (Al99.85) with 29% by volume of Al_2O_3 and three different test temperatures were used in the experiments. As can be seen, this approach works reasonably well at high strain levels over the whole range of temperatures. Because this approach only models crack growth, no allowance is made for crack initiation and at high strain rate crack initiation will be rapid and most of the fatigue life of the metal matrix composite will be involved in crack growth. Once 1000 cycles have been exceeded the specimens, as would be suspected, survive for longer than predicted. Fatigue crack initiation should at these lower strain values, occupy a substantial amount of the life of the material.

Another fracture mechanics approach has been used to predict fatigue life of a fibre reinforced concrete.[61] It uses a Paris based law with a crack tip stress intensity factor and assumes unstable fracture conditions when the crack tip stress intensity factor surpasses the matrix fracture toughness. There is a complication in that the crack tip stress intensity factor is made up of both the stress intensity due to geometry and stress intensity due to crack bridging. The solution to both these

factors and the matrix fracture toughness must be achieved numerically. From this analysis a theoretical S/n curve can be calculated. Figure 3.11 and Figure 3.12 shows this analysis and compare it to experimentally derived data

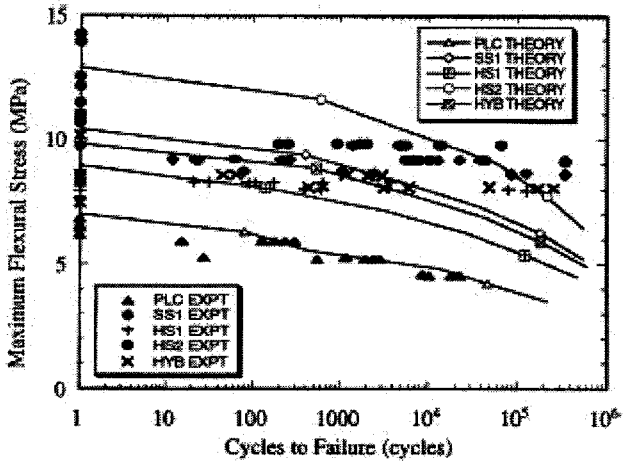

Figure 3.11 S/n diagram of theoretical predictions of plane concrete and four fibre reinforced concretes shown against experimentally derived results for the same concretes.

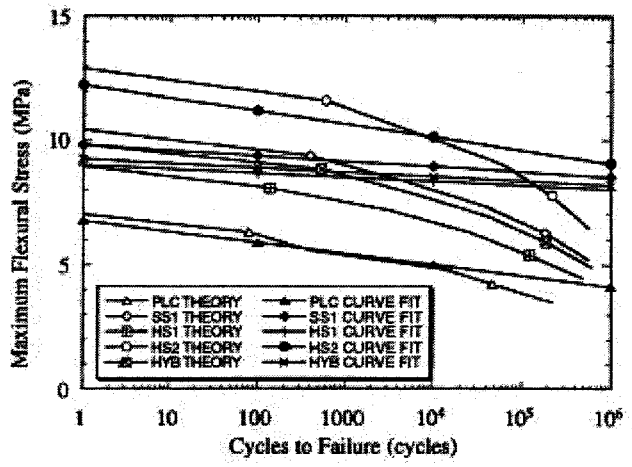

Figure 3.12 Same results as given in Figure 3.11 but with curve fit of experimental results.

Five different materials were analysed and tested: A plain concrete (PLC) and four fibre reinforced concretes (AA1, HS1, HS2 and HYB). As can be seen from these

graphs, correlation between theory and experimental data is rather patchy. The plain concrete correlates rather well for all results over 30 cycles. However for all the fibre reinforced concretes it would be difficult to make any correlation between the experimental results and the predicted values. Figure 3.12 is an attempt to make some sense out of this conflicting data by curve fitting the experimental results. Although this looks better for one or two of the fibre reinforced composites one could argue that this has only been achieved by using the many 1 cycle to failure results to skew the results towards the predicted results.

A different approach to fatigue prediction is by using a micromechanical analytical model associated with some assumptions about fatigue damage. A mechanistic life fraction model has been proposed[62] and, in association with a two dimensional version of the Theory of Cells, predications can be made on the fatigue life of unidirectional long fibre metal matrix composites.[63] The modified Theory of Cells along with Bodner-Partom's theory of viscous-plasticity[64 65] are used to calculate stresses around a single fibre within a composite then, using a simplified life fraction model of fatigue, fatigue life can be evaluated. This life fraction model assumes that fatigue life is dependant on both a time dependant factor and a cyclic factor and also introduces a term to take account of the interaction between the two factors.

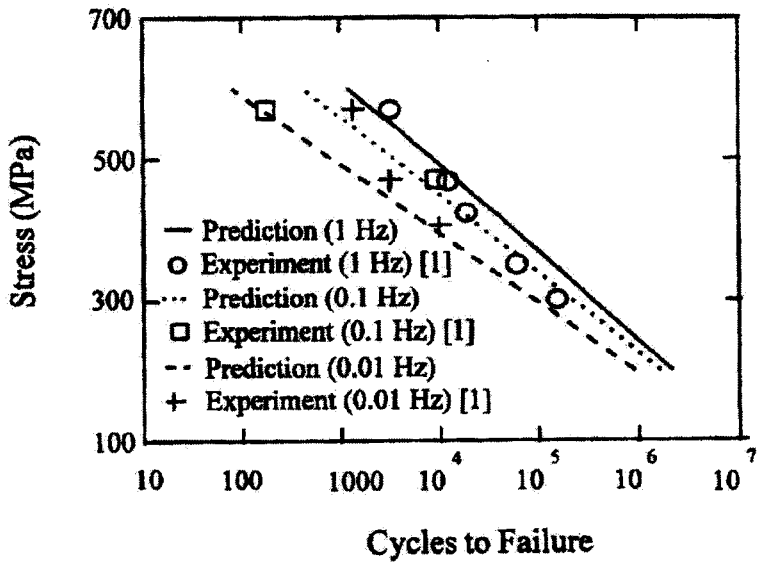

Figure 3.13 S/n curve for SCS-6/TIMETAL 21s cross-ply composite at 650°C.
with predicted results for various frequencies.

Initially, static testing needed to be carried out on the composite material to obtain both the material properties, such as Young's Modulus, and the stress strain curve and also to calculate information necessary to carry out the fatigue life analysis. The results from both experimental and theoretical analysis for ScS-6/TIMETAL21s cross ply titanium metal matrix composite are shown in Figure 3.13 and Figure 3.14

These two figures are different ways to represent the same results and perhaps Figure 3.14 gives a better summary of the results as it shows clearly how the predicted results correlate experimental evidence. Poor correlation is observed for low cycle life tests with some improvement as the cycle life increases. The weakness of this method is that results are only given for long fibre composites and it cannot be used to predict the fatigue life of proposed metal matrix composite systems.

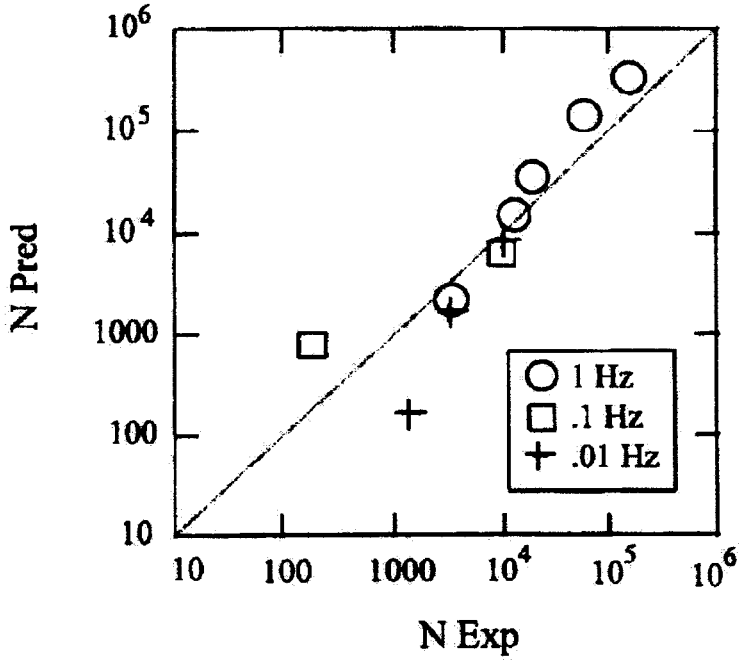

Figure 3.14 Predicted fatigue results against experimental results SCS-6/TIMETAL 2ls cross-ply composite at 650°C. at various frequencies.

Chapter 4

4.0 Theoretical Aspects: Development of Mathematical Models

4.1 Theory of Cells

4.1.1 Introduction

In Chapter 3 a number of mathematical methods to predict the mechanical properties of metal matrix composites were introduced. Of these, the Theory of Cells offers a wide range of application over all types of composite systems. Three separate versions of the theory have been produced; one for long fibre composites comprising four sub-cells (see Figure 3.3), one for short fibre composites comprising eight sub-cells (see Figure 4.1 and Figure 4.2) and a generalised form comprising any number of sub-cells (Figure 3.6). The sub-cell number indicates the complexity of analysis required in the process. As the computation required to make a prediction of mechanical properties within this system is time consuming a computer program is required no matter which version of the theory is used. The present author has written two such programmes, one for long fibres and one for short and particulate fibres (see Appendix A and Appendix B). All Theory of Cells predictions shown in this document were carried out using the short fibre and particulate program.

4.1.2 Assumptions Made in the Theory

In the simplest form of the Theory of Cells, the composite is assumed to have only two constituents, the fibre and the matrix. Both fibre and matrix are assumed linear elastic and for given fibre and matrix materials a whole range of composite mechanical properties can be predicted. Development of this version of the theory

allows for creep, yield and elasto-plastic behaviour of both fibre and matrix. A review of this method is given in a review article published in 1989.[66]

The Theory of Cells (TOC) for short fibre and particulate metal matrix composites has been further developed by Aboudi [67]. In this method, an elastic matrix is considered which is reinforced by unidirectional fibres of short length. The fibres are assumed rectangular with dimensions of d_1, l_1 and h_1 and arranged in the matrix as shown in Figure. 4.1.

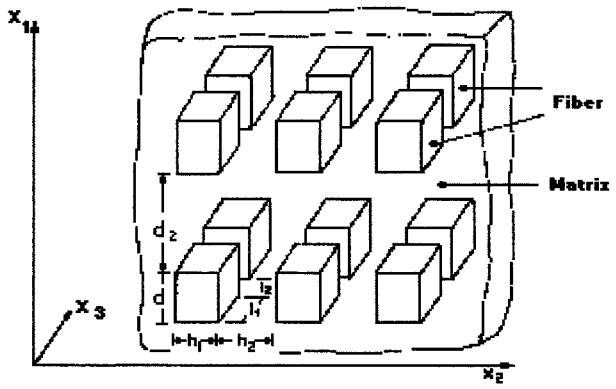

Figure 4.1 Schematic of an MMC with periodic array of fibres

In a particulate metal matrix composite h_1 will have a similar value to l_1.

4.1.3 Designation of a Sub-Cell Position.

Given that the arrangement of fibre and matrix are periodic, only one fibre and its surrounding matrix need be analysed to give a representative section of the composite material. This area is called a cell and is shown in Figure 4.2. This cell is divided into eight sub-cells and to allow analysis, each sub-cell must be uniquely labelled. As is seen in Figure 4.2 each area is given a three digit reference which depends on its position in the cell. For example the fibre is referenced 1,1,1 and when considering stress and strain this is used as a super script notation, i.e. for stress the fibre would be written $\sigma^{(1,1,1)}$. This super-script notation is necessary to

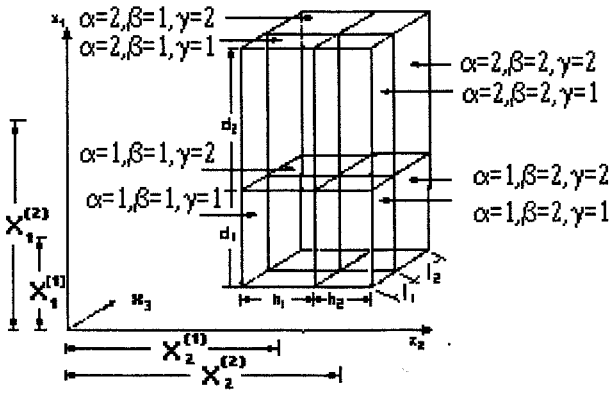

Figure 4.2 A representative cell of the composite showing the eight subs cells

distinguish it from the stress or strain direction which of course uses a sub-script notation. For example the direct stress in the x_1 direction is labelled σ_{11}. The full notation for the direct stress on the fibre in the x_1 direction will be $\sigma_{11}^{(1,1,1)}$. This is then repeated for all other sub cells. For example stresses in the sub cell above the fibre, as shown in Figure 4.2, are labelled. $\sigma^{(1,1,2)}$ and for example the direct stress in the x_2 direction would be $\sigma_{22}^{(1,1,2)}$.

4.1.4 Development of the Theory.

It is assumed, initially, that both fibres and matrix are perfectly elastic materials and the stresses are related to the strains as follows

$$\sigma^{(\alpha,\beta,\gamma)} = \mathbf{C}^{(\alpha\beta\gamma)}\ \mathbf{Z}^{(\alpha\beta\gamma)} - \Gamma^{(\alpha\beta\gamma)}\ \Delta T$$

where

$\sigma^{(\alpha\beta\gamma)}$ being the stress matrix of each sub-cell

$\mathbf{C}^{(\alpha\beta\gamma)}$ the stiffness matrix representing mechanical properties of each sub-cell

$\Gamma^{(\alpha\beta\gamma)}$ a matrix representing thermal properties of each sub-cell

ΔT the temperature difference between a reference stress free temperature and the working temperature

while

Z, the strain micro-variables is given by

$$\mathbf{Z}^{(\alpha\beta\gamma)} = \Phi_1{}^{(\alpha\beta\gamma)}, X_2{}^{(\alpha\beta\gamma)}, \Psi_3{}^{(\alpha\beta\gamma)}, X_1{}^{(\alpha\beta\gamma)} + \Phi_2{}^{(\alpha\beta\gamma)}, \Psi_1{}^{(\alpha\beta\gamma)} + \Phi_3{}^{(\alpha\beta\gamma)}, \Psi_2{}^{(\alpha\beta\gamma)} + X_3{}^{(\alpha\beta\gamma)}$$

with

$\Phi_1{}^{(\alpha\beta\gamma)}, \Phi_2{}^{(\alpha\beta\gamma)}, \Phi_3{}^{(\alpha\beta\gamma)}, X_1{}^{(\alpha\beta\gamma)}, X_2{}^{(\alpha\beta\gamma)}, X_3{}^{(\alpha\beta\gamma)}, \Psi_1{}^{(\alpha\beta\gamma)}$, $\Psi_2{}^{(\alpha\beta\gamma)}, \Psi_3{}^{(\alpha\beta\gamma)}$ representing strain micro-variables

In an expanded form this matrix equality can be written for each sub-cell as follows:

$$\begin{pmatrix} \sigma_{11} \\ \sigma_{22} \\ \sigma_{33} \\ \sigma_{12} \\ \sigma_{13} \\ \sigma_{23} \end{pmatrix} = \begin{pmatrix} C_{11} & C_{12} & C_{12} & 0 & 0 & 0 \\ C_{12} & C_{22} & C_{23} & 0 & 0 & 0 \\ C_{12} & C_{23} & C_{22} & 0 & 0 & 0 \\ 0 & 0 & 0 & C_{44} & 0 & 0 \\ 0 & 0 & 0 & 0 & C_{44} & 0 \\ 0 & 0 & 0 & 0 & 0 & C_{66} \end{pmatrix} \begin{pmatrix} \varphi_1 \\ \chi_2 \\ \psi_3 \\ \chi_1 + \varphi_2 \\ \psi_1 + \varphi_3 \\ \psi_2 + \chi_3 \end{pmatrix}$$

If this matrix is solved we obtain expressions of the form

$$\sigma_{11}^{a\delta\gamma} = C_{11}^{a\delta\gamma}\varphi_1^{a\delta\gamma} + C_{12}^{a\delta\gamma}\chi_2^{a\delta\gamma} + C_{12}^{a\delta\gamma}\psi_3^{a\delta\gamma\delta}$$

$$\sigma_{22}^{a\delta\gamma} = C_{12}^{a\delta\gamma}\varphi_1^{a\delta\gamma} + C_{22}^{a\delta\gamma}\chi_2^{a\delta\gamma} + C_{23}^{a\delta\gamma}\psi_3^{a\delta\gamma}$$

etc

If continuity of traction between appropriate sub-cells is assumed, certain of the sub-cell will have equality of stress i.e.:-

$$\sigma_{11}^{1\beta\gamma} = \sigma_{11}^{2\beta\gamma}$$

$$\sigma_{22}^{a1\gamma} = \sigma_{22}^{a2\gamma}$$

$$\sigma_{33}^{a\beta1} = \sigma_{33}^{a\beta1}$$

Using a first order approximation the displacement component at any point in the sub-cell can be expressed as

$$u_i^{(\alpha\beta\gamma)} = w_i^{(\alpha\beta\gamma)} + x_1^{(\alpha)} \Phi_i^{(\alpha\beta\gamma)} + x_2^{(\beta)} X_i^{(\alpha\beta\gamma)} + x_3^{(\gamma)} \Psi_i^{(\alpha\beta\gamma)}$$

where

w_i represents the displacement component of the centre of the sub-cell and

Φ_i, X_i, Ψ_i characterises the linear dependence of the displacements on the local co-ordinates. $x_1^{(\alpha)}$, $x_2^{(\beta)}$ and $x_3^{(\gamma)}$

and the displacement can be connected to strain using the expression

$$\varepsilon_{ij}^{(\alpha,\beta,\gamma)} = \tfrac{1}{2} [\partial_j u_i^{(\alpha,\beta,\gamma)} + \partial_i u_j^{(\alpha,\beta,\gamma)}]$$

and $\partial_1 = \partial/\partial x_1^{\alpha}$

$\partial_2 = \partial \partial x_2^{\beta}$

$\partial_3 = \partial/\partial x_3^{\gamma}$

If continuity of traction and displacement between appropriate sub-cells is assumed, it is possible to calculate the 26 strain micro-variables generated by the theory. Once the stresses in each sub-cell are calculated the overall stresses can be found as follows

$$\sigma_{ij} = 1/V \sum_{\alpha,\beta,\gamma=1}^{2} \left(V^{(\alpha,\beta,\gamma)} \sigma_{ij}^{(\alpha,\beta,\gamma)} \right)$$

V represents the total volume of the cell and

$V^{(\alpha,\beta,\gamma)}$ the volume of a particular sub-cell.

By an incremental increase in the strain it is possible to generate the value of stress in each of the sub-cells and also to determine the overall stress for the composite. It is therefore possible to plot a stress strain curve for the proposed composite. A number of strategies are available to take into account any plastic deformation occurring in either the fibre or matrix and therefore calculate the yield stress of the composite and estimate its overall elasto-plastic behaviour.

To obtain values of overall composite properties such as Young's modulus and Poison's ratio, in the axial and transverse ratio an overall elastic matrix can be calculated and from this the overall elastic constant can be determined.

4.1.5 Randomly Reinforced Metal Matrix Composites

The Theory of Cells was developed for unidirectional composites where the fibres are aligned in the X_1 direction as shown in Figures 4.1 & 4.2 This places severe limitations on the type of systems it is possible to analyse. However a transformation can be made on the stiffness matrix of each sub-cell, using a method first suggested by Arridge.[68] It is found that for a material with randomly distributed fibres, the stiffness matrix reduces to three non-zero elements which are related to the aligned fibre matrix in the following manner

$$B_{11}^{(\alpha,\beta,\gamma)} = (3A_1 + 2A_2 + 4A_3) / 5$$

$$B_{12}^{(\alpha,\beta,\gamma)} = (A_1 + 4A_2 + 2A_3) / 5$$

$$B_{66}^{(\alpha,\beta,\gamma)} = (A_1 - 4A_2 + 3A_3) / 5$$

where

$$A_1 = (C_{11}^{(\alpha,\beta,\gamma)} + C_{22}^{(\alpha,\beta,\gamma)} + C_{33}^{(\alpha,\beta,\gamma)}) / 3$$

$$A_2 = (C_{23}^{(\alpha,\beta,\gamma)} + C_{13}^{(\alpha,\beta,\gamma)} + C_{12}^{(\alpha,\beta,\gamma)}) / 3$$

$$A_3 = (C_{44}^{(\alpha,\beta,\gamma)} + C_{55}^{(\alpha,\beta,\gamma)} + C_{66}^{(\alpha,\beta,\gamma)}) / 3$$

$B_{ij}^{(\alpha,\beta,\gamma)}$ is the transformed stiffness matrix, allowing for a fully random fibre distribution in the composite.

$C_{ij}^{(\alpha,\beta,\gamma)}$ is the stiffness matrix for aligned fibres

Using this modified stiffness matrix in the stress strain matrix, the strain in all three dimensions can be calculated for each sub-cell in the MMC with randomly distributed fibres.

4.2 Fatigue Analysis

It can be assumed that fatigue failure will occur when one or more of the sub-cells reach a critical stress level. In a one-dimensional loading system the fatigue failure stress for the matrix material can be obtained from an S/n curve. It can be assumed that failure of the composite will occur, for a similar number of cycles, when any matrix sub-cell reaches this cyclic stress level providing the fibre has not reached its critical level. Therefore the matrix is assumed to fail by fatigue similar to the homogenous material.

The fibres however may behave differently. Silicon carbide fibres are brittle and do not exhibit fatigue failure.[69] In the case of the individual fibres, their critical fatigue stress is assumed to be identical to their tensile failure stress. However, similar fibres exhibit a wide range of tensile failure stresses as can be seen in Figure 4.3. This has important implications on the fatigue life of a metal matrix composite containing such brittle fibres.

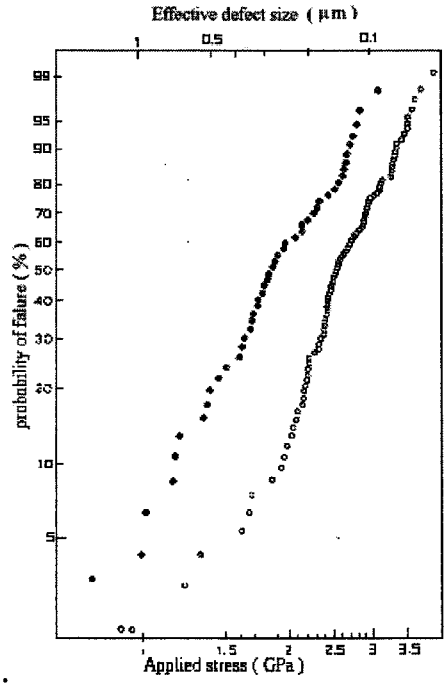

Figure 4.3 Experimental strength behaviour of SiC yarn fibre (Andersson and Warren[70])
○ 10-mm fibre carefully handled ● 100-mm fibre carefully handled

In the present study the Theory of Cells is used to calculate stresses in the eight sub-cells for an increasing load. At each increment of load, a check is made to see if any matrix sub-cell has reached its fatigue limit for a given number of cycles, or if the stress level in the fibres is such that fibre failure is encountered. If the former is the case, the overall composite stress is recorded as the fatigue failure stress for that load. If fibre failure has taken place, the stress on each sub-cell is recalculated, assuming a lower density of fibres and the possibility of more fibre breakage ascertained. An iterative recalculation of stress is then performed until the mode of fatigue failure is determined.

4.3 Elasto-Plastic Models within the Theory of Cells.

A typical MMC comprises a fibre that behaves in an elastic manner up to the breaking stress and a matrix that will show the typical elasto-plastic behaviour of a ductile material. To model a composite an allowance must be made for the plastic deformation of the ductile matrix. In Aboudi's development of the Theory of

Cells[71] he used the unified theory of plasticity developed by Bodner and Partom.[72] In this theory, plasticity is assumed to be always present throughout the loading process. Although rigorous, the Bodner et al. approach adds a level of complexity to the analysis that may not be necessary. In the present study, this has been abandoned in favour of a theory of plasticity proposed by Mendelson[73], in which the total strain experienced by a stressed material is made up of both elastic and plastic strains. Using this approach, plastic strain can be assumed to approximate to zero while the material is within the elastic region. Therefore if $\sigma_{ij} < Y$ the total strain can be written as

$\varepsilon_{ij\,(total)} = \varepsilon_{ij\,(elastic)} = \sigma_{ij}/E$ for a one dimensional direct stress system.

Once the material suffers plastic deformation the relationship changes to:

$$\varepsilon_{ij\,(total)} = \varepsilon_{ij\,(elastic)} + \varepsilon_{ij\,(plastic)}$$

and $\varepsilon_{ij\,(plastic)}$ can be defined as $(\sigma_{ij} - Y)^n / \mu$

and therefore for $\sigma_{ij} > Y$ the total strain is now

$$\varepsilon_{ij} = \sigma_{ij}/E + (\sigma_{ij} - Y)^n / \mu$$

where

σ_{ij} represents the total stress in the ij direction

Y is the material yield stress

n and μ are factors which characterise the plastic behaviour of the material.

This approach assumes simple elastic breakdown at the yield stress. For a bi-axial loading system the failure theory can be modified to include a shear yield component.[74]

4.4 Finite Element Analysis

4.4.1 2-D Approach

As a first approach a simple 2-D Finite Element Analysis was attempted using the EsduFine 2-D modeller produced by Coventry University. This package is restricted to elastic analysis and has limitations on the number of elements that can be used. To accommodate these limitations only a small section containing one fibre and the surrounding matrix was analysed.

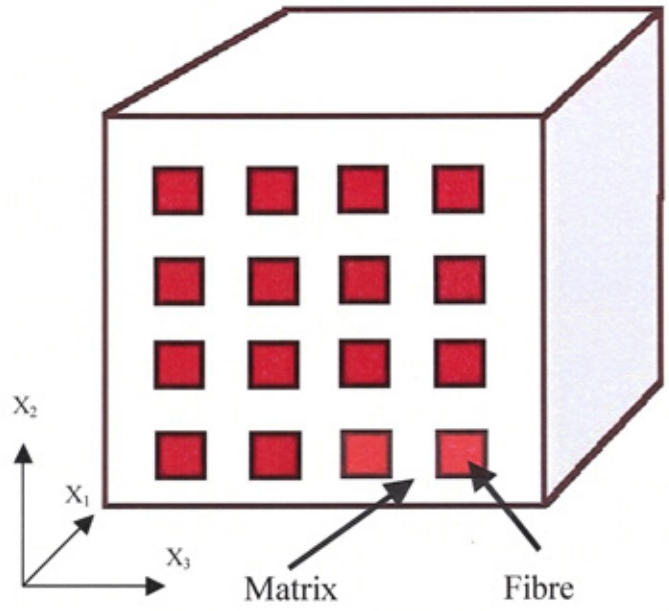

Figure 4.4. Idealised representative area of a metal matrix composite with periodic array of fibres

In finite element analysis, an idealised representation of the composite structure must be chosen. Such a configuration is given in Figure 4.4. where it is assumed that the fibres are arranged in a periodic manner and that all fibres are equally spaced in both the X_2 and X_3 direction.

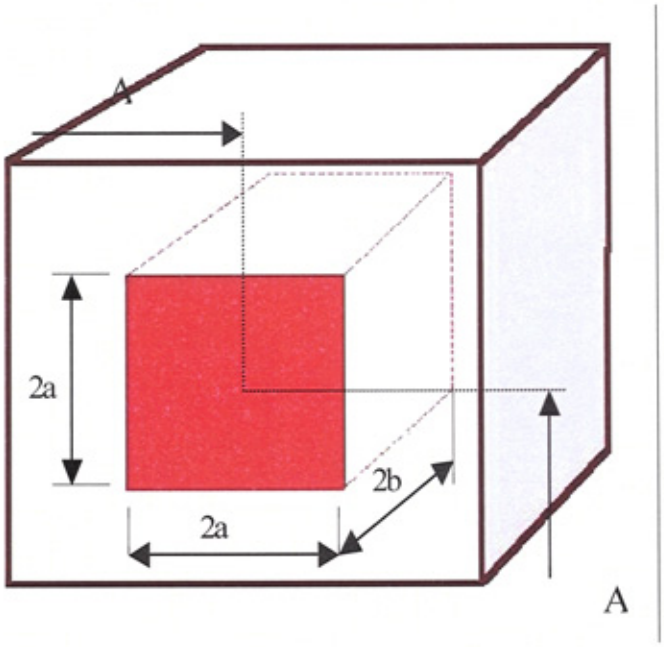

Figure 4.5. Idealized region showing single fibre surround by matrix material.

It not necessary to look at the whole of the multi-fibre region to obtain accurate results from a finite element calculation. Figure 4.5 shows one single fibre and because of symmetry it is possible to take the region A-A which represents a ¼ fibre only and, by imposing certain constrictions, obtain valid results.

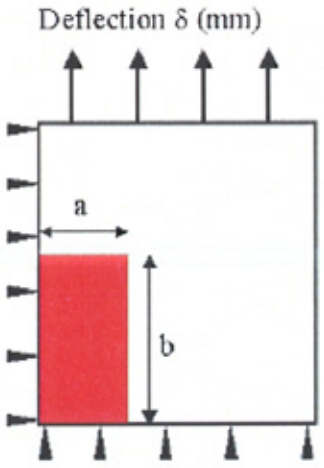

Figure 4.6. Model of ¼ fibre with surrounding matrix used in the EsduFINE analysis.

In Figure 4.6 a ¼ fibre is shown surrounded by matrix material and constraints are placed upon the two faces as shown. By superimposing a deflection in the X_1 direction both the local and global effect upon the metal matrix composite stress fields can be observed. The depth of the fibre, which is not shown on the figure, is the 'a', the same as the width.

4.4.2 3-D Approach

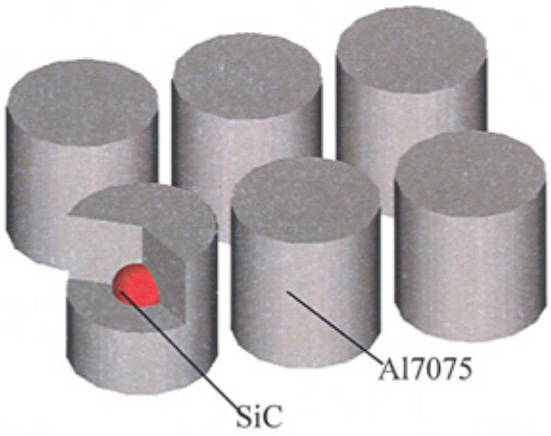

Figure 4.7. Scheme of the MMC structure with periodic array of fibres

The 3-D finite element approach has been used with some success to determine material properties of both long and short fibre metal matrix composites. In the present investigation only the region of high plastic deformation has been analysed. The stress-strain analysis of both the metal matrix composite and the individual cells within it are a 3D plasticity problem. However, as a first approach, the fibres were approximated to a spherical body surrounded by a cylinder of matrix material (see Figure 4.4). The cylinder represented one cell of the MMC. Using a model described elsewhere[75,76,77,78] the cyclic stress-strain response of the matrix material can be developed in terms of the simple relationships. The stress σ_n^* and strain ε_n^* co-ordinates may be related during any half-cycle n by

$$\sigma_n^* = f_n(\varepsilon_n^*), \tag{4.1}$$

where $f_n(\varepsilon_n^*)$ represents some modification of the initial stress-strain response of the matrix material under monotonic loading (i.e. n=0). However other parameters describing the material cyclic stress-strain curve will vary depending on the cyclic history and the number of applied cycles, but, as was shown in previous

publications[77,78,79, 79] ,these changes may not only be dependent on the number of half cycles. To take this into account an alternative approach is used, with the parameters describing the cyclic strain curve dependent on the cumulative plastic strain χ.

This is defined as

$$\chi = \sum_{n=0}^{n_f} \left| \Delta \varepsilon_p \right|, \tag{4.2}$$

The relationship between stress σ_n^* and strain ε_n^* (Figure 5) is represented in the form

$$\sigma^* = \begin{cases} E_\chi \varepsilon^* & \varepsilon^* \le \varepsilon_{s\chi}^* \\ E_\chi \varepsilon_{s\chi}^* + b_\chi d_\chi \left\{ f\left[\varepsilon_s + \dfrac{\left(\varepsilon^* - \varepsilon_{s\chi}^*\right)}{b_\chi} \right] - \sigma_s \right\} & \varepsilon^* > \varepsilon_{s\chi}^* \end{cases} \tag{4.3}$$

$$\varepsilon_{s\chi}^* = \left(\frac{a_\chi}{d_\chi} \right) \varepsilon_s; \quad d_\chi = E_\chi / E$$

where σ_s^* and ε_s^* are the initial stress and strain values at 0.02% offset yield; a_χ, b_χ and d_χ are material-sensitive parameters describing plastic deformation response of the material under cyclic load; E_χ is a plastic strain path χ-dependant modulus such that $E = E_{\chi(\chi=0)}$. In practice, due to the Bauschinger effect, a_χ may be defined as $\sigma_{s\chi}/\sigma_s$, d_χ is defined as stated above and a transformation coefficient b_χ relates the non-linear portion of the stress–strain curve under monotonic loading to that observed under dynamic loading conditions.

This relationship is valid for the matrix material, which under cyclic loading has an alternating elasto–plastic strain while the fibre material remains elastic. Material constants describing the above mentioned parameters of cyclic stress-strain were defined on the base of experimental results obtained for an equivalent material to that of the Al 7075 alloy.[80]

These constitutive equations lead to the non-linear FE problem, the solution of which requires special iterative procedure at every half cycle of the loading or unloading.

Tests conducted for different engineering materials show that for constant–amplitude stress, constant–amplitude strain and stress random–amplitude loading the number of half-cycles n_f before failure at alternating–sign plastic deformation is related to the limiting value $\chi_{\max}$ by the power law:

$$n_f = \left(\chi_{\max} / \delta \right)^{\gamma}, \tag{4.4}$$

here δ is the constant depending on the residual plastic strain value, γ is the parameter that characterises the material's ability "to cure" the cyclic loading damage.

The model, based on the relationship 4.3, allows simulating the cyclic life exhaust process of the specimens under all conditions. At the same time, the accumulated plastic strain may be plotted on the co-ordinate plane χ, n by the function $\ln(\chi)$ of $\ln(n)$. Moreover, if $\Delta\varepsilon_p$ does not change sign in going from half-cycle to half-cycle, then χ increases and n_f remains constant. If, in the two adjoining half-cycles $\Delta\varepsilon_p$ changes sign then n increases by one. If the value $D = \chi(n)/\chi_{\max}(n)$ is taken as the damage measure its equality to unit defines the amount of half-cycles loading where the alternating–sign plastic deformation takes place. If for different loading processes the parameters defining the material's mathematical model at cyclic deformation are equivalent to the same damage measure D, all functions of χ in equation 4.3 may be replaced by the functions of the dimensionless parameter D.

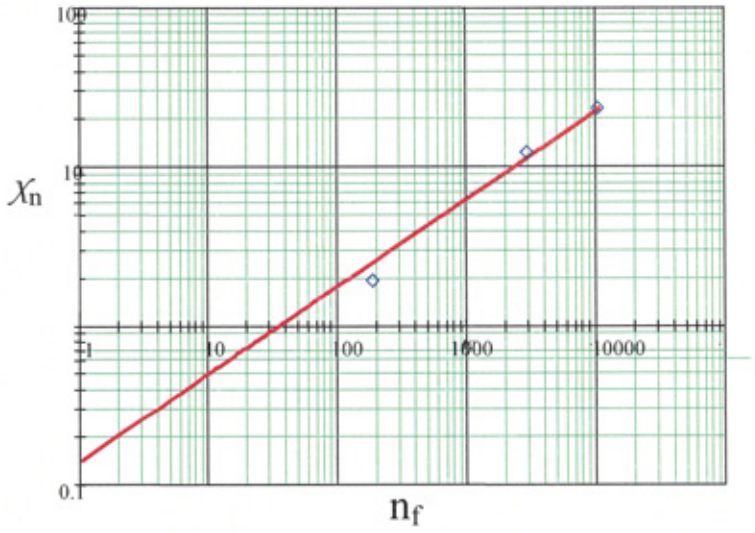

Figure 4.8. Experimental and analytical relationship between the ultimate accumulated plastic strain and the number of half-cycles before failure.

Taking into account that parameter χ in these tests can be obtained by the following relationship :- $\chi = n_f \left(2\Delta\varepsilon_{ay} - \frac{a_\chi \sigma^* \left(2\Delta\varepsilon_{ay}\right)}{E_\chi} \right)$ the results of which are shown in Figure 4.8 where n_f is the number of half-cycles to failure for un-notched Al specimens and $\Delta\varepsilon_{ay}$ is the specimen's elongation amplitude. Figure 4.8 is an approximation of these experimental points. The point of intersection with the Y-axis gives the value of δ=0.1328. The line tangent is γ=2.005.

Chapter 5

5. 0 Experimental Aspects: Techniques Adopted and Materials Used

5.1 Strain control testing

5.1.1 Testing Procedure

Tests were carried out on a PC driven Dartec 50 kN. capacity servo-hydraulic testing machine. All tests were conducted under strain control and constant amplitude. Tests were conducted in air at a frequency of 0.25 Hz using fully reversed loading (R=-1.0) with stress and strain data being recorded for each cycle.

5.1.2 Material

The material under consideration in this section was an aluminium alloy Al 7075 and a metal matrix composite with an identical material for the matrix plus 12% SiC fibres, in particulate form. The chemical composition of the composite was 6.2% Zn, 1.5% Cu, 2.3% Mg, 0.2% Cr., 0.3% Fe and the remainder aluminium. The monolithic material had a Young's modulus of 72 GPa, a Poisson's ratio of 0.33, a 0.2% proof stress of 416 MPa, UTS of 565 MPa and an elongation at failure of 14%.

The SiC particles had the following specification[81]. Diameters range from 0.25 to 20 microns with an average diameter of 3 micron to 4 microns. The average effective aspect ratio was 1.3 while the Young's modulus was 468 GPa and the Poisson's ratio was 0.25. The particulate strength was assumed to be statistical in nature, 5% of the particulates failing at a stress of 1.6 GPa and 90% having failed at an average stress of 3.1 GPa.

The metal matrix composites were produced by spray forming followed by extrusion. Heat treatment of the material consisted of an initial high temperature solution treatment at 465 °C held for 45 minutes followed by a cold-water quench and the material aged for 16 hours at 135 °C. The measured Young's modulus was then 84 GPa, the 0.2% Proof stress 404 MPa, the UTS 490 MPa and its elongation at failure was 2%.

5.2 Stress control testing

5.2.1 Testing Procedure

Tests were carried out on a PC driven Dartec 50 kN. capacity servo-hydraulic testing machine or on a PC driven Mayes electrically driven testing machine. Both units are shown in Figure 5.1. The particular machine used in any test is indicated in the results section.

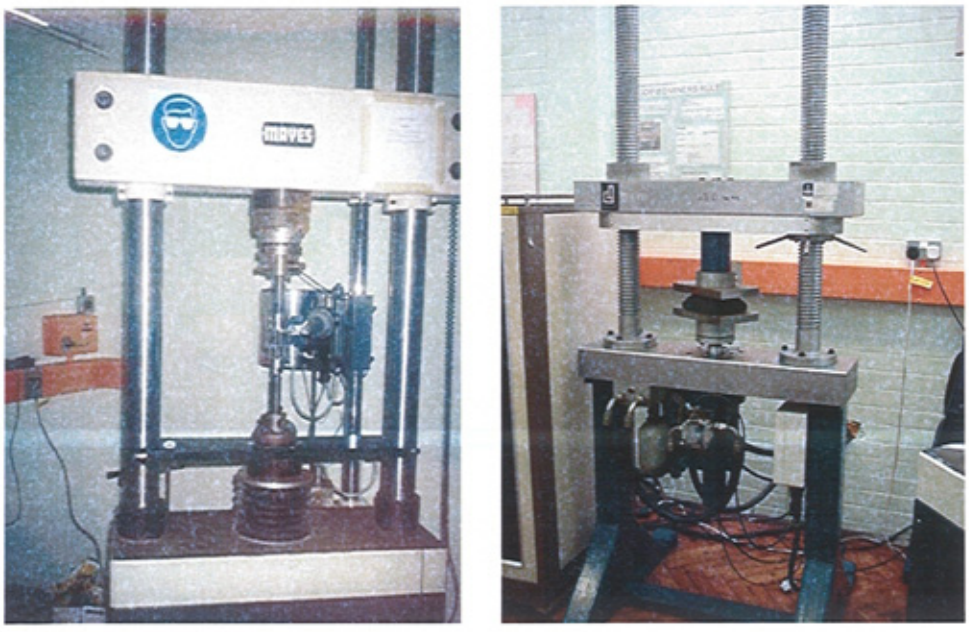

Figure 5.1 Electrically driven Mayes dynamic testing machine and Dartec servo-hydraulic dynamic machine

All tests were conducted under strain control using sinusoidal constant amplitude. Tests were conducted in air at frequency ranging from of 0.5 to 8.0 Hz, using an R ratio of 0.1 with load and displacement being recorded for each cycle. Both machines were controlled using a Dartec modular 9500 controller capable of both controlling and monitoring all necessary parameters. All information from the controller was stored on a standard PC using Dartec Easy software. Setting up the machine and all adjustments were carried out using the same PC. The 9500 controller and PC are shown in Figure 5.2.

Figure 5.2 A Dartec series M9000 controller that is used in conjunction with the Mayes dynamic testing machine.

In the tests carried out above ambient temperature a three-zone furnace was used. This unit was connected, as an integral part, to the Mayes testing machine. This furnace was controlled by the use of a K type thermocouple connected to a Eurotherm controller/programer TRI-24-ZV. During these tests a mineral insulated

K type thermocouple was attached to the fatigue specimen and an Orion data logger was used to record the temperature every 2 minutes. The furnace is shown in Figure 5.3 and 5.4 in both the open and closed position.

All static and dynamic bend tests were carried out in four point bending. The central span of the four-point bend cradle being 0.02m and the outer span 0.054m. This is shown in position on the Mayes dynamic testing machine in Figure 5.5.

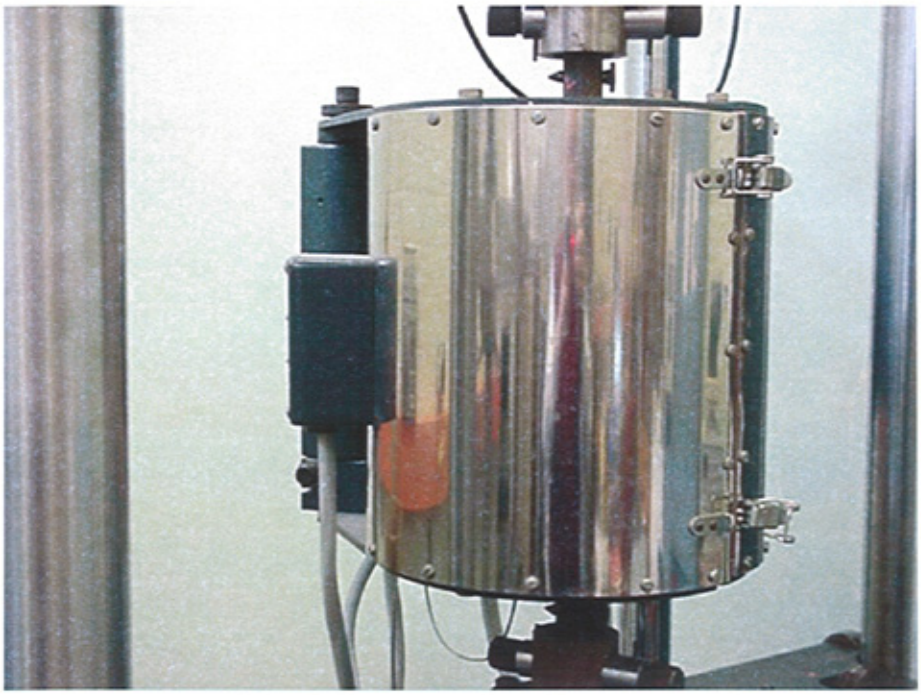

Figure 5.3 Three-zone furnace shown in its closed position.

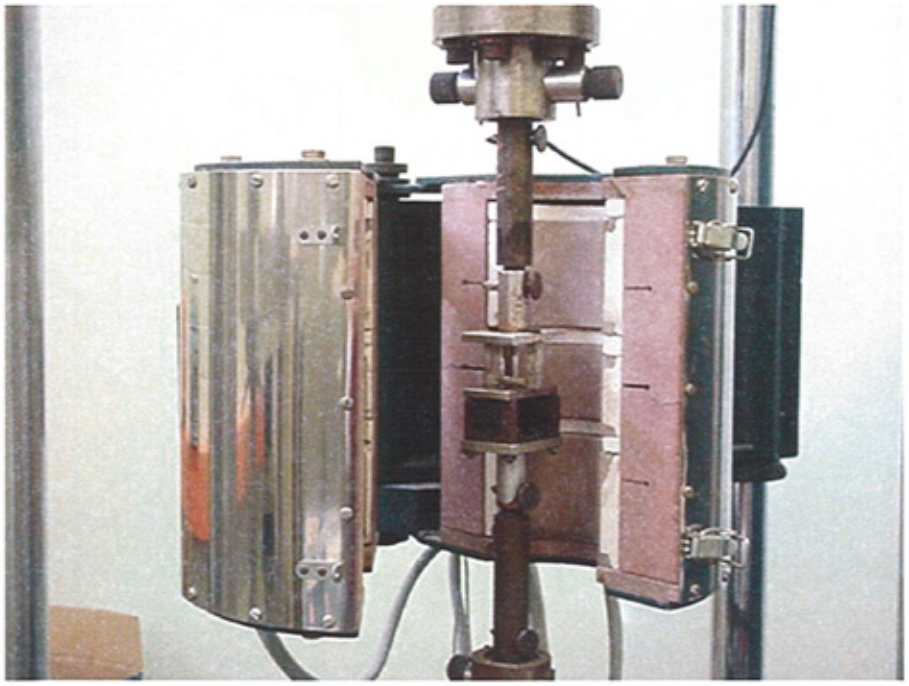

Figure 5.4 Three-zone furnace shown in its open position.

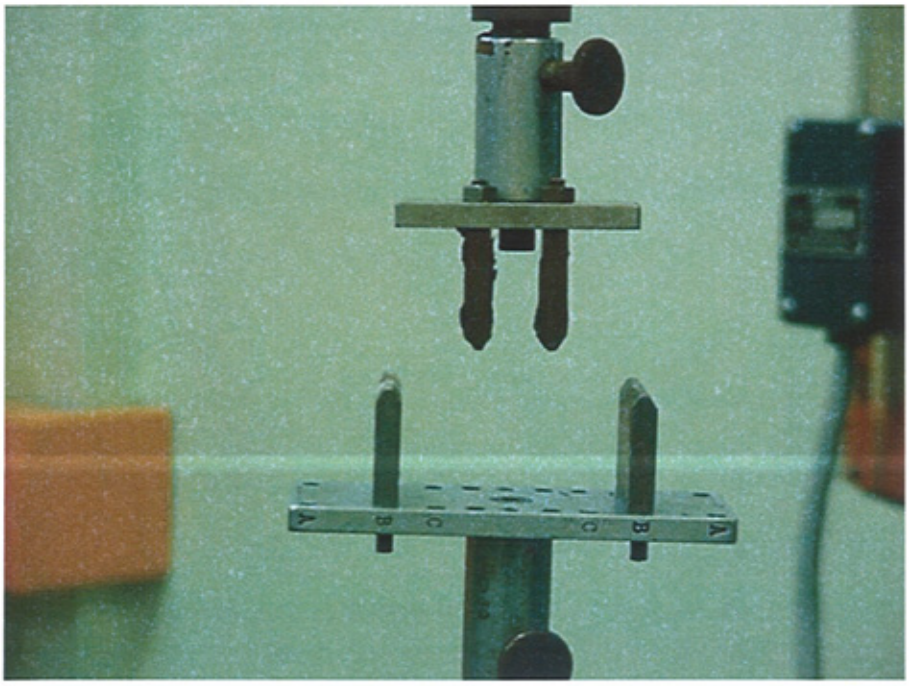

Figure 5.5 Four Point Bend Testing Cradle

5.2.2 Materials

A number of different metal matrix composites and matrix materials were used in this series of tests, details of each material are given below.

5.2.2.1 Aluminium Al 2618

The metal matrix composite in this section was an Al 2618 alloy and a metal matrix composite with identical base material with an addition of 20% volume silicon carbide particulates. The chemical composition of this alloy was Cu 2.5%, Fe 1.1 %, Mg 1.5 %, Ni 1.10 % the rest being aluminium. The base matrix material had a Young's modulus of 72GPa, a 0.2% proof stress of 428 MPa and a UTS of 459Mpa, while for the metal matrix composite the Young's modulus was 92GPa, the 0.2% proof stress was 484 MPa and it had a UTS of 510 MPa. The material was spray formed and formed as an extruded bar. After extrusion both the monolithic material and the metal matrix composite were solution treated at 530°C for 1 hour, then water quenched and cold stretched up to 2%. Afterwards, they were artificially aged at 190°C. for 10 to 20 hours to reach peak-aged condition (T6).

The fibres were the same as reported for the Al 7075 material and had an aspect ratio of 1.3 and a statistical type failure mode.

5.2.2.2 Aluminium Al 2014

The metal matrix composite was a copper based aluminium alloy designated Al 2014 with an addition of 15% volume $Al_2 O_3$ fibres. The reported chemical composition of both the monolithic material and the composite base material was Al 93.5%, Cu 3.9 –4.5%, Mg 0.2 – 0.8%, Mn 0.4 – 1.2%, Si 0.5 – 1.2%. It was experimentally determined that the composite had a yield strength of 359 MPa and a UTS of 468 MPa. The Young's modulus for the monolithic material is 72.4 GPa with a Poisson's ratio of 0.33. The yield stress of this alloy was 290MPa and the

UTS was 425MPa. The reported Young's Modulus of the $Al_2 O_3$ is 532 MPa and the Poisson's Ratio is 0.25. The failure stress of the fibre is again of a statistical nature, with the reported maximum strength being 7.0 GPa. In this metal matrix composite they had an average aspect ratio of 8.

The composite was solution treated for 2 hours at 500°C. It was then water quenched and naturally aged for 2 days and finally aged for 16 hours at 160°C. The comparison is with a monolithic Al 2614 alloy given identical heat treatment to that of the metal matrix composite.

5.2.2.3 Aluminium AE 109

The monolithic material used in these tests was a standard AE 109 being a high purity eutectic aluminium/ silicon-casting alloy. To achieve high rates of solidification and good structural refinement the alloys were manufactured using the squeeze casting method. The alloying elements used with the aluminium were 12% Si, 1.0% Cu, 1.0% Ni, 1.1% Mg, with no more than 0.5% Fe, 0.25% Mn and 0.2% Zn.

The metal matrix composite had a base material of AE109 and was manufactured in an identical manner to the monolithic material except with the addition of 15% Fibrefrax fibres.

Fibrefrax is a commercially available material being a mixture of $AL_2 O_3$ and SiO_2 and has a measured Young's Modulus of 103Gpa and a Poisson's Ratio of 0.25. The fibres range in diameter from 1 to 2.5 microns and in this metal matrix composite the aspect ratio of the fibres was 30.

5.3 Replica work

As the outer surface of a bend specimen under load is the area of highest stress this is also likely to be the area of crack initiation. As it would be difficult to constantly

observe the outer surface of a bend specimen for signs of crack initiation a process of surface replication has been developed.[82] In this method the machine was paused at various stages of the test and a softened acetate strip was applied to the surface of the specimen. Softening was achieved by applying a small amount of acetone to the acetate strip a few seconds before applying the strip to the specimen. A small pressure was applied while the strip remains in place for 15 to 20 seconds. Upon removal the strip was carefully stored to allow hardening of the acetate. All strips could then be microscopically observed at a later date for signs of crack initiation or crack growth.

Figure 5.5 shows the set up for later observation of the replica slides

Figure 5.5 Set up for observation of the replica slides

5.4 Finite Element

5.4.1 2-D Finite Element Model

As the 2-D finite element analysis was carried out using a purely elastic model the matrix material could represent any aluminium alloys with a modulus of 72 MPa while the fibre material was SiC with a Young's modulus of 468 GPa and the Poisson's ratio was 0.25. Because of the simplicity of both the mesh and the model it was possible to carry out the analysis over a range of aspect ratios and volume fractions of fibres. Figure 5.6 shows the mesh used for the 12% volume fraction 2-D finite element analysis. Elements representing matrix material are marked '5' while fibre elements are labelled '8'. A similar mesh was used for all tests with only the ratio of matrix to fibre elements being varied.

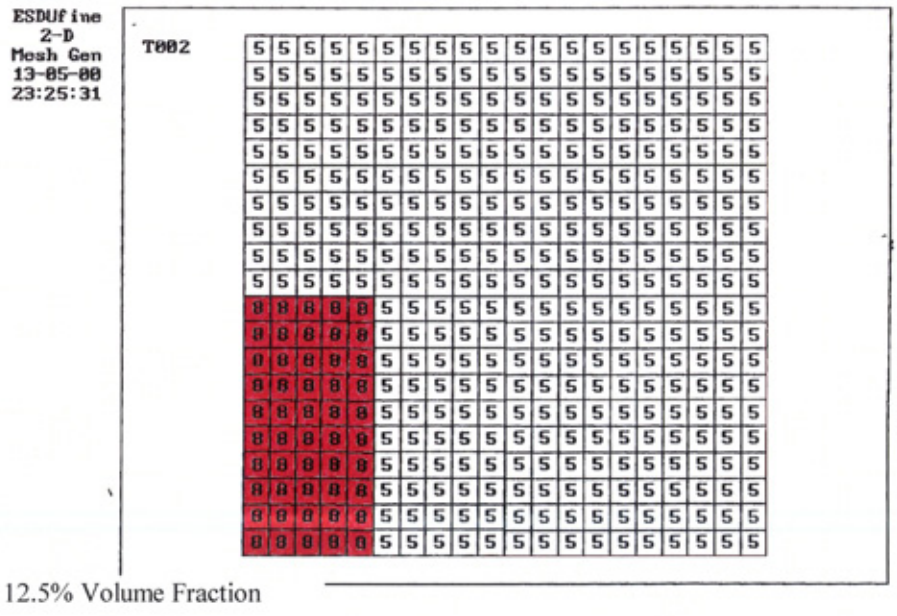

Figure 5.6 Mesh used in 2-dimensional finite element analysis.

5.4.2 3-D Finite Element model

The testing of the material has been reported in section 5.1.1 and 5.1.2. and comprises an aluminium alloy, Al 7075, and a metal matrix composite with an identical matrix material plus 12% SiC by volume, of particulate fibres. In all studies, the fibres are approximated to an elastic body with a Young's modulus of 468 GPa and a Poisson's ratio of 0.25. The Al 7075 had a Young's modulus of 72 GPa, a Poisson's ratio of 0.33, and a yield stress of 416 MPa and an ultimate stress of 565 MPa with an elongation of 14%.

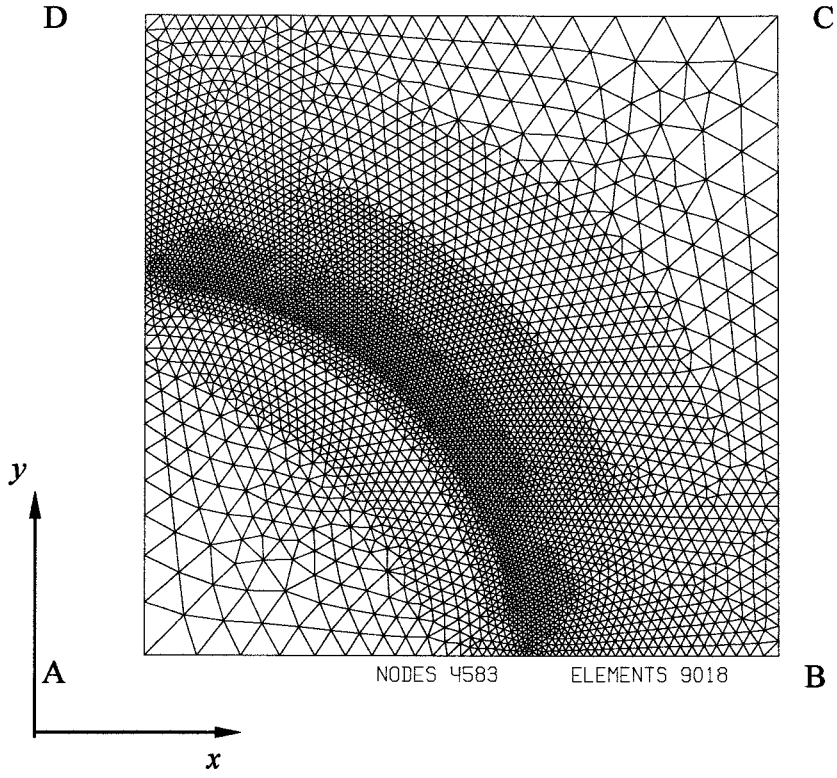

Figure 5.7. 3-Dimesional finite element mesh for MMC with spherical fibre.

When considering the behaviour of the MMC under monotonic loading a finite element model with spherical fibres containing 4583 nodal points and 9018 axi-symmetric simplex finite elements was used as shown in Figure 5.7.

When cyclic deformation was analysed, the meshes needed to be refined to decrease approximation errors and to increase the stability of FE models during the various steps of mathematical simulation. While analysing an MMC with spherical fibres the number of nodes in the FE model during cyclic plasticity analysis was above 7000.

Chapter 6

6.0 Results

6.1 Aluminium Al 7075 and its Equivalent Metal Matrix Composite Al 7075/ 12% SiCp

6.1.1 Strain Controlled Testing.

A spray formed aluminium zinc alloy was tested under four point bending. In this series of tests, upper and lower strain levels were kept constant while the stress levels and number of cycles were recorded. The results are shown below in Figure 6.1

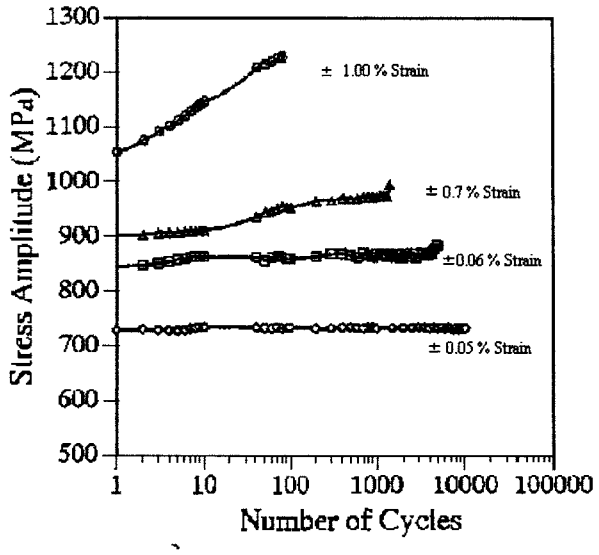

Figure 6.1 Strain controlled fatigue test on monolithic Al 7075

An equivalent metal matrix composite comprising a matrix of Al 7075 with 12% SiCp particulates added during the spay forming processes, was tested in an identical manner and these results are shown in Figure 6.2.

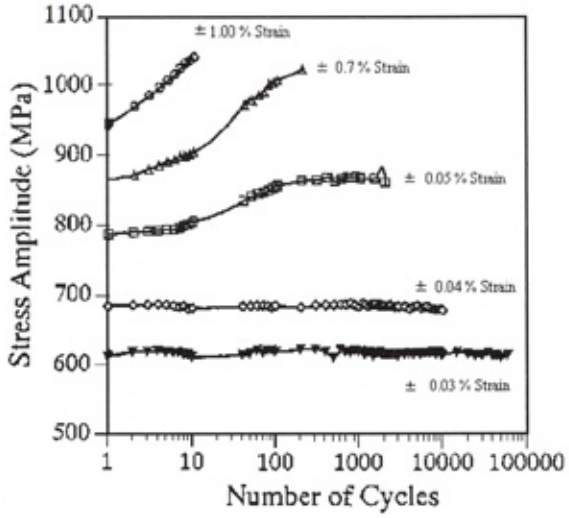

Figure 6.2 Strain controlled fatigue tests on Al 7075/ 12 SiCp

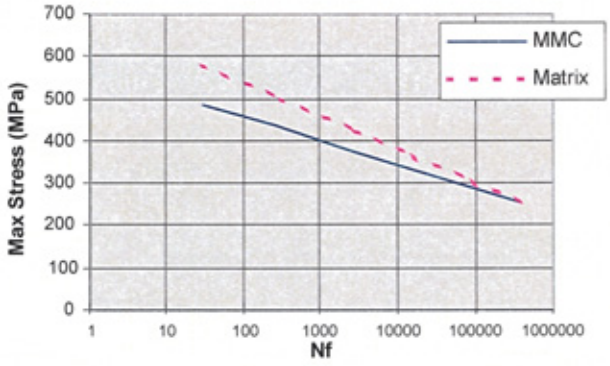

Figure 6.3 Strain controlled experimental S/n curve for monolithic Al 7075 and MMC Al 7075 + 12% SiCp.

The results from Figure 6.1 and Figure 6.2 are used to construct Figure 6.3, which is an S/n curve for both the matrix material and the equivalent metal matrix composite. The maximum stresses shown in these curves are the maximum stresses encountered in each individual test.

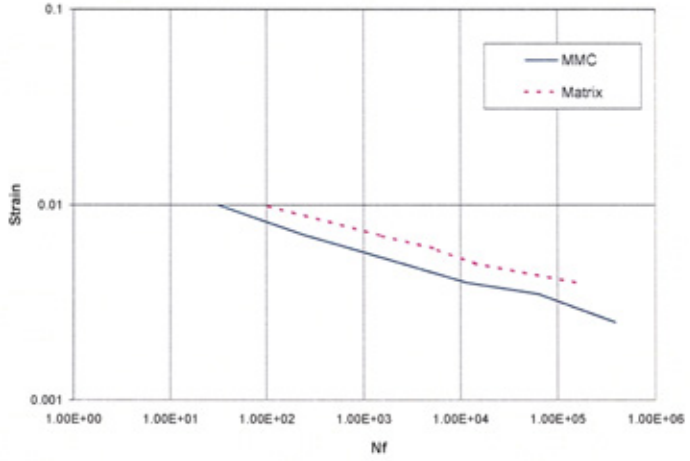

Figure 6.4 Strain controlled experimental results of constant strain against Cycles to Failure for monolithic Al 7075 and MMC Al 7075 + 12% SiCp

Using the results from Figure 6.1 and Figure 6.2 a Strain against Fatigue Life curve was plotted for both the matrix material and the metal matrix composite. This is shown in Figure 6.4 with the strain being the maximum strain encountered in each individual test.

As both the Young's Modulus and the yield stress can be predicted by the Theory of Cells for any metal matrix composite, a comparison is made between the prediction for this material and those obtained from experimental results. This comparison can be seen in Table 6.1.

	Young's Modulus	*Poisson's Ratio*	*Yield Stress*
Experimental	84.1 Gap	Not Available	404 MPa
TOC	83.3 GPa	0.324	391 MPa

Table 6.1 Experimental and Theoretical values of Modulus and Poisson's Ratio for metal matrix composite Al 7075 + 12% SiCp

The comparison between experimental results for the composite Al 7075 + 12% SiCp and the predictions for fatigue life given by the Theory of Cells is given in Figure 6.5. This figure shows life against Maximum Stress while Figure 6.6 is a similar prediction of Maximum Strain for the same material and the same experimental results.

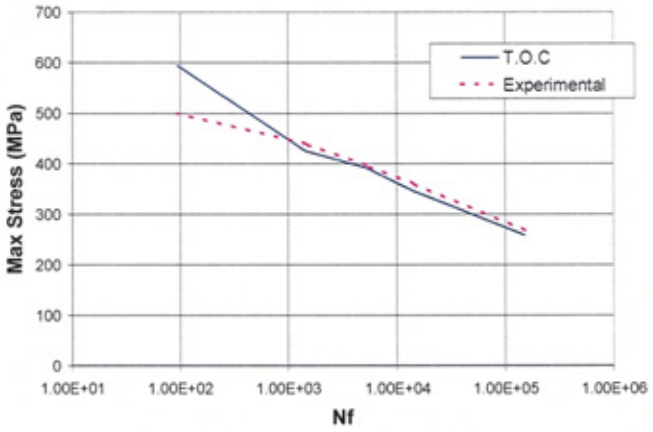

Figure 6.5 S/n Curve of experimental results and TOC predicted life of metal matrix composite Al7075 + 12% SiCp

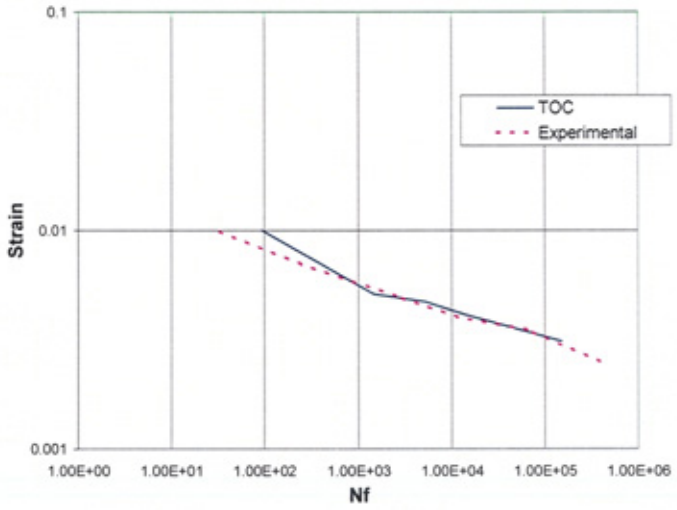

Figure 6.6 Constant Strain against Cycles to Failure: experimental results and TOC predicted life of metal matrix composite Al7075 + 12% SiCp

6.1.2 Two Dimensional Finite Element Prediction for Strain Controlled Testing on an Aluminium Metal Matrix Composite with SiC Inclusions.

A 2 dimensional model was generated for a metal matrix composite having a perfectly elastic aluminium matrix whose Young's Modulus was 72 GPa and SiC inclusions whose volume fraction of the composite were varied from 10% to 32.5%. The aspect ratio for each of these varying fractions was, to a large degree, dictated by the finite element mesh and is shown in Table 6.2

Aspect Ratio	2.5	2	1.66	1.43	1.25	1.0	1.1	1.2	1.3
Volume Fraction	0.1	0.125	0.15	0.175	0.20	0.25	0.275	0.30	0.325

Table 6.2 Aspect ratio used in the 2-dimensional finite element analysis of the individual volume fractions

Because of the simplicity of the 2-D model it was possible to predict both the Young's modulus and the Poisson's ratio for a series of metal matrix composites with varying volume fractions of fibres. These results are shown in Figure 6.7 and Figure 6.8.

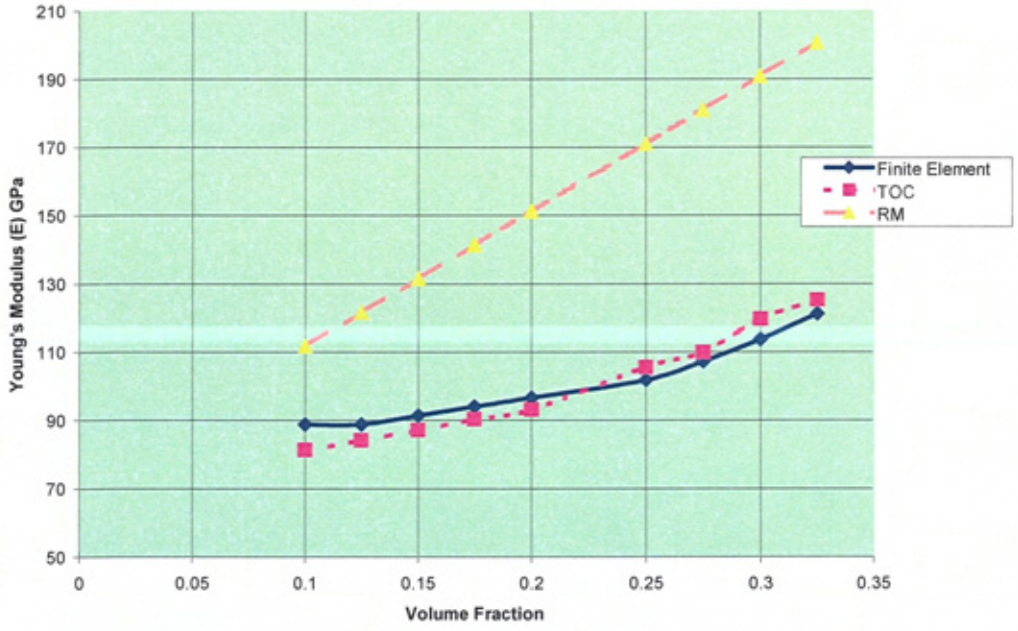

Figure 6.7 Prediction of Young's Modulus using different methods of analysis for a series of metal matrix composites

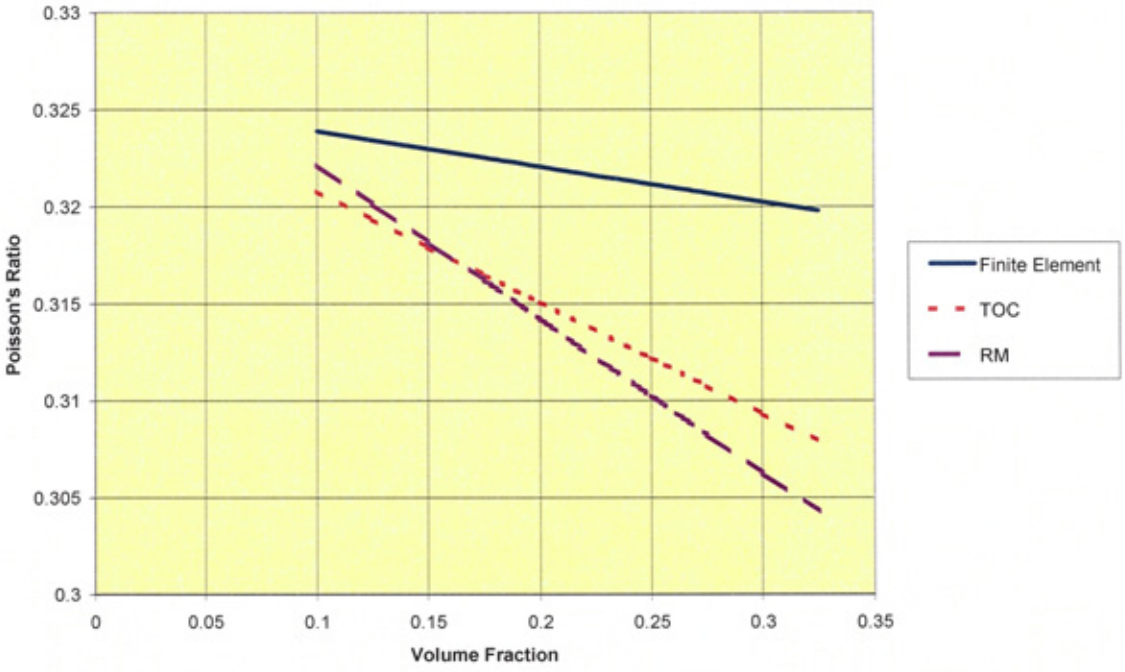

Figure 6.8 Prediction of Poisson's ratio using different methods of analysis for a series of metal matrix composites.

The two graphs not only show the change of Young's Modulus and Poisson's ratio over a range of volume fractions as predicted by the 2-dimension finite analysis but also for a comparison similar predictions using Theory of Cells and Rule of Mixtures. The results for the Poisson's ratio have been smoothed and drawn as a straight line for ease of reference.

As a comparison with events happening in the Al 7075/ 12% SiCp metal matrix composite, a 2-D finite element analysis was carried out around a ¼ fibre and its surrounding matrix. The results are show in Figure 6.9.

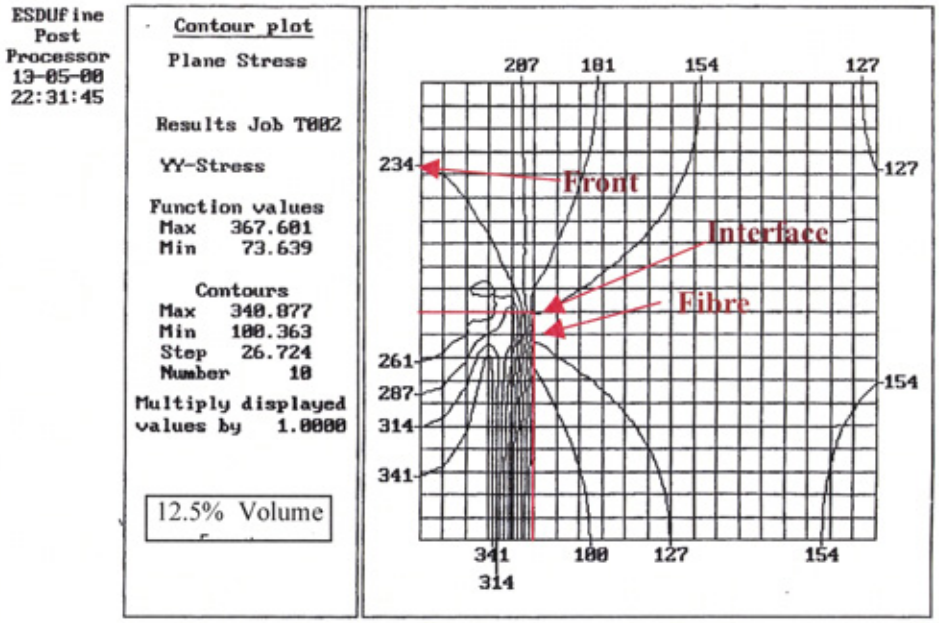

Figure 6.9 Stress Contour around ¼ fibre using 2-D finite element simulation

The overall strain in this simulation was 1%, but due to mesh limitation the volume fraction was 12.5 % and the aspect ratio used was 2. This compares with 12% volume fraction and 1.4 aspect ratio for the results show in Figure 6.10 and 6.11.

6.1.3 Three Dimensional Finite Element Prediction for Strain Controlled Testing on Aluminium Al 7075 and its Equivalent Metal Matrix Composite Al 7075/ 12% SiCp.

A three-dimensional theoretical finite element model was generated for the composite Al 7075/ 12% SiCp and the stress gradient, produced around a quarter fibre after five half cycles, is shown in Figure 6.10. The maximum areas of stress are labelled 'Interface', being one particular interfacial area between matrix and fibre, and 'Front', being located ahead of the fibre in the direction of the applied load. The elongation amplitude used in this case was 1% strain.

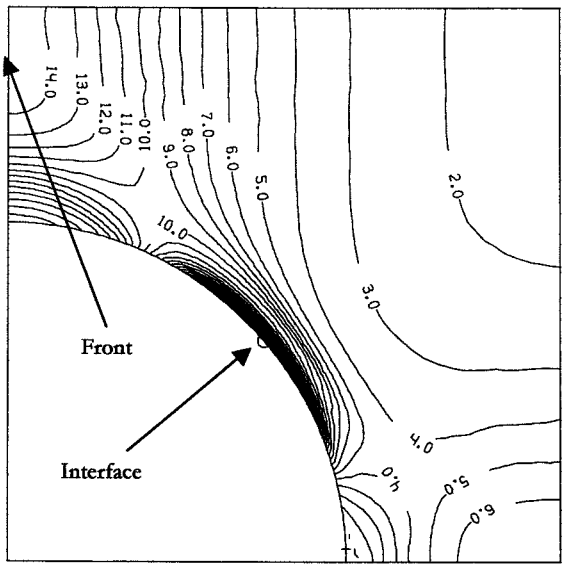

Figure 6.10. Distribution of the accumulated plastic strain in the composite after 5 half-cycles with elongation amplitude of 1%. I denotes the concentration zone of accumulated plastic strain on the interface between fibre and matrix. F denotes the concentration zone in the direction of load action

The Theory of Cells does not produce stress or strain contours but predicts average stress over pre-defined areas called sub-cells. For comparison, these average stresses are given in Figure 6.11 and this covers the same region of the metal matrix composite as shown in the finite element plot of Figure 6.10.

Matrix Sub Cell2,1,1 223 MPa	*Matrix* Sub Cell 2,2,1 187 MPa
Fibre Sub Cell 1,1,1, 269 MPa	*Matrix* Sub Cell1,2,1 213 MPa

Figure 6.11. Distribution of localised stress within and around the fibre as predicted by the Theory of Cells. An overall strain of 0.24% was used in the TOC analysis.

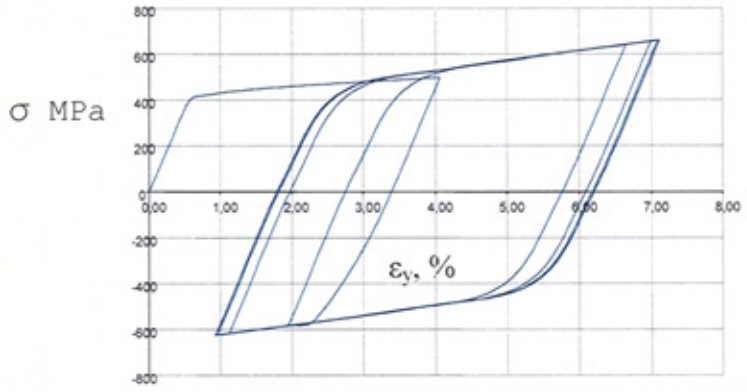

Figure 6.12 Numerically (FE) simulated cyclic stress-strain curves interface zone

Figure 6.12 and Figure 6.13 presents the stress/ plastic strain diagram for both the 'interface' and 'front' regions for the first five cycles of the finite element simulation under a constant strain of 0.7%.

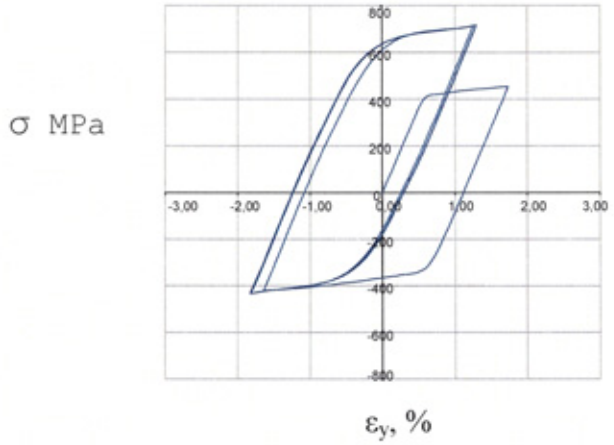

Figure 6.13 Numerically (FE) simulated cyclic stress-strain curves frontal zone

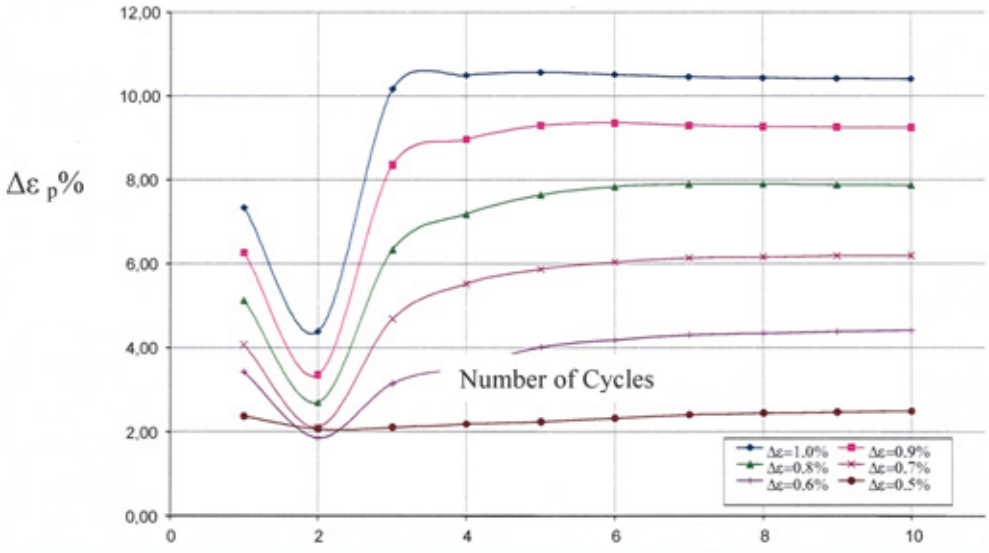

Figure 6.14 Relationship between the width of cyclic deformation loop and the number of half-cycles for the interface zone at different values of the specimen's elongation amplitude:

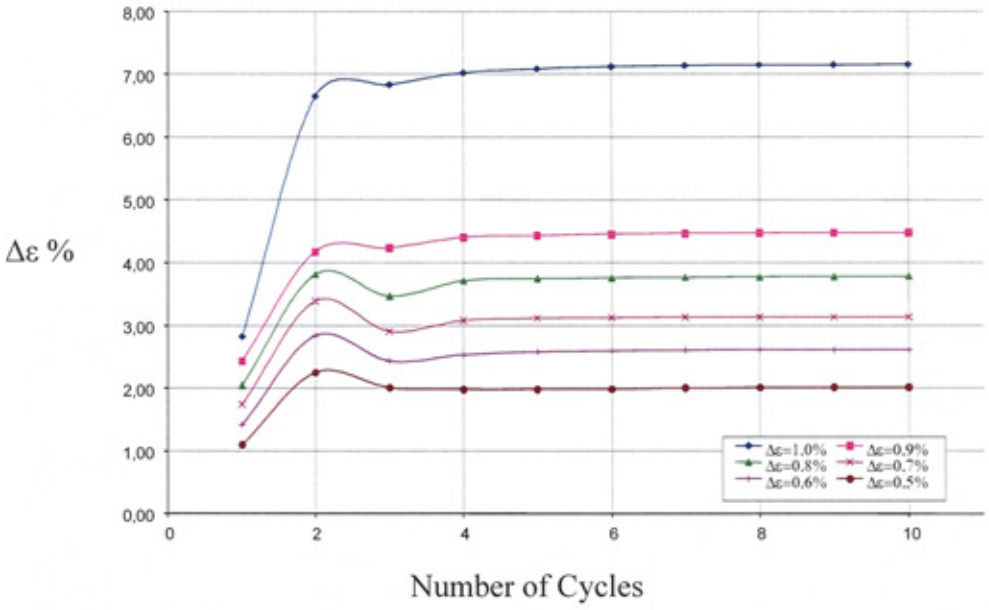

Figure 6.15 Relationship between the width of cyclic deformation loop and the number of half-cycles for the frontal zone at different values of the specimen's elongation amplitude.

A clearer view of what is happening in both the 'interface' and 'front' zones during load cycling is shown in Figure 6.14 and Figure 6.15. The graphs include results over the full range of strain amplitudes and show the local strain differences between each cycle.

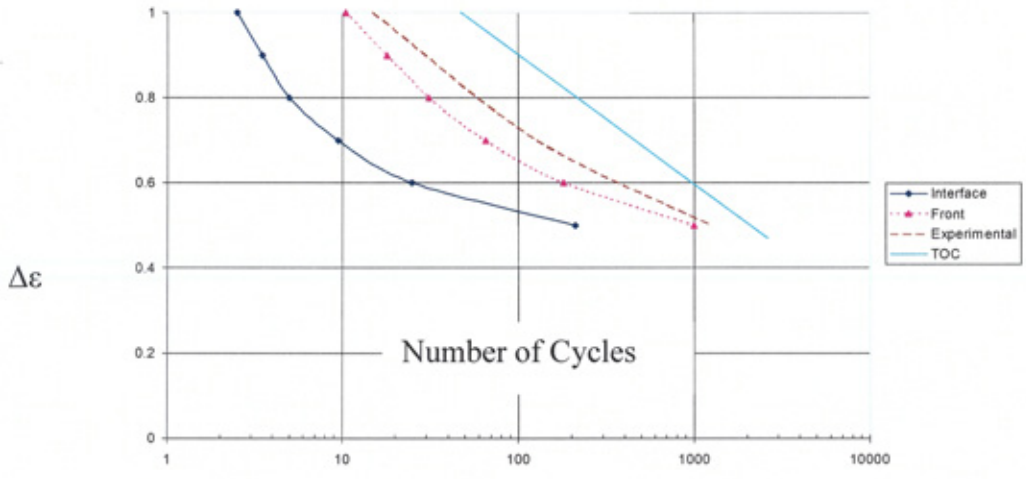

Figure 6.16 Results of the local strain against life for 3-D finite element simulation compared to Theory of Cells analysis and experimental results.

Figure 6.16 gives a summary of strain against cycles to failure results for experimental, finite element and Theory of Cells. Results are given for low cycle fatigue only.

6.2 Stress Controlled Testing on Aluminium AE 109 and its Equivalent Metal Matrix Composite AE 109 with 15% SiC Fibrefrax

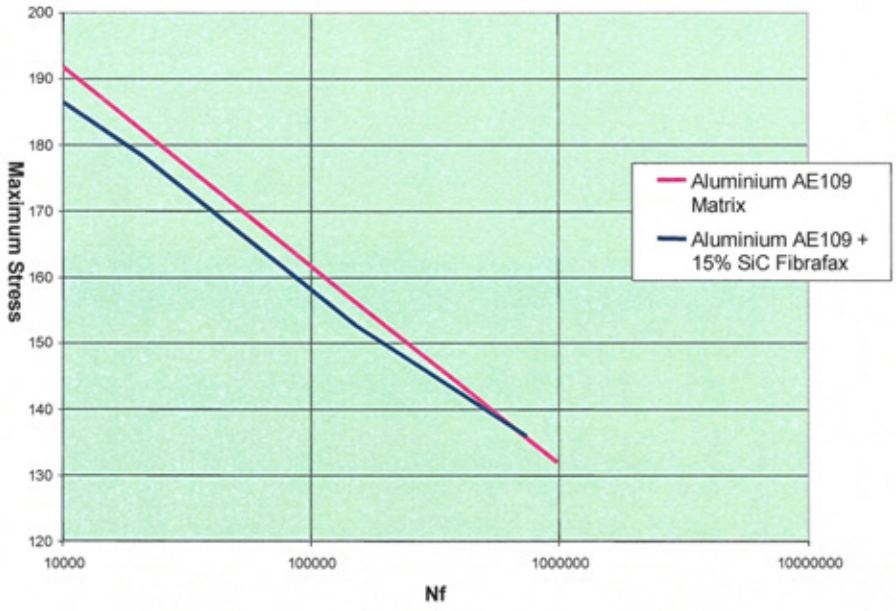

Figure 6.17 Experimental ambient temperature S/n curve of AE 109 aluminium alloy

The material reported in this section was a commercially available metal matrix composite used in the automotive diesel engine industry. Figure 6.17 shows a comparison between the fatigue life of Aluminium AE109 and its equivalent metal matrix composite. Both sets of results were obtained at ambient temperature and under identical test methods.

The Theory of Cells was then used to give a fatigue life prediction and the results of this are given in Figure 6.18. For comparison the experimentally obtained fatigue life of the composite is shown on the graph.

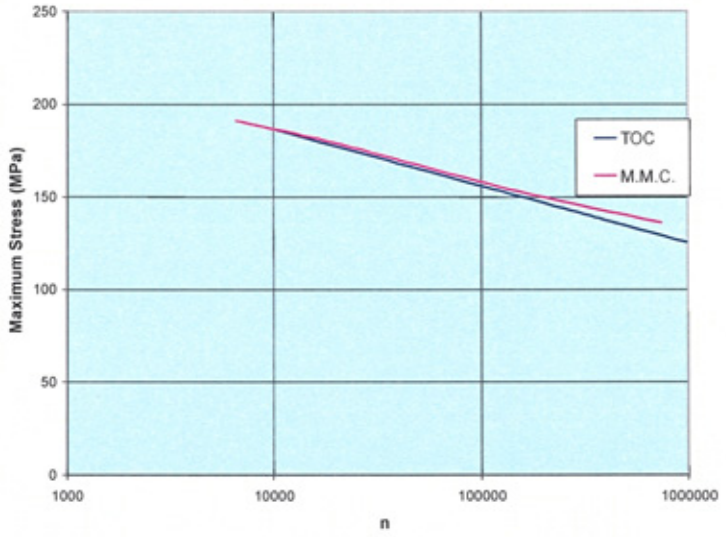

Figure 6.18 Experimental data for ambient temperature S/n curve of metal matrix composite AE 109 aluminium alloy with 15% Sic Fibrefrax fibres compared To TOC fatigue life predictions for the same material.

Figure 6.19 is identical to Figure 6.18, except that for comparison purposes a fatigue life prediction for a theoretical AE 109 metal matrix composite with fibres whose Young's Modulus is 300 GPa. instead of the actual value 105 GPa. All other properties of both the matrix material and the fibres were assumed to be identical with the actual original metal matrix composite.

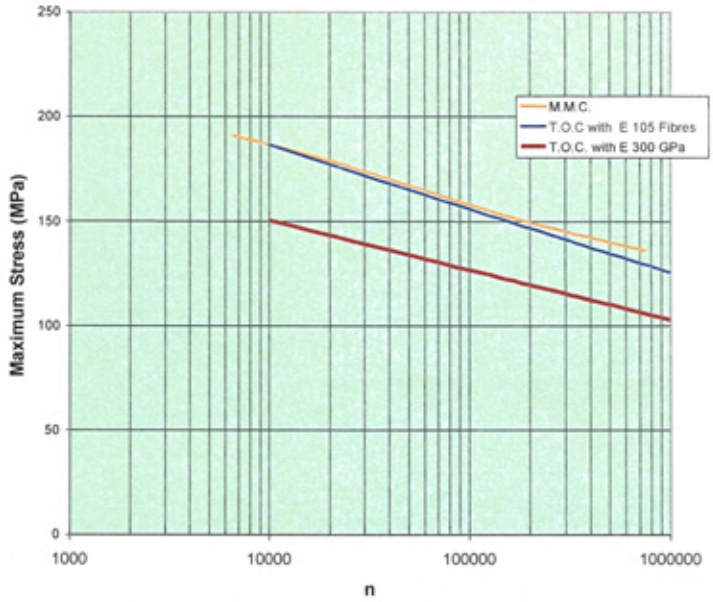

Figure 6.19 Two predictions of fatigue life of a metal matrix composite using Theory of Cells compared to experimental data. The only variation in information used in the predictions is in fibre Young's Modulus value.

6.3 Stress Controlled Testing on Aluminium Al 2618 and its Equivalent Metal Matrix Composite with 20% SiC Fibres

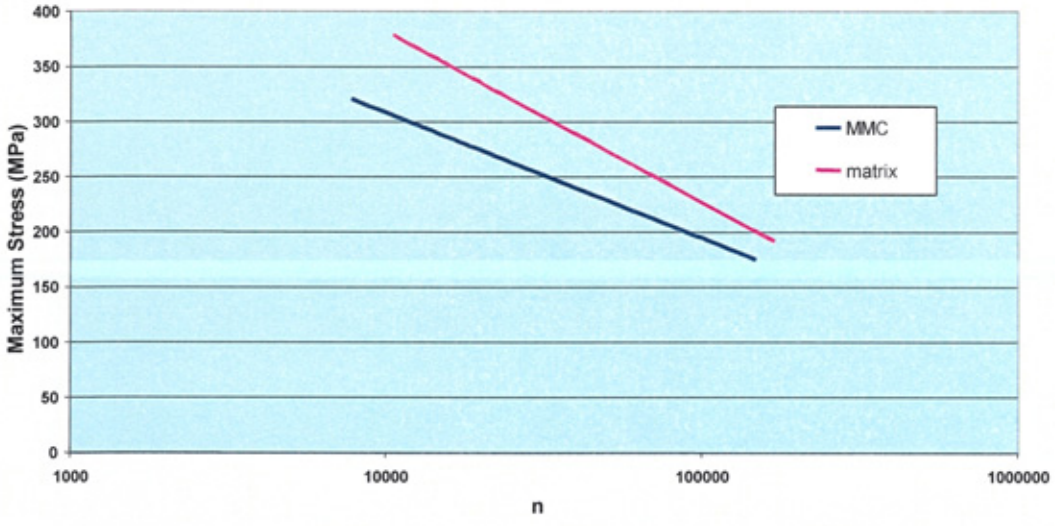

Figure 6.20 Experimental results of an Al 2618 aluminium and a metal matrix composite with a matrix of Al 2618 containing 20% SiC fibres. Test carried out under tension-tension loading at ambient temperature.

The Stress / Cycles to failure graph shown in Figure 6.20 was produced from experimental results determined for Al 2618 and a metal matrix composite comprising the same grade of aluminium with an addition of 20% SiC fibres.

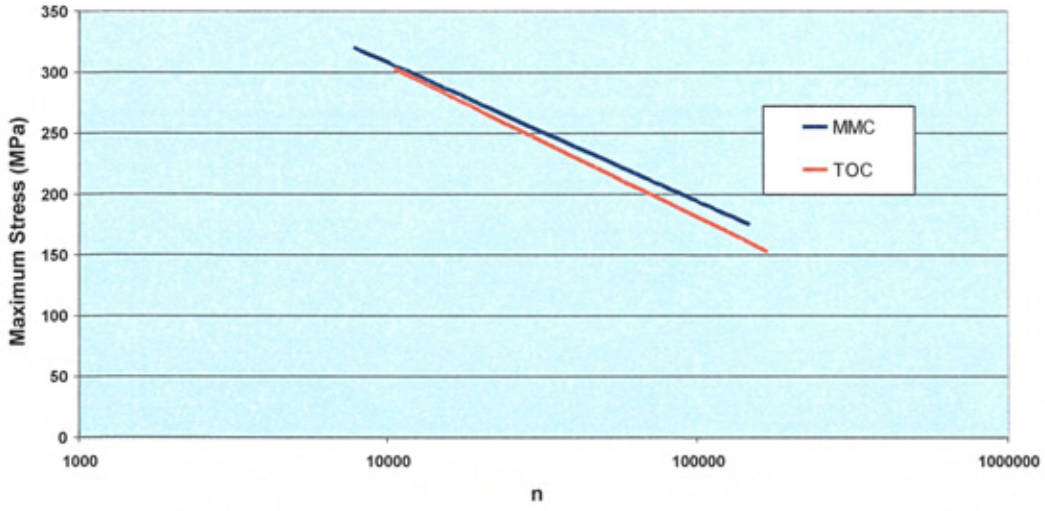

Figure 6.21 The S/n Curve for the Al 2618 metal matrix composite containing 20% SiC fibres shown in Figure 6.10 compared to the theoretical predictions of fatigue life using the Theory of Cells.

The experimental results for the metal matrix composite was then compared to a prediction from the Theory of Cells and these results are shown in Figure 6.21

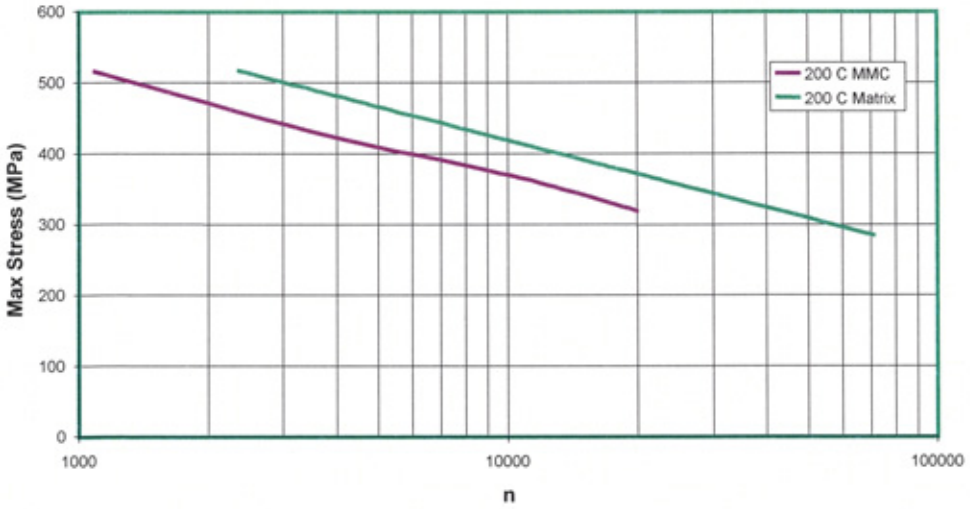

Figure 6.22 Experimental results of an Al 2618 aluminium and a metal matrix composite with a matrix of Al 2618 containing 20% SiC fibres fatigue testing carried in 4-point bending at 200°C.

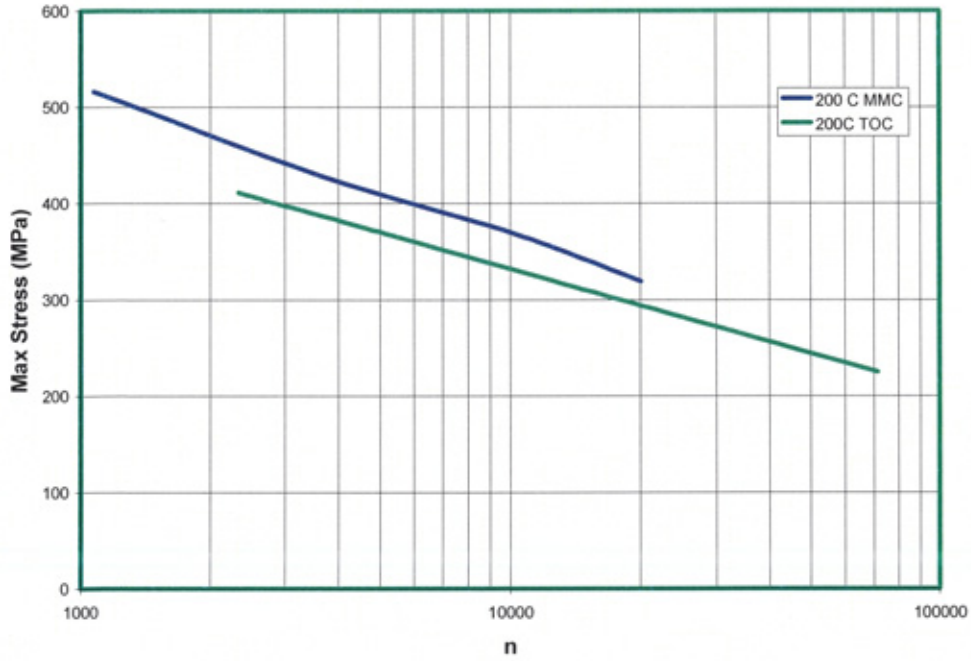

Figure 6.23 The S/n Curve for the Al 2618 metal matrix composite containing 20% SiC fibres compared to the theoretical predictions of fatigue life using the Theory of Cells.

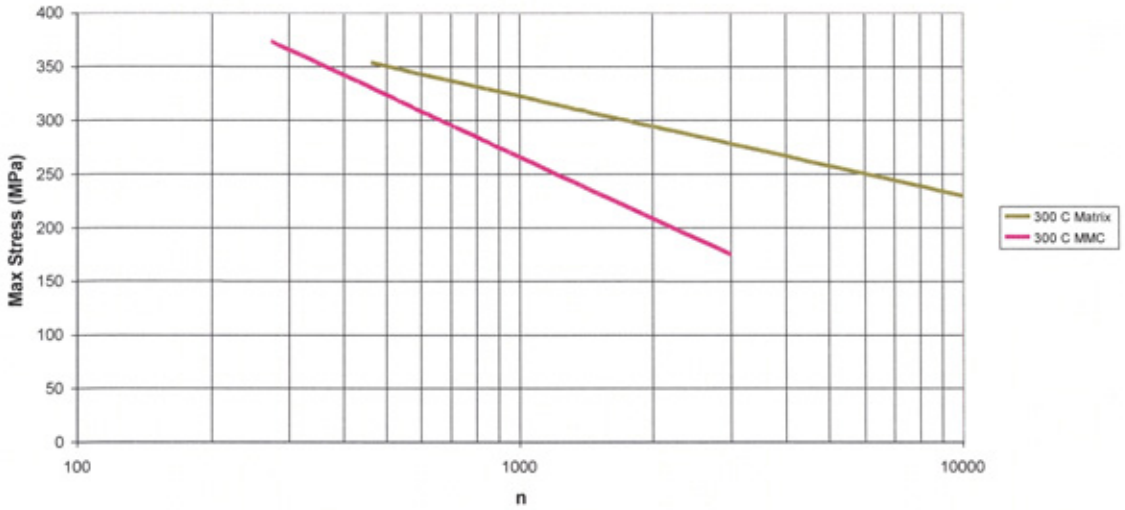

Figure 6.24 Experimental Results of an Al 2618 aluminium and a metal matrix composite with a matrix of Al 2618 containing 20% SiC fibres. Fatigue testing carried in 4-point bending at 300°C.

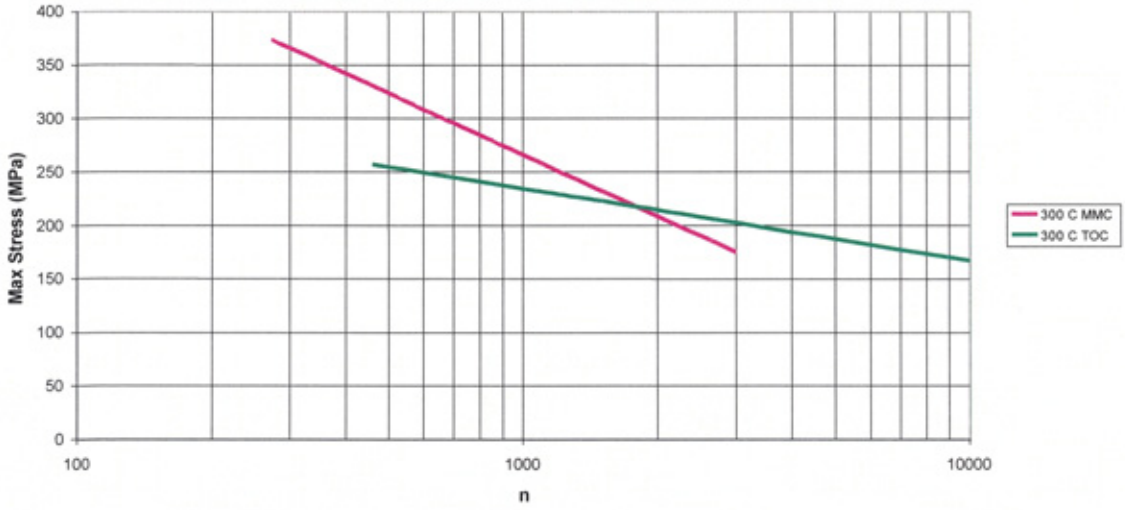

Figure 6.25 The S/n curve for the Al 2618 metal matrix composite containing 20% SiC fibres shown in Figure 6.15 compared to the theoretical predictions of fatigue life using the Theory of Cells.

For this material, tests were carried out on both the matrix material and its equivalent metal matrix composite at 200˚C and 300˚C. The results for this are shown in Figure 6.22 and Figure 6.24. The comparison between the experimental

results for the metal matrix composite and the Theory of Cells predictions is given in Figure 6.23 and Figure 6.25.

A series of micrographs was taken of the fracture surface for both the monolithic material and its equivalent metal matrix composite. These images were taken of material tested under ambient temperatures and in the low cycle regime, with the number of cycles to failure being 30,000 cycles or less.

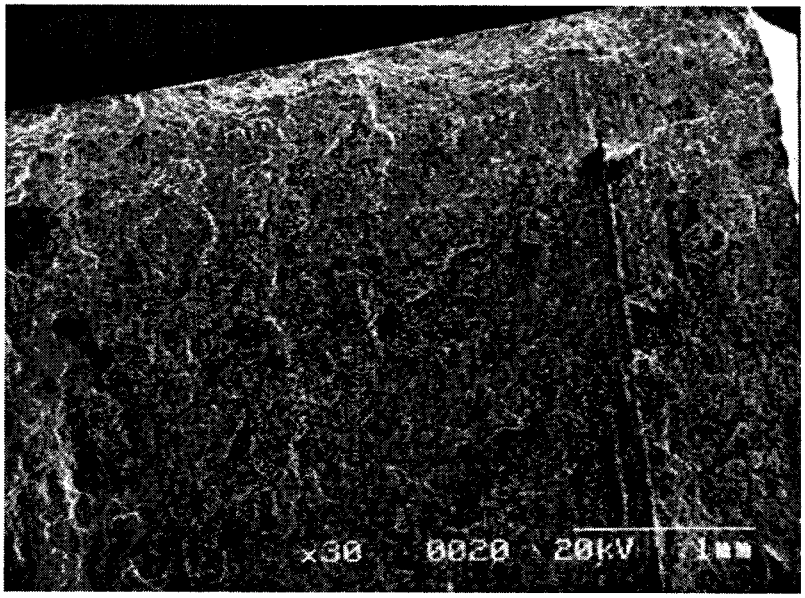

Figure 6.26 Al 2618 + (20%)SiC x 30 Magnification showing fracture surface of metal matrix composite.

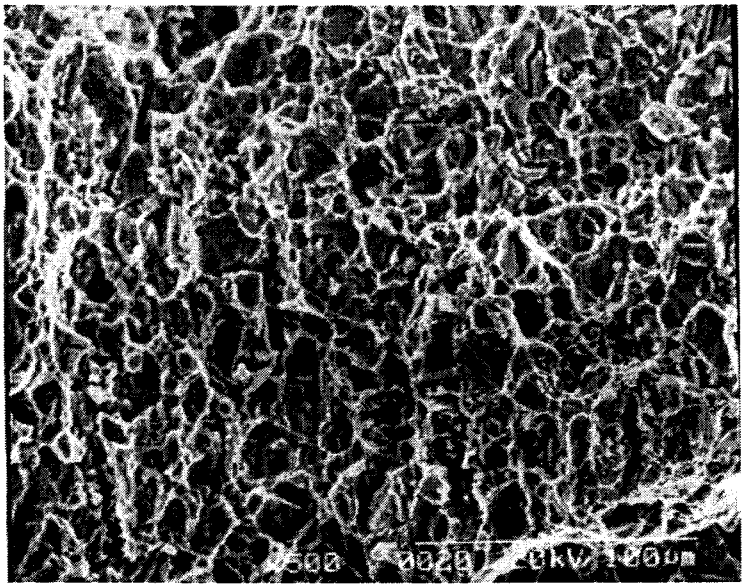

Figure 6.27 Al 2618 + (20%) SiC. The same fracture surface at 500 magnification.

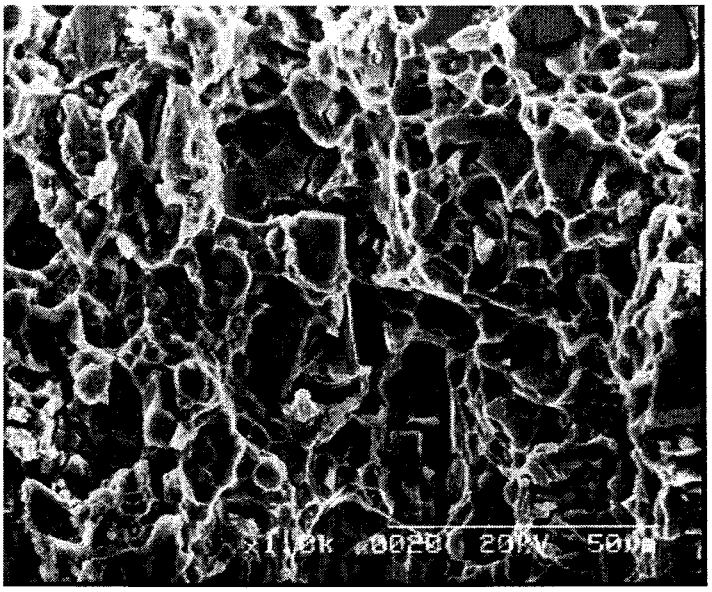

Figure 6.28 Al 2618 + (20%) Sic. The same fracture surface at 1000 magnification.

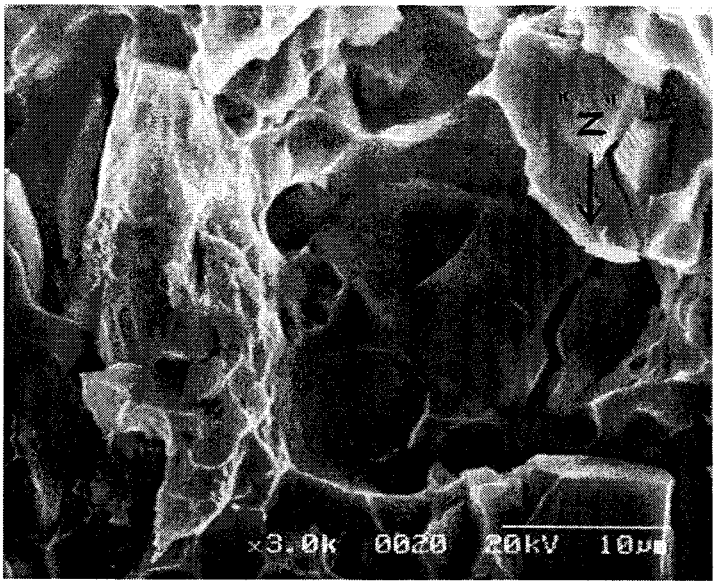

Figure 6.29 Al 2618 + (20%)SiC. The same fracture surface at 3000 magnification.
"Z" indicates a fractured fibre.

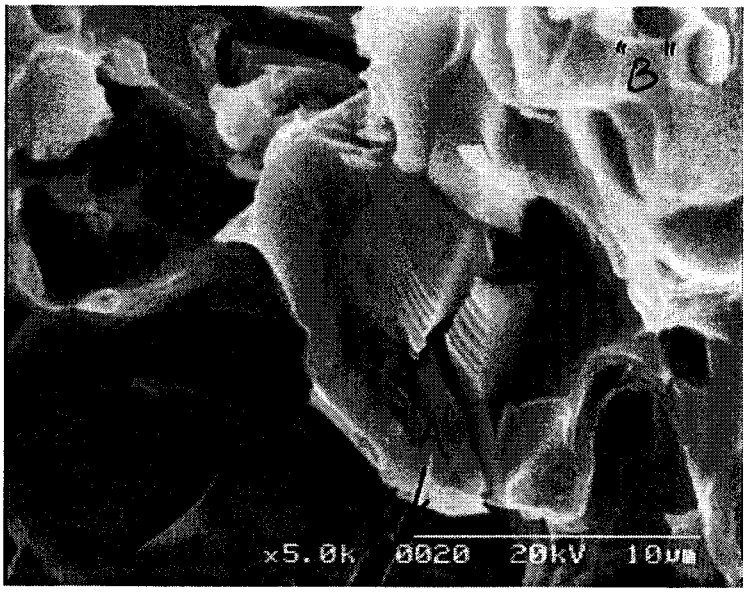

Figure 6.30 Al 2618 + 20%SiC. The same fracture surface at 5000 magnification.
"A" indicates a fractured fibre and "B" indicates stepped features typical of fatigue fracture.

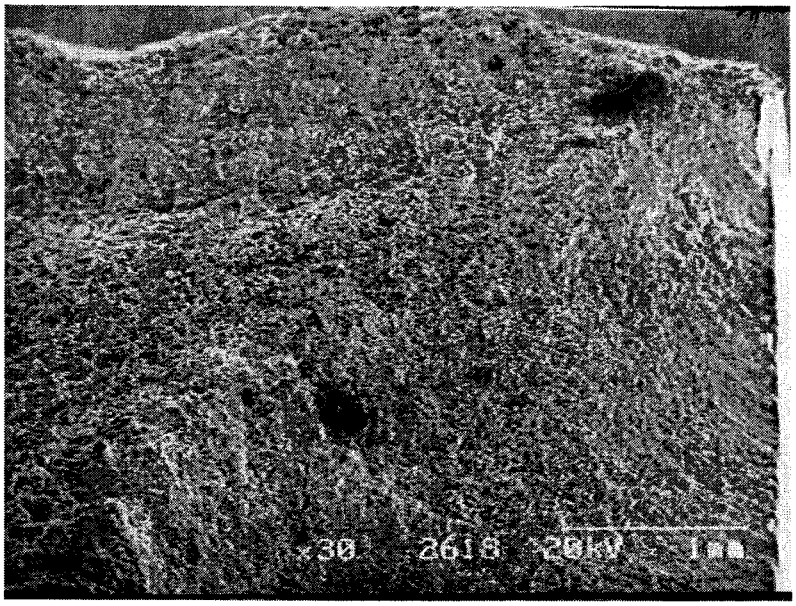

Figure 6.31 Fracture surface of fatigue specimen with the magnification at 30 times. The material is monolithic Al 2618

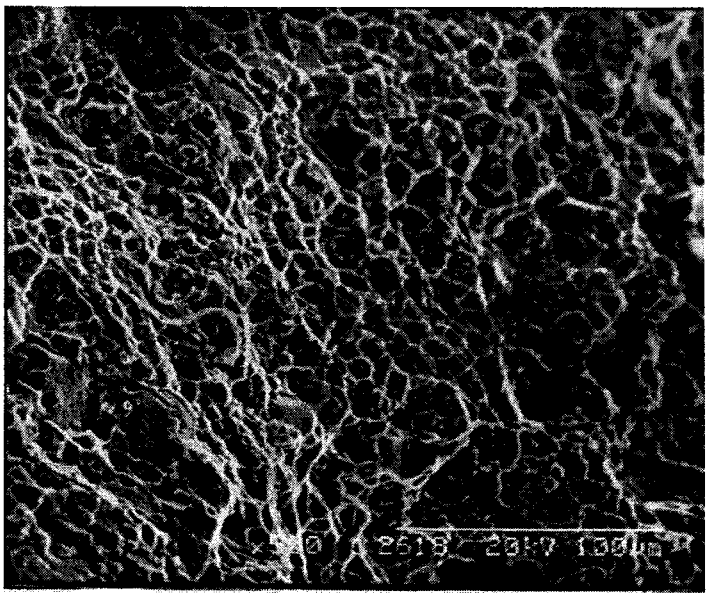

Figure 6.32. The same surface of the same material at a magnification of 500.

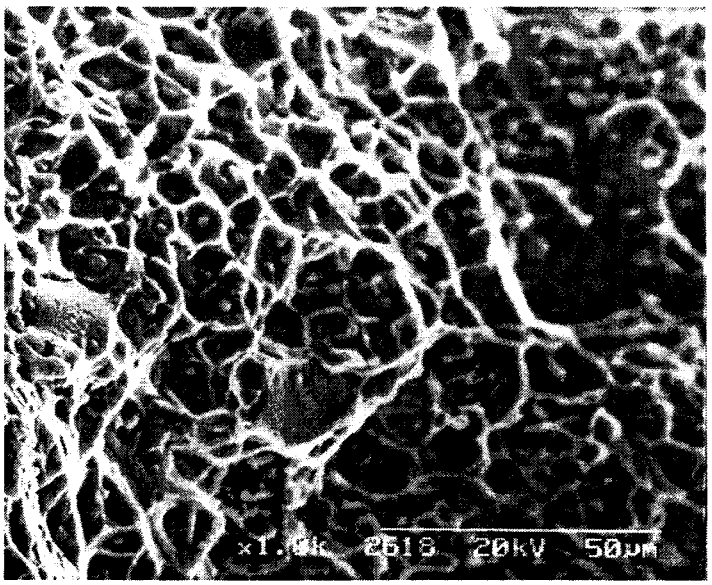

Figure 6.33 Al 2618 fracture surface at a magnification of 1000

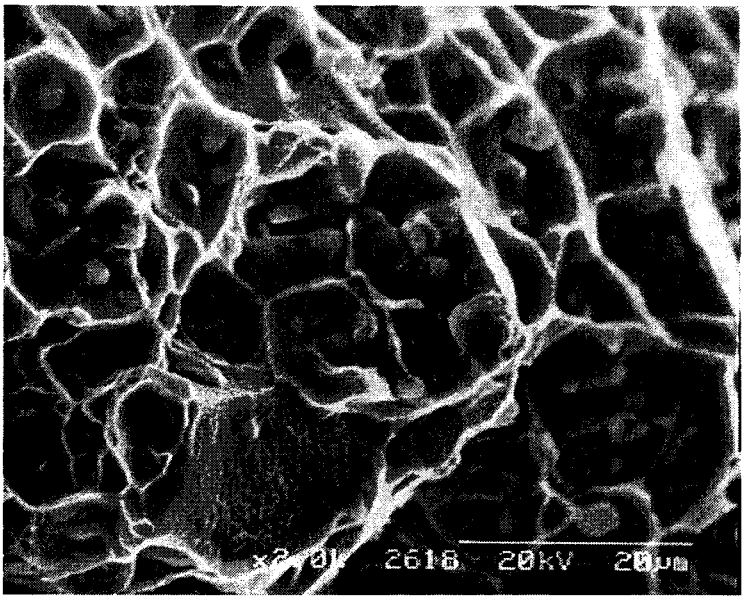

Figure 6.34 Al 2618 fracture surface at 3000 magnification.

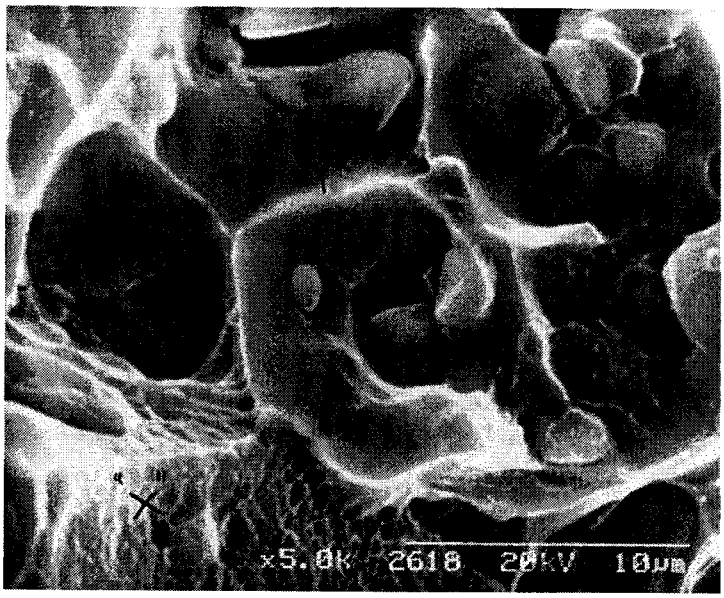

Figure 6.35 Fracture surface of Al 2618 at 5000 magnification. "Y" indicates a circular feature at the centre of which is a ferrite particle.

Some verification of the material has been made using an Energy Dispersion Spectrograph and the results are given in Figure 6.34 to 6.36.

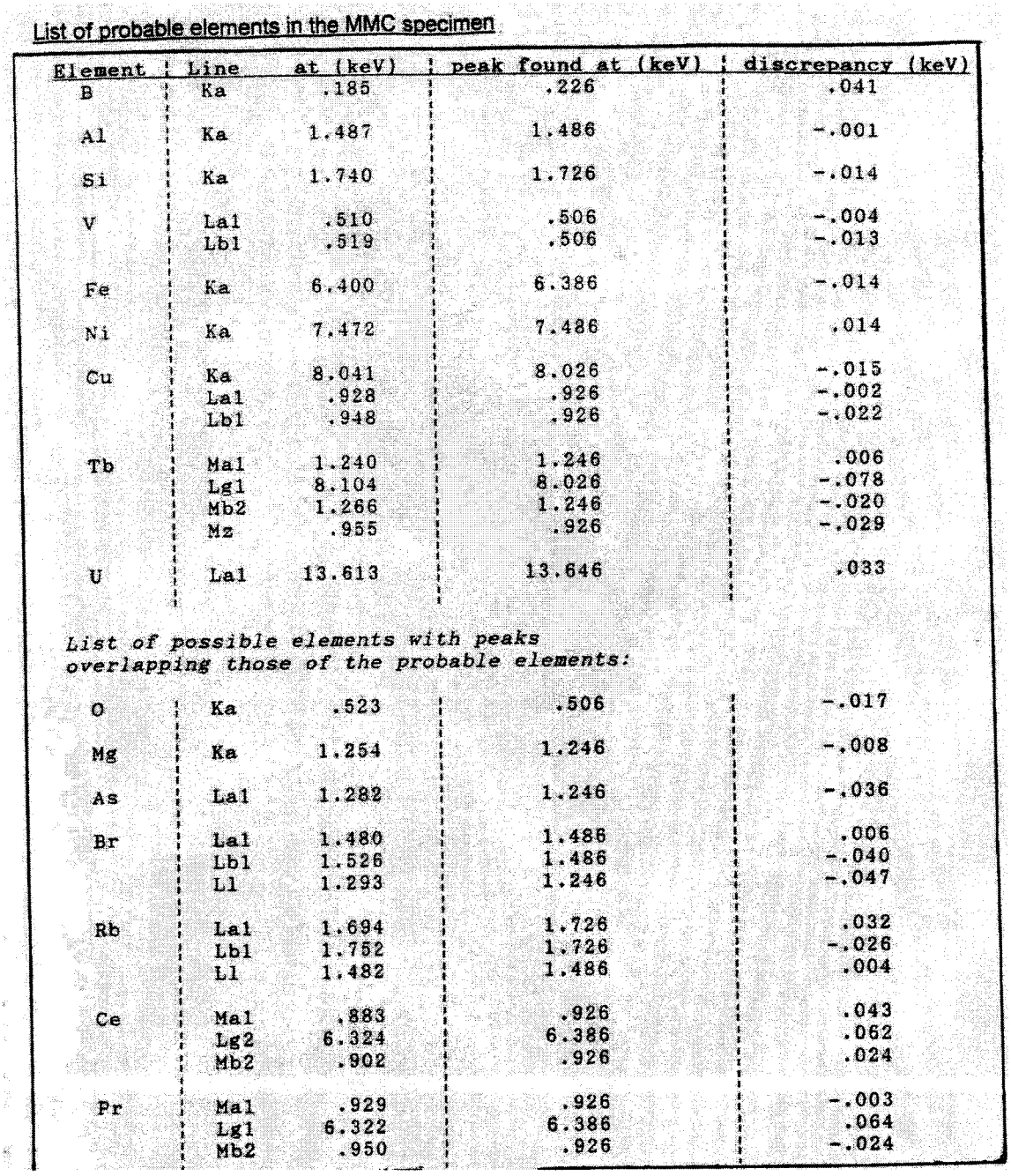

List of probable elements in the MMC specimen

Element	Line	at (keV)	peak found at (keV)	discrepancy (keV)
B	Ka	.185	.226	.041
Al	Ka	1.487	1.486	-.001
Si	Ka	1.740	1.726	-.014
V	La1	.510	.506	-.004
	Lb1	.519	.506	-.013
Fe	Ka	6.400	6.386	-.014
Ni	Ka	7.472	7.486	.014
Cu	Ka	8.041	8.026	-.015
	La1	.928	.926	-.002
	Lb1	.948	.926	-.022
Tb	Ma1	1.240	1.246	.006
	Lg1	8.104	8.026	-.078
	Mb2	1.266	1.246	-.020
	Mz	.955	.926	-.029
U	La1	13.613	13.646	.033

List of possible elements with peaks overlapping those of the probable elements:

O	Ka	.523	.506	-.017
Mg	Ka	1.254	1.246	-.008
As	La1	1.282	1.246	-.036
Br	La1	1.480	1.486	.006
	Lb1	1.526	1.486	-.040
	Ll	1.293	1.246	-.047
Rb	La1	1.694	1.726	.032
	Lb1	1.752	1.726	-.026
	Ll	1.482	1.486	.004
Ce	Ma1	.883	.926	.043
	Lg2	6.324	6.386	.062
	Mb2	.902	.926	.024
Pr	Ma1	.929	.926	-.003
	Lg1	6.322	6.386	.064
	Mb2	.950	.926	-.024

Figure 6.36 Table of elements from an Energy Dispersion Spectrograph of Al 2618 + 20% SiC showing typical chemical composition.

List of probable elements in AL2618.

Element	Line	at (keV)	peak found at (keV)	discrepancy (keV)
B	Ka	.185	.226	.041
Al	Ka	1.487	1.486	-.001
Fe	Ka	6.400	6.386	-.014
Ni	Ka	7.472	7.486	.014
Cu	Ka	8.041	8.026	-.015
	La1	.928	.926	-.002
	Kb	8.907	8.866	-.041
	Lb1	.948	.926	-.022
Tb	Ma1	1.240	1.246	.006
	Lg1	8.104	8.026	-.078
	Mb2	1.266	1.246	-.020
	Mz	.955	.926	-.029
Os	La1	8.910	8.866	-.044
	Mz	1.485	1.486	.001
List of possible elements with peaks overlapping those of the probable elements:				
Mg	Ka	1.254	1.246	-.008
As	La1	1.282	1.246	-.036
	Kesc	8.800	8.866	.066
Br	La1	1.480	1.486	.006
	Lb1	1.526	1.486	-.040
	Ll	1.293	1.246	-.047
Ce	Ma1	.883	.926	.043
	Lg2	6.324	6.386	.062
	Mb2	.902	.926	.024
Pr	Ma1	.929	.926	-.003
	Lg1	6.322	6.386	.064
	Mb2	.950	.926	-.024
Dy	Ma1	1.293	1.246	-.047
Tm	Ma1	1.462	1.486	.024
	Lb1	8.103	8.026	-.077
	Ll	6.341	6.386	.045
	Mb2	1.503	1.486	-.017
Yb	La1	7.414	7.486	.072
	Ma1	1.521	1.486	-.035

68

Figure 6.37 Table of elements from an Energy Dispersion Spectrograph of Al 2618 showing typical chemical composition.

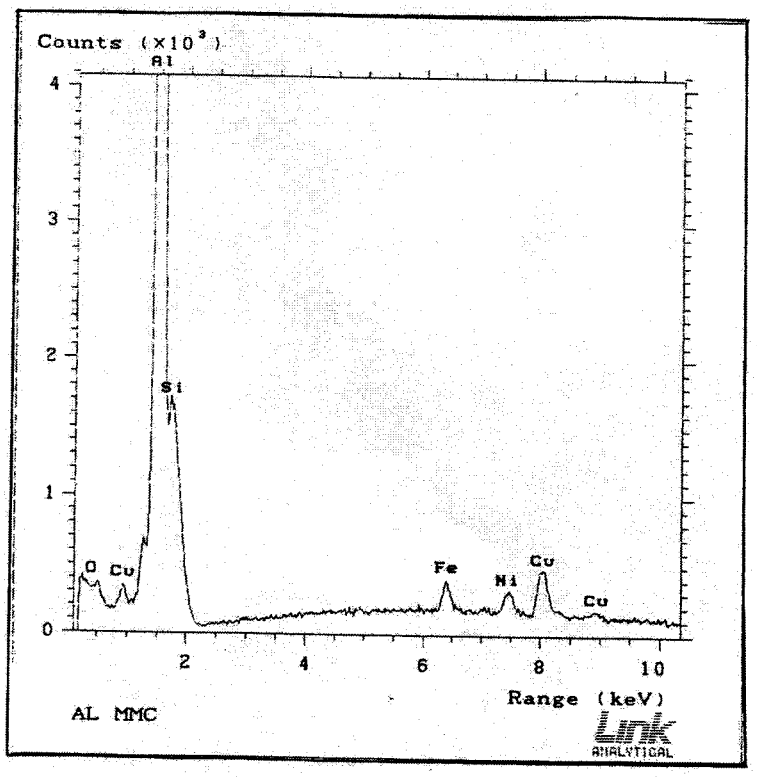

Figure 6.38 Energy Dispersion Spectrograph of AL 2618 + 20% SiC showing typical chemical composition.

6.4 Stress Controlled Testing on Aluminium Al 2014 and its Equivalent Metal Matrix Composite.

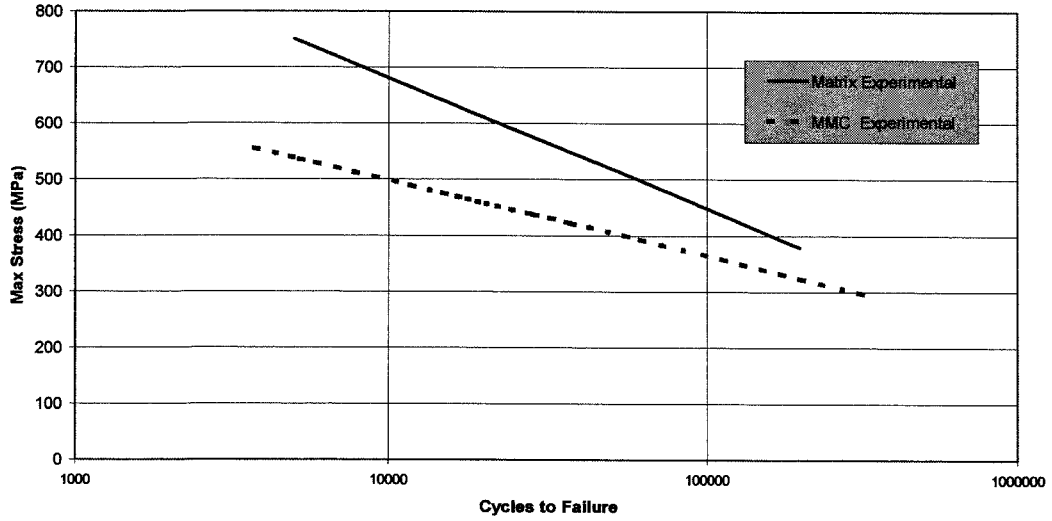

Figure 6.39 Experimental obtained data showing Maximum Stress plotted against Cycles to Failure for aluminium Al 2014 and a metal matrix composite with an identical matrix material +15% by volume $Al_2 O_3$ fibres.

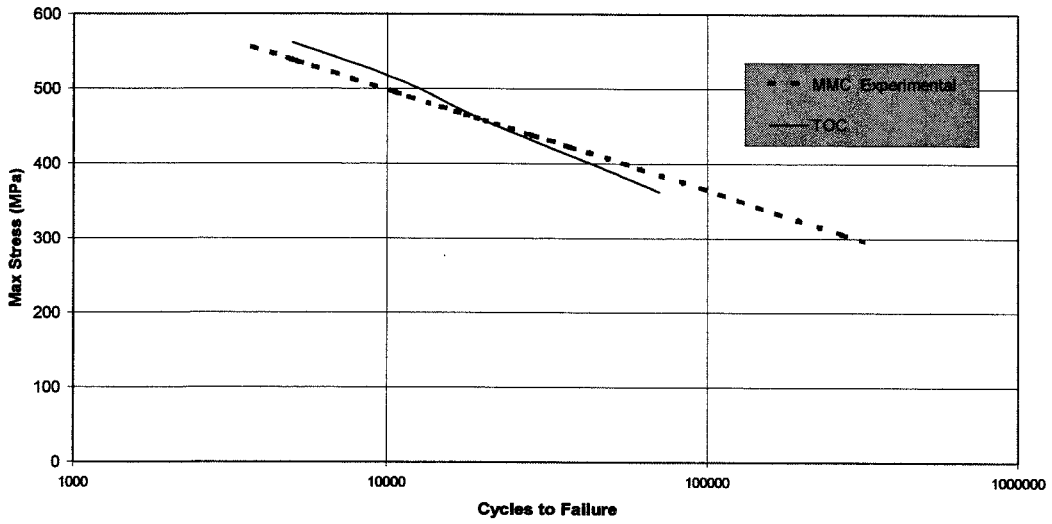

Figure 6.40. The fatigue data for the metal matrix composite compared to the fatigue life predictions given by the Theory of Cells.

The data presented in Figure 6.39 was obtained in a four point bend test and shows the fatigue life of an Al 2014 compared to an equivalent metal matrix composite tested under identical conditions. The fatigue life of the metal matrix composite was then compared to the results obtained from a Theory of Cells analysis and the results are given in Figure 6.40.

Test Number	Max Stress	No of Cycles to Crack Initiation	No of Cycles to Failure	% of Fatigue Life at Which Crack Initiated
1	493	14250	16435	87
2	500	10000	11711	86
3	498	8500	10076	85
4	544	3000	3725	82

Table 6.3 Summary of test results using replica technique showing number of cycles to crack initiation and number of cycles to failure.

During the experimental testing of the Al 2014 metal matrix composite the tests were interrupted at regular intervals. A replica was taken of the top surfaces of each test specimen and checked to ascertain the number of cycles to crack initiation and then the rate of crack growth up to failure. The results from this replica technique testing are given in Table 6.3

In almost all cases, once crack initiation had been detected it was only possible to obtain one replica image before failure took place. Crack initiation was assumed to be represented by the appearance of a small gas bubble as indicated in Figure 6.41. This

image was obtained from test 1 after 14250 cycles. In the same test after 15000 cycles the crack has grown and can clearly be seen on the next replica plate, Figure 6.42.

A number of micrographs were obtained from this material using a scanning electro-microscope. An estimation of the fibre diameter can be obtained from Figure 6.43, which shows a fracture fibre surrounded by matrix aluminium. The fibre failure happened during the reported fatigue tests. Both the diameter and length of the fractured fibre can be estimated from Figure 6.44.

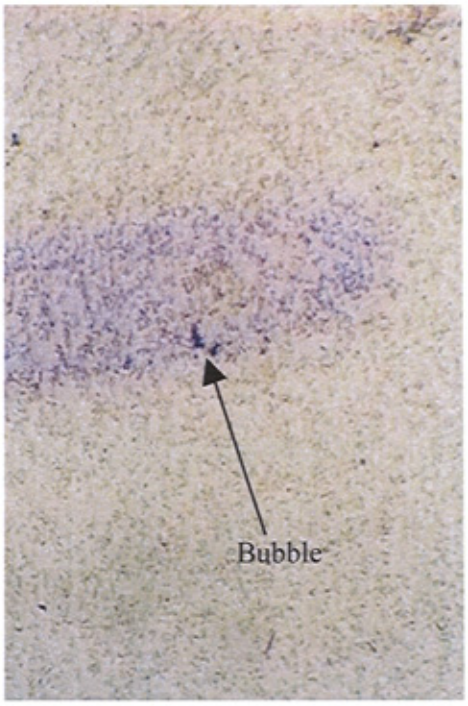

Figure 6.41. Optical micrograph showing the start of crack growth. Starts by showing a bubble.

Figure 6.42 Optical micrograph of crack growth. Crack was 2.3 mm length

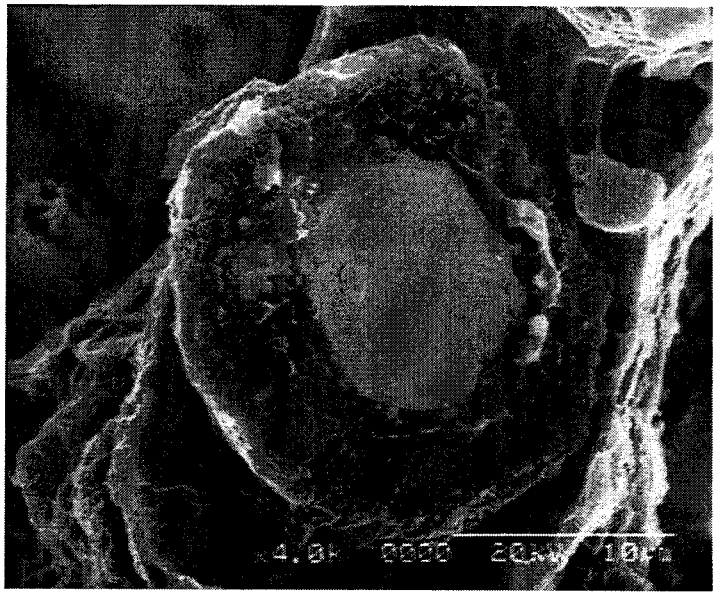

Figure 6.43. Scanning electron microscope micrograph showing fractured fibre.

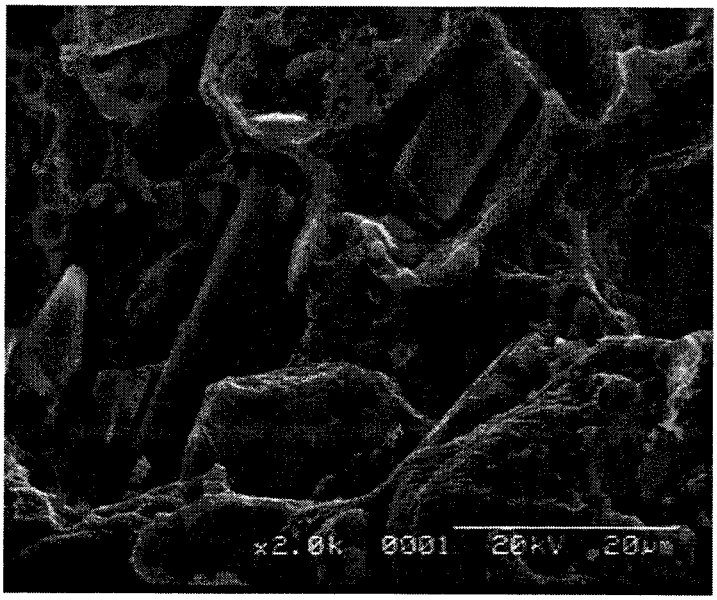

Figure 6.44 Scanning electron microscope micrograph showing fibre length and diameter.

Some evidence of fibre clustering can be seen in Figure 6.45 while a typical fracture surface is shown in Figure 6.46.

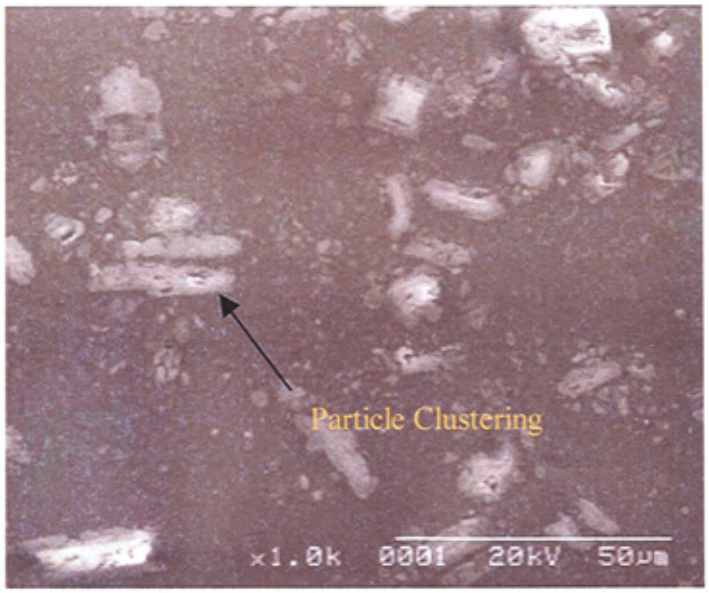

Figure 6.45 Scanning electron microscope micrograph showing region of particle clustering.

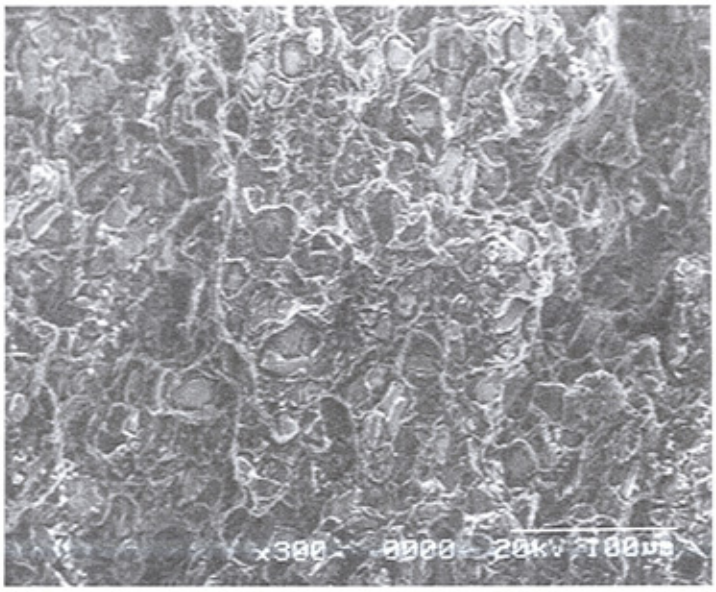

Figure 6.46. Fracture surface showing fibre at the centre of circular features.

Two energy dispersion spectrographs are shown in Figures 6.47 and 6.48. The first is of the base aluminium, the second is of the fibre itself.

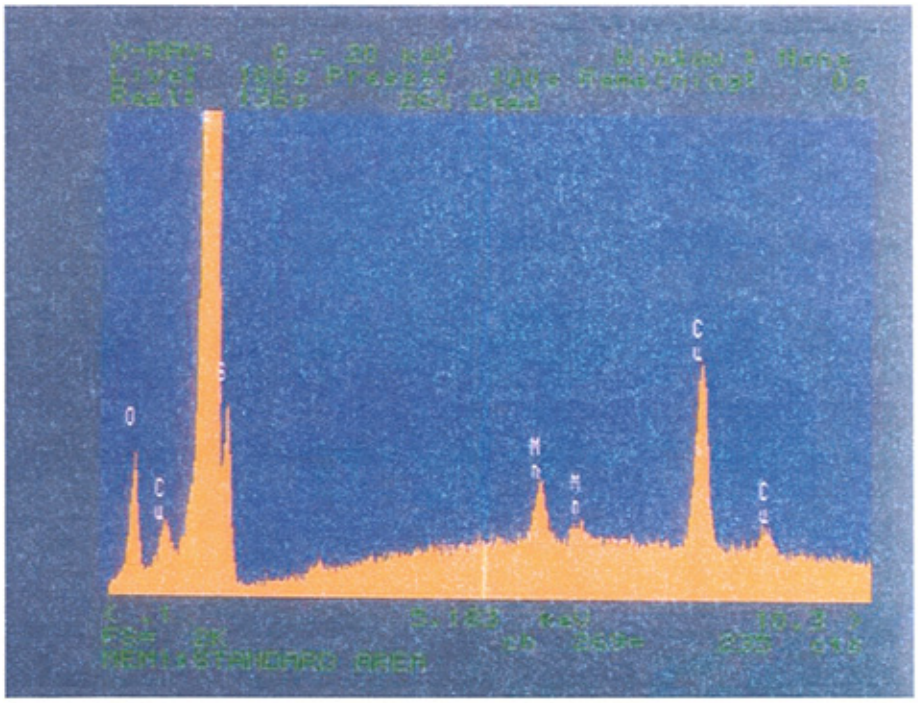

Figure 6.47 Energy Dispersion Spectrograph of Al 2014 showing typical chemical composition.

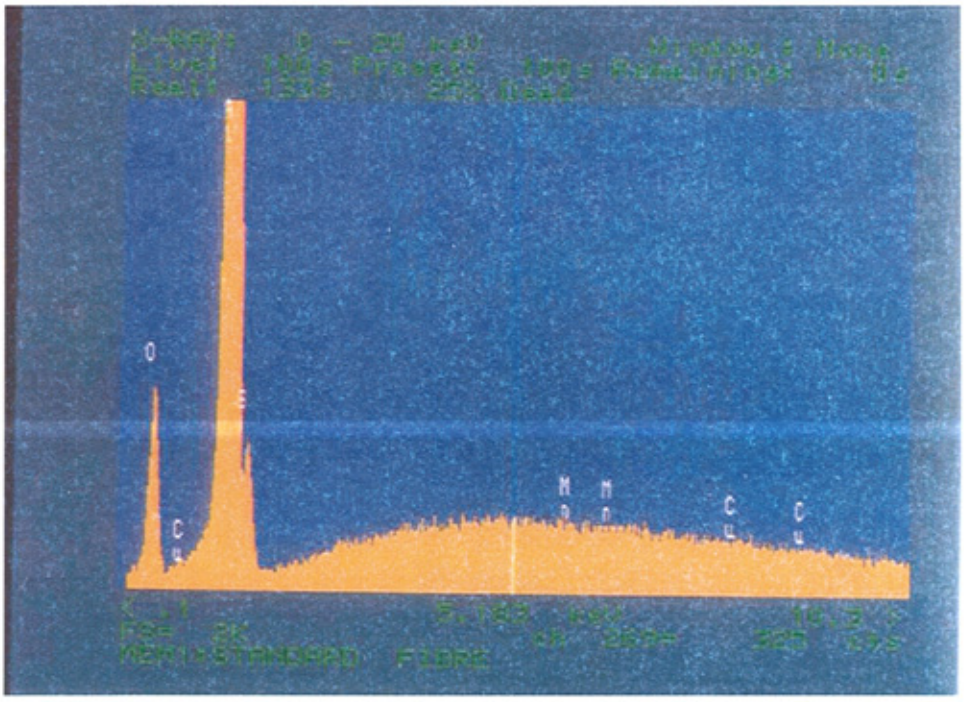

Figure 6.48 Energy Dispersion Spectrograph of Al_2O_3 fibre used in the metal matrix composite showing typical chemical composition.

Chapter 7

7.0 Discussion

7.1 Aluminium Al 7075 and its Equivalent Metal Matrix Composite Al 7075/ 12% SiCp

Initially, a monotonic stress strain curve was generated for both the monolithic material and its equivalent metal matrix composite, the results of which are given in Section 5. However during fatigue testing the strain levels were kept constant and so it was necessary to monitor the stress levels as each of the fatigue tests progressed. The results of these tests are shown in Figure 6.1 and Figure 6.2, the former being for the monolithic material and the latter for the metal matrix composite. From these curves, results can be generated showing the fatigue life of both materials. In all but the lowest stresses, the monolithic material exhibits a superior fatigue life to that of the metal matrix composite. The difference in fatigue life is more apparent in the strain plot shown in Figure 6.4 than the conventional S/n curve of Figure 6.3.

As reported in Chapter 5, the monolithic material had a 0.2% proof stress of 416 MPa, and so the result for yield stress of 404 MPa for the metal matrix composite was somewhat surprising. It might be expected that the inclusion of particulates in the aluminium would improve both its yield and ultimate strength. However, it can be seen from Table 6.1 that the experimental yield stress is at the level predicted by the Theory of Cells; the experimental and theoretical values being 404 MPa and 391 MPa respectively. The reason why the metal matrix composite yields at a lower stress than the monolithic material is to do with the particulate inclusions. Under load, the particulates will create stress gradients within the aluminium matrix. As predicted in the Theory of Cells some areas of matrix will be yielding, other areas will still be at sub-yield levels of stress. The overall stress of the metal matrix composite is the average of the particulate stress and the stress experienced by each matrix sub-cell, so

that while areas of the metal matrix composite may have started to exhibit plastic behaviour, the overall stress may not have reached the value of the yield stress of the monolithic material.[83,84] Although this is what has happened to this composite it may not necessarily be the case for another composite of different particulate volume fraction and different constituent mechanical properties.[85,86] Yield stress of a composite is not only dependent on the yield stress of the matrix, but is a complex relationship between particulate and matrix properties and particulate volume fraction, aspect ratio and orientation.[87] The overall stress of the metal matrix composite will, of course be a summation of the stresses in the particulate or fibre and each sub-cell of the matrix. So while one or two sub-cells of matrix material may be yielding other sub-cells may be well below the yielding stress. In this case, the summed stress for the metal matrix composite at yield was lower than the yield stress of the monolithic material.

Table 6.1 also compares an experimentally derived Young's modulus with that predicted by Theory of Cells. The experimental result indicating a modulus of 84.1 GPa. while the Theory of Cells gives 83.3 GPa. The TOC result, in this case, is within 1 % of the experimental result.

Both the S/n results given in Figure 6.5 and the Strain/N results given in Figure 6.6 show good agreement between Theory of Cells and the experimental results. At stress levels below 450 MPa the agreement is well within the experimental error of the test. However once stresses are in the plastic region of the metal matrix composite, the prediction value of fatigue failure starts to deviate from the experimental results. At these levels, the stress in the particulates is significantly higher than those experienced in any sub-cell of the matrix. The matrix accommodates the increase in overall loading on the metal matrix composite by yielding, but the particulates are still deforming elastically. As the load increases some of the weaker particulates fail and there is a redistribution of the load between particulate and matrix. The theory predicts that, for this metal matrix composite, the stress level in the individual particulates falls, causing a corresponding increase in the

stress on the matrix. So failure throughout these tests should have been by matrix fatigue failure.

It could be assumed that once a particulate has failed, the broken portion is then available to take load. This could be true of inclusions that are of significant length, but in this case we are not dealing with fibres but particulates and it would seem that failed particulates are not available to take load. This would explain the significant short fall in fatigue life in cyclic stresses above 450 MPa. The broken particulates, rather than taking load, may be areas of weakness and could cause premature fatigue failure of the composite. As the stress increases, more particulates break, causing more fatigue damage to the material. Failure at these stresses could also be initiated by imperfections in the matrix material itself.

Although this difference between experimental and theoretical fatigue life under gross plastic deformation is of some importance, it must be remembered that this only involves the first thousand cycles of the S/n curve. Once beyond this value the predicted life from the Theory of Cells is in close agreement with that obtained from experiment.

As a comparison to the predictions offered by the Theory of Cells a simple 2-D finite element was used to predict both material properties and stresses around the inclusion in the metal matrix composite. Due to the limitations of the finite element package used, the number of mesh that could be used in any model was severely limited and as a consequence the mesh around the inclusion was fairly coarse. Due to these restrictions, for any volume fraction, the choice of aspect ratio was limited to a small number of choices. For example for a volume fraction of 0.1 the aspect ratio could have been chosen as 2.5 or 1.6. Ideally, identical aspect ratios would have been used for comparing properties of metal matrix composites across the range of volume fractions, instead because of the mesh constraints the aspect ratios used for each volume fraction are shown in Table 6.2.

Because of the flexibility of the Theory of Cells it was possible to make a prediction of the mechanical properties of each of the metal matrix composites with identical volume fraction and aspect ratio as that used in the finite element prediction. This

allows a simple evaluation between the two methods over a wide range of possible metal matrix composite systems. A comparison of the predicted value of Young's Modulus, using both the Theory of Cells and this 2-D finite element model is shown in Figure 6.7. In the Theory of Cells prediction, the Young's Modulus rises in a linear fashion up to a volume fraction of 0.2. After this point the rise is no longer linear but shows some small amount of irregularity. A similar but not identical trend can be seen in the results predicted by the finite element method. This is due to the varying aspect ratio as, over this range, not only the volume ratio but also the aspect ratio is increasing. Most material properties in metal matrix composites are affected not only by the amount of fibres included in the structure but also by the length of fibre within the composite.

The results predicted by both methods are in a large measure in good agreement with one another, the maximum discrepancy being in the region of 9%. For comparison a prediction using the Rule of Mixtures is shown plotted on the same graph. A brief résumé of the Rule of Mixtures is given in Chapter 3. The results for this technique show a linear increase in value of Young's Modulus but compared to the other two methods it over predicts the value by between 24% and 64%.

A prediction of the Poisson's ratio was also made by the finite element method and the results for this are show in Figure 6.8. Also shown on this graph are the predictions given by the Theory of Cells and the Rule of Mixtures. At first glance it appears as though the finite element prediction is at variance with the other two methods and that the Rule of Mixtures and Theory of Cells prediction look in good agreement. However, in general the change in the Poisson's ratio is small over the whole range of volume fractions, with small changes in any of the results being capable of drastically altering the trend of the curve.

As the Theory of Cells compares stresses within the composite with known fatigue failure stresses, it would be interesting to know the predicted stress distribution within the metal matrix composite as forecast by the 2-D finite element prediction. This is shown in Figure 6.9 with the overall strain on the composite being 0.1% and the position of the fibre being outlined in red. It will be noticed that stress within the

fibre ranges from 341 MPa and 161 MPa, which is way below the minimum failure stress for a SiC fibre.

Within the aluminium matrix this finite element model predicts an area of high stress, with a value of 234 MPa, in front of the fibre and another of 207 MPa at the interface. These areas are marked Front and Interface in the figure.

The mesh limitations imposed by the 2-D finite element study could only be overcome by moving to a more sophisticated programme. Developing such a program was outside the capabilities of this study and so a method, developed by collaborators, was used to compare with results produced by the Theory of Cells. By using a fully 3-D package, that also allows modelling the material in a non-linear fashion, the solution to the problem then requires a special iterative procedure at every half cycle of the loading or unloading.

The effective plastic strains were determined for different values of strain ε_y in the direction of the cylinder axis. The effective plastic strain distribution in the cylinder with an overall strain of $\varepsilon_y = 0.01$ after 5 cycles is shown in Figure 6.10. It can be seen that the residual strains reach maximum value on the interface between the inclusion and the matrix. There is a second area on the cylinder axis in front of the inclusion where plastic strain reaches a maximum value.

The Theory of Cells, by using an analytical approached to the problems of stress and strain within a metal matrix composite, allows simple, quick calculations to be undertaken over a range of situations. For comparison between the methods already described, Figure 6.11 is included and shows stresses predicted by the Theory of Cells in the same orientation to those for the finite element methods given in Figure 6.10 and Figure 6.9. In each of the methods, an area of high stress just ahead of the fibre is predicted. This area is marked 'Front' for both of the finite element methods and is the area sub-cell 2,1,1 in the Theory of Cells. In the finite element analysis, areas of high stress are also predicted in the position marked 'Interface' in Figure 6.10 and Figure 6.9. This corresponds with sub-cell 1,2,1 in the Theory of Cells. However in the 3-D analysis it is the interfacial area that is forecast to have the higher stress,

where as the other two methods indicate it is the frontal area with the higher stress. The discrepancy as far as the Theory of Cells is concerned could be that this interface area, as predicted by the 3-D finite element model, lies at the cross over point between all 4 cells shown in the figure. We will see later that this 'interfacial' high stress region presents a problem for the 3-D finite element model when compared to the experimental model.

The numerical investigation of the composite was carried out in strain-controlled tests for the following strain amplitudes of symmetric cycles: $\Delta\varepsilon_{ay}$= 0.5%, 0.6%, 0.7%, 0.8%, 0.9%, 1%. At each calculation point the current values of χ and damage measure D were defined. The calculation process stops when $D=1$.

It follows from what has been said that it can be assumed that the first fatigue crack forms on the inclusion matrix interface, but it is soon followed by a second crack that forms in the frontal zone after a certain number of loading and unloading half-cycles. Obviously these cracks precede the overall metal matrix composite's failure. As long as some region of the composite is at high enough stress this process will occur at all levels of strain amplitude.

In the zones marked 'Interface' and 'Front' in Figure 6.10, the process of alternating-sign deformation occurs in different ways. Figure 6.12 and Figure 6.13 are two cyclic diagrams of the global co-ordinates $\sigma(\varepsilon)$ for a strain amplitude of 0.7%. Figure 6.12 shows that the process of cyclic deformation on the interface between inclusion and matrix is subject to greater strain levels than in the zone Front, shown in Figure 6.13.

Despite the fact that the overall loading process occurs at constant strain amplitude, the zones, Interface and Face, see a different stress and strain range. However, as the number of cycles increases the dimensions of the hysteresis loop stabilises. This is confirmed by the results given in Figure 6.14 and Figure 6.15, showing the behaviour of the loop's width versus the number of half-cycles. Initially, the cyclic behaviour of the material is dependent on the value of the specimen's elongation amplitude. However, by the tenth half-cycle the process of cyclic deformation may be considered stabilised. In many respects, it depends on the value of the hardening parameter b_{χ}.It

should be noted that the process of cyclic elasto-plastic deformation brings an essential non-homogeneity in the distribution of plastic strain in the region close to the inclusion matrix interface (see Figure 6.10). Due to the non-uniformity of aluminium's hardening in the region near the interface, a zone with wave-like distribution of plastic strain arises. However, with the number of half-cycles increasing, such wave-like pattern is smoothed out. Thus maximum plastic strain on the interface and frontal zones are not consistent from the cycle to cycle. This is clearly indicated in Figure 6.14 and Figure 6.15.

On the basic assumption that the number of half-cycles before the appearance of a low-cycle fatigue crack is defined by the condition $D = 1$, the number of cycles for crack initiation were calculated. Figure 6.16 is a plot of cycles before failure, versus the localised strain for region within the metal matrix composite. Results from the 3-D finite element analysis are indicated as 'Front' and 'Interface' and for comparison both experimental and Theory of Cells results are shown.

It must be remembered that we are not strictly comparing like with like on this graph. This finite element analysis only allows prediction of the number of cycles to crack initiation, while the experimental and Theory of Cells results are for prediction of fatigue failure. For this type of fatigue loading it would be expected that the number of cycles from first crack until failure is around 70-80% of specimen cyclic lifetime. It should be expected therefore that, for a given strain level, the finite element prediction would under estimate the life of the material compared to results obtained experimentally and it can be seen from Figure 6.16 that this is the case.

In the above section, experimental results for a series of constant strain fatigue tests on Al 7075 were used along with the Theory of Cells to make a prediction of the fatigue life of an equivalent Al 7075 metal matrix composite. These results were then compared to constant strain fatigue tests of the metal matrix composite itself. The results were then compared to the prediction made by the Theory of Cells with good correlation in all but the low cycle fatigue regime.

A comparison has also been made of the results of Young's modulus, Poisson's Ratio and Yield Stress of experimentally obtained values and those predicted by the Theory

of Cells. Then using a simple 2-Dimensional finite element model the predicted values of Young's Modulus and Poisson's ratio over a wide range of volume fractions was compared to the results obtained from the Theory of Cells. For both the experimental and finite element results there is good agreement with the Theory of Cells. Although not the main point of the study, this correlation between experiment and finite element with the Theory of Cells gives some confidence that the model can predict a wide range of mechanical properties of metal matrix composites.

A crucial point about the Theory of Cells is that it can predict average stresses in and around a fibre within a metal matrix composite. Comparison is shown of the stresses predicted in this region by the Theory of Cells and by the simple 2-Dimensional finite element model and a much more powerful 3-dimensionl non-linear finite element model. The results from these studies are in agreement that there will be a highly stressed area in the matrix material ahead of the fibre but there is disagreement about the level of stress at the fibre-matrix interface.

The 3-dimensional finite element model was then used to forecast the fatigue life of the metal matrix composite and the results were compared to the forecast made by the Theory of Cells but due to computational limitation the comparison could only be made at the low-cycle fatigue end of life prediction. The finite element method indicated a high area of stress at the interface which was not shown using the Theory of Cells. This would predict fatigue failure, for a given stress, at a lower number of cycles to that given by the Theory of Cells or experimental evidence. The frontal area of high stress indicated by the finite element gives a much close correlation to both Theory of Cells and experimental evidence. Perhaps the simplification of the fibre into a sphere has over predicted the stress in the interfacial area and thus forecast a very pessimistic fatigue life compared to the other two results. Both the simple 2-dimensional finite element model and the Theory of Cells use a model of the fibre which is more in line with the real fibre than the more complex 3-dimensional analysis.

7.2 Stress Controlled Testing on Aluminium AE 109 and its Equivalent Metal Matrix Composite AE 109 With 15% SiC Fibrefrax

Aluminium AE109 and its associated metal matrix composite is a commercially produced material used in diesel engine pistons. Although general information on this material are available[88] details of comprehensive mechanical data is difficult to obtain due to both its commercial sensitivity and constant material development. The material tested in this section was a standard AE109 alloy and an equivalent metal matrix composite with a commercially available refractory fibre 'Fibrefrax '. Both composite and base materials were tested in tension-tension mode under constant stress control.

The S/n curve generated from these tests can be seen in Figure 6.17. At high maximum stress the aluminium alloy had superior fatigue strength to that of the metal matrix composite, but at low stresses the fatigue strength of both materials was identical. When the results from the metal matrix composite were compared to those predicted by the Theory of Cells, as shown in Figure 6.18, the correlation of the two was very close indeed. At the low-cycle end of the curve, the experimental results correlated exactly with those of the prediction and only at a very high number of cycles did prediction and experimental results differ by more than a few percent.

Although the deviation of the predicted values from those of the experimental is only slight, it can be seen from Figure 6.17 that the experimental curve deviates from linearity at the low stress section of the curve. This non-linearity could be a real effect or in fact could be generated by a single result. Unfortunately, this issue could not be resolved due to time and material limitations. If this was a spurious result and the S/N curve was in fact linear, the correspondence between theory and experiment would be more striking.

At ambient temperatures the difference between the fatigue strength of the composite and that of the original alloy is comparatively slight. It might be felt, therefore, that the accurate prediction of the Theory of Cells is only to be expected. Fatigue is

predicted in this modification of the Theory of Cells by comparing the stress levels around a fibre with known values of matrix material fatigue strength. Obviously, the mis-matching in Young's modulus between fibre and matrix could have a major effect on the composite fatigue life. Figure 6.19 has the same information as that presented in Figure 6.18 but also includes a prediction of a similar composite to the one used in the study, but with the fibres having a Young's modulus of 300 GPa. As can be seen, for this composite, the fatigue life is greatly reduced over the whole stress range. This is a significant result because it shows how important the relative stiffness of the fibre and matrix can be in the fatigue life of the metal matrix composite. By selecting a fibre and matrix of similar stiffness, a superior fatigue life was obtained for this composite to that obtained by having a high fibre stiffness with an identical base matrix. With materials of similar stiffness all components will experience similar levels of stress during initial loading. This will mean that fatigue damage to the matrix material occurs later in a loading sequence than would occur in a material with a high fibre stiffness. In this manner, the similarity between the S/n curve of matrix and composite can be explained.

Using a simple tension-tension series of tests the fatigue life of a metal matrix composite and its equivalent aluminium alloy has been predicted and good correlation is shown between the composite life and predictions made by the Theory of Cells. This material also shows clearly the effects of fibre Young's modulus on the fatigue life of a metal matrix composite.

7.3 Stress Controlled Testing on Aluminium Al 2618 and its Equivalent Metal Matrix Composite with 20% SiC Fibres

The test data shown in Figure 6.20 was obtained from a four-point bend test, with an R ratio for all tests being 0.1. The fatigue life of the metal matrix composite was, in all cases, inferior to that of the matrix material, with the low cycle fatigue life showing a greater difference compared to that obtained in the high cycle testing.

Compared to the material studied in the last section, the difference between the fatigue life of the composite and the aluminium alloy is significantly different.

However when, we compare the results of the composite fatigue testing with the prediction given by the Theory of Cells, as shown in Figure 6.21, a very good correlation exists between the two. Again at high maximum stress the correlation between Theory of Cells and experimental results are much better than at the lower maximum stress fatigue region but even here the error difference between the predicted value and experimentation is still only 6%.

For this material, fatigue testing on both the composite material and its associated metal matrix composite were also carried out at elevated temperatures. Figure 6.22 shows fatigue results for both the matrix and composite at 200°C while Figure 6.24 shows the results at 300°C. In both cases we can see that the matrix material appears to have superior fatigue properties to that of the metal matrix composite. The results from the 200°C Theory of Cells analysis compared to the experimental results for metal matrix composite are shown in Figure 6.23. In all cases, the Theory of Cells underestimates the fatigue life of the composite. For example with a maximum stress of 400 MPa the Theory of Cells predicts failure at 3000 stress reversals while the composite in fact withstood 6000 stress reversals before failure. Although this result was a disappointment at least the prediction was conservative and consistent as the slope of both lines were virtually identical.

When we look at the results for the 300°C Theory of Cells prediction, a much more confused picture emerges. The results of both the experimental data and the prediction are shown in Figure 6.25. As can be seen the Theory of Cells has failed to predict the fatigue life of the metal matrix composite at this temperature. The slopes of both lines are different and nothing positive can be said about this result.

For both these results we must look at what is meant by fatigue failure. At room temperature, failure occurs because of the fracture of the specimen. Crack initiation and then growth has occurred and finally the material fails in a ductile or brittle fashion, depending on the material type and the stress levels. However fatigue failure at these elevated temperatures must be defined in a different way from the type of

failure which occurs at ambient temperatures. Some elevated temperature tests fail in a manner similar to that experienced at ambient temperature, but more often failure occurs because displacement of the specimen is such that testing can no longer be carried out. Some of the metal matrix composite specimens tested at 200°C failed by simple fracture but all other specimens, both metal matrix composite and matrix material, failed by excessive displacement. This excessive bending of the specimen is a mixture of both fatigue and creep damage. It is not surprising, therefore, that the predictions from the Theory of Cells do not match the results from experimentation. With greater knowledge of the mechanical properties of both materials at higher temperatures it may be possible to modify the Theory of Cells to accommodate both creep and temperature effects but this was felt to be beyond the scope of this study. Also, the monolithic matrix material and the metal matrix composite are subject to different creep rates thus confusing the analysis even further. In these high temperature tests both fatigue failure and creep failure are signified by gross deformation of the test specimen. This deformation will be caused by creep and fatigue damage but as the temperature rises, creep will be more prevalent in the matrix than the metal matrix composite.

To better understand the events surrounding fatigue of both the aluminium alloy and its associated metal matrix composite, a micrographic study was undertaken of some of the failed specimens tested at ambient temperatures. The two lower power micrographs, Figure 6.26 and Figure 6.31, of the metal matrix composite and the matrix material do not show sufficient detail to reveal any difference in the way fatigue has taken place in both materials. Once the magnification is increased however, significant differences can be noticed. The metal matrix composite micrograph, Figure 6.27, shows a non-uniform dimpled structure in which the bottom of many of the dimples have fibre particles. Notice that these dimples are irregular in both size and shape, the shape often being determined by the particle size and orientation.

Compare this micrograph with Figure 6.32, which is one of similar magnification of the matrix material. The dimples here are of a more uniform circular nature and many

have a hollow bottom indicating that they were produced during extended plastic deformation[89].

With higher magnification of the metal matrix composite fracture surface, we see more clearly both the uneven dimple effect and fibre particles. This is very evident in Figure 6.28 where many SiC particles are observed. Figure 6.29 gives evidence of particle fracture, this being marked by "Z" on the micrograph and "A" on Figure 6.30. All of these micrographs are typical of a fatigue fracture in a metal matrix composite including the stepped feature marked "B" on Figure 6.30.

The micrographs of the matrix material are also very typical of fatigue fracture surfaces. Figure 6.33 and Figure 6.34 clearly show the circular nature of the fractured surface. We also notice small particles protruding from many of the dimples and for a clear view of this feature a micrograph at a higher magnification was obtained, (Figure 6.35). A particle is labelled "Y" on this figure. In an earlier report[90] a similar feature was noted and it was stated that these features were eutectic silicon particles. However the material under study in this section was a copper based aluminium alloy with no silicon present. An energy dispersion spectrograph was obtained both for the metal matrix composite, Figures 6.36 and 6.38, and for the base material, Figure 6.37. This indicates that while the composite contained silicon from the fibres, none was present in the base material. However as ferrite was an alloying element in the aluminium it is likely that these inclusions were composed of particles of pure ferrite[91] produced during material processing.

In the modified form of the Theory of Cells presented in this study, it has been shown, that the fatigue life of a metal matrix composite over a wide range of stress/strain levels can be predicted. At elevated temperature where creep damage may be occurring, the predictive power of the Theory of Cells are somewhat restricted. Results at both 200°C and 300°C are shown and compared to theoretical results derived from the Theory of Cells.

To obtain some understanding of the failure process encountered for this alloy and its associated metal matrix composite, a series of micrographs are shown and it was noted that both the matrix material and the metal matrix composite had similar

features at high magnification. The fracture surface of both materials are covered with dimples but the reason for their being there is different for each of the materials. In the composite, the centre of the dimple is of course the fibre, but in the matrix material it is probably a ferrite particle.

One assumption made in the modified Theory of Cells is that fatigue failure occurs when the matrix or fibre material reaches an appropriate stress caused by the elastic-plastic interplay of fibre and matrix. In the current modification, no allowance is made for pre-existing 'faults' in the material. These can take the form of cracks, inclusions or problems associated with fibres and these are alternative areas from which fatigue failure could be initiated. The micrographs from this section of the study do not unfortunately indicate by which of these two methods fatigue initiation occurs. It therefore became necessary to use more indirect means to ascertain whether the assumption made by the modified Theory of Cells were correct. This is dealt with in the next section of this study.

7.4 Stress Controlled Testing on Aluminium Al 2014 and its Equivalent Metal Matrix Composite.

If a material is going to fail in fatigue by stress raisers such as cracks and inclusions, or from problems associated with fibres, most of the cyclic fatigue life will be involved in the process of crack growth. If, on the other hand, this is not the case, most of the material's life will be involved in causing enough fatigue damage to start crack initiation, followed by a short period of crack growth and then failure. One method of investigating crack initiation is the replica technique as described in Section 5.3. This method has to be applied with some caution being both tedious and time consuming. As a consequence only moderately low cycle tests could be undertaken.

The first results from this section are S/n data, generated while using the replica technique. Not only is the data from this technique shown, but for completeness a number of high cycle tests were also undertaken and are included in the information given in Figure 6.39. As with previous materials, we have a matrix material which in

all cases has a fatigue life greater than its metal matrix composite counterpart. Figure 6.39 also shows the now familiar convergence of the two curves in the very high cycle region.

When we come to compare the metal matrix composite results with the theoretical prediction, shown in Figure 6.40, we again see a reasonable correlation between the two. At high maximum stress levels the Theory of Cells over-predicts the life of the composite and at lower stress levels it under-predicts the life of the composite. When using the replica technique, the fatigue test must be constantly stopped and re-started and it was felt that this might have some effect on the results of the fatigue test. When these results are compared to others given in earlier sections there is little evidence that this was the case.

The replicas produced in this series of tests were in every case taken from the top surface of a four-point bend test specimen. This is of course the area of highest stress and is where a fatigue crack would be expected to initiate. The results, which are summarised in Table 6.3., show that for all these low cycle tests the fatigue crack did not appear until quite late in the fatigue life of the specimen. The number of cycles to failure range from 3725 to 16435, but on all occasions it took over 80% of the testing time to initiate the fatigue crack. This is consistent with the Theory of Cells' assumption that fatigue cracks are not growing from faults around the fibre or from inclusions within the metal matrix composite but the crack that causes failure is caused by the same initiation process as that experienced by the aluminium alloy.

Two pictures of replicates are shown in Figure 6.41 and Figure 6.42. These pictures are taken from the same test. The Figure 6.41 shows the first signs of crack initiation, and this is signified by a small bubble appearing on the replicate slide. Figure 6.42 shows the same area after 750 further stress reversals and, as we see, a crack has appeared and grown to a length of 2.5mm. Failure followed quickly after this. In each of the tests carried out in this section, a bubble was observed just prior to the appearance of the fatigue crack. It was decided to define the point of crack initiation to be co-incidental with the appearance of this bubble. In practical testing it was only

after failure had occurred and the replicate slides were being reviewed that it was realized that the bubble feature had occurred.

On close inspection of the fracture surface we can see a number of interesting features. Use of a scanning electron microscope, detailed in Figure 6.43, shows a fractured fibre surrounded by matrix material. The fibre shows a clear, brittle fracture consistent with Al_2O_3 with the matrix showing ductile failure. By decreasing the magnification, as shown in Figure 6.44, a good view of the length and diameter of the fibre can be estimated. This gives an aspect ratio of approximately 6.5, which is close to the reported average aspect ratio of 8. It is also likely that the fibre image shown in the micrograph is slightly foreshortened which would give an aspect ratio closer to the quoted average.

In the next micrograph, Figure 6.45, we see evidence of particle clustering that is often quoted in the literature as phenomena causing composite weakness and an area from which fatigue crack growth could occur. Clustering is a natural effect caused during the production of the metal matrix composite. In a system like squeeze casting, molten matrix material is mixed with a block of fibre material and although the design of the whole system is arranged to allow maximum dispersion of the fibre, inevitably this cannot be completely successful. The clustering we see here is only of two fibres and is what would be expected in a well-dispersed metal matrix composite. Statistically you would expect at least two or three fibres to be in close proximity at intervals throughout the material. A weakening of the composite would only be expected if there were large areas of clustering and other areas devoid of fibres.

As with the material reviewed in the previous section, Figure 6.46 shows us a dimpled fracture surface and at the centre of the larger dimple is a fibre. This is what we would expect from a metal matrix composite. Comments have been made on this type of surface in the previous section.

The final two figures in this section are energy dispersion spectrographs of the matrix material, Figure 6.47, and the fibre, Figure 6.48. The matrix material shows an abundance of aluminium with significant levels of copper, manganese and silicon. This analysis is consistent with the reported makeup of this particular alloy. One

surprising trace element is oxygen. This also occurs in the energy dispersion spectrographs of the fibre, along with aluminium. However as the fibre is Al_2O_3 this was to have been expected. Also shown on this spectrograph are traces of all the elements seen in the matrix spectrograph. As the fibre is small, and a difficult target to isolate, it would seem that small amounts of matrix material are involved in the analysis. The oxygen shown in the matrix analysis could have come from the fibre or could have been defused into the matrix from the fibre during production.

In this section the Theory of Cells has been used once again to predict the fatigue life of a metal matrix composite and again good correlation has been achieved between the theory and experimental results. During the fatigue testing, replicas were taken of the most highly stressed part of the test specimen and upon examination it was determined that fatigue crack initiation did not occur until late in the fatigue life of the metal matrix composite. This result was consistent with fatigue cracks not emanating from pre-existing cracks or faults already present in the material before fatigue testing was undertaken. Micrographs of the material show a typical failure mode of the fibres and also some clustering of the fibres within the material but not enough to cause weakness of the composite.

7.5 Overall Fatigue Behaviour of Metal Matrix Composite

In each test reported in this study, an analysis using the modified Theory of Cells has been used to predict the fatigue life of a different metal matrix composite. Four different aluminium alloys were used comprising a zinc-based alloy, two copper based alloys and a silicon-based alloy. Both SiC and Al_2O_3 fibres have formed the reinforcement in the metal matrix composite and both stress controlled testing and strain controlled testing have formed part of the study. Both tension/tension and four point bending tests have been carried out. At ambient temperature the modified Theory of Cells has demonstrated an ability to forecast, to close accuracy, the fatigue life of all these metal matrix composites. Looking at the various results, no type of

alloy or fibre reinforcement can be claimed to be favoured by the analysis. Neither can it be said that strain testing produced closer correlation than stress testing. It seems the theory works equally well for all the different parameters tested. The simple assumption of the modified Theory of Cells is that fatigue failure will occur when the matrix or the fibre reaches a critical stress and it is on this basis that the fatigue predictions shown in this study are forecast. It may be inferred that when two dissimilar materials such as aluminium alloy and a ceramic fibre are cast together there must be many other possible candidates for initiating fatigue failure than the simple assumption given above. The fibres themselves and the area around them are likely areas of weakness, as are any inclusions which may be present when production takes place. It has been reported[92] that during the production of SiC fibres a round inclusion called "shot" can be seen in the fibre mix.

All metal matrix composites examined in this study are either commercial materials or candidate commercial materials. Such materials would be produced to minimise any unwanted inclusions. Also such materials would be expected to have good adhesion between fibre and matrix, in fact a lot of effort would have been expended to ensure that matrix and fibre bonded well together. For these reasons the materials scrutinised in this study would be expected to follow the fatigue assumption in the modified Theory of Cells.

The Theory of Cells calculates the stress within and around a fibre by dividing this area into eight sub-cells. By doing this, a fairly quick analysis can be carried out for a range of composites over all nominal strains. To check that this was not an over-simplification of the situation, some results were compared with both a 2-D and 3-D finite element analysis. All methods forecast an area of high stress just in front of the fibre within the composite but the 3-D finite element study also forecast a high interfacial stress between fibre and matrix and this would more probably be the area causing fatigue damage. When compared with experimental evidence it turned out that, using the stress from this interfacial area, the fatigue life was grossly under estimated compared to both the Theory of Cells and the stress from the frontal area forecast by the 3-D finite element analyse.

It was only possible to carry out a small number of tests at elevated temperatures and these were only on one material. The results from this are disappointing, as the Theory of Cells becomes less accurate in its prediction of fatigue life as the temperature around the composite increases. This inaccuracy is a result of the interaction of fatigue damage with creep of the material. Several attempts were made by the Author to incorporate creep into the modified Theory of Cells, but with little success.

It has been shown that the Theory of Cells can be used to forecast the fatigue life of a range of aluminium composites at ambient temperature. The use of the computer program used in the Theory of Cells predictions is not difficult and has been used by a number of under-graduate students with only minimum training. Although only aluminium alloys have been used in this study, there appears to be no reason why the analysis cannot be tested with other types of metal matrix composite or indeed with certain polymeric composites.

Chapter 8

8.1 Conclusion

1. For a range of aluminium metal matrix composites the prediction of modulus and yield stress from the Theory of Cells was in good agreement with experimental results.
2. Using a modified version of the Theory of Cells with fatigue data obtained from aluminium matrix materials and information on the failure stress of fibres or particulates, it was possible to make a prediction of the fatigue life of a variety of metal matrix composite materials.
3. The Theory of Cells could be used successfully to predict constant stress and constant strain fatigue life.
4. At ambient temperature, the predicted fatigue lives of the metal matrix composites were in close agreement with the experimental results in all cases except for the low cycle fatigue regime of 1000 cycles or less.
5. Failure when material life expectancy was below 1000 cycles may have been due to failed particulates causing high stress concentrations, or to metallurgical faults in the matrix material.
6. In the low cycle fatigue regime, the fatigue life as predicted by the Theory of Cells and a fatigue life prediction by a 3-D finite element analysis were compared to experimental results. Both theoretical methods have a similar accuracy in their predictive capabilities.
7. The Theory of Cells indicated an area of high stress in the matrix ahead of the fibre and this was confirmed using both a 2-D and 3-D finite element analysis.
8. The fatigue life predictions using the Theory of Cells became less accurate as the working temperature of the composite was increased.

9. A replica technique was used to show that fatigue crack initiation, for commercial metal matrix composites, did not occur before 80% of the total fatigue life of the composite.
10. A good agreement was obtained for the values of Young's Modulus and Poisson's ratio over a wide range of volume fractions for both a 2 dimensional finite element model and the Theory of Cells.
11. The Theory of Cells has been used to show that the match between the Young's Modulus of the fibre and the matrix material has a significant effect on the fatigue life of a metal matrix composite.

8.2 Suggestions for Future Work

1. Further development of the Theory of Cells needs to be made to allow accurate fatigue predictions at elevated temperatures. A creep component needs to be incorporated into the theory and a consistent fatigue failure criterion developed.
2. More investigation needs to be carried out into the low cycle –high stress region of fatigue failure and, if possible, modifications made to the theory to allow more accurate fatigue predictions in this region.

[1] Clyne, T.W. and Withers P.J. "An Introduction To Metal Matrix Composites", Cambridge University Press, 1993 p 467
[2] Holoway, S.R "Designing with Continuous Aluminium Matrix Composites", Composite Manufacturing and Tooling, Society of Manufacturing Engineers, 2000
[3] Rajagopal, S. "Squeeze Casting: A Review and Update", *J. Appl. Metalworking*, **1**, 1981 pp 503-8
[4] Stanford-Beal, C.A. and Clyne, T. W. "Extrusion and High Temperature Deformation of Fibre-Reinforced Aluminium", *Comp. Sci and Tech*, **35**, 1989, pp249-54
[5] Automotive Data Sheet "Saffil" http://www.saffil.com/pdfs/automotive/data/mmcprop.pdf
[6] Avezou J.C., Cole A.T., Gazzard S.T and Munro R "The Application of Squeeze Casting to Piston Technology" *T & N Technology for the 90's*, **19**, T & N Plc. Publication
[7] "Discontinuously Reinforced Aluminium Has Come Of Age". Aluminium Metal Matrix Composites Consortium. www.almmc.com
[8] Clyne, T.W. and Withers P.J. "An Introduction To Metal Matrix Composites", Cambridge University Press, 1993, p 461.
[9] Taya, M and Arsenault, R. J. "Metal Matrix Composites", Pergamon Press, 1989, pp1
[10] Backe, P, Schurmans, H. and Verhoest, J. "Inorganic Fibre and Composite Materials", Pergamon Press 1983
[11] Yuen J.L. and Petrasek D.W. "Elevated Temperature Fatigue Behaviour of Tungsten Fiber Reinforced Super-alloy Composites" *Journal of Composite Technology and Research*, **16**, 4, 1994, pp 343-351
[12] Taya, M and Arsenault, R. J. "Metal Matrix Composites", Pergamon Press, 1989, pp 238
[13] Llorca J. "Fatigue of Particle and Whisker Reinforced Metal Matrix Composites" *Progress in Material Science*, **47**, 3, 2002, p 303
[14] Clyne, T.W. and Withers P.J. "An Introduction To Metal Matrix Composites", Cambridge University Press, 1993, p 3.
[15] Brown A "Metal Matrix Composites on the Road", *Material World*, January 1993, pp 20 -21
[16] King J. E. and Bhattacharjee "Interfacial Effects on Fatigue and Fracture in Discontinuously Reinforced Metal Matrix Composites", *Material Science Forum*, **189-190**, 1995, pp43 -56
[17] Harris B. "Engineering Composite Materials" Institute of Materials, UK, pp 45 (1999)
[18] Bigelow C.A., Johnson W.S. and Naik R.A. " A Comparison of Various Micromechanical Models for Metal Matrix Composites" *Mechanics of Composite Materials and Structures*, **100**, 1989, pp 21-31
[19] Foye, R.L., "An evaluation of Various Engineering Estimates of the Transverse Properties of Unidirectional Composites" *Proceedings of the Tenth National SANPE Symposium - Advanced Fibrous Reinforced Composites.* November 1966.
[20] Dvorak G.L and Bahei-El-Din "Elastic-Plastic Behavior of Fibrous Composites" *J. Mech Phys. Solids* Vol. 27, 1979,pp51-72
[21] Hokins, D.A. and Chamis, C.C., "A Unique Set of Micromechanical Equations for High Temperature Metal Matrix Composites" *NASA* TM 87154 (1985)
[22] Aboudi, J,. "Elastoplasticity Theory for Composite Materials" *Solid Mechanics Archives* **11** pp. 141-183 (1986)
[23] Hill R. "A Self Consistent Mechanics of Composite Materials" *Journal of the Mechanics and Physics of Solids*, **13**, 1965 pp213-222
[24] Eshelby J. D. "The Determination of the Elastic of an Ellipsoidal Inclusion, and Related Problems" *Proc. Royal Society*, **A241**, 1957, pp376 -396.
[25] Dvorak G.L and Bahei-El-Din "Elastic-Plastic Behavior of Fibrous Composites" *J. Mech Phys. Solids* Vol. 27, 1979,pp51-72
[26] Bodner, S.R., "Review of a Unified Elastic Viscoplastic Theory" in "Unified Constitution Equations for Plastic Deformation and Creep in Engineering Alloys" Miller., A.K., ed. Elservier, New York pp. 273 -301 (1987)
[27] Benveniste Y. and Aboudi J. "A Continuum Model for Fiber Reinforced Materials with Debonding" *Int J Solds Structures*, **20**, 11/12, 1984, pp 935-951.
[28] Drumheller An effect of debonding on stress wave propagation in a composite material J. Appl. Mech 40 1146-1147 (1973)

[29] Aboudi J." Constitutive Equations for Elastioplastic Composites with Imperfect Bonding" *International Journal of Plasticit,* **4**, 1988,pp 103 - 125
[30] Jones J.P. and Whittier J.S. "Waves at a Flexibly Bonded Interface", *J. Appl. Mech*, **34**, pp 905-909
[31] Bodner, S.R., "Review of a Unified Elastic Viscoplastic Theory" in "Unified Constitution Equations for Plastic Deformation and Creep in Engineering Alloys" Miller., A.K., ed. Elservier, New York pp. 273 -301 (1987)
[32] Paley M. and Aboudi J." Micromechanical Analysis of Composites by the Generalized Cell Model" *Mechanics of Materials*, **14**, pp 127-139 (1992)
[33] Chawla K.K. "Composite Materials" .Springer-Verlag New York p79 (1987)
[34] Jero P.D. and Kearans R.J. "The Computation of Interfacial Roughness of Friction of Ceramic Fibres in a Glass Matrix", *Scripta Metall Mater.*, **24**, pp2315 –1318 (1990)
[35] Jang-Kyo Kim and Yiu-Wing Mai "Effect of Interface Strength on Metal Matrix Composite Properties", *Comprehensive Composite Materials*,**3**, Elservier. (2000)
[36] Watson M.C. and Clyne T. W. "The use of Single Fibre Push-Out Testing to Explore Interfacial Mechanics in SiC Monofilament Reinforced Ti", *Acta Metallt Mat.*, **40**, pp135 –140. (1992)
[37] Damage Mechanics of Composite Materials Ed R. Talreja Elservier Science 1994 p 246
[38] Jang-Kyo Kim and Yiu-Wing Mai "Effect of Interface Strength on Metal Matrix Composite Properties", *Comprehensive Composite Materials*,**3**, Elservier. (2000)
[39] A.F. Whitehouse and T.W. Clyne "Cavity Formation during Tensile Straining of Particulate and Short Fibre Metal Matrix Composites", *Acta Metall Mater.*, 41, 1701-1711, (1993)
[40] Aboudi J., "Constitutive Equations for Elastoplastic Composites with Imperfect Bonding", *International Journal of Plasticity,* **4**, pp 103-125 (1988).
[41] Suresh S. "Fatigue of Materials", Cambridge Solid State Science Series pp 405 (1991)
[42] Suresh S. "Fatigue of Materials", Cambridge Solid State Science Series pp 10 (1991)
[43] Harris B. "Engineering Composite Materials" Institute of Materials, UK, pp219 (1999)
[44] Johnson W. S. "fatigue Testing and Damage Development in Continues Fibre Reinforced Metal Matrix Composites" *Metal Matrix Composite : Testing, Analysis and Failure Modes,* **ASTM STP 1032,** American Society for Testing and Materials, Philadelphia pp 194 –224 (1989)

[45] Cook J and Gordon J.E. "A Mechanism for the Control of Crack Propagation in All-Brittle Systems", *Proc Roy Soc,* **282A**, pp 508-520 (1964)
[46] Sims G D And Gladman D G, "Effect of test conditions on the fatigue strength of a glass-fibre laminate: Part A. Frequency", *Plastics and Rubber: Materials and Applications,* **1**, p 41, (1978).
[47] Sensmeire M.D. and Wright. P.K., "The Effect of Fibre Bridging on Fatigue Crack Growth in Titanium Matrix Composites" in *Fundamentals Relationships Between Microstructures and Mechanical Properties of Metal Matrix Composites.* TMS. pp 441 –457 (1991)
[48] Johnson W. S. "Fatigue Testing and Damage Development in Continues Fibre Reinforced Metal Matrix Composites" *Metal Matrix Composite : Testing, Analysis and Failure Modes,* **ASTM STP 1032,** American Society for Testing and Materials, Philadelphia pp 194 –224 (1989)"
[49] Johnson W. S. "Fatigue Testing and Damage Development in Continues Fibre Reinforced Metal Matrix Composites" *Metal Matrix Composite : Testing, Analysis and Failure Modes,* **ASTM STP 1032,** American Society for Testing and Materials, Philadelphia pp 194 –224 (1989)
[50] Fleming W.J. and Dowson A.L. "Prediction of the Fatigue Life of an Aluminium Metal Matrix Composite Using Theory of Cells". *Science and Engineering of Composite Materials*, **8**, 4, 181-189. (1999).
[51] Clyne, T.W. and Withers P.J. "An Introduction To Metal Matrix Composites", Cambridge University Press, 1993 pp 117-120
[52] Fu L, Schmerling M and Marcus H.L. "Interfacial Studies of Aluminium Metal Matrix Composites" *Composite Materials- Fatigue and Fracture* ,**STP 907**, pp51 –72 (1986)
[53] Gouda M., Prewo, K. M. and McEvily, A. J., *Fatigue of Fibrous Composite Materials* , **ASTM STP 723** pp 639- 670, (1981)
[54] Taya M and Arsenault R.J "Metal Matrix Composite", Pergamon Press pp 155(1989)

[55] Botstein O, Arone R and Shipigler "Fatigue Crack Growth Mechanism in Al – SiC Particulate Metal Matrix Composite", *Material Science and Engineering*, **A128,** pp 15-22, (1990)
[56] Pearson S. "Initiation Of Fatigue Cracks In Commercial Aluminium Alloys And The Subsequent Propagation Of Very Short Cracks", *Eng Fracture Mechanics,***7**, pp235-247, (1975)
[57] Richie R O and Landford J. "Small Fatigue Cracks: A Statement Of The Problem And Potential Solution". *Mater Sci Eng*, **84**, pp11-16, (1996)
[58] Bruzzi MS and McHughs PE. "Methodology For Modelling The Small Crack Fatigue Behaviour Of Aluminium Alloys", *Int J Fatigue* **;24(10)**, pp1071-1078 (2002)
[59] Bruzzi MS and McHughs PE. "Application Of Closure Based Fatigue Modelling Methodology To Al-Sic Metal Matrix Composites", *Int J Fatigue* ,**25,** pp577-584 (2003)
[60] Ding, H. Z, Biermann, H., and Hartmann, O. "Low Cycle Fatigue Crack Growth And Life Prediction Of Short-Fibre Reinforced Aluminium Matrix Composites", *Int J Fatigue*,**25,** pp209-220, (2003)
[61] Matsumoto T and Victor C Li "Fatigue Life Analysis Of Fibre Reinforced Concrete With A Fracture Mechanics Based Model", *Cement & Concrete Composites,* **21** , pp249-261, (1999)
[62] Neu R W. "A Mechanistic Based Thermomechanical Fatigue Life Prediction Model For Metal Matrix Composites", *Fatigue Fracture Mater Struct*, **16**, 8, pp 811-828 (1993)
[63] Foringer M A, Robertson D D and Mall S "A Micromechanistic-Based Approach To Fatigue Life Modelling Of Titanium Matrix Composites",. *Composites Part B*, **28B**, pp507-521 (1997)
[64] Robertson D D and Mall S A "Micromechanical Relations for Fibre Reinforced Composite Using Free Transvers Shear Approach" Unpublished Paper.
[65] Robertson D D and Mall S A "Nonlinear Micromechanicals Based Analysis of Metal Matrix Composite Laminates", *Composite Science and Technology*, **52**, 3, pp 319 -331. (1994)
[66] Aboudi, J,. "Micromechanical Analysis of Composites by the Method of Cells" *Applied Mechanical Review* **42 (7)** pp.193 - 221 (1989)
[67] Aboudi, J,. "Mechanics of Composite Materials" *Studies in Applied Mechanics* **29** Elservier, New York pp. 76 -82 (1991)
[68] Arridge, R.G.C., "An Introduction to Polymer Mechanics" Taylor and Francis, London pp.142 -158 (1985)
[69] Rosenthal, D., and Asimow, R.A., "Introduction to Properties of Materials" Van Nostrand Reinhold, London pp. 184 (1971)
[70] Andersson, C.H., and Warren, R., "Silicon Carbide Fibers and their Potential for Use in Composite Materials: Part 1" *Composites* **15 (1)** pp. 21 (1984)
[71] Aboudi J "Micromechanical Analysis of Composites by the Method of Cells", *Applied Mechanics Review,* **42,** 7, pp193 –221, (1989)
[72] Bodner S. R. and Partom Y "Constitutive Equations for Elastic-Visco-Plastic Strain Hardening Materials", *J ApplMech,* **42**, pp385 –389, (1975)
[73] Mendelson, A., "Plasticity, Theory and Application" Kriegar Publishing Co., Melbourne pp. 20 (1988)
[74] Aboudi, J,. "Mechanics of Composite Materials" *Studies in Applied Mechanics* **29** Elservier, New York pp. 116 (1991)
[75] Temis, Y.M. Plasticity and Creep in engineering analysis. Analytical and Numerical Methods of Plasticity and Viscous-Elasticity Boundary Problems Solution. Sverdlovsk, Ac.of Sc of USSR, pp.100-106, 1986 (in Russian).
[76] Putchkov, I.V., Temis, J.M. Elastoplastic and damage model of structure material. Fifth USSR Symposium Low Cycle Fatigue.- *Failure Criteria and Material Structures*. Volgograd 1987. V2 pp. 50-52. (in Russian)
[77] Putchkov, I.V., Temis, J.M. Analytical formulas for elastoplastic response of structure materials under cyclic loading. *Problems of Strength.*1988, No9. pp.18-22. (in Russian)
[78] Putchkov I.V., Temis J.M. Elastoplastic and damage parameters of structures materials under cyclic loading. *Applied Problems of Strength and Plasticity*. University of N. Novgorod, 1992. pp.82-89

[79] Putchkov I.V., Temis Y.M., Dowson A.L., Damri D. Development of a finite element based strain accumulation model for the prediction of fatigue lives in highly stressed Ti components. *Int.J. Fatigue.* Vol.17, No 6, pp. 385-398, 1995

[80] Shnaderovich R. M. Strength under monotonic and cyclic loading. Mashinostroenie. Moscow. 1968. 343p. (in Russian).

[81] Dowson, A.L., Kwon, J.W., Healy, J.C., and Beevers, C.J., "Innovative Manufacturing, Design and Assessment of Aluminium Matrix Composites for High Temperature Performance" *Brite Euram Project* **BE 3398-89** (1993)

[82] Akid R. and Miller K. J. "The Effect of Solution pH on the Initiation and Growth of Short Fatigue Cracks". *Fracture Behaviour and Design of Materials and Structures*, **Proc ECF8,** Emas pp 11403-1411 (1990)

[83] Clyne T W and Withers P J, "An Introduction to Metal Matrix Composites" Cambridge University Press pp 73 (1993)

[84] Nieh T and G, Chellman D , " Modulus Measurement in Discontinuous Reinforced Al Composites" *Scripta Metallurgica* **18 (9)** pp 925-8 (1984)

[85] Llorca J, Suresh S, Needleman A, "An Experimental and Numerical Study of Cyclic Deformation in Metal Matrix Composites" *Metallurgical Transactions A* **23** pp. 925 (1992)

[86] Han H.L, Wang Z.G, Lizhi Sun, "Effects of Reinforcements Size on Low Cycle Fatigue Behaviour of SiC Particle Reinforced Aluminium Matrix Composites" *Scripa Metallurgica et Materiala* **33 (5)** pp. 782 (1995)

[87] Taya M and Arsenault R J, " Metal Matrix Composites" Pergamon Press, Oxford pp 49-50 (1989)

[88] Avezou J.C., Cole A.T., Gazzard S.T and Munro R "The Application of Squeeze Casting to Piston Technology" *T & N Technology for the 90's,* **19**, T & N Plc. Publication

[89] Zhang R.J. Wanh Z. and Simpson C. "Fatigue Fractography of Particulate SiC Reinforced Al(A356) Cast Alloy",*Materials Science and Engineering,* **A148**, pp 53 –66, (1991)

[90] Zhang R.J. Wanh Z. and Simpson C. "Fatigue Fractography of Particulate SiC Reinforced Al(A356) Cast Alloy",*Materials Science and Engineering,* **A148**, pp 53 –66, (1991)

[91] "An Experimental and Numerical Study of Cyclic Deformation in Metal-Matrix Composites" by Llorca J, Suresh S and Needleman A. Metallurgical Transactions A Volume 23A 1992 919-934

[92] Avezou J.C., Cole A.T., Gazzard S.T and Munro R "The Application of Squeeze Casting to Piston Technology" *T & N Technology for the 90's,* **19**, T & N Plc. Publication

Appendix A

Program for Predicting the Fatigue Life of Long Fibre Metal Matrix Composites

```
COMMON CM(10,10),CF(10,10),V(2,2),B(10,10),E(10,10)
       COMMON AS(3,3),ST(3,3),SA(3,3),PSI1(3,3),PSI2(3,3)
       COMMON PSI3(3,3),FI1(3,3),FI2(3,3),FI3(3,3),SIB(3,3)
       COMMON BD(10,10),BDT(10,10),B11(4,4),B22(4,4),B21(4,4 )
       COMMON B12(4,4),N(2),V1
       COMMON H,H1,H2,DW1DX2,DW2DX1,DW1DX3,DW3DX1,DW2DX3,DW3DX2
       COMMON T1,T2,T3,T4,T5,T6,T7,T8,T9,T10,T11,T12,T13,T14,T15
       COMMON T16,DELTA,DELTA1
       DIMENSION FAT(4),WP(3,3),L11(3,3),L22(3,3),L12(3,3),L21(3,3),
     * LAM(2,2),HN(2,2),TN(2,2),DNOUGHT(2,2),BA(6,6),EPL(3,3)
       DIMENSION J2(2,2),HK(3,3),TM(2,2),Z0(2,2),Z1(2,2),L33(3,3)
     * ,L13(3,3),L23(3,3),S11(2,2),S22(2,2),S33(3,3),S12(2,2)
       DIMENSION S23(2,2),Z(2,2),SL11(2,2),SL22(2,2),SL33(2,2),
     * SL12(2,2),SL13(2,2),SL23(2,2),WPD(2,2),S13(2,2)
       REAL KM,KF,J1,J2,J3,J4
       CHARACTER DATE*12,TIME*12
C      ***************************************************

       OPEN (UNIT=2,FILE='A5.DAT')
       WRITE(*,*) '                    '
       WRITE(*,*) ' WHAT IS THE DATE '
       WRITE(*,*) '  '
       READ(*,*) DATE
       WRITE(*,*) '                    '
       WRITE(*,*) ' WHAT IS THE TIME '
       WRITE(*,*) '  '
       READ(*,*) TIME
       WRITE(2,*) '    '
       WRITE(2,*) '       EDITION 6.0'
       WRITE(2,*) '       DATE: ',DATE
       WRITE(2,*) '       TIME ',TIME
       WRITE(2,*) '                          '
       WRITE(2,*) '                          '
       WRITE(2,*) 'HELLO EVERYBODY'
       WRITE(2,*) 'THE STRESS STRAIN CURVE PROGRAME'
C      ***************************************************
C       THE PLASTIC PROGRAMME
      EAM=72.5
```

```
      POSTM=.33
      POSAM=.33
      ETM=72.5
      EAF=400.
      POSTF=0.2
      POSAF=0.2
      ETF=400
      GAM=31.
      GAF=250.
      MUF=0
      TN(1,1)=0.000001
      TN(1,2)=10
      TN(2,1)=10
      TN(2,2)=10
      TM(1,1)=0.000001
      TM(1,2)=70
      TM(2,1)=70
      TM(2,2)=70
      Z0(1,1)=0.0000001
      Z0(1,2)=100
      Z0(2,1)=100
      Z0(2,2)=100
      Z1(1,1)=0.0000001
      Z1(1,2)=190
      Z1(2,1)=190
      Z1(2,2)=190
      DNOUGHT(1,1)=10E-15
      DNOUGHT(1,2)=10E-4
      DNOUGHT(2,1)=10E-4
      DNOUGHT(2,2)=10E-4
      H1=1
      DO 1 JJJ=1,60
      WRITE(*,*) '      '
1     CONTINUE
      WRITE(*,*) '  '
      WRITE(*,*) 'WHAT IS THE VOLUME FRACTION?'
      WRITE(*,*) '   '
      READ(*,*) VF


      CALL MATPROPS (EAM,POSTM,POSAM,ETM,EAF,POSTF,POSAF,ETF,
     *GAM,GAF,VF,ESTARA,POSTARA,ESTART,POSTART,GSTARA)
      CALL PRINTPROP(VF,ESTARA,ESTART,POSTARA,POSTART,
     *GSTARA)
      V1=H**2
      DO 470 K1=1,3
      DO 472 JJ=1,3
      ST(K1,JJ)=0
      L11(K1,JJ)=0
      L22(K1,JJ)=0
      L33(K1,JJ)=0
      L12(K1,JJ)=0
      L13(K1,JJ)=0
```

```
      L23(K1,JJ)=0
      WP(K1,JJ)=0
472   CONTINUE
470   CONTINUE

      ST(1,1)=0.1
      ST(2,2)=-ST(1,1)*POSTART
      ST(3,3)=ST(2,2)
      ST(1,2)=ST(1,1)
      ST(1,3)=0.0
      ST(2,3)=0.0
      DW1DX2=ST(1,2)
      DW2DX1=ST(1,2)
      DW1DX3=ST(1,3)
      DW3DX1=ST(1,3)
      DW2DX3=ST(2,3)


      DO 500 K=1,20
       CALL ALL
      MUM=CM(4,4)
      S1111=CF(1,1)*ST(1,1)+CF(1,2)*(FI2(1,1)+PSI3(1,1))
     * -2*MUF*L11(1,1)
      S1112=CM(1,1)*ST(1,1)+CM(1,2)*(FI2(1,2)+PSI3(1,2))
     * -2*MUM*L12(1,1)
       S1122=CM(1,1)*ST(1,1)+CM(1,2)*(FI2(2,1)+PSI3(2,1))
     * -2*MUM*L21(1,1)
      S2211=CF(1,2)*ST(1,1)+CF(2,2)*FI2(1,1)+CF(2,3)*PSI3(1,1)
     * -2*MUF*L11(2,2)
      S2212=CM(1,2)*ST(1,1)+CM(2,2)*FI2(1,2)+CM(2,3)*PSI3(1,2)
     * -2*MUM*L12(2,2)
      S2221=CM(1,2)*ST(1,1)+CM(2,2)*FI2(2,1)+CM(2,3)*PSI3(2,1)
     * -2*MUM*L21(2,2)
      S2222=CM(1,2)*ST(1,1)+CM(2,2)*FI2(2,2)+CM(2,3)*PSI3(2,2)
     * -2*MUM*L22(2,2)
      S3311=CF(1,2)*ST(1,1)+CF(2,3)*FI2(1,1)+CF(2,2)*PSI3(1,1)
     * -2*MUF*L11(3,3)
      S3312=CM(1,2)*ST(1,1)+CM(2,3)*FI2(1,2)+CM(2,2)*PSI3(1,2)
     * -2*MUM*L12(3,3)
      S3321=CM(1,2)*ST(1,1)+CM(2,3)*FI2(2,1)+CM(2,2)*PSI3(2,1)
     * -2*MUM*L21(3,3)
      S3322=CM(1,2)*ST(1,1)+CM(2,3)*FI2(2,2)+CM(2,2)*PSI3(2,2)
     * -2*MUM*L22(3,3)
      S1211=CF(4,4)*(DW2DX1+FI1(2,1))-2*CF(4,4)*L21(1,2)
      S1212=CM(4,4)*(DW2DX1+FI1(1,2))-2*CM(4,4)*L12(1,2)
      S1222=CM(4,4)*(DW2DX1+FI1(2,2))-2*CM(4,4)*L22(1,2)
      S1311=CF(4,4)*(DW3DX1+PSI1(1,1))-2*CM(4,4)*L11(1,3)
      S1312=CM(4,4)*(DW3DX1+PSI1(1,2))-2*CM(4,4)*L12(1,3)
      S1321=CM(4,4)*(DW3DX1+PSI1(2,1))-2*CM(4,4)*L21(1,3)
      S1322=CM(4,4)*(DW3DX1+PSI1(2,2))-2*CM(4,4)*L22(1,3)
      S2311=CF(6,6)*N(1)-2*CF(6,6)*L11(2,3)
      S2321=CM(6,6)*N(2)-2*CM(6,6)*L21(2,3)
      S2312=CM(6,6)*N(2)-2*CM(6,6)*L12(2,3)
      S2322=CM(6,6)*N(2)-2*CM(6,6)*L22(2,3)
```

```
      S11(1,1)=(2*S1111-S2211-S3311)/3
      S11(1,2)=(2*S1112-S2212-S3312)/3
      S11(2,1)=(2*S1121-S2221-S3321)/3
      S11(2,2)=(2*S1122-S2222-S3322)/3
      S22(1,1)=(2*S2211-S3311-S1111)/3
      S22(1,2)=(2*S2212-S3312-S1112)/3
      S22(2,1)=(2*S2221-S3321-S1121)/3
      S22(2,2)=(2*S2222-S3322-S1122)/3
      S12(1,1)=S1211
      S12(2,1)=S1221
      S12(1,2)=S1212
      S12(2,2)=S1222
      S23(1,1)=S2311
      S23(1,2)=S2312
      S23(2,1)=S2321
      S23(2,2)=S2322
      S13(1,1)=S1311
      S13(1,2)=S1312
      S13(2,1)=S1321
      S13(2,2)=S1322
      J2(1,1)=((S1111+S2211)**2+(S2211-S3311)**2+(S3311-S1111)**2)
      J2(1,1)=(J2(1,1)+6*(S1211**2+S2311**2+S1311**2))/6
      J2(1,2)=(S1112+S2212)**2+(S2212-S3312)**2+(S3312-S1112)**2
      J2(1,2)=(J2(1,2)+6*(S1212**2+S2312**2+S1312**2))/6
      J2(2,1)=(S1121+S2221)**2+(S2221-S3321)**2+(S3321-S1121)**2
      J2(2,1)=(J2(2,1)+6*(S1221**2+S2321**2+S1321**2))/6
      J2(2,2)=(S1122+S2222)**2+(S2222-S3322)**2+(S3322-S1122)**2
      J2(2,2)=(J2(2,2)+6*(S1222**2+S2322**2+S1322**2))/6
      DO 502 K1=1,2
      DO 504 JJ=1,2
      HN(K1,JJ)=0.5*(TN(K1,JJ)+1)/TN(K1,JJ)
      EX=-TM(K1,JJ)*WP(K1,JJ)/Z0(K1,JJ)
      Z(K1,JJ)=Z1(K1,JJ)+(Z0(K1,JJ)-Z1(K1,JJ))*EXP(EX)
      XP=-HN(K1,JJ)*(Z(K1,JJ)**2/(3*J2(K1,JJ)))**(TN(K1,J))
      XP=XP/J2(K1,JJ)**0.5
      LAM(K1,JJ)=DNOUGHT(KJ,JJ)*EXP(XP)
      SL11(K1,JJ)=LAM(K1,JJ)*S11(K1,JJ)
      SL22(K1,JJ)=LAM(K1,JJ)*S22(K1,JJ)
      SL33(K1,JJ)=LAM(K1,JJ)*S33(K1,JJ)
      SL12(K1,JJ)=LAM(K1,JJ)*S12(K1,JJ)
      SL13(K1,JJ)=LAM(K1,JJ)*S13(K1,JJ)
      SL23(K1,JJ)=LAM(K1,JJ)*S23(K1,JJ)
      WPD(K1,JJ)=LAM(K1,JJ)*2*J2(K1,JJ)
504   CONTINUE
502   CONTINUE

      HK(1,1)=2*Q1*MUM*(L12(2,2)-L22(2,2))+2*Q2*(MUM*L21(2,2)
     * -MUF*L11(2,2))
      HK(1,1)=HK(1,1)+(2*Q3*(MUM*L12(3,3)-MUF*L11(3,3))
     *+2*Q4*MUM*(L21(3,3)-L22(3,3)))
      HK(1,1)=HK(1,1)+2*(MUF*V(1,1)*L11(1,1)+MUM*(V(1,2)*L12(1,1)
     *+V(2,1)*L21(1,1)+V(2,2)*L22(1,1)))
      HK(1,1)=HK(1,1)/V1
      HK(2,2)=2*QD1*MUM*(L12(2,2)-L22(2,2))+2*QD2*(MUM*L21(2,2)
```

```
     * -MUF*L11(2,2))
      HK(2,2)=HK(2,2)+2*QD3*(MUM*L12(3,3)-MUF*L11(3,3)
     *+2*QD4*MUM*(L21(3,3)-L22(3,3)))
      HK(2,2)=HK(2,2)+2*(MUF*V(1,1)*L11(2,2)+MUM*(V(1,2)*L12(2,2)
     *+V(2,1)*L21(2,2)+V(2,2)*L22(2,2)))
      HK(2,2)=HK(2,2)/V1
      HK(3,3)=HK(2,2)
      HK(1,2)=2*(V(1,1)*CF(4,4)*L11(1,2)+CM(4,4)*(V(1,2)*L12(1,2)
     *+V(2,1)*L21(1,2)+V(2,2)*L22(1,2)))
      HK(1,2)=HK(1,2)-2*(V(1,1)*H2*CF(4,4)-V(2,1)*H1*CM(4,4))
     * *(CF(4,4)*L11(1,2)-CM(4,4)*L12(2,1))
      HK(1,2)=HK(1,2)/V1
      HK(2,3)=2*CF(6,6)*CM(6,6)

HK(2,3)=HK(2,3)*(V(1,1)*L11(2,3)+V(1,2)*L12(2,3)+V(2,1)*L21(2,3)
     *+V(2,2)*L22(2,3))/DELTA1
      A=B(2,2)**2*B(1,1)+(2*B(1,2)**2*B(2,3))
      A=A-(2*B(1,2)**2*B(2,2))-(B(2,3)**2*B(1,1))
      BA(1,1)=(B(2,2)**2-B(2,3)**2)/A
      BA(1,2)=B(1,2)*(B(2,2)-B(2,3))/A
      BA(1,3)=B(1,2)*(B(2,3)-B(2,2))/A
      BA(2,2)=(B(1,1)*B(2,2)-B(1,2)**2)/A
      BA(4,4)=1/B(4,4)
      BA(6,6)=1/B(6,6)
      BA(3,2)=(B(1,2)**2+B(1,1)*B(2,3))/A
      EPL(1,1)=BA(1,1)*HK(1,1)+BA(1,2)*HK(2,2)+BA(1,3)*HK(3,3)
      EPL(2,2)=BA(1,2)*HK(1,1)+BA(2,2)*HK(2,2)+BA(3,2)*HK(3,3)
      EPL(3,3)=BA(1,1)*HK(1,1)+BA(3,2)*HK(2,2)+BA(2,2)*HK(3,3)
      EPL(1,2)=BA(4,4)*HK(1,2)
      EPL(1,3)=BA(4,4)*HK(1,3)
      EPL(2,3)=BA(6,6)*HK(2,3)
      AS(1,1)=E(1,1)*(ST(1,1)-EPL(1,1))+E(1,2)*(ST(2,2)-EPL(2,2))
      AS(1,1)=AS(1,1)+E(3,2)*(ST(3,3)-EPL(3,3))
      AS(2,2)=E(1,2)*(ST(1,1)-EPL(1,1))+E(3,2)*(ST(2,2)-EPL(2,2))
      AS(2,2)=AS(2,2)+E(2,2)*(ST(3,3)-EPL(3,3))
      AS(3,3)=E(1,2)*(ST(1,1)-EPL(1,1))+E(3,2)*(ST(2,2)-EPL(2,2))
      AS(3,3)=AS(3,3)+E(2,2)*(ST(3,3)-EPL(3,3))
      AS(1,2)=E(4,4)*(ST(1,2)-EPL(1,2))
      AS(1,3)=E(4,4)*(ST(1,3)-EPL(1,3))
      AS(2,3)=E(6,6)*(ST(2,3)-EPL(2,3))

      DO 510 K1=1,2
      DO 512 JJ=1,2
      L11(K1,JJ)=L11(K1,JJ)+SL11(K1,JJ)
      L22(K1,JJ)=L22(K1,JJ)+SL22(K1,JJ)
      L33(K1,JJ)=L33(K1,JJ)+SL33(K1,JJ)
      L12(K1,JJ)=L12(K1,JJ)+SL12(K1,JJ)
      L13(K1,JJ)=L13(K1,JJ)+SL13(K1,JJ)
      L23(K1,JJ)=L23(K1,JJ)+SL23(K1,JJ)
      WP(K1,JJ)=(WP(K1,JJ)+LAM(K1,JJ)*.01*2*J2(K1,JJ))
  512 CONTINUE
  510 CONTINUE
```

Appendix B

Program for Predicting the Fatigue Life of Short Fibre Metal Matrix Composites

```
      PROGRAM SHORT51
C       THREE DIMENSIONAL METHOD OF CELLS FOR ISOTROPIC PHASES
C       IMPLICIT DOUBLE PRECISION (A-H,O-Z)

C       ************************************
C       *                                  *
C       *      SHORT FIBRE  PROGRAMME      *
c       *         RANDOM FIBERS            *
C       *           EDITION 6R.0.1         *
C       *         July 17th 2000           *
C       *                                  *
C       *  Modified Plastic deformation    *
C       *  included and Cleaned up         *
C       ************************************

      COMMON /PLASTIC/ E1P(2,2,2), E2P(2,2,2), E3P(2,2,2)
      REAL L1,L2,N1,N2,MU1,MU2

C       DIFINE THE GEOMETRICAL DIMENSIONS OF THE SUBCELLS
C       VOL=INCLUSION VOLUME RATIO,ASP=ASPECT RATIO= DI/HI

      VOL=0.35
      ASP=1.3
      H1=ROOT(-VOL*(ASP-1)/ASP,-VOL/ASP)
      L1=H1
      D1=ASP*H1
      H2=1-H1
      L2=1-L1
      D2=H2

C      DEFINE THE PROPERTIES OF MATERIAL 1 (INCLUSION)IN
SUBCELL(1,1,1),
C      AND MATERIAL 2 (MATRIX ) IN THE OTHER 7 SUBCELLS
C      E=YOUNG , FN= POISSON , ALPHA= CTE
```

```
      E1=468.0E9
      FN1=0.25
      ALPHA1=5.0E-6
C       Y IS THE MATERIAL YIELD STRESS
C       N IS THE PLASTIC INDEX
C       MU IS THE PLASTIC MODULUS

      Y1=111200.E6
      N1=4.0
      MU1=2.0E8

      E2=72.E9
      FN2=0.33
      ALPHA2=5.1E-6

      Y2=3591.E6
      N2=1.03
      MU2=4.E9

      OPEN(UNIT=2,FILE='t029.DAT')

      WRITE(2,*) 'RESULTS USING DATA FROM'
      WRITE(2,*) 'Stokes          '
      WRITE(2,*) 'ASP=2.5           '
      WRITE(2,*) 'July 1 2002         '
      WRITE(2,*) 'e 72 GPa              '
      WRITE(2,*) '                    '

C       SET THE PLASTIC STRAINS OF THE 8 SUBCELLS = 0
(INITIALIZATION)
      DO 1 I=1,2
      DO 1 J=1,2
      DO 1 K=1,2
      E1P(I,J,K)=0.
      E2P(I,J,K)=0.
   1    E3P(I,J,K)=0.

C       DETERMINE THE EFFECTIVE STIFFNESS MATRIX [B] OF THE COMPOSITE
C       SEE EQN.(3.101) IN THE BOOK.
      E1B=1.
      E2B=0.
      E3B=0.
      TEM=0.
      E4B=0.
      E5B=0.
      E6B=0.
      II=1


      CALL MOC3D (D1,H1,L1,D2,H2,L2,E1,FN1,ALPHA1,E2,FN2,ALPHA2,
     1              E1B,E2B,E3B,TEM,S1B,S2B,S3B,
     2              E4B,E5B,E6B,S4B,S5B,S6B,II
     3              ,Y1,N1,MU1,Y2,N2,MU2)
      B11=S1B/E1B
```

```
      B21=S2B/E1B
      B31=S3B/E1B

      E1B=0.
      E2B=1.
      E3B=0.
      TEM=0.
      E4B=0.
      E5B=0.
      E6B=0.
      II=2

      CALL MOC3D (D1,H1,L1,D2,H2,L2,E1,FN1,ALPHA1,E2,FN2,ALPHA2,
     1               E1B,E2B,E3B,TEM,S1B,S2B,S3B,
     2               E4B,E5B,E6B,S4B,S5B,S6B,II
     3               ,Y1,N1,MU1,Y2,N2,MU2)

      B12=S1B/E2B
      B22=S2B/E2B
      B32=S3B/E2B

      E1B=0.
      E2B=0.
      E3B=1.
      TEM=0.
      E4B=0.
      E5B=0.
      E6B=0.
      II=3


       CALL MOC3D (D1,H1,L1,D2,H2,L2,E1,FN1,ALPHA1,E2,FN2,ALPHA2,
     1               E1B,E2B,E3B,TEM,S1B,S2B,S3B,
     2               E4B,E5B,E6B,S4B,S5B,S6B,II
     3               ,Y1,N1,MU1,Y2,N2,MU2)

      B13=S1B/E3B
      B23=S2B/E3B
      B33=S3B/E3B



C       EFFECTIVE SHEAR MODULI
      E1B=0.
      E2B=0.
      E3B=0.
      TEM=0.
      E4B=1.
      E5B=1.
      E6B=1.
      II=4

      CALL MOC3D (D1,H1,L1,D2,H2,L2,E1,FN1,ALPHA1,E2,FN2,ALPHA2,
     1               E1B,E2B,E3B,TEM,S1B,S2B,S3B,
```

```
     2               E4B,E5B,E6B,S4B,S5B,S6B,II
     3               ,Y1,N1,MU1,Y2,N2,MU2)

      B44=S4B/(2*E4B)
      B55=S5B/(2*E5B)
      B66=S6B/(2*E6B)


      AAA=(B11+B22+B33)/3
      BBB=(B23+B13+B12)/3
      CCC=(B44+B55+B66)/3
      RB11=(3*AAA+2*BBB+4*CCC)/5
      RB12=(AAA+4*BBB-2*CCC)/5
      RB66=(AAA-BBB+3*CCC)/5
      E1B=3.
      E2B=2
      E3B=1
      RS11=RB11*E1B+RB12*E2B+RB12*E3B
      RS22=RB11*E2B+RB12*E1B+RB12*E3B
      RS33=RB11*E3B+RB12*E1B+RB12*E2B
      XODR=RB66*(3*RB12+2*RB66)/(RB12+RB66)
      POSR= RB12/(2*(RB12+RB66))
      WRITE(2,*) 'RESULTS USING THE OVERALL B MATRIX'
      WRITE(2,*) '                              '
      WRITE(2,*) '  '
      WRITE(2,*) 'RMOD RPOS          ',XODR,POSR
      WRITE(2,*) '                   '


C       WORK OUT THE RANDOM STRESS ON THE CELLS
        WRITE(2,*) '       FIBRE       MATRIX      OVERALL  OVERALL'
        WRITE(2,*) '      STRESS      STRESS     STRESS    STRAIN  '
        WRITE(2,*) '        MPa           MPa          MPa        '

      DO 345 XCT=.00001,.0002,.00001
      E1B=XCT
      E2B=-E1B*POSR
      E3B=E2B
      TEM=0.
      E4B=0.
      E5B=0.
      E6B=0.
      II=5


      CALL MOC3D (D1,H1,L1,D2,H2,L2,E1,FN1,ALPHA1,E2,FN2,ALPHA2,
     1              E1B,E2B,E3B,TEM,S1B,S2B,S3B,
     2              E4B,E5B,E6B,S4B,S5B,S6B,II
     3              ,Y1,N1,MU1,Y2,N2,MU2)

 345   CONTINUE
C       DETERMINE THE EFFECTIVE GAMA AND CTE
      E1B=0.
      E2B=0.
```

```
      E3B=0.
      TEM=1.
      E4B=0.
      E5B=0.
      E6B=0.
      II=0

      CALL MOC3D (D1,H1,L1,D2,H2,L2,E1,FN1,ALPHA1,E2,FN2,ALPHA2,
     1              E1B,E2B,E3B,TEM,S1B,S2B,S3B,
     2              E4B,E5B,E6B,S4B,S5B,S6B,II
     3              ,Y1,N1,MU1,Y2,N2,MU2)

      GAMA1S=-S1B/TEM
      GAMA2S=-S2B/TEM
      GAMA3S=-S3B/TEM

      ALPHA2S=(GAMA1S*B12-GAMA2S*B11)/(2*B12**2-B11*(B22+B23))
      ALPHA1S=(GAMA1S-2*B12*ALPHA2S)/B11

      E11=B11
      E12=B12
      E13=E12
      E22=0.75*B22+0.25*B23+0.5*B66
      E33=E22
      E23=(B22+B33)/8.
      E23=E23+0.75*B23
      E23=E23-B66/2.
      E44=(B44+B55)/2.
      E55=E44
      E66=(E22-E33)*0.5

      ESTARA=B11-2*B12**2/(B22+B23)
      POSTARA=B12/(B22+B23)
      ESTART=B11*(B22+B23)-2*B12**2
      ESTART=ESTART*(B22-B23)/(B11*B22-B12**2)
      POSTART=(B11*B23-B12**2)
      POSTART=POSTART/(B11*B22-B12**2)
      GSTARA=B44
       WRITE(2,*) '                                    '
       WRITE(2,*) '                                    '
       WRITE(2,*) 'THIS IS THE NON RANDOM FIBER RESULTS'
       WRITE(2,*) 'ORIGINAL MODUL FIBRE      ',E1
       WRITE(2,*) 'ORIGINAL MU  FIBRES       ',FN1
       WRITE(2,*) 'ORIGINAL MODUL MATRIX     ',E2
       WRITE(2,*) 'ORIGINAL MU  MATRIX       ',FN2
       WRITE(2,*) 'PLASTIC MODULUS           ',MU2
       WRITE(2,*) 'N2                        ',N2

       WRITE(2,*) 'WIDTH OF FIBRE          = ',D1
       WRITE(2,*) 'LENGTH OF FIBRE         = ',L1
       WRITE(2,*) 'HEIGHT OF FIBRE         = ',H1
       WRITE(2,*) 'MATRIX H2               = ',H2
       WRITE(2,*) 'MATRIC L2               = ',L2
       WRITE(2,*) 'MATRIX D2               = ',D2
```

```
      WRITE(2,*) 'ASPECT RATIO            = ',ASP
      WRITE(2,*) 'VOLUME RATIO OF FIBRE   = ',VOL
      WRITE(2,*) 'AXIAL YOUNGS MODULUS    = ',ESTARA
      WRITE(2,*) 'TRANSVERE YOUNGS MODULUS= ',ESTART
      WRITE(2,*) 'AXIAL POSIONS RATIO     = ',POSTARA
      WRITE(2,*) 'TRANSVERE POSIONS RATIO = ',POSTART
      WRITE(2,*) 'AXIAL SHEAR MODULUS     = ',GSTARA
      WRITE(2,*) 'THIS IS THE END OF THE NON RANDOM FIBER RESULTS'

C     NOW DETERMINE THE STRESS CONCENTRATION MATRIX BY SETTING
C     ALL STRESSES TO ZERO EXCEPT ONE ( PAGE 114)

      END


      SUBROUTINE MOC3D
(D1,H1,L1,D2,H2,L2,E1,FN1,ALPHA1,E2,FN2,ALPHA2,
     1                    E1B,E2B,E3B,TEM,S1B,S2B,S3B,
     2                    E4B,E5B,E6B,S4B,S5B,S6B,II
     3                    ,Y1,N1,MU1,Y2,N2,MU2)

C     THE 3-D VERSION OF THE METHOD OF CELLS
C     REF: JACOB ABOUDI MECHANICS OF COMPOSITE MATERIALS
C
C
C
C     E1B,E2B,E3B,E4B,E5B,E6B ARE THE APPLIED TOTAL STRAINS
C     TEM= TEMPERATURE
C     S1B,S2s,S3B,S4B,S5B,S6B ARE THE RESULTING AVERAGE STRESSES
C     SI, s2, S3 ,S4, S5, S6 ARE THE STRESSES IN THE 8 SUBCELLS
C     NOTE : PLASTICITY IS INCORPOBATED IN THE NOR@WiL DIRECTIONS
ONLY,
C     I.E., NO PLASTICITY EFFECTS EXIST IN SHEAR

C     IMPLICIT DOUBLE PRECISION (A-H,O-Z)

      DIMENSION A(24,25), B(24)
      COMMON /PLASTIC/ E1P(2,2,2), E2P(2,2,2), E3P(2,2,2)
      DIMENSION S1(2,2,2), S2(2,2,2), S3(2,2,2)
      DIMENSION S4(2,2,2), S5(2,2,2), S6(2,2,2)
      DIMENSION VN(2,2,2), WN(2,2,2), XN(2,2,2)
      DIMENSION B111(6,6),B112(6,6),B122(6,6),B222(6,6)
      DIMENSION B212(6,6),B221(6,6),B121(6,6),B211(6,6)
      DIMENSION RB111(6,6),RB112(6,6),RB122(6,6),RB222(6,6)
      DIMENSION RB212(6,6),RB221(6,6),RB121(6,6),RB211(6,6)
      DIMENSION RS1(2,2,2),RS2(2,2,2),RS3(2,2,2)
      REAL L1,L2,N1,N2,MU1,MU2

C       FL,FM=LAME CONSTANTS

      FL1=E1*FN1/((1+FN1)*(1-2*FN1))
      FM1=0.5*E1/(1+FN1)
      GAMA1=(3*FL1+2*FM1)*ALPHA1
      FL2=E2*FN2/((1+FN2)*(1-2*FN2))
```

```
      FM2=0.5*E2/(1+FN2)
      GAMA2=(3*FL2+2*FM2)*ALPHA2

      DO 1 I=1,24
           B(I)=0
      DO 1 J=1,24
    1       A(I,J)=0
      DO 333 I=1,2
      DO 333 J=1,2
      DO 333 KM=1,2
      E1P(I,J,KM)=0.0
      E2P(I,J,KM)=0.0
      E3P(I,J,KM)=0.0
  333   CONTINUE

C       EQNS. (3.95) :
      A(1,1)=FL1+2*FM1
      A(1,9)=FL1
      A(1,17)=FL1
      A(1,5)=-(FL2+2*FM2)
      A(1,13)=-FL2
      A(1,21)=-FL2

      A(2,2) =FL2+2*FM2
      A(2,10)=FL2
      A(2,18)=FL2
      A(2,6)=-(FL2+2*FM2)
      A(2,14)=-FL2
      A(2,22)=-FL2

      A(3,3)=FL2+2*FM2
      A(3,11)=FL2
      A(3,19)=FL2
      A(3,7)=-(FL2+2*FM2)
      A(3,23)=-FL2
      A(3,15)=-FL2

      A(4,4)=FL2+2*FM2
      A(4,12)=FL2
      A(4,20)=FL2
      A(4,8)=-(FL2+2*FM2)
      A(4,16)=-FL2
      A(4,24)=-FL2

      A(5,9)=FL1+2*FM1
      A(5,1)=FL1
      A(5,17)=FL1
      A(5,11)=-(FL2+2*FM2)
      A(5,3)=-FL2
      A(5,19)=-FL2

      A(6,10)=FL2+2*FM2
      A(6,2)=FL2
      A(6,18)=FL2
```

```
      A(6,12)=-(FL2+2*FM2)
      A(6,4)=-FL2
      A(6,20)=-FL2

      A(7,13)=FL2+2*FM2
      A(7,5)=FL2
      A(7,21)=FL2
      A(7,15)=-(FL2+2*FM2)
      A(7,7)=-FL2
      A(7,23)=-FL2

      A(8,14)=FL2+2*FM2
      A(8,6)=FL2
      A(8,22)=FL2
      A(8,16)=-(FL2+2*FM2)
      A(8,8)=-FL2
      A(8,24)=-FL2

      A(9,17)=FL1+2*FM1
      A(9,1)=FL1
      A(9,9)=FL1
      A(9,18)=-(FL2+2*FM2)
      A(9,2)=-FL2
      A(9,10)=-FL2

      A(10,19)=FL2+2*FM2
      A(10,3)=FL2
      A(10,11)=FL2
      A(10,20)=-(FL2+2*FM2)
      A(10,4)=-FL2
      A(10,12)=-FL2

      A(11,21)=FL2+2*FM2
      A(11,5)=FL2
      A(11,13)=FL2
      A(11,22)=-(FL2+2*FM2)
      A(11,6)=-FL2
      A(11,14)=-FL2

      A(12,23)=FL2+2*FM2
      A(12,7)=FL2
      A(12,15)=FL2
      A(12,24)=-(FL2+2*FM2)
      A(12,8)=-FL2
      A(12,16)=-FL2

C               EQNS. (3.90)    :
      A(13,1)=D1
      A(13,5)=D2

      A(14,2)=D1
      A(14,6)=D2

      A(15,3)=D1
```

```
      A(15,7)=D2

      A(16,4)=D1
      A(16,8)=D2

      A(17,9)=H1
      A(17,11)=H2

      A(18,10)=H1
      A(18,12)=H2

      A(19,13)=H1
      A(19,15)=H2

      A(20,14)=H1
      A(20,16)=H2

      A(21,17)=L1
      A(21,18)=L2

      A(22,19)=L1
      A(22,20)=L2

      A(23,21)=L1
      A(23,22)=L2

      A(24,23)=L1
      A(24,24)=L2

C       R.H.S. :
      B(1)=(GAMA1-GAMA2)*TEM+2*FM1*E1P(1,1,1)-2*FM2*E1P(2,1,1)
      B(2)=2*FM2*(E1P(1,1,2)-E1P(2,1,2))
      B(3)=2*FM2*(E1P(1,2,1)-E1P(2,2,1))
      B(4)=2*FM2*(E1P(1,2,2)-E1P(2,2,2))

      B(5)=(GAMA1-GAMA2)*TEM+2*FM1*E2P(1,1,1)-2*FM2*E2P(1,2,1)
      B(6)=2*FM2*(E2P(1,1,2)-E2P(1,2,2))
      B(7)=2*FM2*(E2P(2,1,1)-E2P (2,2,1))
      B(8)=2*FM2*(E2P(2,1,2)-E2P(2,2,2))

      B(9)=(GAMA1-GAMA2)*TEM+2*FM1*E3P(1,1,1)-2*FM2*E3P(1,1,2)
      B(10)=2*FM2*(E3P(1,2,1)-E3P(1,2,2))
      B(11)=2*FM2*(E3P(2,1,1)-E3P(2,1,2))
      B(12)=2*FM2*(E3P(2,2,1)-E3P(2,2,2))

      B(13)=(D1+D2)*E1B
      B(14)=(D1+D2)*E1B
      B(15)=(D1+D2)*E1B
      B(16)=(D1+D2)*E1B

      B(17)=(H1+H2)*E2B
      B(18)=(H1+H2)*E2B
      B(19)=(H1+H2)*E2B
      B(20)=(H1+H2)*E2B
```

```
      B(21)=(L1+L2)*E3B
      B(22)=(L1+L2)*E3B
      B(23)=(L1+L2)*E3B
      B(24)=(L1+L2)*E3B

C       SOLUTIoN OF THE 24 EQNS.:

      CALL SOLVEQ(A,B,24,B,DTR)

C       THE STRESSES IN THE 8 SUBCELLS (SEE EQNS.(8.76)) :
C       FIRST CALCULATE THE PLASTIC COMPONENT

      S1(1,1,1)=(FL1+2*FM1)*B(1)+FL1*(B(9)+B(17))-2*FM1*E1P(1,1,1)
     &              -GAMA1*TEM
      S1(1,1,2)=(FL2+2*FM2)*B(2)+FL2*(B(10)+B(18))-2*FM2*E1P(1,1,2)
     &              -GAMA2*TEM
      S1(1,2,1)=(FL2+2*FM2)*B(3)+FL2*(B(11)+B(19))-2*FM2*E1P(1,2,1)
     &              -GAMA2*TEM
      S1(1,2,2)=(FL2+2*FM2)*B(4)+FL2*(B(12)+B(20))-2*FM2*E1P(1,2,2)
     &              -GAMA2*TEM
      S1(2,1,1)=(FL2+2*FM2)*B(5)+FL2*(B(13)+B(21))-2*FM2*E1P(2,1,1)
     &              -GAMA2*TEM
      S1(2,1,2)=(FL2+2*FM2)*B(6)+FL2*(B(14)+B(22))-2*FM2*E1P(2,1,2)
     &              -GAMA2*TEM
      S1(2,2,1)=(FL2+2*FM2)*B(7)+FL2*(B(15)+B(23))-2*FM2*E1P(2,2,1)
     &              -GAMA2*TEM
      S1(2,2,2)=(FL2+2*FM2)*B(8)+FL2*(B(16)+B(24))-2*FM2*E1P(2,2,2)
     &              -GAMA2*TEM


      S2(1,1,1)=(FL1+2*FM1)*B(9)+FL1*(B(1)+B(17))-2*FM1*E2P(1,1,1)
     &              -GAMA1*TEM
      S2(1,1,2)=(FL2+2*FM2)*B(10)+FL2*(B(2)+B(18))-2*FM2*E2P(1,1,2)
     &              -GAMA2*TEM
      S2(1,2,1)=(FL2+2*FM2)*B(11)+FL2*(B(3)+B(19))-2*FM2*E2P(1,2,1)
     &              -GAMA2*TEM
      S2(1,2,2)=(FL2+2*FM2)*B(12)+FL2*(B(4)+B(20))-2*FM2*E2P(1,2,2)
     &              -GAMA2*TEM
      S2(2,1,1)=(FL2+2*FM2)*B(13)+FL2*(B(5)+B(21))-2*FM2*E2P(2,1,1)
     &              -GAMA2*TEM
      S2(2,1,2)=(FL2+2*FM2)*B(14)+FL2*(B(6)+B(22))-2*FM2*E2P(2,1,2)
     &              -GAMA2*TEM
      S2(2,2,1)=(FL2+2*FM2)*B(15)+FL2*(B(7)+B(23))-2*FM2*E2P(2,2,1)
     &              -GAMA2*TEM
      S2(2,2,2)=(FL2+2*FM2)*B(16)+FL2*(B(8)+B(24))-2*FM2*E2P(2,2,2)
     &              -GAMA2*TEM
      S3(1,1,1)=(FL1+2*FM1)*B(17)+FL1*(B(9)+B(1))-2*FM1*E3P(1,1,1)
     &              -GAMA1*TEM
      S3(1,1,2)=(FL2+2*FM2)*B(18)+FL2*(B(10)+B(2))-2*FM2*E3P(1,1,2)
     &              -GAMA2*TEM
      S3(1,2,1)=(FL2+2*FM2)*B(19)+FL2*(B(11)+B(3))-2*FM2*E3P(1,2,1)
     &              -GAMA2*TEM
      S3(1,2,2)=(FL2+2*FM2)*B(20)+FL2*(B(12)+B(4))-2*FM2*E3P(1,2,2)
```

```
     &              -GAMA2*TEM
      S3(2,1,1)=(FL2+2*FM2)*B(21)+FL2*(B(13)+B(5))-2*FM2*E3P(2,1,1)
     &              -GAMA2*TEM
      S3(2,1,2)=(FL2+2*FM2)*B(22)+FL2*(B(14)+B(6))-2*FM2*E3P(2,1,2)
     &              -GAMA2*TEM
      S3(2,2,1)=(FL2+2*FM2)*B(23)+FL2*(B(15)+B(7))-2*FM2*E3P(2,2,1)
     &              -GAMA2*TEM
      S3(2,2,2)=(FL2+2*FM2)*B(24)+FL2*(B(16)+B(8))-2*FM2*E3P(2,2,2)
     &              -GAMA2*TEM
  23    CONTINUE
C       THE RESULTING AVERAGE STRESSES ,SEE EQNS. (3.97)
       S1B=(D1*H1*L1*S1(1,1,1)+D1*H1*L2*S1(1,1,2)+D1*H2*L1*S1(1,2,1)+
     1  D1*H2*L2*S1(1,2,2)+D2*H1*L1*S1(2,1,1)+D2*H1*L2*S1(2,1,2)+
     2
D2*H2*L1*S1(2,2,1)+D2*H2*L2*S1(2,2,2))/((D1+D2)*(H1+H2)*(L1+L2))
       S2B=(D1*H1*L1*S2(1,1,1)+D1*H1*L2*S2(1,1,2)+D1*H2*L1*S2(1,2,1)+
     1  D1*H2*L2*S2(1,2,2)+D2*H1*L1*S2(2,1,1)+D2*H1*L2*S2(2,1,2)+
     2
D2*H2*L1*S2(2,2,1)+D2*H2*L2*S2(2,2,2))/((D1+D2)*(H1+H2)*(L1+L2))
       S3B=(D1*H1*L1*S3(1,1,1)+D1*H1*L2*S3(1,1,2)+D1*H2*L1*S3(1,2,1)+
     1  D1*H2*L2*S3(1,2,2)+D2*H1*L1*S3(2,1,1)+D2*H1*L2*S3(2,1,2)+
     2
D2*H2*L1*S3(2,2,1)+D2*H2*L2*S3(2,2,2))/((D1+D2)*(H1+H2)*(L1+L2))


C       SHEAR EFFECTIVE MODULI :
C       REF: J. ABOUDI , SOLID MECH. ARCHIVE ,VOL.11, PP.141-183
(1986)
C       SEE EQNS. 67,68,69,70 IN THIS PAPER (GIVEN FOR EPS12B)
C       E4B= EPS12B , S4B=S12B

      COF1=(D1+D2)*(H1+H2)*2*E4B
      VN(1,1,1)=COF1/(D1*H1+D2*H2*FM1/FM2+D2*H1*FM1/FM2+D1*H2*FM1/FM2
)
      VN(2,2,2) =COF1/(D2*H2+D1*H1+D2*H1+D1*H2)
      VN(1,1,2)=VN(2,2,2)
      VN(1,2,1)=FM1*VN(1,1,1)/FM2
      VN(1,2,2)=VN(2,2,2)
      VN(2,1,1)=FM1*VN(1,1,1)/FM2
      VN(2,1,2)=VN(2,2,2)

      VN(2,2,1)=FM1*VN(1,1,1)/FM2
      S4(1,1,1)=FM1*VN(1,1,1)
      S4(1,1,2)=FM2*VN(1,1,2)
      S4(1,2,1)=FM2*VN(1,2,1)
      S4(1,2,2)=FM2*VN(1,2,2)
      S4(2,1,1)=FM2*VN(2,1,1)
      S4(2,1,2)=FM2*VN(2,1,2)
      S4(2,2,1)=FM2*VN(2,2,1)
      S4(2,2,2)=FM2*VN(2,2,2)
      S4B=(D1*H1*L1*S4(1,1,1)+D1*H1*L2*S4(1,1,2)+D1*H2*L1*S4(1,2,1)+
     1  D1*H2*L2*S4(1,2,2)+D2*H1*L1*S4(2,1,1)+D2*H1*L2*S4(2,1,2)+
     2
D2*H2*L1*S4(2,2,1)+D2*H2*L2*S4(2,2,2))/((D1+D2)*(H1+H2)*(L1+L2))
```

```
C       E5B= EPS13B , S5B=S13B
       COF2=(D1+D2)*(L1+L2)*2*E5B
       WN(1,1,1)=COF2/(D1*L1+D2*L2*FM1/FM2+D1*L2*FM1/FM2+D2*L1*FM1/FM2
)
       WN(2,2,2)=COF2/(D2*L2+D1*L1+D2*L1+D1*L2)
       WN(1,1,2)=FM1*WN(1,1,1)/FM2
       WN(1,2,1)=WN(2,2,2)
       WN(1,2,2)=WN(2,2,2)
       WN(2,1,1)=FM1*WN(1,1,1)/FM2
       WN(2,1,2)=FM1*WN(1,1,1)/FM2
       WN(2,2,1)=WN(2,2,2)
       S5(1,1,1)=FM1*WN(1,1,1)
       S5(1,1,2)=FM2*WN(1,1,2)
       S5(1,2,1)=FM2*WN(1,2,1)
       S5(1,2,2)=FM2*WN(1,2,2)
       S5(2,1,1)=FM2*WN(2,1,1)
       S5(2,1,2)=FM2*WN(2,1,2)
       S5(2,2,1)=FM2*WN(2,2,1)
       S5(2,2,2)=FM2*WN(2,2,2)
       S5B=(D1*H1*L1*S5(1,1,1)+D1*H1*L2*S5(1,1,2)+D1*H2*L1*S5(1,2,1)+
      1  D1*H2*L2*S5(1,2,2)+D2*H1*L1*S5(2,1,1)+D2*H1*L2*S5(2,1,2)+
      2
D2*H2*L1*S5(2,2,1)+D2*H2*L2*S5(2,2,2))/((D1+D2)*(H1+H2)*(L1+L2))

C       E6B= EPS23B , S6B=S23B
       COF3=(H1+H2)*(L1+L2)*2*E6B
       XN(1,1,1)=COF3/(H1*L1+FM1*(H2*L2/FM2+H2*L1/FM2+H1*L2/FM2) )
       XN(2,2,2)=COF3/(H2*L2+H1*L1+H2*L1+H1*L2)
       XN(1,1,2)=FM1*XN(1,1,1)/FM2
       XN(1,2,1)=FM1*XN(1,1,1)/FM2
       XN(1,2,2)=FM1*XN(1,1,1)/FM2
       XN(2,1,1)=XN(2,2,2)
       XN(2,1,2)=XN(2,2,2)
       XN(2,2,1)=XN(2,2,2)
       S6(1,1,1)=FM1*XN(1,1,1)
       S6(1,1,2)=FM2*XN(1,1,2)
       S6(1,2,1)=FM2*XN(1,2,1)
       S6(1,2,2)=FM2*XN(1,2,2)
       S6(2,1,1)=FM2*XN(2,1,1)
       S6(2,1,2)=FM2*XN(2,1,2)
       S6(2,2,1)=FM2*XN(2,2,1)
       S6(2,2,2)=FM2*XN(2,2,2)

        S6B=(D1*H1*L1*S6(1,1,1)+D1*H1*L2*S6(1,1,2)+D1*H2*L1*S6(1,2,1)
+
      1  D1*H2*L2*S6(1,2,2)+D2*H1*L1*S6(2,1,1)+D2*H1*L2*S6(2,1,2) +
      2
D2*H2*L1*S6(2,2,1)+D2*H2*L2*S6(2,2,2))/((D1+D2)*(H1+H2)*(L1+L2))

C       WORK OUT THE STRESS CONCENTRATION MATRIX
C       FOR EACH OF THE EIGHT SUB CELLS
C       NOTE MUST ONLY HAVE ONE OVERALL STRESS IN ONE DIRECTION
C       EACH TIME
```

```
IF (II.EQ.1) THEN

B111(1,1)= S1(1,1,1)/E1B
B112(1,1)= S1(1,1,2)/E1B
B122(1,1)= S1(1,2,2)/E1B
B222(1,1)= S1(2,2,2)/E1B
B212(1,1)= S1(2,1,2)/E1B
B221(1,1)= S1(2,2,1)/E1B
B121(1,1)= S1(1,2,1)/E1B
B211(1,1)= S1(2,1,1)/E1B

B111(2,1)= S2(1,1,1)/E1B
B112(2,1)= S2(1,1,2)/E1B
B122(2,1)= S2(1,2,2)/E1B
B222(2,1)= S2(2,2,2)/E1B
B212(2,1)= S2(2,1,2)/E1B
B221(2,1)= S2(2,2,1)/E1B
B121(2,1)= S2(1,2,1)/E1B
B211(2,1)= S2(2,1,1)/E1B

B111(3,1)= S3(1,1,1)/E1B
B112(3,1)= S3(1,1,2)/E1B
B122(3,1)= S3(1,2,2)/E1B
B222(3,1)= S3(2,2,2)/E1B
B212(3,1)= S3(2,1,2)/E1B
B221(3,1)= S3(2,2,1)/E1B
B121(3,1)= S3(1,2,1)/E1B
B211(3,1)= S3(2,1,1)/E1B

ELSE IF (II.EQ.2) THEN

B111(1,2)= S1(1,1,1)/E2B
B112(1,2)= S1(1,1,2)/E2B
B122(1,2)= S1(1,2,2)/E2B
B222(1,2)= S1(2,2,2)/E2B
B212(1,2)= S1(2,1,2)/E2B
B221(1,2)= S1(2,2,1)/E2B
B121(1,2)= S1(1,2,1)/E2B
B211(1,2)= S1(2,1,1)/E2B

B111(2,2)= S2(1,1,1)/E2B
B112(2,2)= S2(1,1,2)/E2B
B122(2,2)= S2(1,2,2)/E2B
B222(2,2)= S2(2,2,2)/E2B
B212(2,2)= S2(2,1,2)/E2B
B221(2,2)= S2(2,2,1)/E2B
B121(2,2)= S2(1,2,1)/E2B
B211(2,2)= S2(2,1,1)/E2B

B111(3,2)= S3(1,1,1)/E2B
B112(3,2)= S3(1,1,2)/E2B
B122(3,2)= S3(1,2,2)/E2B
B222(3,2)= S3(2,2,2)/E2B
```

```
B212(3,2)= S3(2,1,2)/E2B
B221(3,2)= S3(2,2,1)/E2B
B121(3,2)= S3(1,2,1)/E2B
B211(3,2)= S3(2,1,1)/E2B


ELSE IF (II.EQ.3) THEN

B111(1,3)= S1(1,1,1)/E3B
B112(1,3)= S1(1,1,2)/E3B
B122(1,3)= S1(1,2,2)/E3B
B222(1,3)= S1(2,2,2)/E3B
B212(1,3)= S1(2,1,2)/E3B
B221(1,3)= S1(2,2,1)/E3B
B121(1,3)= S1(1,2,1)/E3B
B211(1,3)= S1(2,1,1)/E3B

B111(2,3)= S2(1,1,1)/E3B
B112(2,3)= S2(1,1,2)/E3B
B122(2,3)= S2(1,2,2)/E3B
B222(2,3)= S2(2,2,2)/E3B
B212(2,3)= S2(2,1,2)/E3B
B221(2,3)= S2(2,2,1)/E3B
B121(2,3)= S2(1,2,1)/E3B
B211(2,3)= S2(2,1,1)/E3B

B111(3,3)= S3(1,1,1)/E3B
B112(3,3)= S3(1,1,2)/E3B
B122(3,3)= S3(1,2,2)/E3B
B222(3,3)= S3(2,2,2)/E3B
B212(3,3)= S3(2,1,2)/E3B
B221(3,3)= S3(2,2,1)/E3B
B121(3,3)= S3(1,2,1)/E3B
B211(3,3)= S3(2,1,1)/E3B

ELSE IF (II.EQ.4) THEN

B111(4,4)= S4(1,1,1)/(2*E4B)
B112(4,4)= S4(1,1,2)/(2*E4B)
B122(4,4)= S4(1,2,2)/(2*E4B)
B222(4,4)= S4(2,2,2)/(2*E4B)
B212(4,4)= S4(2,1,2)/(2*E4B)
B221(4,4)= S4(2,2,1)/(2*E4B)
B121(4,4)= S4(1,2,1)/(2*E4B)
B211(4,4)= S4(2,1,1)/(2*E4B)

B111(5,5)= S5(1,1,1)/(2*E5B)
B112(5,5)= S5(1,1,2)/(2*E5B)
B122(5,5)= S5(1,2,2)/(2*E5B)
B222(5,5)= S5(2,2,2)/(2*E5B)
B212(5,5)= S5(2,1,2)/(2*E5B)
B221(5,5)= S5(2,2,1)/(2*E5B)
B121(5,5)= S5(1,2,1)/(2*E5B)
B211(5,5)= S5(2,1,1)/(2*E5B)
```

```
      B111(6,6)= S6(1,1,1)/(2*E6B)
      B112(6,6)= S6(1,1,2)/(2*E6B)
      B122(6,6)= S6(1,2,2)/(2*E6B)
      B222(6,6)= S6(2,2,2)/(2*E6B)
      B212(6,6)= S6(2,1,2)/(2*E6B)
      B221(6,6)= S6(2,2,1)/(2*E6B)
      B121(6,6)= S6(1,2,1)/(2*E6B)
      B211(6,6)= S6(2,1,1)/(2*E6B)

      ELSE IF (II.EQ.5) THEN

C     RANDOMIZE THE STRESS INTESITY MATRIX
C
C
C
C
C

      AAA=(B111(1,1)+B111(2,2)+B111(3,3))/3
      BBB=(B111(2,3)+B111(1,3)+B111(1,2))/3
      CCC=(B111(4,4)+B111(5,5)+B111(6,6))/3
      RB111(1,1)=(3*AAA+2*BBB+4*CCC)/5
      RB111(1,2)=(AAA+4*BBB-2*CCC)/5
      RB111(6,6)=(AAA-BBB+3*CCC)/5
      RS1(1,1,1)=RB111(1,1)*E1B+RB111(1,2)*E2B+RB111(1,2)*E3B
      RS2(1,1,1)=RB111(1,1)*E2B+RB111(1,2)*E1B+RB111(1,2)*E3B
      RS3(1,1,1)=RB111(1,1)*E3B+RB111(1,2)*E2B+RB111(1,2)*E1B

      XODR=RB111(6,6)*(3*RB111(1,2)+2*RB111(6,6))
      XODR=XODR/(RB111(1,2)+RB111(6,6))
      POSR= RB111(1,2)/(2*(RB111(1,2)+RB111(6,6)))

      AAA=(B112(1,1)+B112(2,2)+B112(3,3))/3
      BBB=(B112(2,3)+B112(1,3)+B112(1,2))/3
      CCC=(B112(4,4)+B112(5,5)+B112(6,6))/3
      RB112(1,1)=(3*AAA+2*BBB+4*CCC)/5
      RB112(1,2)=(AAA+4*BBB-2*CCC)/5
      RB112(6,6)=(AAA-BBB+3*CCC)/5

      RS1(1,1,2)=RB112(1,1)*E1B+RB112(1,2)*E2B+RB112(1,2)*E3B
      RS2(1,1,2)=RB112(1,1)*E2B+RB112(1,2)*E1B+RB112(1,2)*E3B
      RS3(1,1,2)=RB112(1,1)*E3B+RB112(1,2)*E2B+RB112(1,2)*E1B

      XODR=RB112(6,6)*(3*RB112(1,2)+2*RB112(6,6))
      XODR=XODR/(RB112(1,2)+RB112(6,6))
      POSR= RB112(1,2)/(2*(RB112(1,2)+RB112(6,6)))

       AAA=(B122(1,1)+B122(2,2)+B122(3,3))/3
       BBB=(B122(2,3)+B122(1,3)+B122(1,2))/3
       CCC=(B122(4,4)+B122(5,5)+B122(6,6))/3
       RB122(1,1)=(3*AAA+2*BBB+4*CCC)/5
       RB122(1,2)=(AAA+4*BBB-2*CCC)/5
       RB122(6,6)=(AAA-BBB+3*CCC)/5
```

```
RS1(1,2,2)=RB122(1,1)*E1B+RB122(1,2)*E2B+RB122(1,2)*E3B
RS2(1,2,2)=RB122(1,1)*E2B+RB122(1,2)*E1B+RB122(1,2)*E3B
RS3(1,2,2)=RB122(1,1)*E3B+RB122(1,2)*E2B+RB122(1,2)*E1B
XODR=RB122(6,6)*(3*RB122(1,2)+2*RB122(6,6))
XODR=XODR/(RB122(1,2)+RB122(6,6))
POSR= RB122(1,2)/(2*(RB122(1,2)+RB122(6,6)))


AAA=(B222(1,1)+B222(2,2)+B222(3,3))/3
BBB=(B222(2,3)+B222(1,3)+B222(1,2))/3
CCC=(B222(4,4)+B222(5,5)+B222(6,6))/3
RB222(1,1)=(3*AAA+2*BBB+4*CCC)/5
RB222(1,2)=(AAA+4*BBB-2*CCC)/5
RB222(6,6)=(AAA-BBB+3*CCC)/5

RS1(2,2,2)=RB222(1,1)*E1B+RB222(1,2)*E2B+RB222(1,2)*E3B
RS2(2,2,2)=RB222(1,1)*E2B+RB222(1,2)*E1B+RB222(1,2)*E3B
RS3(2,2,2)=RB222(1,1)*E3B+RB222(1,2)*E2B+RB222(1,2)*E1B
XODR=RB222(6,6)*(3*RB222(1,2)+2*RB222(6,6))
XODR=XODR/(RB222(1,2)+RB222(6,6))
POSR= RB222(1,2)/(2*(RB222(1,2)+RB222(6,6)))


AAA=(B211(1,1)+B211(2,2)+B211(3,3))/3
BBB=(B211(2,3)+B211(1,3)+B211(1,2))/3
CCC=(B211(4,4)+B211(5,5)+B211(6,6))/3
RB211(1,1)=(3*AAA+2*BBB+4*CCC)/5
RB211(1,2)=(AAA+4*BBB-2*CCC)/5
RB211(6,6)=(AAA-BBB+3*CCC)/5
RS1(2,1,1)=RB211(1,1)*E1B+RB211(1,2)*E2B+RB211(1,2)*E3B
RS2(2,1,1)=RB211(1,1)*E2B+RB211(1,2)*E1B+RB211(1,2)*E3B
RS3(2,1,1)=RB211(1,1)*E3B+RB211(1,2)*E2B+RB211(1,2)*E1B
 XODR=RB211(6,6)*(3*RB211(1,2)+2*RB211(6,6))
XODR=XODR/(RB211(1,2)+RB211(6,6))
POSR= RB211(1,2)/(2*(RB211(1,2)+RB211(6,6)))


AAA=(B221(1,1)+B221(2,2)+B221(3,3))/3
BBB=(B221(2,3)+B221(1,3)+B221(1,2))/3
CCC=(B221(4,4)+B221(5,5)+B221(6,6))/3
RB221(1,1)=(3*AAA+2*BBB+4*CCC)/5
RB221(1,2)=(AAA+4*BBB-2*CCC)/5
RB221(6,6)=(AAA-BBB+3*CCC)/5

RS1(2,2,1)=RB221(1,1)*E1B+RB221(1,2)*E2B+RB221(1,2)*E3B
RS2(2,2,1)=RB221(1,1)*E2B+RB221(1,2)*E1B+RB221(1,2)*E3B
RS3(2,2,1)=RB221(1,1)*E3B+RB221(1,2)*E2B+RB221(1,2)*E1B
XODR=RB221(6,6)*(3*RB221(1,2)+2*RB221(6,6))
XODR=XODR/(RB221(1,2)+RB221(6,6))
POSR= RB221(1,2)/(2*(RB221(1,2)+RB221(6,6)))


AAA=(B212(1,1)+B212(2,2)+B212(3,3))/3
BBB=(B212(2,3)+B212(1,3)+B212(1,2))/3
```

```
      CCC=(B212(4,4)+B212(5,5)+B212(6,6))/3
      RB212(1,1)=(3*AAA+2*BBB+4*CCC)/5
      RB212(1,2)=(AAA+4*BBB-2*CCC)/5
      RB212(6,6)=(AAA-BBB+3*CCC)/5

      RS1(2,1,2)=RB212(1,1)*E1B+RB212(1,2)*E2B+RB212(1,2)*E3B
      RS2(2,1,2)=RB212(1,1)*E2B+RB212(1,2)*E1B+RB212(1,2)*E3B
      RS3(2,1,2)=RB212(1,1)*E3B+RB212(1,2)*E2B+RB212(1,2)*E1B
      XODR=RB212(6,6)*(3*RB212(1,2)+2*RB212(6,6))
      XODR=XODR/(RB212(1,2)+RB212(6,6))
      POSR= RB212(1,2)/(2*(RB212(1,2)+RB212(6,6)))

      AAA=(B121(1,1)+B121(2,2)+B121(3,3))/3
      BBB=(B121(2,3)+B121(1,3)+B121(1,2))/3
      CCC=(B121(4,4)+B121(5,5)+B121(6,6))/3
      RB121(1,1)=(3*AAA+2*BBB+4*CCC)/5
      RB121(1,2)=(AAA+4*BBB-2*CCC)/5
      RB121(6,6)=(AAA-BBB+3*CCC)/5



      RS1(1,2,1)=RB121(1,1)*E1B+RB121(1,2)*E2B+RB121(1,2)*E3B
      RS2(1,2,1)=RB121(1,1)*E2B+RB121(1,2)*E1B+RB121(1,2)*E3B
      RS3(1,2,1)=RB121(1,1)*E3B+RB121(1,2)*E2B+RB121(1,2)*E1B
       XODR=RB121(6,6)*(3*RB121(1,2)+2*RB121(6,6))
      XODR=XODR/(RB121(1,2)+RB121(6,6))
      POSR= RB121(1,2)/(2*(RB121(1,2)+RB121(6,6)))


      JKL=0
      IF(II.EQ.5) THEN
      DO 22,I=1,2
      DO 22,J=1,2
      DO 22 K=1,2
      JKL=JKL+1
      IF(JKL.EQ.1) THEN
C       MUST DO FIBRE FIRST
      IF(RS1(1,1,1).GT.Y1) THEN
      YOUNG=FM1*(3*FL1+2*FM1)/(FM1+FL1)
      RS1(1,1,1)=(E1B+(Y1/MU1))/(1/E1+1/MU1)
       ENDIF
       ELSE
      YOUNG=FM2*(3*FL2+2*FM2)/(FM2+FL2)
      IF(RS1(I,J,K).GT.Y2) THEN
      YYY=Y2
      RRSS11=YYY
      TEST=1.0
      EEE2=E2
      UUUMMM=MU2
 15     RRSS11=RRSS11+1E6
      TEST=RRSS11/EEE2-E1B+((RRSS11-YYY)**N2)/UUUMMM
C        EAT=RRSS11/EEE2+((RRSS11-YYY)**N2)/UUUMMM
C        WRITE(2,*) 'TEST              ',TEST
```

```
C         WRITE(2,*) 'STRESS,Y,MU            ',RRSS11,YYY,UUUMMM
C         WRITE(2,*) 'IJK              ',I,J,K
C         WRITE(2,*) 'STRain  EAT N2         ',E1B,EAT,N2

       IF ( TEST .LT. 0.0 ) GOTO 15
       RS1(I,J,K)=RRSS11
C         RS1(I,J,K)=(E1B+(Y2/MU2))/(1/E2+1/MU2)
       ENDIF
       ENDIF
 22      CONTINUE
       ENDIF

        S1B=(D1*H1*L1*RS1(1,1,1)+D1*H1*L2*RS1(1,1,2)+D1*H2*L1
      1       *RS1(1,2,1)+D1*H2*L2*RS1(1,2,2)+D2*H1*L1*RS1(2,1,1)
      2       +D2*H1*L2*RS1(2,1,2)+D2*H2*L1*RS1(2,2,1)+D2*H2*L2
      3       *RS1(2,2,2))/((D1+D2)*(H1+H2)*(L1+L2))
        S2B=(D1*H1*L1*RS2(1,1,1)+D1*H1*L2*RS2(1,1,2)+D1*H2*L1
      1       *RS2(1,2,1)+D1*H2*L2*RS2(1,2,2)+D2*H1*L1*RS2(2,1,1)
      2       +D2*H1*L2*RS2(2,1,2)+D2*H2*L1*RS2(2,2,1)+D2*H2*L2
      3       *RS2(2,2,2))/((D1+D2)*(H1+H2)*(L1+L2))
        S3B=(D1*H1*L1*RS3(1,1,1)+D1*H1*L2*RS3(1,1,2)+D1*H2*L1
      1       *RS3(1,2,1)+D1*H2*L2*RS3(1,2,2)+D2*H1*L1*RS3(2,1,1)
      2       +D2*H1*L2*RS3(2,1,2)+D2*H2*L1*RS3(2,2,1)+D2*H2*L2
      3       *RS3(2,2,2))/((D1+D2)*(H1+H2)*(L1+L2))


        RPOS=((S1B/E1B)-(S2B/E2B))/((S2B+S3B)/E1B-(S1B+S3B)/E2B)
        RYOUNG=(S1B-RPOS*(S2B+S3B))/E1B
       XSTRESS=0.0
       KOUNT=0
       DO 25,I=1,2
       DO 25,J=1,2
       DO 25 K=1,2
       KOUNT=KOUNT+1
       IF(KOUNT.EQ.1) GOTO 25
       IF(XSTRESS.LT.RS1(I,J,K)) THEN
       XSTRESS=RS1(I,J,K)
       III=I
       JJJ=J
       KKK=K
       ENDIF
 25      CONTINUE

        WRITE(2,99) RS1(1,1,1)/1E6,XSTRESS/1E6,S1B/1E6,
      1    E1B
  99      FORMAT(F14.2,F14.2,F14.2,F14.4)
        ENDIF

        END

       SUBROUTINE SOLVEQ(A,E,N,X,DTR)
C        TO SOLVE A(N,N)*X(N)=E(N)
```

```
C       NEED A STOBAGE OF A(N,N+1)
C       IMPLICcIT DOUBLE PRECISION (A-H,O-Z)
      DIMENSION A(N,*),E(N),X(N)
      M=N+1
      DO  1 I=1,N
    1       A(I,M)=E(I)
        N1=N-1
      DO 20 K=1,N1
         CALL PIVOT(A,K,N)
         K1=K+1
      DO 20 I=K1,N
         EM=A(I,K)/A(K,K)
         A(I,K)=0
      DO 20 J=K1,M
   20      A(I,J)=A(I,J)-EM*A(K,J)

      DO 2 I=1,N
    2       E(I)=A(I,M)
         X(N)=E(N)/A(N,N)
      DO 6 K=1,N1
         I=N-K
         I1=I+1
         SUM=0
      DO 7 J=I1,N
    7       SUM=SUM+ A(I,J)*X(J)
    6       X(I)=(E(I)-SUM)/A(I,I)



      RETURN
      END

      SUBROUTINE PIVOT(A,K,N)
C       IMPLICIT DOUBLE PRECISION        (A-H,O-Z)
      DIMENSION A(N,*)
      M=N+1
      K1=K+1
      L=K
      DO 2 I=K1,N
         IF(ABS(A(I,K))-ABS(A(L,K))) 2,2,1
    1       L=I
    2    CONTINUE
      IF(L-K) 5,5,3
    3    DO 4 J=K,M
         TT=-A(K,J)
         A(K,J)=A(L,J)
    4       A(L,J)=TT
    5    RETURN
      END



      FUNCTION ROOT(A,B)
```

```
C       TO SOLVE THE CUBIC EQN.: X**3+A*X+B=0
C       IMPLICIT DOUBLE PRE@ISION (A-H,O-Z)
      DEL=B**2/4+A**3/27
      IF(DEL) 2,1,1
   1    SD=SQRT(DEL)
      R1=-B/2+SD
      R2=-B/2-SD
      P=1./3.
      IR1=1
      IR2=1
      R1P=(ABS(R1))**P
      R2P=(ABS(R2))**P
      IF(R1.LT.0.) IR1=-1
      IF(R2.LT.0.) IR2=-1
      ROOT=IR1*R1P+IR2*R2P

      RETURN
   2    R=SQRT(-A**3/27)
      TE=ACOS(-0.5*B/R)
      ROOT=2*R**(1./3)*COS(TE/3)
      RETURN
      END
```

```
      WRITE(2,*) 'STRAIN(1,1)=',ST(1,1)
      WRITE(2,*) 'STRAIN(2,2)=',ST(2,2)
      WRITE(2,*) 'STRAIN(3,3)=',ST(3,3)
      WRITE(2,*) 'STRAIN(1,2)=',ST(1,2)
      WRITE(2,*) 'STRAIN(2,3)=',ST(2,3)
      WRITE(2,*) 'STRAIN(1,3)=',ST(1,3)
      WRITE(2,*) '    '
      WRITE(2,*) 'STRESS(1,1)=',AS(1,1)
      WRITE(2,*) 'STRESS(2,2)=',AS(2,2)
      WRITE(2,*) 'STRESS(3,3)=',AS(3,3)
      WRITE(2,*) 'STRESS(1,2)=',AS(1,2)
      WRITE(2,*) 'STRESS(2,3)=',AS(2,3)
      WRITE(2,*) 'STRESS(1,3)=',AS(1,3)
      WRITE(2,*) '    '
      ST(1,1)=ST(1,1)+.01
500   CONTINUE
      END


      SUBROUTINE MATPROPS(EAM,POSTM,POSAM,ETM,EAF,POSTF,POSAF,ETF,
     *GAM,GAF,VF,ESTARA,POSTARA,ESTART,POSTART,GSTARA)
      COMMON CM(10,10),CF(10,10),V(2,2),B(10,10),E(10,10)
      COMMON AS(3,3),ST(3,3),SA(3,3),PSI1(3,3),PSI2(3,3)
      COMMON PSI3(3,3),FI1(3,3),FI2(3,3),FI3(3,3),SIB(3,3)
      COMMON BD(10,10),BDT(10,10),B11(4,4),B22(4,4),B21(4,4 )
      COMMON B12(4,4),N(2),V1
      COMMON H,H1,H2,DW1DX2,DW2DX1,DW1DX3,DW3DX1,DW2DX3,DW3DX2
      COMMON T1,T2,T3,T4,T5,T6,T7,T8,T9,T10,T11,T12,T13,T14,T15
      COMMON T16,DELTA,DELTA1
      REAL KM,KF,J1,J2,J3,J4


      H2=SQRT((H1**2)/VF)-H1
C                                                     *
C                                                     *
C                                                     *
C       MATERIAL PROPERTIES EQUATIONS                 *
C                                                     *
C                                                     *
C                                                     *
      KM= 0.25*EAM/(0.5*(1-POSTM)*(EAM/ETM)-POSAM**2)
      CM(1,1)= EAM+(4*KM*POSAM**2)
      CM(1,2)=2*KM*POSAM
      CM(2,2)=KM+0.5*ETM/(1+POSTM)
      CM(2,3)=KM-0.5*ETM/(1+POSTM)
      CM(4,4)=GAM
      CM(6,6)=(CM(2,2)-CM(2,3))/2
```

```
KF= 0.25*EAF/(0.5*(1-POSTF)*(EAF/ETF)-POSAF**2)
CF(1,1)= EAF+(4*KF*POSAF**2)
CF(1,2)=2*KF*POSAF
CF(2,2)=KF+0.5*ETF/(1+POSTF)
CF(2,3)=KF-.5*ETF/(1+POSTF)
CF(4,4)=GAF
CF(6,6)=(CF(2,2)-CF(2,3))/2
A1=CM(2,2)*(1+(H2/H1))
A2=CM(2,3)*(H1/H2)
A3=CM(2,3)
A4=CM(2,2)*(H1/H2)+CF(2,2)
A5=CF(2,3)
A6=H2*CM(2,3)/H1
A7=CF(2,3)
A8=A6
A9=A4
A10=H1*CM(2,3)/H2
A11=A3
A12=A1
D=A1*(A12*(A5*A7-A4*A9)+A6*A9*A10)
D=D+A2*((A4*A8*A12)+A6*(A7*A11-A8*A10))
D=D+A3*(A4*A9*A11+A5*(A8*A10-A7*A11))
T1=-(A5*A8*A12+A6*A9*A11)/D
T2=(A2*A8*A12+A3*A9*A11-A1*A9*A12)/D
T3=(A1*A5*A12+A2*A6*A11-A3*A5*A11)/D
T4=(A1*A6*A9+A8*(A3*A5-A2*A6))/D
T5=(A6*A9*A10+A12*(A5*A7-A4*A9))/D
T6=-(A2*A7*A12+A3*A9*A10)/D
T7=(A3*A5*A10+A2*(A4*A12-A6*A10))/D
T8=(A2*A6*A7+A3*(A4*A9-A5*A7))/D
T9=(A4*A8*A12+A6*(A7*A11-A8*A10))/D
T10=(A1*A7*A12+A3*(A8*A10-A7*A11))/D
T11=(A3*A4*A11+A1*(A6*A10-A4*A12))/D
T12=-(A1*A6*A7+A3*A4*A8)/D
T13=(A4*A9*A11+A5*(A8*A10-A7*A11))/D
T14=(A1*A9*A10+A2*(A7*A11-A8*A10))/D
T15=-(A1*A5*A10+A2*A4*A11)/D
T16=(A1*(A5*A7-A4*A9)+A2*A4*A8)/D
H=H1+H2
V1=H**2
V(1,1)=H1*H1
V(1,2)=H1*H2
V(2,2)=H2*H2
V(2,1)=H2*H1
Q1=V(1,1)*CF(1,2)*(T1+T9)
Q1=Q1-V(1,2)*CM(1,2)*(H2*T5/H1+H1*T9/H2)
Q1=Q1-V(2,1)*CM(1,2)*(H1*T1/H2+H2*T13/H1)
Q1=Q1+V(2,2)*CM(1,2)*(T5+T13)
Q2=V(1,1)*CF(1,2)*(T2+T10)
Q2=Q2-V(1,2)*CM(1,2)*(H2*T6/H1+H1*T10/H2)
Q2=Q2-V(2,1)*CM(1,2)*(H1*T2/H2+H2*T14/H1)
Q2=Q2+V(2,2)*CM(1,2)*(T6+T14)
Q3=V(1,1)*CF(1,2)*(T3+T11)
Q3=Q3-V(1,2)*CM(1,2)*(H2*T7/H1+H1*T11/H2)
```

```
Q3=Q3-V(2,1)*CM(1,2)*(H1*T3/H2+H2*T15/H1)
Q3=Q3+V(2,2)*CM(1,2)*(T7+T15)
Q4=V(1,1)*CF(1,2)*(T4+T12)
Q4=Q4-V(1,2)*CM(1,2)*(H2*T8/H1+H1*T12/H2)
Q4=Q4-V(2,1)*CM(1,2)*(H1*T4/H2+H2*T16/H1)
Q4=Q4+V(2,2)*CM(1,2)*(T8+T16)
QD1=V(1,1)*(CF(2,2)*T1+CF(2,3)*T9)
QD1=QD1-V(1,2)*(CM(2,2)*H2*T5/H1+CM(2,3)*H1*T9/H2)
QD1=QD1-V(2,1)*(CM(2,2)*H1*T1/H2+CM(2,3)*H2*T13/H1)
QD1=QD1+V(2,2)*(CM(2,2)*T5+CM(2,3)*T13)
QD2=V(1,1)*(CF(2,2)*T2+CF(2,3)*T10)
QD2=QD2-V(1,2)*(CM(2,2)*H2*T6/H1+CM(2,3)*H1*T10/H2)
QD2=QD2-V(2,1)*(CM(2,2)*H1*T2/H2+CM(2,3)*H2*T14/H1)
QD2=QD2+V(2,2)*(CM(2,2)*T6+CM(2,3)*T14)
QD3=V(1,1)*(CF(2,2)*T3+CF(2,3)*T11)
QD3=QD3-V(1,2)*(CM(2,2)*H2*T7/H1+CM(2,3)*H1*T11/H2)
QD3=QD3-V(2,1)*(CM(2,2)*H1*T3/H2+CM(2,3)*H2*T15/H1)
QD3=QD3+V(2,2)*(CM(2,2)*T7+CM(2,3)*T15)
QD4=V(1,1)*(CF(2,2)*T4+CF(2,3)*T12)
QD4=QD4-V(1,2)*(CM(2,2)*H2*T8/H1+CM(2,3)*H1*T12/H2)
QD4=QD4-V(2,1)*(CM(2,2)*H1*T4/H2+CM(2,3)*H2*T16/H1)
QD4=QD4+V(2,2)*(CM(2,2)*T8+CM(2,3)*T16)
DELTA=H1*CM(4,4)+H2*CF(4,4)
DELTA1=V(1,1)*CM(6,6)+(V(1,2)+V(2,1)+V(2,2))*CF(6,6)
B(1,1)=V(1,1)*CF(1,1)+CM(1,1)*(V(1,2)+V(2,1)+V(2,2))
B(1,1)=(B(1,1)+(CM(1,2)-CF(1,2))*(Q2+Q3))/V1
B(1,2)=(H/H1)*(CM(1,2)*V(1,2)+Q1*CM(2,2)+Q3*CM(2,3))
X=CM(1,2)*V(2,1)+Q2*CM(2,2)+Q4*CM(2,3)
X=(H/H2)*X
B(1,2)=(B(1,2)+X)/V1
B(1,3)=B(1,2)
X=H/H1*(CM(2,2)*(V(1,2)+QD1)+QD3*CM(2,3))
Y=(H/H2)*(CM(2,2)*(V(2,1)+QD2)+QD4*CM(2,3))
B(2,2)=(X+Y)/V1
X=(H/H1)*(CM(2,3)*(V(2,1)+QD2)+QD4*CM(2,2))
Y=(H/H2)*(CM(2,3)*(V(1,2)+QD1)+QD3*CM(2,2))
B(2,3)=(X+Y)/V1
B(3,3)= B(2,2)
X=H*(V(1,1)+V(2,1))+H2*(V(1,2)+V(2,2))
B(4,4)=CF(4,4)*X
X=CM(4,4)*(V(1,2)+V(2,2))*H1
B(4,4)=(CM(4,4)*(B(4,4)+X))/(V1*DELTA)
B(5,5)=B(4,4)
B(6,6)=CF(6,6)*CM(6,6)*H*H/DELTA1

BDT(2,2)=0.0
BDT(2,3)=0.0
BDT(6,6)=0.0

ANG=0.0
DO 22 J=1,18
X=(COS(ANG))**4+(SIN(ANG))**4
Y=((SIN(ANG))**2)*((COS(ANG))**2)
BD(2,2)=B(2,2)*X+2*(B(2,3)+2*B(6,6))*Y
```

```
      BD(2,3)=B(2,3)*X+2*(B(2,2)-2*B(6,6))*Y
      BD(6,6)=B(6,6)*X+2*(B(2,2)-B(2,3)-B(6,6))*Y
      BDT(2,2)=BDT(2,2)+BD(2,2)
      BDT(2,3)=BDT(2,3)+BD(2,3)
      BDT(6,6)=BDT(6,6)+BD(6,6)
      ANG=ANG+10*3.142/180
      ANGLE=ANG*180/3.142
   22 CONTINUE
      B(2,2)=BDT(2,2)
      B(2,3)=BDT(2,3)
      B(6,6)=BDT(6,6)

      B(2,2)=B(2,2)/18
      B(2,3)=B(2,3)/18
      B(6,6)=B(6,6)/18
C      WRITE(2,*) '   '
C      WRITE(2,*) 'SUMMED QUANITITY'
C
C      WRITE(2,*) 'B(2,2)=',B(2,2),'B(2,3)=',B(2,3),'B(6,6)',B(6,6)

      E(1,1)=B(1,1)
      E(1,2)=B(1,2)
      E(2,2)=0.75*B(2,2)
      E(2,2)=E(2,2)+B(2,3)/4
      E(2,2)=E(2,2)+B(6,6)/2
      E(2,3)=B(2,2)*.25+.75*B(2,3)-B(6,6)*.5
      E(4,4)=B(4,4)
      E(6,6)=(E(2,2)-E(2,3))/2
      ESTARA=E(1,1)-2*E(1,2)**2/(E(2,2)+E(2,3))
     POSTARA=E(1,2)/(E(2,2)+E(2,3))
      ESTART=E(1,1)*(E(2,2)+E(2,3))-2*E(1,2)**2
      ESTART=ESTART*(E(2,2)-E(2,3))
      ESTART=ESTART/(E(1,1)*E(2,2)-E(1,2)**2)
     POSTART=(E(1,1)*E(2,3)-E(1,2)**2)
     POSTART=POSTART/(E(1,1)*E(2,2)-E(1,2)**2)
      GSTARA=E(4,4)
     RETURN
     END

      SUBROUTINE  PRINTPROP(VF,ESTARA,ESTART,POSTARA,POSTART,
     *GSTARA)
      COMMON CM(10,10),CF(10,10),V(2,2),B(10,10),E(10,10)
      COMMON AS(3,3),ST(3,3),SA(3,3),PSI1(3,3),PSI2(3,3)
      COMMON PSI3(3,3),FI1(3,3),FI2(3,3),FI3(3,3),SIB(3,3)
      COMMON BD(10,10),BDT(10,10),B11(4,4),B22(4,4),B21(4,4 )
      COMMON B12(4,4),N(2),V1
      COMMON H,H1,H2,DW1DX2,DW2DX1,DW1DX3,DW3DX1,DW2DX3,DW3DX2
      COMMON T1,T2,T3,T4,T5,T6,T7,T8,T9,T10,T11,T12,T13,T14,T15
      COMMON T16,DELTA,DELTA1
C                                                    *
C                                                    *
C                                                    *
C     WRITING RESULTS                                *
C     MATERIAL PROPERTIES                            *
```

```
C                                                                *
C                                                                *
      WRITE(2,*) '       '
      WRITE(2,*) '       '
      WRITE(2,*) '       '
      WRITE(2,*) 'DIAMETER OF FIBRE       = ',H1
      WRITE(2,*) 'DIMENSIONP OF MATRIX     = ',H2
      WRITE(2,*) 'VOLUME RATIO OF FIBRE   = ',VF
      WRITE(2,*) 'AXIAL YOUNGS MODULUS    = ',ESTARA
      WRITE(2,*) 'TRANSVERE YOUNGS MODULUS= ',ESTART
      WRITE(2,*) 'AXIAL POSIONS RATIO     = ',POSTARA
      WRITE(2,*) 'TRANSVERE POSIONS RATIO = ',POSTART
      WRITE(2,*) 'AXIAL SHEAR MODULUS     = ',GSTARA
      RETURN
      END



      SUBROUTINE ALL


      COMMON CM(10,10),CF(10,10),V(2,2),B(10,10),E(10,10)
      COMMON AS(3,3),ST(3,3),SA(3,3),PSI1(3,3),PSI2(3,3)
      COMMON PSI3(3,3),FI1(3,3),FI2(3,3),FI3(3,3),SIB(3,3)
      COMMON BD(10,10),BDT(10,10),B11(4,4),B22(4,4),B21(4,4 )
      COMMON B12(4,4),N(2),V1
      COMMON H,H1,H2,DW1DX2,DW2DX1,DW1DX3,DW3DX1,DW2DX3,DW3DX2
      COMMON T1,T2,T3,T4,T5,T6,T7,T8,T9,T10,T11,T12,T13,T14,T15
      COMMON T16,DELTA,DELTA1
      REAL KM,KF,J1,J2,J3,J4
      CHARACTER A*3,K1*1
C     ****************************************************


     J1=H*CM(2,2)*ST(2,2)/H1+H*CM(2,3)*ST(3,3)/H2
     J2=(CM(1,2)-CF(1,2))*ST(1,1)+(CM(2,2)*H*ST(2,2))/H2
     J2=J2+CM(2,3)*H*ST(3,3)/H1
     J3=(CM(1,2)-CF(1,2))*ST(1,1)+H*CM(2,3)*ST(2,2)/H1
     J3=J3+H*CM(2,2)*ST(3,3)/H2
     J4=H*CM(2,3)*ST(2,2)/H2+H*CM(2,2)*ST(3,3)/H1
      FI1(1,1)=DW1DX2*H*CM(4,4)
      WRITE(*,*) DELTA

      FI1(1,1)=(FI1(1,1)-(DW2DX1*(CF(4,4)-CM(4,4)))*H2)/DELTA
      FI1(2,2)=DW1DX2
      FI1(1,2)=(H*DW1DX2-H2*FI1(2,2))/H1
      FI1(2,1)=(H*DW1DX2-H1*FI1(1,1))/H2
      PSI1(1,1)=DW1DX3*H*CM(4,4)
      PSI1(1,1)=PSI1(1,1)-DW3DX1*(CF(4,4)-CM(4,4))*H2
      PSI1(1,1)=PSI1(1,1)/DELTA
```

```
PSI1(2,2)=DW1DX3
PSI1(1,2)=(H*DW1DX3-H1*PSI1(1,1))/H2
PSI1(2,1)=DW1DX3

N(1)=2*H*H*CM(6,6)*ST(2,3)/DELTA1
N(2)=CF(6,6)*N(1)/CM(6,6)


PSI3(2,2)=(T13*J1+T14*J2+T15*J3+T16*J4)
PSI3(2,1)=(H*ST(3,3)-H2*PSI3(2,2))/H1
PSI3(1,1)=(T9*J1+T10*J2+T11*J3+T12*J4)
FI2(1,1)=(T1*J1+T2*J2+T3*J3+T4*J4)
FI2(2,2)=(T5*J1+T6*J2+T7*J3+T8*J4)
PSI3(1,2)=(H*ST(3,3)-H1*PSI3(1,1))/H2
FI2(2,1)=(H*ST(2,2)-H1*FI2(1,1))/H2
FI2(1,2)=(H*ST(2,2)-H2*FI2(2,2))/H1


RETURN
END
```

Prediction of the Fatigue Life of an Aluminium Metal Matrix Composite Using the Theory of Cells

[1]W J Fleming, [2]A L Dowson

Abstract

An analytical micromechanical model is employed to predict the fatigue life of an aluminium SiC metal matrix composite. From data obtained from the monolithic matrix material and the individual SiC fibres theoretical S/N and Strain/N curves were produced. This was possible by assuming that the matrix material in the composite fails at the same fatigue stress level as does the monolithic matrix material or, if fibres fail, this will be at the failure level of the individual fibres. These curves were then compared to experimental data and good agreement was obtained for all but the low cycle fatigue regime.

1. Introduction

The introduction of fibres into a base metal will give greatly enhanced mechanical properties to the resultant metal matrix composite. These will be dependent on both the properties of the base matrix and the fibre used. The volume ratio of fibre to matrix will of course also be important as will the interface between fibre and matrix. Some early attempts were made to forecast the resultant composite properties using known properties of the constituents.(1)(2)(3)(4). All these theories were initially formulated for continuous fibre composites in which it was assumed the interface played no part.

In a series of papers, Aboudi(5)(6)(7) has extended his Theory of Cells to include both short and particulate fibres. The range of properties that can be predicted is Young's Modulus, Poisson's ratio and shear modulus. It is also possible to predict the composite yield stress and by modelling the plastic behaviour of the matrix to predict the failure stress and the composite stress-strain curve.

Aboudi (8) has given some indication of how the Theory of Cells may be extended to include fatigue behaviour of a composite material. The work reported here has developed these ideas to estimate the fatigue life of a SiC particulate reinforced aluminium alloy. The assumptions made is that the fatigue behaviour of the matrix will be the same as the fatigue behaviour of the bulk homogeneous material, whilst the fibres will fail statistically as they reach their overall failure stress. At most stresses, it is expected that fatigue failure will be due to matrix failure and only at high stresses, when plastic deformation is encountered in the matrix will failure be caused by the fibres failing.

2. Theory of Cells.

The Theory of Cells (TOC) for short fibre and particulate metal matrix composites has been developed by Aboudi (9). In the method an elastic matrix is considered which is reinforced by unidirectional fibres of short length. The fibres are assumed rectangular with dimensions of d_1, l_1 and h_1 and arranged in the matrix as shown in Fig. 1.

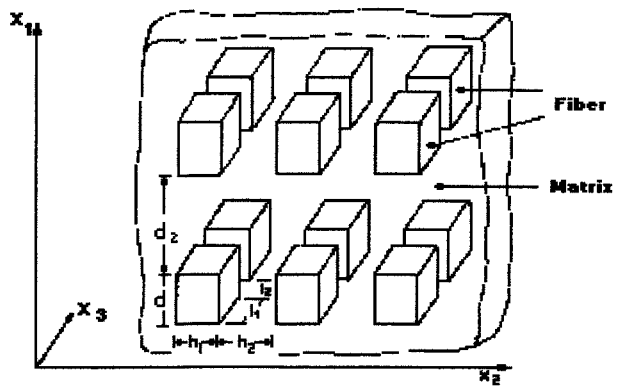

Fig.1 Schematic of an MMC with periodic array of fibres

1 Senior Lecture School of Engineering University of Northumbria at Newcastle, UK

2 Research Fellow IRC in Materials for High Performance Applications, The University of Birmingham, UK

In a particulate metal matrix composite h_1 will have a similar value to l_1.

Given that the arrangement of fibre and matrix are periodic, only one fibre and its surround matrix need be analysed to give a representative section of the composite material. This area is called a cell and is shown in Fig.2.

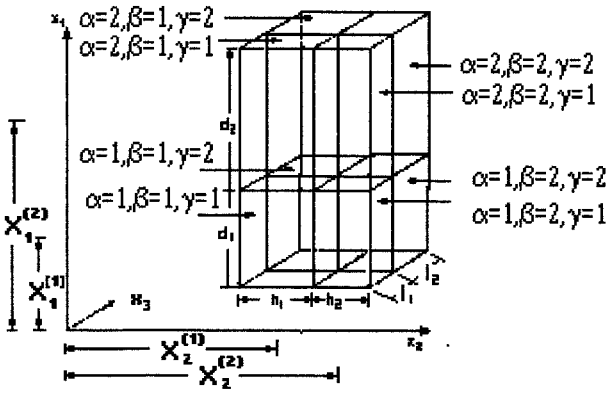

Fig.2 A representative cell of the composite showing the eight sub cells

As can be seen each cell comprises eight sub cells, one of fibre, labelled 1,1,1, and seven of matrix material. It is assumed, initially, that both fibres and matrix are perfectly elastic materials and the stresses are related to the strains as follows

$$\sigma^{(\alpha,\beta,\gamma)} = \mathbf{C}^{(\alpha\beta\gamma)}\ \mathbf{Z}^{(\alpha\beta\gamma)} - \Gamma^{(\alpha\beta\gamma)}\ \Delta T$$

where

$\sigma^{(\alpha\beta\gamma)}$ being the stress matrix of each sub cell

$\mathbf{C}^{(\alpha\beta\gamma)}$ the stiffness matrix representing mechanical properties of each sub cell

$\Gamma^{(\alpha\beta\gamma)}$ a matrix representing thermal properties of each sub cell

ΔT the temperature difference between a reference stress free temperature and the working temperature

whilst $\mathbf{Z}$, the strain microvariables is given by

$$\mathbf{Z}^{(\alpha\beta\gamma)} = \Phi_1^{(\alpha\beta\gamma)}, X_2^{(\alpha\beta\gamma)}, \Psi_3^{(\alpha\beta\gamma)}, X_1^{(\alpha\beta\gamma)} + \Phi_2^{(\alpha\beta\gamma)}, \Psi_1^{(\alpha\beta\gamma)} - \Phi_3^{(\alpha\beta\gamma)}, \Psi_2^{(\alpha\beta\gamma)} + X_3^{(\alpha\beta\gamma)}$$

with $\Phi_1^{(\alpha\beta\gamma)}, \Phi_2^{(\alpha\beta\gamma)}, \Phi_3^{(\alpha\beta\gamma)}, X_1^{(\alpha\beta\gamma)}, X_2^{(\alpha\beta\gamma)}, X_3^{(\alpha\beta\gamma)}, \Psi_1^{(\alpha\beta\gamma)}$, $\Psi_2^{(\alpha\beta\gamma)}, \Psi_3^{(\alpha\beta\gamma)}$ representing strain microvariables

Note that when discussing the position of a sub cell a super script notation is used, i.e., $\sigma^{(1,1,1)}$ refers to the fibre whilst, for instance $\sigma^{(1,2,1)}$ is the matrix material to the right of the fibre and subscript notation is used for the stress direction, e.g. σ_{11} is the direct stress in the x_1 direction.

Using a first order approximation the displacement component at any point in the sub cell can be expressed as

$$u_i^{(\alpha\beta\gamma)} = W_i^{(\alpha\beta\gamma)} + x_1^{(\alpha)}\,\Phi_i^{(\alpha\beta\gamma)} + x_2^{(\beta)}\,X_i^{(\alpha\beta\gamma)} + x_3^{(\gamma)}\,\Psi_i^{(\alpha\beta\gamma)}$$

where

W_i represents the displacement component of the centre of the sub cell and

Φ_i, X_i, Ψ_i characterises the linear dependence of the displacements on the local co-ordinates. $x_1^{(\alpha)}$, $x_2^{(\beta)}$ and $x_3^{(\gamma)}$

and the displacement can be connected to strain using the expression

$$\varepsilon_{ij}^{(\alpha,\beta,\gamma)} = \tfrac{1}{2}\left[\partial_j u_i^{(\alpha,\beta,\gamma)} + \partial_i u_j^{(\alpha,\beta,\gamma)}\right]$$

and $\partial_1 = \partial/\partial x_1^{\alpha}$
$\partial_2 = \partial\,\partial x_2^{\beta}$
$\partial_3 = \partial/\partial x_3^{\gamma}$

If continuity of traction and displacement between appropriate sub cells is assumed, it is possible to calculate the 26 strain microvariables generated by the theory. Once the stresses in each sub cell is calculated the overall stresses can be found as follows

$$\sigma_{ij} = 1/V \sum_{\alpha,\beta,\gamma=1}^{2} \left(V^{(\alpha,\beta,\gamma)} \sigma_{ij}^{(\alpha,\beta,\gamma)}\right)$$

V represents the total volume of the cell and
$V^{(\alpha,\beta,\gamma)}$ the volume of a particular sub cell.

3. Inelastic Behaviour of Metal Matrix Composites

A typical MMC comprises a fibre that behaves in an elastic manner up to the breaking stress and a matrix that will show the typical elastoplastic behaviour of a ductile material. To model a composite an allowance must be made for the plastic deformation of the ductile matrix. In Aboudi's development of the theory of cells (10) he used the unified theory of plasticity developed by Bodner and Pardom.(11) In this theory, plasticity is assumed to be always present throughout the loading process. Although rigorous, the Bodner et al. approach adds a level of complexity to the analysis that may not be necessary. In the present study, this has been abandoned in favour of a theory of plasticity proposed by Mendelson (12), in which the total strain experienced by a stressed material is made up of both elastic and plastic strains. Using this approach, plastic strain can be assumed to approximate to zero whilst the material is within the elastic region. Therefore if $\sigma_{ij} < Y$ the total strain can be written as

$\varepsilon_{ij\,(total)} = \varepsilon_{ij\,(elastic)} = \sigma_{ij}/E$ for a one dimensional direct stress system.

Once the material suffers plastic deformation the relationship changes to:

$$\varepsilon_{ij\,(total)} = \varepsilon_{ij\,(elastic)} + \varepsilon_{ij\,(plastic)}$$

and $\varepsilon_{ij\,(plastic)}$ can be defined as $(\sigma_{ij} - Y)^n/\mu$

and therefore for $\sigma_{ij} > Y$ the total strain is now

$$\varepsilon_{ij} = \sigma_{ij}/E + (\sigma_{ij} - Y)^n/\mu$$

where

σ_{ij} represents the total stress in the ij direction
Y is the material yield stress
n and μ are factors which characterise the plastic behaviour of the material.

This approach assumes simple elastic breakdown at the yield stress. For a biaxial loading system the failure theory can be modified to include a shear yield component. (13)

4. Randomly Reinforced Metal Matrix Composites

The theory developed so far is for unidirectional short fibre and particulate composites where the fibres are aligned in the X_1 direction as shown in fig. 1. This places severe limitations on the type of systems it is possible to analyse. However a transformation can be made on the stiffness matrix of each sub cell, using a method first suggested by Arridge (14). It is found that for a material with randomly distributed fibres, the stiffness matrix reduces to three non-zero elements which are related to the aligned fibre matrix in the following manner

$$B_{11}^{(\alpha,\beta,\gamma)} = (3A_1 + 2A_2 + 4A_3) / 5$$
$$B_{12}^{(\alpha,\beta,\gamma)} = (A_1 + 4A_2 + 2A_3) / 5$$
$$B_{66}^{(\alpha,\beta,\gamma)} = (A_1 - 4A_2 + 3A_3) / 5$$

where

$$A_1 = (C_{11}^{(\alpha,\beta,\gamma)} + C_{22}^{(\alpha,\beta,\gamma)} + C_{33}^{(\alpha,\beta,\gamma)}) / 3$$
$$A_2 = (C_{23}^{(\alpha,\beta,\gamma)} + C_{13}^{(\alpha,\beta,\gamma)} + C_{12}^{(\alpha,\beta,\gamma)}) / 3$$
$$A_3 = (C_{44}^{(\alpha,\beta,\gamma)} + C_{55}^{(\alpha,\beta,\gamma)} + C_{66}^{(\alpha,\beta,\gamma)}) / 3$$

$B_{ij}^{(\alpha,\beta,\gamma)}$ is the transformed stiffness matrix, allowing for a fully random fibre distribution in the composite.

$C_{ij}^{(\alpha,\beta,\gamma)}$ is the stiffness matrix for aligned fibres

Using this modified stiffness matrix in the stress strain matrix, the strain in all three dimensions can be calculated for each sub cell in the MMC with randomly distributed fibres.

5. Fatigue Failure and the Theory of Cells

It can be assumed that fatigue failure will occur when one or more of the sub cells reaches a critical stress level. In a one-dimensional loading system the fatigue failure stress for the matrix material can be obtained from an S/N curve. It can be assumed that failure of the composite will occur, for a similar number of cycles, when any matrix sub cell reaches this cyclic stress level providing the fibre has not reached its critical level. Therefore the matrix is assumed to fail by fatigue similar to the homogenous material.

The fibres however may behave differently. Silicon carbide fibres are brittle and do not exhibit fatigue failure (15). In the case of the individual fibres, their critical fatigue stress is assumed to be identical to their tensile failure stress. However similar fibres exhibit a wide range of tensile failure stresses as can be seen in Fig.3. This has important implications on the fatigue life of an MMC containing such brittle fibres

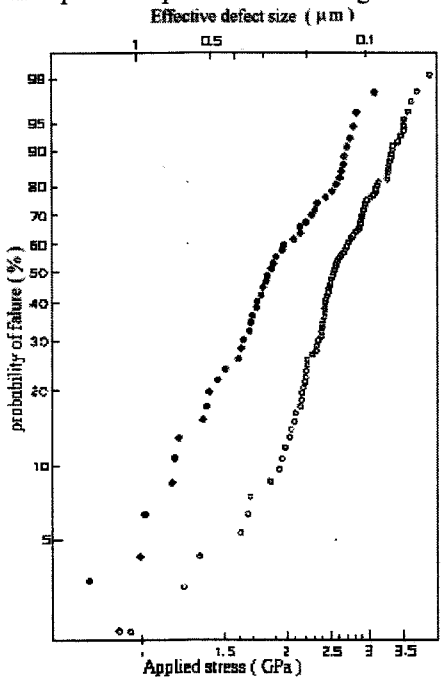

Fig.3 Experimental strength behaviour of SiC yarn fibre (Andersson and Warren (16))

○ 10-mm fibre carefully handled ● 100-mm fibre carefully handled

When the cyclic loading is high enough to break fibres, the outcome will be one of two possible behaviour patterns.. First is that only a certain percentage of fibres break due to the fatigue loading and the resulting redistribution of stresses ensures no more fibre breakage. In this event, the composite will eventually fracture by

matrix fatigue failure. The second possibility is that as the fibres break the stress redistribution ensures more fibres will fail. Fatigue failure of the MMC is then by fibre failure.
In the present study the theory of cells is used to calculate stresses in the eight sub cells for an increasing load. At each increment of load a check is made to see if any matrix sub cell has reached its fatigue limit for a given number of cycles or that the stress level in the fibres is such that fibre failure is encountered. If the former is the case, the overall composite stress is recorded as the fatigue failure stress for that load. If fibre failure has taken place, the stress on each subcell is recalculated, assuming a lower density of fibres ,and the possibility of more fibre breakage ascertained. An iterative recalculation of stress is then performed until the mode of fatigue failure is determined.

6. Material

The materials under consideration in this report are an aluminium alloy Al 7075 and a metal matrix composite with an identical material for the matrix plus 12% SiC fibres, in particulate form. The chemical composition of the composite was 6.2% Zn, 1.5% Cu, 2.3% Mg, 0.2% Cr, 0.3% Fe and the remainder aluminium. The monolithic material had a Young's modulus of 72 GPa, a Possions ratio 0.33, a 0.2% proof stress of 416 MPa, a UTS of 565 MPa and an elongation at failure of 14%.
The SiC particles had the following specification (17). Diameters range from 0.25 to 20 microns with an average diameter of 3 micron to 4 microns. The average effective aspect ratio was 1.3 whilst the Young's modulus was 468 GPa and the Poisson's ratio was 0.25. The particulate strength was assumed to be statistical in nature, 5% of the particulates failing at a stress of 1.6 GPa and 90% having failed at an average stress of 3.1 GPa.
The MMC's were produced by spray forming followed by extrusion. Heat treatment of the material consisted of an initial high temperature solution treatment at 465 °C held for 45 minutes followed by a cold water quench and the material aged for 16 hr at 135 °C. The measured Young's modulus was then 84 GPa, the 0.2% Proof stress 404 MPa, the UTS 490 MPa and its elongation at failure was 2%.

7. Testing Procedure

Tests were carried out on a PC driven 50 kN. capacity Dartec servo hydraulic testing machine. All tests were conducted under strain control and constant amplitude. Tests were conducted in air at a frequency of 0.25 Hz using fully reversed loading (R=-1.0) with stress and strain data being recorded for each cycle.

8. Results

The tests were carried out at a constant strain rate with the stress being allowed to vary. Fig.4 and Fig. 5 show how the stress varied over the life of the specimen, Fig. 4 being for the monolithic material and Fig.5 being for the MMC. In both cases, for the low strain rates the stress was fairly constant throughout each individual experiment. However once the material was strained into the plastic region, work hardening took place and therefore the stress increased throughout the life of the test

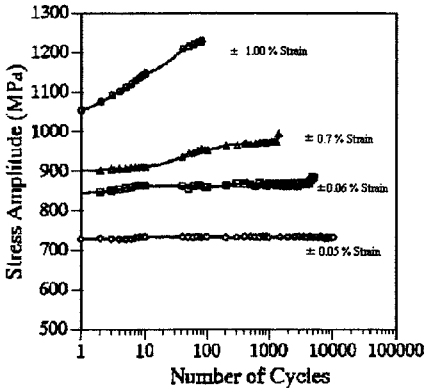

Fig.4 Strain controlled fatigue test on monolithic Al 7075

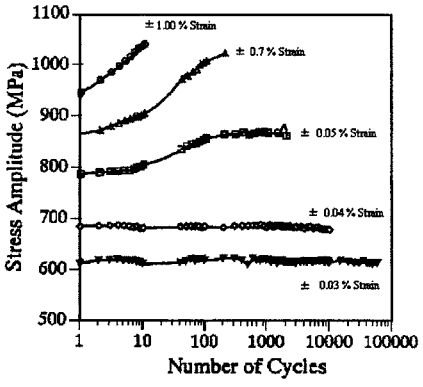

Fig.5 Strain controlled fatigue test on Al 7075/ 12 SiCp

All results from the tests on both monolithic and MMC materials were plotted on an S/N curve as shown in Fig.6. The stress in all cases being the initial stress recorded after one cycle. The same test results are also shown in Fig. 7, only this time, strain is plotted as one of the axes instead of stress. Note that in Fig. 7 both axis of the graph are logarithmic.

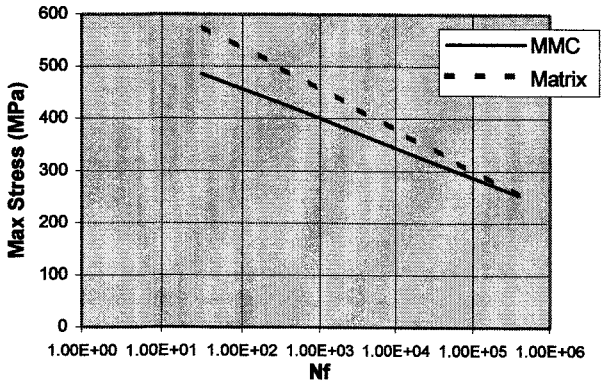

Fig. 6 Strain controlled experimental S/N curve for monolithic Al 7075 and MMC Al 7075 + 12% SiCp.

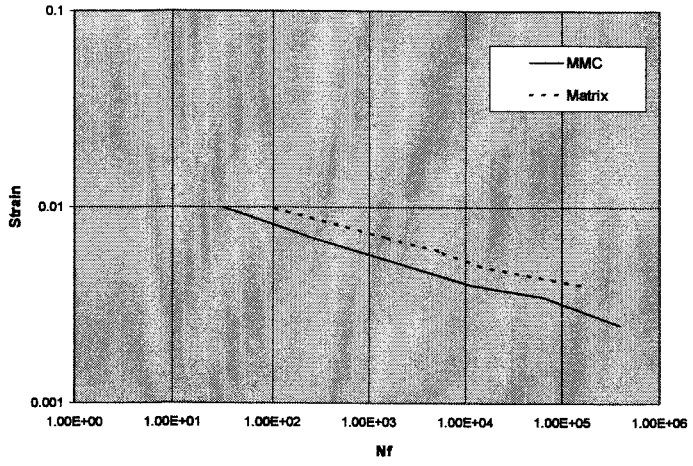

Fig.7 Strain controlled experimental results of constant strain against cycles to failure for monolithic Al 7075 and MMC Al 7075 + 12% SiCp

During the experiment carried out on the MMC the Young's modulus was monitored. Fig.8 gives the average experimental value of modulus, the Poisson's ratio and the Yield stress against the predicted values produced from the Theory of Cells (TOC)

	Young's Modulus	*Poisson's Ratio*	*Yield Stress*
Experimental	84.1 GPa	Not Available	404 MPa
TOC	83.3 GPa	0.324	391 MPa

Fig.8 Experimental and Theoretical values of Modulus and Poisson's Ratio

Using the data experimentally obtained on the monolithic material it was possible to predict the fatigue life of

the MMC using the Theory of Cells. These predictions are shown in Fig.9 and Fig.10. In Fig.9, a conventional S/N curve is produced and both the TOC prediction and experimental results are shown. In both cases the stress plotted on the graph is the stress measured after one cycle of the test. In Fig. 10, the same TOC predictions and experimental data are used as in Fig. 9 but this time, strain is plotted against fatigue life for both experimental and predicted results.

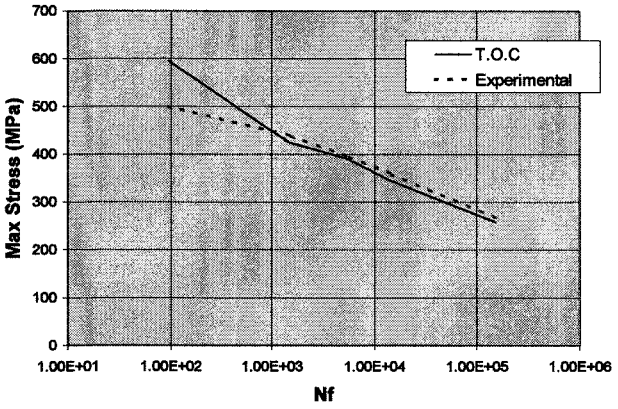

Fig.9 S/N Curve of experimental results and TOC predicted life of MMC Al7075 + 12% SiCp

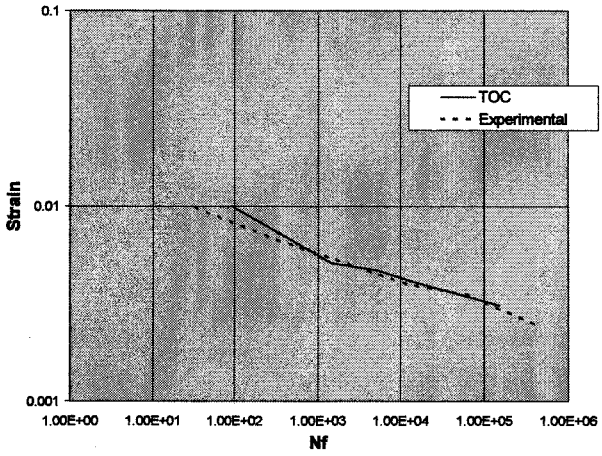

Fig.10 Constant Strain against Cycles to failure experimental results and TOC predicted life of MMC Al7075 + 12% SiCp

10. Discussion

Comparing the monolithic material with the MMC we find that both the experimentally obtained yield stress and failure stress of the MMC were inferior to that of the monolithic material (see section 6). Similarly at all but the lowest stresses, the monolithic material exhibits a superior fatigue life to that of the MMC. The difference in fatigue life is more apparent in the strain plot shown in Fig.7 than the conventional S/N curve of Fig.6.
The results for yield and failure stress were somewhat surprising, as it would be expected that the inclusion of particulates in the aluminium would improve both its yield and ultimate strength. However it can be seen from Fig.8 that the experimental yield stress is at the level predicted by the theory of cells; the experimental and theoretical values being 404 MPa and 391 MPa respectively. The reason why the MMC yields at a lower stress than the monolithic materials is to do with the particulate inclusions. Under load, the particulates will create stress gradients within the aluminium matrix. This means that whilst some areas of matrix will be yielding other areas will still be at sub yield levels of stress. The overall stress of the MMC is the average of the particulate stress and the stress experienced by each matrix sub cell. So that whilst areas of the MMC may have started to exhibit plastic behaviour the overall stress may not have reached the value of the yield stress of the monolithic material. Although this is what has happened to this composite it may not necessarily be the case for another composite of different particulate volume fraction and different constituent mechanical properties. Yield stress of a composite is not only dependent on the yield stress of the matrix but is a complex relationship between particulate and matrix properties and particulate volume fraction and orientation. The overall stress of the MMC will of course be a summation of the stresses in the fibre and each sub cell of matrix. In this case the summed stress at yield was lower for the MMC than that of the monolithic material.
Fig. 8 also compares experimentally derived Young's modulus with that predicted by TOC. The experimental result indicating a modulus of 84.1 GPa. whilst TOC gives 83.3 GPa. This result is 1 % of the experimental result.
Both the S/N results given in Fig.9 and the Strain/N results given in Fig.10 show good agreement between TOC and the experimental results. At stress levels below 450 MPa the agreement is well within the experimental error of the test. However once stresses are in the plastic region of the MMC, the prediction value of fatigue failure starts to deviate from the experimental results. At these levels, the stress in the particulates is significantly higher than those experienced in any sub-cell of the matrix. The matrix accommodates the increase in overall loading on the MMC by yielding but the particulates are still deforming elastically. As the load increases some of the weaker particulates fail and there is a redistribution of the load between particulate and matrix. The theory predicts that, for this MMC, the stress level in the individual particulates falls causing a corresponding increase in the stress on the matrix. So failure throughout the test should have been by matrix fatigue failure.
It could be assumed that once a particulate has failed, the broken portion is then available to take load. This could be true of inclusions that are of significant length but in this case we are not dealing with fibres but particulates and it would seem that failed particulates are not available to take load. This would explain the significant short fall in fatigue life in cyclic stresses above 450 MPa. The broken particulates, rather than taking load, are areas of weakness and cause premature fatigue failure of the composite. As the stress increases, more particulates break, causing more fatigue damage to the material. Failure at these stresses could also be initiated by imperfections in the matrix material itself.
Although this difference between experimental and theoretical fatigue life under gross plastic deformation is of some importance, it must be remembered that this only involves the first thousand cycles of the S/N curve. Once beyond this the predicted life from the theory of cells is in close agreement with that obtained from experiment.

Conclusion

1. For this particular aluminium metal matrix composite the prediction of Young's modules and yield stress from the theory of cells was in good agreement with experimental results.
2. Using fatigue data obtained from the matrix material and information on the failure stress of the particulate, it was possible to make a prediction of the fatigue life of a metal matrix composite material.
3. The predicted fatigue life of the MMC was in close agreement with the experimental results for life outside of the low cycle fatigue regime of 1000 cycles or less.
4. Failure when material life expectancy was below 1000 cycles may have been due to failed particulates causing high stress concentrations or to metallurgical faults in the matrix material.

References

(1) Dvorak, G.J., and Bahei-El-Din, Y.A., "Elastic - Plastic Behaviour of Fibrous Composites" *Journal of Mechanics & Physics of Solids* **27** pp. 141-183 (1979)

(2) Hokins, D.A. and Chamis, C.C., "A Unique Set of Micromechanical Equations for High Temperature Metal Matrix Composites" *NASA* TM 87154 (1985)
(3) Foye, R.L., "An evaluation of Various Engineering Estimates of the Transverse Properties of Unidirectional Composites" *Proceedings of the Tenth National SANPE Symposium - Advanced Fibrous Reinforced Composites.* November 1966
(4) Aboudi, J,. "Elastoplasticity Theory for Composite Materials" *Solid Mechanics Archives* **11** pp. 141-183 (1986)
(5) Aboudi, J,. "Micromechanical Analysis of Composites by the Method of Cells" *Applied Mechanical Review* **42 (7)** pp.193 - 221 (July 1989)
(6) Aboudi, J,. "The Effective Moduli of Short Fibre Composites" *Int. J. Solids Structures* **19 (8)** pp. 693 -707 (1983)
(7) Paley, M., & Aboudi, J,. "Micromechanical Analysis of Composites by the Generalized Cells Model" *Mechanics of Materials* **14** pp. 127- 139 (1992)
(8) Aboudi, J,. "Mechanics of Composite Materials" *Studies in Applied Mechanics* **29** Elservier, New York pp. 112 (1991)
(9) Aboudi, J,. "Mechanics of Composite Materials" *Studies in Applied Mechanics* **29** Elservier, New York pp. 76 -82 (1991)
(10) Aboudi, J,. "Mechanics of Composite Materials" *Studies in Applied Mechanics* **29** Elservier, New York pp. 230 - 233 (1991)
(11) Bodner, S.R., "Review of a Unified Elastic Viscoplastic Theory" in "Unified Constitution Equations for Plastic Deformation and Creep in Engineering Alloys" Miller., A.K., ed. Elservier, New York pp. 273 -301 (1987)
(12) Mendelson, A., "Plasticity, Theory and Application" Kriegar Publishing Co., Melbourne pp. 20 (1988)
(13) Aboudi, J,. "Mechanics of Composite Materials" *Studies in Applied Mechanics* **29** Elservier, New York pp. 116 (1991)
(14) Arridge, R.G.C., "An Introduction to Polymer Mechanics" Taylor and Francis, London pp.142 -158 (1985)
(15) Rosenthal, D., and Asimow, R.A., "Introduction to Properties of Materials" Van Nostrand Reinhold, London pp. 184 (1971)
(16) Andersson, C.H., and Warren, R., "Silicon Carbide Fibers and their Potential for Use in Composite Materials: Part 1" *Composites* **15 (1)** pp. 21 (1984)
(17) Dowson, A.L., Kwon, J.W., Healy, J.C., and Beevers, C.J., "Innovative Manufacturing, Design and Assessment of Aluminium Matrix Composites for High Temperature Performance" *Brite Euram Project* **BE 3398-89** (1993)

06/03/2006
12:55:15

Numerical Simulation of Cyclic Plasticity and Damage of an Aluminium Metal Matrix Composite with Particulate SiC Inclusions

W.J.Fleming[1], J.M.Temis[2]

[1]Senior Lecturer, School of Engineering, University of Northumbria at Newcastle, U.K.
[2]Professor of Applied Mathematics, Bauman Moscow State Technical University, Moscow, Russia.

ABSTRACT

Models of strain cyclic plasticity and strain-accumulated damage were employed to analysis an aluminium SiC metal matrix composite behaviour under cyclic loading. From the data obtained from the monolithic matrix material, a model for the mathematical simulation of matrix material response under monotonic and cyclic loading was produced. This model and data from individual SiC inclusions was employed to an FE simulation of cyclic plasticity to prediction low fatigue lives of composite. It was shown that cyclic damage of matrix material on the interface between Al and SiC is responsible for the number of cycles to composite failure. Theoretical Strain/N curve is compared with experimental data for an MMC in low cyclic fatigue.

1. INTRODUCTION

The introduction of inclusions into a base metal will give greatly enhanced mechanical properties to the resultant metal matrix composite. However, these properties will depend on the properties of both the base matrix and the inclusions used. The inclusion volume ratio and its geometrical form will, of course, also be important. These parameters and the parameters of the interface between matrix and inclusion define both the composite ultimate strength under monotonic loading and fatigue strength under cyclic loading. The main problem facing the material designer is to create composite materials or structure with superior mechanical properties. To solve this problem experimental research is mainly employed. This method is expensive and it does not allow an easy optimisation of the material or component properties. The use of mathematical simulation methods appears to offer scope for focusing onto the more likely material and inclusion combinations and thus limiting the amount of experimentation necessary to produce successful materials. Simultaneously this method will allow more accurate predictions of the mechanical behaviour of any components and structure that may go into production.

Mathematical and numerical procedures which are capable of modelling the physical processes that underwrite the fracture behaviour of engineering materials and structures have become essential tools in both the both the design process and in defining the philosophies of life prediction of a material. As such, they promote the concepts of safe-life design and can reduce the need for investment in expensive materials and component evolution trials. For future development of these procedures it is necessary to further improve the mathematical models so that they more fully conform to the complex stress and strain histories associated with testing or in-service loading.

One of these models based on the theory of cells was employed to predict the fatigue life of an aluminium metal matrix composite with short SiC inclusions[1]. As was shown, the prediction of Young's modulus and yield stress by the theory of cells was in good agreement with experimental

results. Also the predicted fatigue failure life of the aluminium SiC MMC was in close agreement with the experimental results for life outside of the low cycle fatigue regime of 1000 cycles or less. The high stress concentration on the interface between matrix and inclusion in the low cycle zone exerts an influence on material cyclic behaviour. On the base of this theory alone the prediction of low cyclic failure is difficult because the definition of material cyclic behaviour subject to the stress-strain distribution inhomogeneity inside the cell is needed. Such a problem requires a detailed analysis of the stress-strain history on the base of cyclic plasticity theory. A theory of cyclic strain plasticity accompanied by damage model based on the concepts of ultimate accumulated plasticity strain[2-5] has been successfully employed for the prediction of fatigue lives in highly stressed Ti components[6]. In the current paper, an application of the theory of cyclic strain plasticity and the cyclic damage model to the lifetime prediction of MMC in the area of low fatigue is considered.

2. TESTING, MATERIAL AND FE MODEL

Testing procedure

The testing of the material has been previously reported[1] and comprise an aluminium alloy, Al 7075, and a metal matrix composite with an identical matrix material plus 12% SiC by volume, of particulate inclusions. Tests were carried out on a PC driven 50 kN capacity Dartec servo-hydraulic testing machine. All tests were conducted under strain control and constant amplitude. Tests were conducted in air at ambient temperature (20-25°C) using a frequency of 0.25 Hz with fully reversed loading (R= - 1.0) the stress and strain data being recorded for each cycle. The tests were carried out at a constant strain rate with the stress being allowed to vary. In every case tests were not terminated until fracture of the material took place.

The main aim of the present paper is to compare previously reported results with a finite element simulation based on the accumulated strain cyclic plasticity theory and connected damage model.

MMC material parameters

In all studies the inclusion are approximated to an elastic body with a Young's modulus of 468 GPa and a Poisson's ratio of 0.25. The Al 7075 had a Young's modulus of 72 GPa, a Poisson's ratio of 0.33, a yields stress of 416 MPa and an ultimate stress of 565 MPa with an elongation of 14%.

The SiC, which was introduced into the matrix as particles, had the following specification [7]. Diameter range of inclusion changed from 0.25 to 20 microns with an average diameter of 3 micron to 4 microns. The average aspect ratio was 1.3.

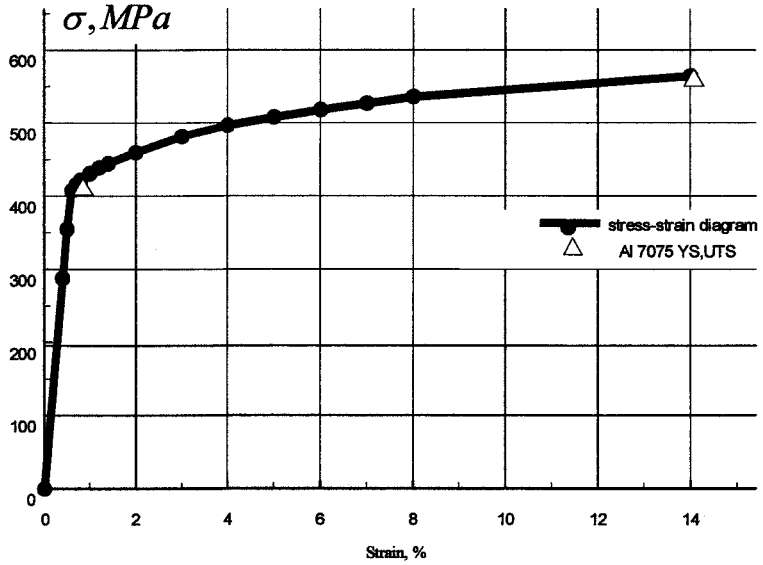

Fig.1 Stress-strain curve of B95 Al alloy.

The MMC's were produced by spray forming followed by extrusion. Heat treatment of both the MMC and the matrix material consisted of an initial high temperature solution treatment of 465°C held for 45 minutes followed by a cold water quench after which the material was aged for 16 hr at 135°C. The measured Young's modulus was then 84 GPa, the 0.2% Proof stress 404 MPa, the UTS 490 and its elongation at failure was 2%.

The Al 7075 matrix material in the following analysis was assumed, as far as cyclic plasticity properties are concerned, to be equivalent to its Russian counterpart, aluminium alloy B95. Both alloys are manufactured under similar technical conditions and the chemical composition of Al 7075 and B95 [8] are shown for a comparison in the Table.1. Further figure 1 shows the stress strain curve for the B75 aluminium alloy with values of yield and ultimate tensile stress for the Al 7075 alloy superimposed upon it. From these reasons it is assumed equivalence exists between the two material for the purpose of plastic analysis.

Table 1.
Al 7075 and B95 alloys chemical formulae

Material	Zn	Cu	Mg	Cr	Fe	Mn
Al 7075	6.2%	1.5%	2.3%	0.2%	<0.5%	-
B95	5.0%-7.0%	1.4%-2.0%	1.8%-2.8%	0.1%-0.25%	0.3%	0.2%-0.6%

Model of structure

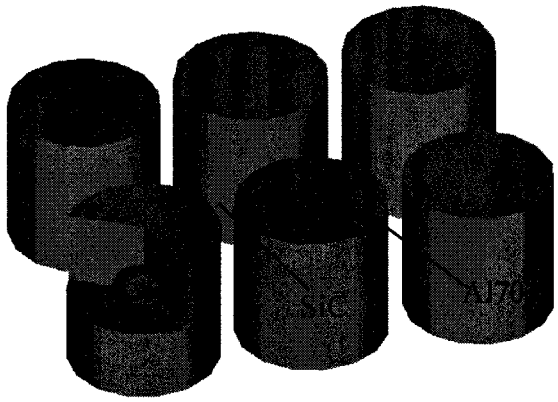

Fig.2 Scheme of the MMC structure with periodic array of fibers.

In general the stress-strain analysis of both the MMC and the individual cells within it are a 3D plasticity problem. However in the present report, as a first approach, the inclusions were approximated to a spherical body surrounded by a cylinder of matrix material (see Fig.2). The cylinder represented one cell of the MMC. The cylinder dimensions were defined from the condition that it was inscribed in the parallelepiped with height H and the base side $2R$. Taking into account that the inclusion volume ratio is 0.12 and that the inclusions are approximated to a sphere of radius r, we get

$$r^3 = \frac{0.36}{\pi} R^2 H,$$

and therefore, all calculations were conducted for model with $H = 2 \cdot R$, where $R = 20$ mm

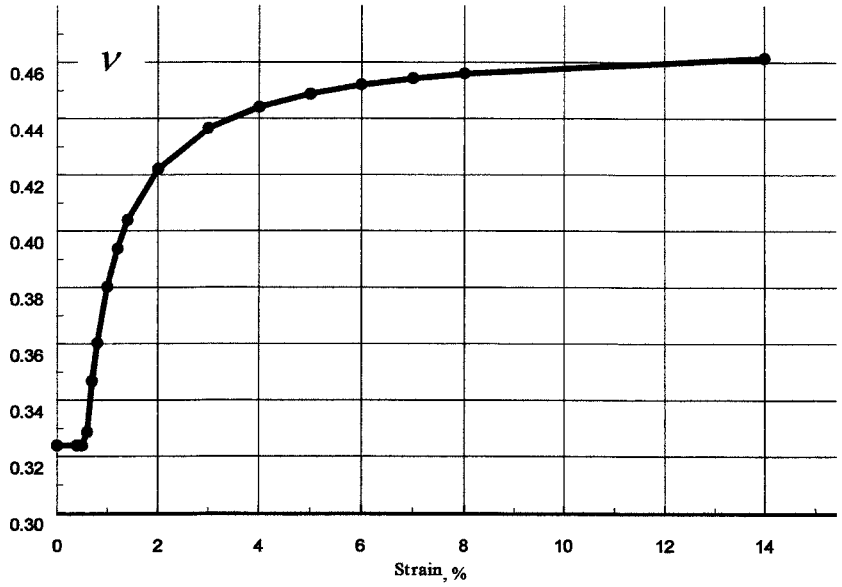

Fig.3 Poisson's ratio for Al 7075 - SiC MMC in plasticity area

The strain in the direction of cylinder axis was equal to the strain in the specimen. The strains in the transverse directions were equal to $-\nu_{MMC}\varepsilon_y$, where ν_{MMC} is the Poisson's ratio of the MMC. In the elasticity region when ε_y<0.008 a value of ν_{MMC} = 0.324 was used for calculations carried out using the theory of cells [1]. However, in the plastic region the Poisson's ratio must be continuously

calculated as its value varies with increasing strain. For the first approach we shall calculate ν_{MMC} on the base of volume mixed model.

$$\nu_{MMC} = \frac{\nu_{Al(elast)}\varepsilon_e + 0.5*\varepsilon_p}{\varepsilon_y} * 0.88 + \nu_{SiC} * 0.12.$$

Here ε_e is elastic part of matrix material strain, ε_p is plastic part of material strain, $\varepsilon_y = \varepsilon_e + \varepsilon_p$.

Fig.3 shows the Poisson's ratio of the MMC calculated in the plastic region on the bases of the stress-strain curve presented in Fig.1 These values of the Poisson's ratio were used in the boundary conditions of FE model.

FE model

When considering the behaviour of the MMC under monotonic loading a FE model with spherical inclusions containing 4583 nodal points and 9018 axisymmetric simplex finite elements was used (Fig.4).

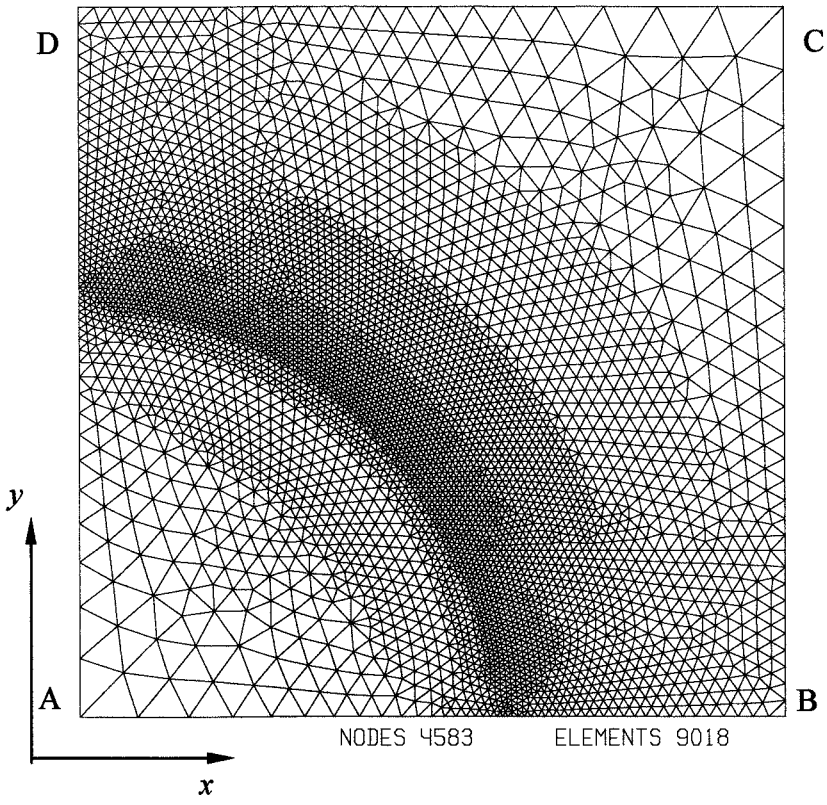

Fig.4 Finite element mesh for MMC with spherical fibre.

When cyclic deformation was analysed the meshes needed to be refined to decrease approximation errors and to increase the stability of FE models during the various steps of mathematical simulation Whilst analysing an MMC with spherical inclusions the number of nodes in the FE model during cyclic plasticity analysis was above 7000.

On the boundary AD displacements in the x (radial) direction were fixed whilst displacements on the boundary AB were fixed in the y (cylinders axial) direction. On the boundary DC displacements $v = \varepsilon_y R$ in the y direction were given. Corresponding displacements $u = -\nu_{MMC}\varepsilon_y R$ were given in the x direction on the boundary BC.

3. CYCLIC STRAIN PLASTICITY

Model of material response under cyclic loading.

Using a model described elsewhere[2-5] the cyclic stress-strain response of the matrix material can be developed in terms of the simple relationships. The stress σ_n^* and strain ε_n^* co-ordinates may be related during any half-cycle n by

$$\sigma_n^* = f_n(\varepsilon_n^*), \qquad (3.1)$$

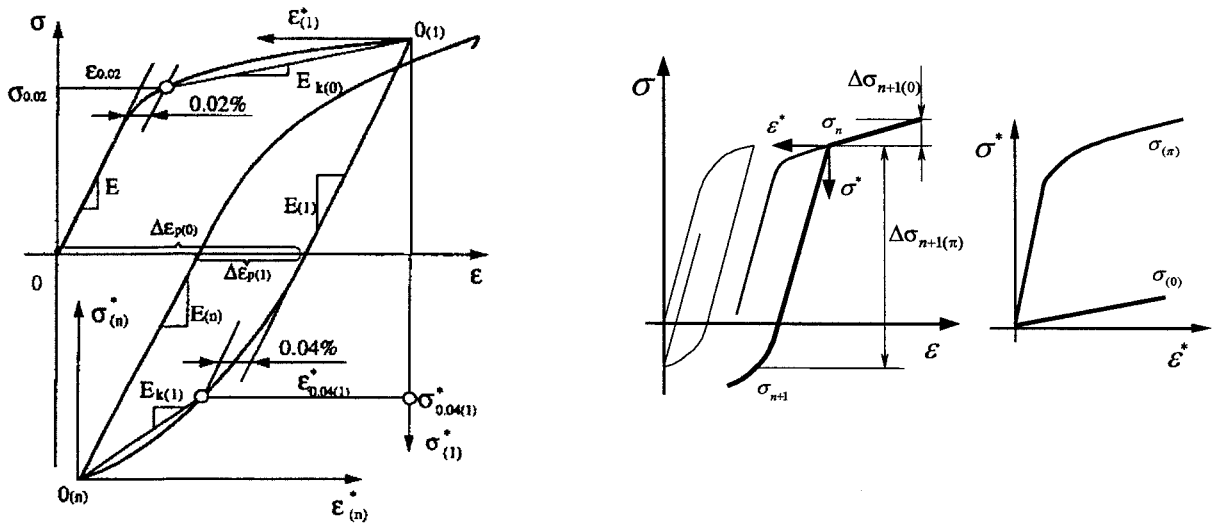

Fig.5. Scheme of stress-strain material response under cyclic loading; a) cyclic stress-strain curve parameters; b) stress-strain curve for $n+1$ loading step; c) unified deformation curve on the $n+1$ step.

where $f_n(\varepsilon_n^*)$ represents some modification of the initial stress-strain response of the matrix material under monotonic loading $f(\varepsilon)$ (i.e. n=0). However other parameters describing the material cyclic stress-strain curve vary depending on the cyclic history and the number of applied cycles but as was shown in previous works[3-6] these changes may not only be dependent on the number of half cycles. To take this into account an alternative approach is used with the parameters describing the cyclic strain curve dependent on the cumulative plastic strain χ.
This is defined as

$$\chi = \sum_{n=0}^{n_f} \left| \Delta\varepsilon_p \right|, \tag{3.2}$$

The relationship between stress σ_n^* and strain ε_n^* (Fig. 5) is represented in the form

$$\sigma^* = \begin{cases} E_\chi \varepsilon^* & \varepsilon^* \le \varepsilon_{s\chi}^* \\ E_\chi \varepsilon_{s\chi}^* + b_\chi d_\chi \left\{ f\left[\varepsilon_s + \dfrac{\left(\varepsilon^* - \varepsilon_{s\chi}^*\right)}{b_\chi} \right] - \sigma_s \right\} & \varepsilon^* > \varepsilon_{s\chi}^* \end{cases}, \tag{3.3}$$

$$\varepsilon_{s\chi}^* = \left(\frac{a_\chi}{d_\chi} \right) \varepsilon_s; \quad d_\chi = E_\chi / E$$

where σ_s and ε_s are the initial stress and strain values at 0.02% offset yield; a_χ, b_χ and d_χ are material-sensitive parameters describing plastic deformation response of the material under cyclic load; E_χ is a plastic strain path χ-dependant modulus such that $E = E_{\chi(\chi=0)}$. In practice due to the Bauschinger effect a_χ may be defined as $a_\chi = \sigma_{y\chi}/\sigma_s$, d_χ is defined as stated above and a transformation coefficient b_χ relates the non-linear portion of the stress–strain curve under monotonic loading to that observed under cyclic loading conditions.
This relationship is valid for the matrix material, which under cyclic load has an alternating elasto–plastic strain whilst the inclusion material remains elastic. Material constants describing the above mentioned parameters of cyclic stress-strain were defined on the base of experimental data obtained for B95 Al alloy[10], whose parameters are equivalent to that of the Al 7075 alloy. The aluminium alloy B95 under cyclic loading shows a decrease in the amplitude of plastic strain and the hardness effect with an increase in the number of cycles. The results from this previous work[10] are shown in

Fig.6 and Fig.7. The parameter, describing Baushinger effect under cyclic loading, is shown in Fig.6. In Fig.7 the parameter d_χ , corresponding to the Young's modulus changing under cycling loading, is shown. It should be noted that the Young's modulus of the Al alloy under cyclic loading decreases in the first cycles and recovers its value with increasing number of cycle.

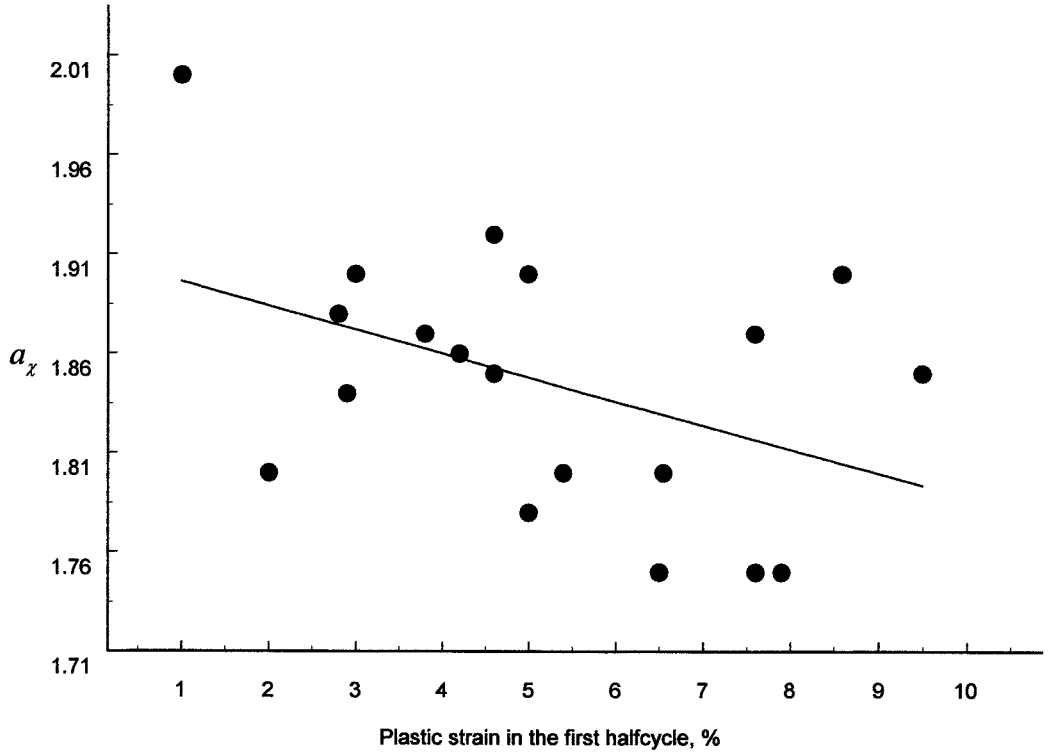

Fig.6. Baushinger parameter in Al alloy

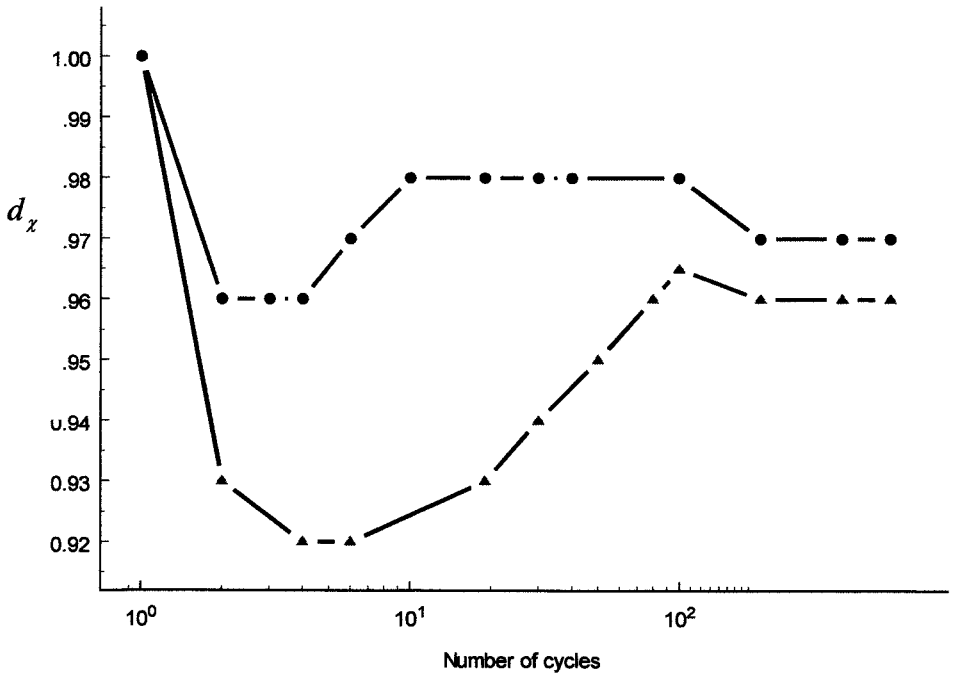

Fig.7. Cyclic modulus of elasticity d_χ

The non-linear parts of cyclic stress-strain diagram for different numbers of cycles are shown in Fig.8, which demonstrates Al alloy hardening under increasing number of cycle. This effect

influences the parameter b_χ. Follows from Fig.8, the main changes in the non-linear part of the Al alloy stress-strain curve take place in the first few half-cycles with maximum change taking place between the first and the third cycles. After the third cycle the modulus slowly increases until the 100th cycles when the change in modulus ceases.

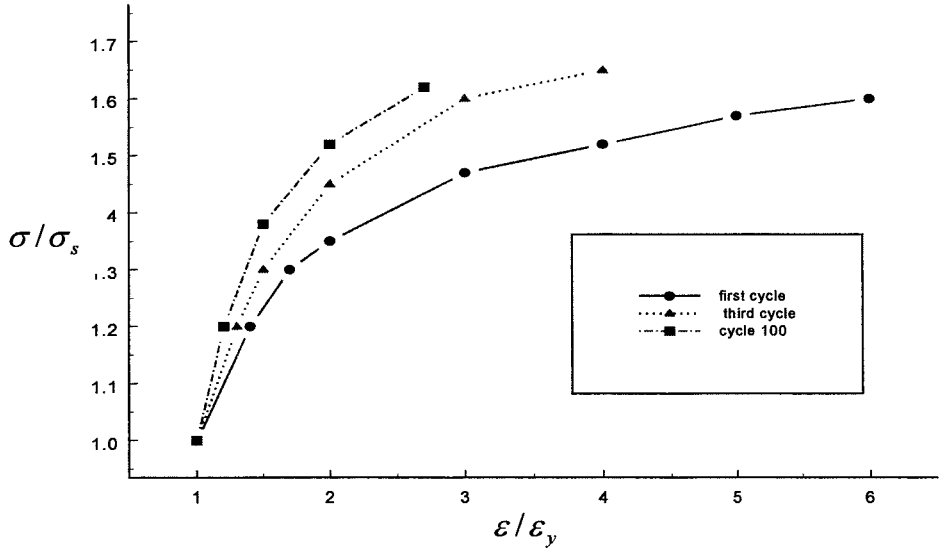

Fig.8. Nonlinear parts of stress-strain curves for B95 Al alloy different loading cycles

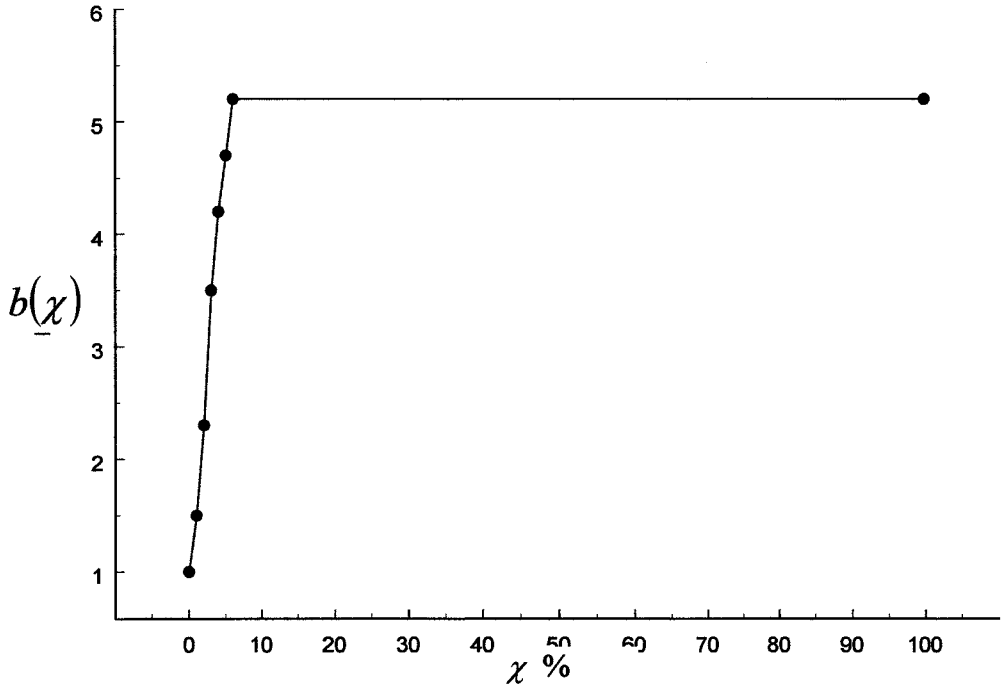

Fig.9. b_χ versus the accumulated plastic strain χ

On the base of this information about cyclic parameters of Al alloy and using the least-squares method the following results were obtained: $d_\chi = 0.95$; $a_\chi = 1.86$; for all values χ. Only average values of d_χ and a_χ are used because the experimental data presented in Fig.7 and Fig.8 was obtained over a limited number of cycles and a similar method was used to obtain b_χ [6]. From the results presented in Fig.8 values of b_χ were calculated. Fig.9 shows the relationship of b_χ with regards to χ the accumulated plastic strain.

Hypothesis

Cyclic strain plasticity relationships are based on the classical strain plasticity theory hypotheses [11-12], which are accepted as valid for any loading and unloading half-cycle. Unlike the usual approach, the hypothesis of unified deformation curve is replaced at any half-cycle by the hypothesis of unified cyclic deformation branch in the local co-ordinates $\sigma^*_{(n)}$, $\varepsilon^*_{(n)}$, where n is the half-cycle number (Fig. 5). The cyclic deformation curve is plotted on the basis of the material test analysis at the cyclic deformation.

Let us consider that the position of the local co-ordinates of the origin of σ^*, ε^* are specified in the global co-ordinates by the stress tensor σ^n_{ij} and the strain tensor ε^n_{ij}, these tensors may be regarded as the initial stresses and strains for the $n+1$ loading half-cycle.

For the $n+1$ half-cycle, the point representing the deformation process must lie on one of the cyclic deformation curve branches that emerge from the point $\sigma_{ij(n)}$, $\varepsilon_{ij(n)}$. Depending on the loading direction, the $n+1$ loading phase may coincide with the previous loading direction or the stress increments are directed opposite to the vector $\{\sigma_n\}$.

Depending on the load direction, the unified deformation curve for each calculated point coincides either with the curve $\sigma_{(0)}$ or with the curve $\sigma_{(\pi)}$, both curves are shown in Fig. 5b, which represents the relationship between the effective stress $\bar{\sigma}^*$ and the strain $\bar{\varepsilon}^*$.

In the local co-ordinates the following hypotheses of the strain plasticity theory are valid

1. The mean stress and strain lies in the elasticity area

$$\sigma^* = K\varepsilon^*, \quad K = \frac{E_\chi}{3(1-2\nu_\chi)},$$

$$\sigma^* = \frac{1}{3}\sigma^*_{ii}, \quad \varepsilon^* = \frac{1}{3}\varepsilon^*_{ii}$$

2. Stress and strain deviators are related by the following relationships

$$s^*_{ij} = \frac{E_\chi}{2(1+\nu_\chi)\psi} e^*_{ij},$$

$$s_{ij} = \sigma^*_{ij} - \sigma^*\delta_{ij}, \; e_{ij} = \varepsilon^*_{ij} - \varepsilon^*\delta_{ij}$$

Thus, on the basis of the unified curve hypothesis and taking into account that $\bar{\sigma}^* = \left(3/2\, s^*_{ij}s^*_{ij}\right)^{1/2}$ and $\bar{\varepsilon}^* = \left(2/3\, e^*_{ij}e^*_{ij}\right)^{1/2}$, we get

$$\psi = \frac{3E_\chi}{2(1+\nu_\chi)} \frac{\bar{\bar{\varepsilon}}^*}{\bar{\sigma}^*}$$

Here E_χ and ν_χ are the Young's modulus and the Poisson's ratio.

These constitutive equations lead to the non-linear FE problem, solution of which requires special iterative procedure at every half cycle of the loading or unloading. A more complete development of this theory and solution methodology of non-linear FE equations are described elsewhere. [2, 13, 14].

4. DAMAGE MODEL

Tests conducted for different engineering materials show [3-6] that for constant–amplitude stress, constant–amplitude strain and stress random–amplitude loading the number of half-cycles n_f before failure at alternating–sign plastic deformation is related to the limiting value $\chi_{\max}$ by the power law:

$$n_f = \left(\chi_{\max} / \delta \right)^{\gamma}, \tag{4.1}$$

here δ is the constant depending on the residual plastic strain value, γ is the parameter that characterises the material ability "to cure" the cyclic loading damage.

The model based on the relationship (3.3) allows simulating the cyclic life exhaust process of the specimens under all conditions. At the same time, the accumulated plastic strain may be plotted on the co-ordinate plane χ, n by the function $\ln(\chi)$ of $\ln(n)$. Moreover, if $\Delta\varepsilon_p$ does not change sign in going from half-cycle to half-cycle, then χ increases and n_f remains constant. If in the two adjoined half-cycle $\Delta\varepsilon_p$ changes sign then n increases by one. If the value $D = \chi(n)/\chi_{\max}(n)$ is taken as the measure of damage, $D = 1$ defines the amount of half-cycle loading where the alternating–sign plastic deformation takes place until a fatigue crack occurs. If for different loading processes the parameters defining the material mathematical model at cyclic deformation are equivalent to the same damage measure D, all functions of χ in (3.3) may be replaced by the functions of the dimensionless parameter D. The possibility of applying this approach has been studied experimentally [3,5].

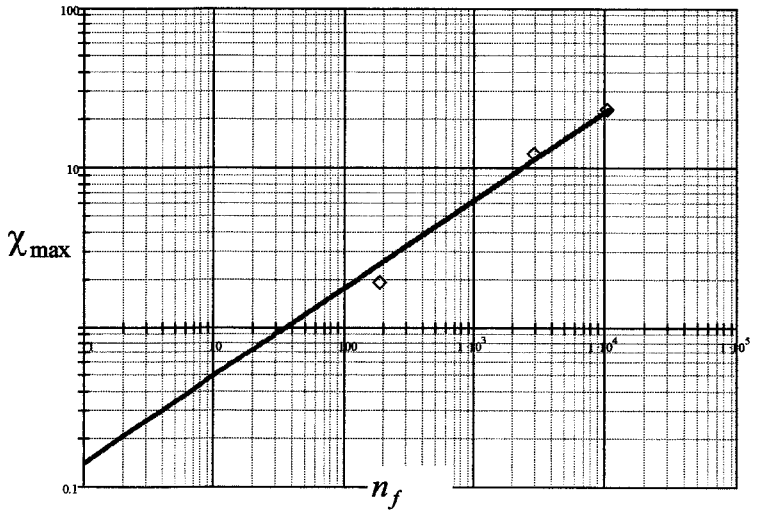

Fig.10. Experimental and analytical relationship between the ultimate accumulated plastic strain and the number of half-cycles before failure.

The values of parameters to be used in (4.1) were calculated on the base of experimental data from the results of constant strain controlled low-cycle fatigue studies that were conducted on un-notched specimens. Taking into account that parameter χ in these tests can be obtained by the following relationship:

$$\chi = n_f \left(2\Delta\varepsilon_{ay} - \frac{a_\chi \sigma^* \left(2\Delta\varepsilon_{ay} \right)}{E_\chi} \right),$$

the results of which are shown in Fig.10 where n_f is the number of half-cycles to failure for un-notched Al specimens and $\Delta\varepsilon_{ay}$ is the specimen's elongation amplitude. Fig. 10 is an approximation of these experimental points. The point of intersection with the Y-axis gives the value of δ=0.1328. The line tangent is γ=2.005.

5. RESULTS OF NUMERICAL SIMULATION

Monotonic loading.

As a first step in this study, the behaviour of the MMC in the plasticity area under monotonic loading was simulated. The effective plastic strains were determined for different values of strain ε_y in the direction of cylinder axis. The effective plastic strain distribution in the cylinder with an overall strain of $\varepsilon_y = 0.01$ is shown in Fig.11. It can be seen that the residual strains reach maximum value on the interface between the inclusion and the matrix. There is a second area on the cylinder axis in front of the inclusion where plastic strain reaches a maximum value. Plastic strains in these two zones are shown in Fig.11 where localised strain in these two regions is plotted against overall material strain.

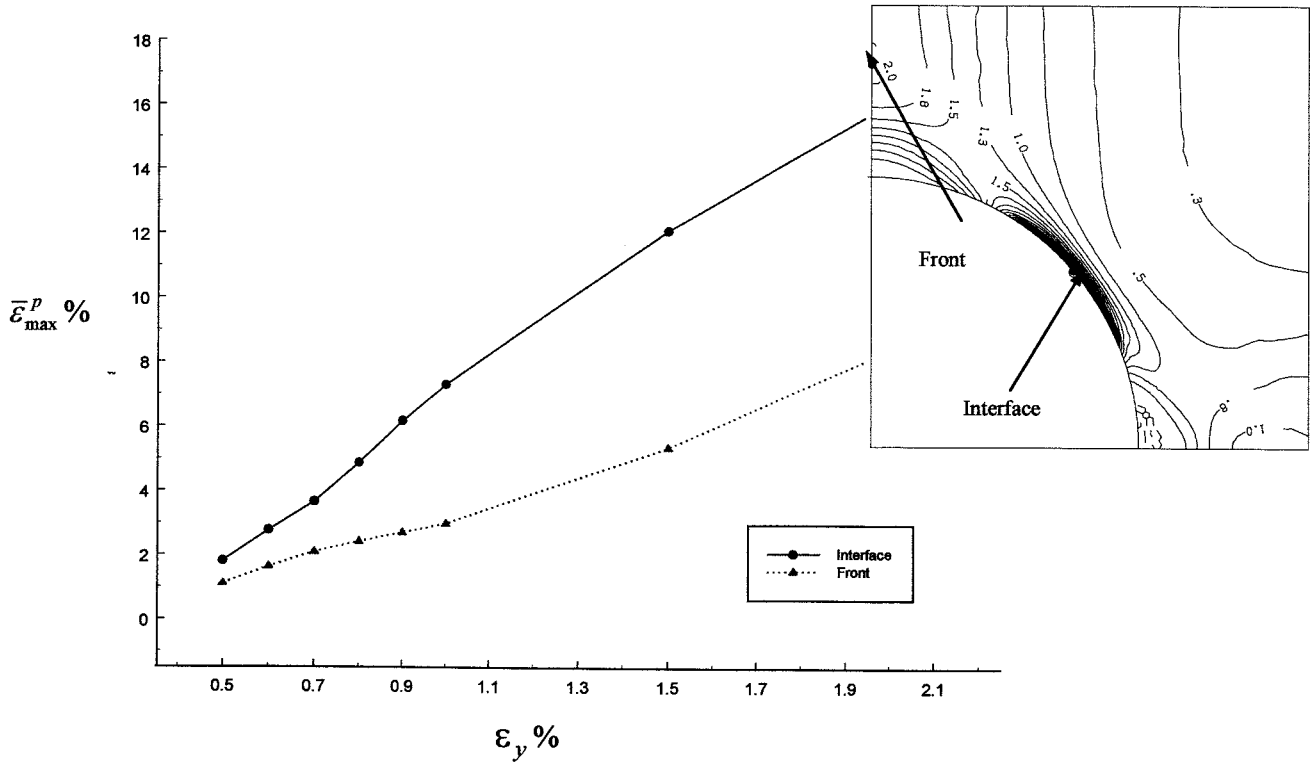

Fig.11. Maximal effective plastic strains $\bar{\varepsilon}^p_{max}$ in the interface and frontal zones versus the specimen's strain ε_y

If it is assumed that failure of the composite will develop from a localised area of maximum strain, it is possible to determine the upper boundary of overall composite strain, by incrementally increasing the value of ε_y to determine those areas within the composite that reach these high strain areas. Using results obtained from Fig.11 we see that with an effective plasticity strain in the MMC of 1.9%-2% certain areas within the composite have strains that have become equal to the failure strains of Al7075. This result is in good agreement with those determined experimentally in which the failure of an MMC's occurs at a strain value of 0.02 [1]. Thus, the above mathematical model is a good estimate of the experimental results and gives some encouragement that this approach may be used in the development of a lifetime prediction model for MMC with short inclusions under cyclic loading. Failure under cyclic loading may be related to the beginning of crack propagation at the interface between inclusion and matrix.

Numerical simulation of MMC behaviour under cyclic loading.

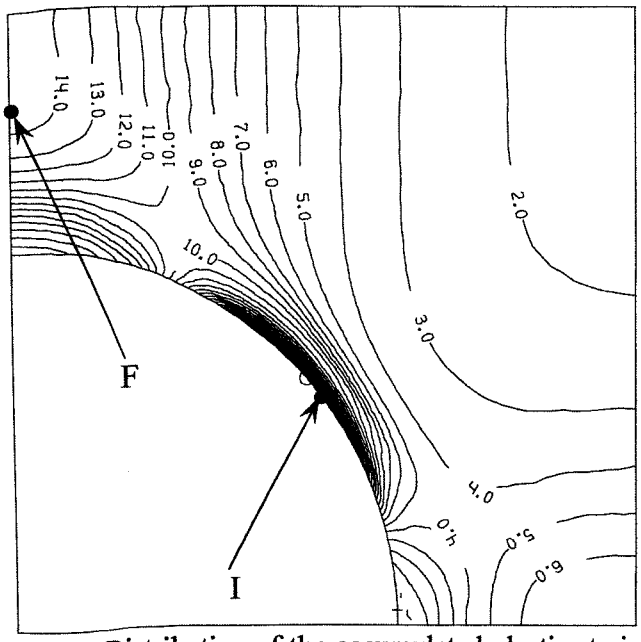

Fig.12. Distribution of the accumulated plastic strain in the composite after 5 half-cycles with elongation amplitude of 1%. I denotes the concentration zone of accumulated plastic strain on the interface between fiber and matrix. F denotes the concentration zone in the direction of load action

The numerical investigation of the composite was carried out in strain-controlled tests for the following strains amplitudes of symmetric cycles, $\Delta\varepsilon_{ay}$= 0.5%, 0.6%, 0.7%, 0.8%, 0.9%, 1%. As for static loading simulation, it was assumed in the analysis that the inclusions in the composite were spherical. Results for the first half-cycle at the deformation amplitude of 1% coincide with results of the monotonic loading presented in Fig.11. At each calculation point the current values of χ and damage measure D were defined. The calculation process stops when $D=1$. Fig.12 represents the accumulated plastic strain distribution after the fifth deforming half-cycles with an elongation amplitude of 1%. One can easily see that two zones (I and F) appear where the accumulated plastic strain is at a maximum. The first zone I, is on the interface between inclusion and matrix. The second zone F is formed at some distance from the inclusion in the direction of deformation, on the cylinder axis. It follows from what has been said that the first fatigue crack forms on the inclusion matrix interface but it is soon followed by a second crack that forms in the frontal zone after a certain number of loading and unloading half-cycles. Obviously these cracks precede the overall MMC's failure. As long as some region of the composite is at high enough stress this process will occurs at all other levels of strain amplitude.

In the zones marked I and F in Fig 12 the process of alternating-sign deformation occurs in different ways. Fig.13 is two cyclic diagrams of the global co-ordinates $\sigma(\varepsilon)$ for a strain amplitude of 0.7%. Fig.13a shows that the process of cyclic deformation on the interface between inclusion and matrix is subject to greater strain levels than in the zone F, shown in Fig.13b.

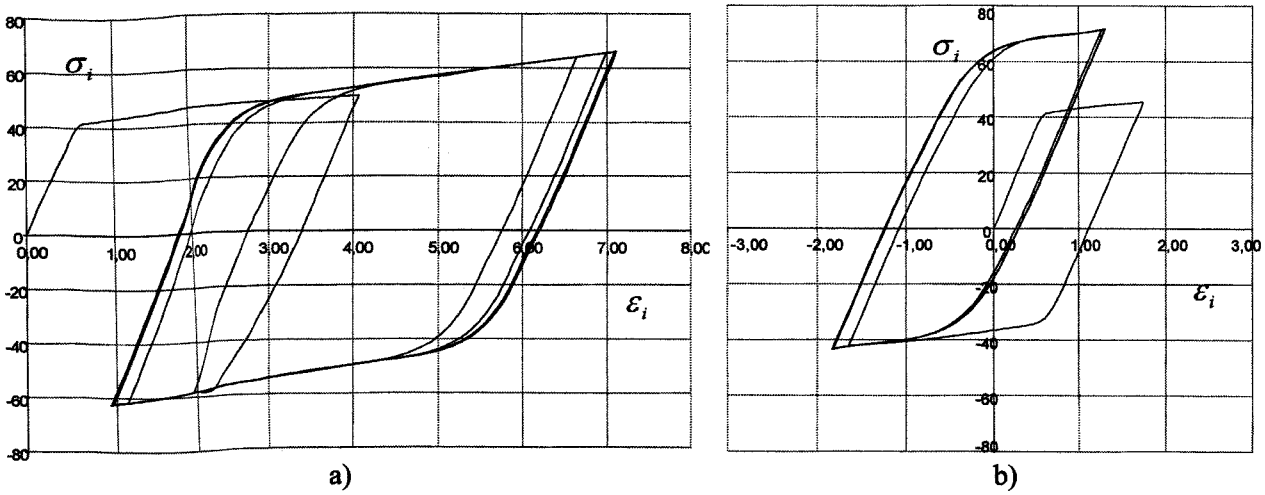

a) b)

Fig.13. Numerically (FE) simulated cyclic stress-strain curves: a) interface zone; b) frontal zone

Despite the fact that the overall loading process occurs at constant strain amplitude, zones I and F see different a different stress and strain range. However, as the number of cycles increase the dimensions of the hysteresis loop stabiles. This is confirmed by the results given in Fig.14 showing the behaviour of the loop's width versus the number of half-cycle. Initially the cyclic behaviour of the material is dependent on the value of the specimen's elongation amplitude. However, by the tenth half-cycle the process of cyclic deformation may be considered stabilised. In many respects, it depends on the value of the hardening parameter b_χ.

It should be noted that the process of cyclic elasto-plastic deformation brings an essential non-homogeneity in the distribution of plastic strain in the region close to the inclusion matrix interface (see Fig.12). Due to the non-uniformity of aluminium's hardening in the region near the interface a zone with wave-like distribution of plastic strain arises. However, with the number of half-cycles increasing, such wave-like pattern is smoothed out. Thus maximal plastic strain on the interface and frontal zones are not consistent from the cycle to cycle (Fig.14).

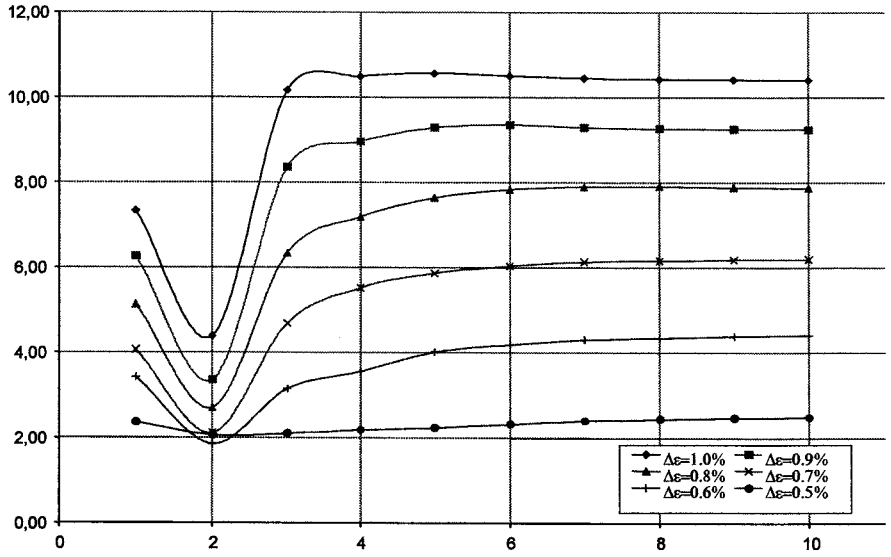

a)

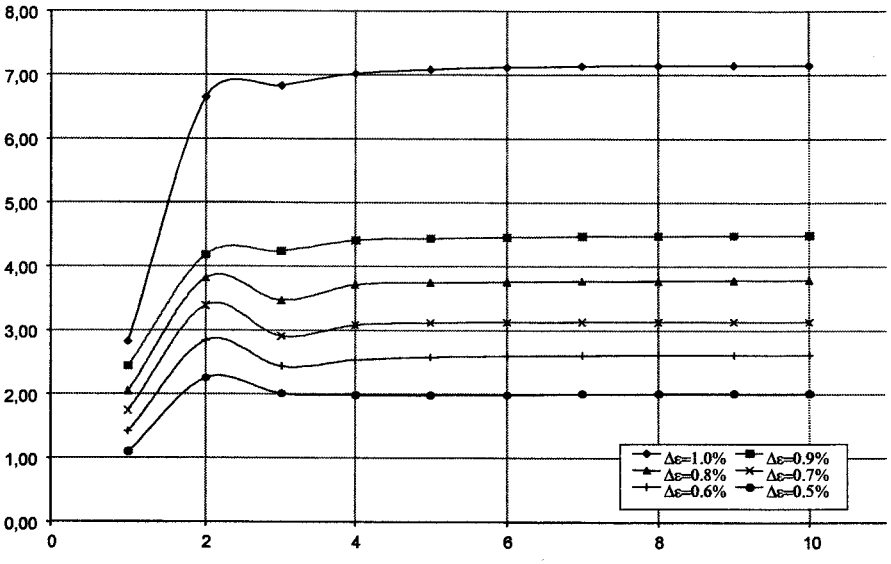

b)

Fig.14. Relationship between the width of cyclic deformation loop and the number of half-cycle at different values of the specimen's elongation amplitude: a) interface zone I; b) frontal zone F.

On the basic assumption that the number of half-cycles before the appearance of a low-cycle fatigue crack is defined by the condition $D = 1$ number of cycles for crack beginning were calculated. Fig.15 is a plot of cycles before failure versus the localised strain for region within the MMC with the interface area of high stress indicated with an I and the highly stressed frontal zone is mark with an F. Experimental results shown on Fig 15 are taken from previous results.[1]
It must be remembered that this finite element analysis only allows prediction of the number of cycles to crack initiation. For this type of fatigue loading it would be expected that number of cycles from first crack until failure lies around 50-80% of specimen cyclic lifetime. It should be expected therefore that, for a given strain level, theoretical predictions would under estimate the life of the material compared to results obtained experimentally and it can be seen from figure 15 that this is the case.

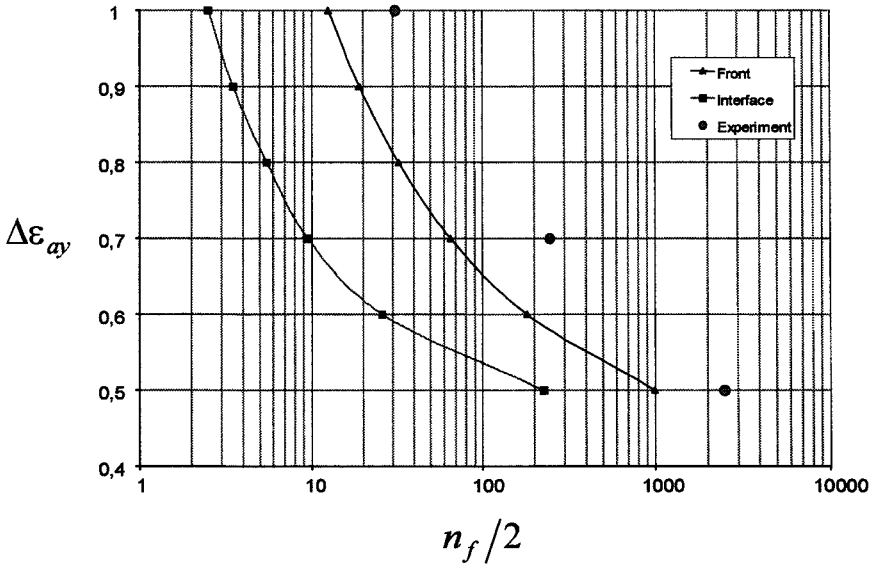

Fig.15. MMC's fatigue diagram.

CONCLUSIONS

A procedure for mathematical modelling the elasto-plastic deformation processes in an MMC with inclusions under cyclic loading is presented. The results obtained show that the failure of the MMC occurs in several steps. First, an internal crack arises on the interfaces between matrix and inclusion. Then, it is possible for further cracks to appear in a frontal zone, situated between inclusions. These two set of cracks do not appear at the same time in the cyclic history of the material but the frontal zone must experience a far larger number of half-cycles before a crack appears compared to the interface area. However, material failure will occurs provided that the system of cracks on the interface is integrated with the cracks in the frontal zones and that the cracks progresses further in the radial direction from interface to the cylinder's surface. The presented results predict time to failure of only some composite's parts and therefore give a low estimate of fatigue lives in comparison with experimental data. Perhaps, a further development of the proposed technique and its application to the bodies with cracks would enable us to simulate the whole process of MMC's failure under cyclic loading.

ACKNOWLEDGEMENT

The authors would like to thank the CIAM research engineers Khakim Azmetov and Andrey Roushnov for great help in analyses and article design, and the student of BMSTU Olga Karasseva for her tireless efforts at the interface in this composite Russian–English article.

REFERENCES

1. Fleming, W.J., Dowson, A.L. Prediction of the Fatigue Life of an Aluminium Metal Matrix Composite Using Theory of Cells. *Science and Engineering of Composite Materials*, **vol.8**, No. 4, 181-189. 1999.
2. Temis, Y.M. Plasticity and Creep in engineering analysis. Analytical and Numerical Methods of Plasticity and Viscous-Elasticity Boundary Problems Solution. Sverdlovsk, Ac.of Sc of USSR, pp.100-106, 1986 (in Russian).
3. Putchkov, I.V., Temis, J.M. Elastoplastic and damage model of structure material. Fifth USSR Symposium Low Cycle Fatigue.- *Failure Criteria and Material Structures*. Volgograd 1987. V2 pp. 50-52. (in Russian)
4. Putchkov, I.V., Temis, J.M. Analytical formulas for elastoplastic response of structure materials under cyclic loading. *Problems of Strength*.1988, No9. pp.18-22. (in Russian)
5. Putchkov I.V., Temis J.M. Elastoplastic and damage parameters of structures materials under cyclic loading. *Applied Problems of Strength and Plasticity*. University of N. Novgorod, 1992. pp.82-89.
6. Putchkov I.V., Temis Y.M., Dowson A.L., Damri D. Development of a finite element based strain accumulation model for the prediction of fatigue lives in highly stressed Ti components. *Int.J. Fatigue*. Vol.17, No 6, pp. 385-398, 1995.
7. Dowson, A.L. Kwon, J.W., Healy, J.C., and Beevers, C.J., "Innovative Manufacturing, Design and Assessment of Aluminium Matrix Composites for High Temperature Performance" *Brite Euram Project* **BE 3398**-89 (1993).
8. Structure materials. Handbook. Ed. in chief B.N.Arsamascev. Mashinostroenie. Moscow. 1990. 667p. (in Russian).
9. Lebedev A.A., Kovalchuk B.I., Gignyak F.F., Lamashevsky V.P. Handbook: Mechanical characteristics of structure materials under multi-axial stress-strain stage. Kiev, Naukova Dumka, 1983. 366p. (in Russian)
10. Shnaderovich R. M. Strength under monotonic and cyclic loading. Mashinostroenie. Moscow. 1968. 343p. (in Russian).
11. Jonson W., Mellor P.B. Engineering Plasticity. Van Nostrand Reinold Company LTD. 1975. 646p.
12. Hill R. The Mathematical Theory of Plasticity. O.U.P., 1950.
13. Temis Y.M. Simulation of non-isothermal elastic-plastic loading in the engine and power station structures. Chapter 4.6.3. *Mechanical engineering. Encyclopaedia*. Ed. In chief K.S.Kolesnikov. Vol.1-3 Book 1. Mashinostroenie. Moscow, pp. 262-268, 1994 (in Russian).
14. Temis Y.M. Plasticity and creep of Gas Turbine Engines components under cyclic loading. *Problems of strength and dynamics in aero engines*. Moscow, 1989. Issue 4 (CIAM reports No 1237) pp.32-50 (in Russian)